Characterization of Mesenchymal Stem Cells for their Use in Cardiovascular Regenerative Medicine

---

Dissertation

zur

Erlangung der naturwissenschaftlichen Doktorwürde
(Dr. sc. nat.)

vorgelegt der

Mathematisch-naturwissenschaftlichen Fakultät

der

Universität Zürich

von

Debora Kehl

von

Zürich ZH

Promotionskommission

Prof. Dr. Arnold von Eckardstein (Vorsitz)

PD Dr. Dr. Benedikt Weber (Leitung der Dissertation)

Prof. Dr. Dr. Simon P. Hoerstrup (Leitung der Dissertation)

Prof. Dr. Christian Grimm

Prof. Dr. Benjamin Gantenbein

Zürich, 2017

for my parents

TABEL OF CONTENT

SUMMARY

Mesenchymal stem cells (MSCs) are multipotent stromal stem cells with the capacity to differentiate into mesodermal lineages and immunomodulatory properties. MSCs have been isolated from several fetal and adult tissue sources with some distinct phenotypic and functional profiles. The clinical benefits exerted by MSCs upon transplantation are due to the release of paracrine factors and biologically relevant molecules to the diseased or injured tissue. The so-called MSC secretome influences the microenvironement following injury, promoting endogenous regeneration of the injured tissue environment via cytoprotection and angiogenesis. Therefore, the interest in MSCs for clinical applications has constantly increased over the last decade, mainly for cell-based therapies but also for cardiovascular tissue engineering. Here, the combination of MSCs with biodegradable scaffold materials enables enhanced extracellular matrix production and *in vivo* tissue formation.

In the presented thesis, different human and animal-derived MSCs were isolated and characterized. Human adult MSCs from the adipose tissue (hADSCs), bone marrow (hBMSCs) and umbilical cord Wharton's jelly (hWJSCs) demonstrated distinct chemoattractive and angiogenic potential. Mass spectrometry analyses revealed that hBMSC and hWJSC secretome possess a more retained pro-angiogenic and inflammatory profile compared to hADSCs. On the other hand, fetal MSCs from the amniotic fluid (AFSCs) were evaluated in the ovine developmental model, which uniquely enables investigation of prenatal cells. In contrast to humans the ovine model maintains two separate extraembryonic cavities, the amniotic and the allantoic fluid cavity. Therefore, several parameters for discrimination of the two fetal fluids over gestation have been defined and isolated cells were systematically compared. Higher expression of pluripotency-related genes was found in ovine AFSCs compared to cells isolated from the allantoic fluid, pointing toward a more pronounced stem cell phenotype. Finally, new scaffolds for cardiovascular tissue engineering applications were evaluated. A jet spinning process for the rapid and automated fabrication of fibrous heart valve scaffolds was established. Tissue engineered heart valves were minimally-invasively deployed into the pulmonary valve position in the ovine model and shown to be functional for 15 hours. However, the *in situ* remodeling was shown to be low in long-term follow up. Therefore the incorporation of either MSCs itself or their secretome might additionally enhance the tissue formation in the future.

ZUSAMMENFASSUNG

Mesenchymale Stammzellen (MSCs) sind multipotente Stammzellen des Bindegewebes, welche in verschiedene mesodermale Gewebe differenzieren können und immunomodulierende Eigenschaften besitzen. MSCs können aus verschiedenen fetalen und adulten Gewebequellen isoliert werden, mit jeweils unterschiedlichen phänotypischen und funktionellen Merkmalen. Die klinischen Vorteile nach MSC Transplantation beruhen auf der Freisetzung von parakrinen Faktoren und biologisch relevanten Molekülen, welche auf das erkrankte oder verletzte Gewebe Einfluss ausüben. Das sogenannte MSC Sekretom beeinflusst die Mikroumgebung nach Verletzung und fördert die körpereigene Wiederherstellung des verletzten Gewebes durch Zellschutz und der Bildung neuer Blutgefässe (Angiogenese). Dementsprechend, stieg das Interesse an MSCs für die klinische Anwendung in den letzten Jahrzehnten stetig, insbesondere für Zelltherapie aber auch für die kardiovaskuläre Geweberekonstruktion (Tissue Engineering). Hierbei, stellt die Kombination aus MSCs und biologisch abbaubarem Zellträger (Scaffold) eine Möglichkeit dar die Produktion von extrazellulärer Matrix und Gewebebildung *in vivo* zu fördern.

In der folgenden Arbeit wurden verschiedene MSCs von Mensch bzw. dem Tiermodell isoliert und charakterisiert. Humane adulte MSCs vom Fettgewebe (hADSCs), Knochenmark (hBMSCs) und der Wharton-Sulze der Nabelschnur (hWJSCs) zeigten unterschiedliches Potential hinsichtlich Chemoattraktion und Angiogenese. Massenspektrometrie zeigte deutlich, dass die Sekretome von hBMSC und hWJSC im Vergleich zu hADSC ein stärker ausgeprägtes pro-angiogenes und entzündliches Potential aufweisen. Zudem wurden die fetalen MSC vom Fruchtwasser (AFSC) im fetal Schafmodell untersucht. Im Gegensatz zum Menschen verbleiben im Schafmodell zwei separate extraembryonale Flüssigkeitsräume, das Fruchtwasser und die Allantois-Kavität. Es wurden Parameter zur spezifischen Diskriminierung der zwei fetalen Flüssigkeiten während der Schwangerschaft analysiert und dessen Zellen systematisch charakterisiert. Ovine AFSC zeigten im Gegensatz zu Zellen aus der Allantois-Flüssigkeit eine erhöhte Expression von mehreren Pluripotenz-assoziierten Genen, was auf einen stärker ausgeprägten Stammzell-Phänotyp schliessen lässt. Zudem wurde ein neuer Scaffold für das kardiovaskuläre Tissue Engineering untersucht. Ein Gerät für die schnelle, automatisierte Herstellung von Herzklappengeweben wurde entwickelt. Tissue engineerte Herzklappen wurden minimal invasiv in die pulmonale Position des Schafmodels implantiert und zeigten 15 Stunden Funktionalität. Allerdings, war der *in situ* Gewebeumbau langfristig niedrig. Jedoch könnte die Einarbeitung von den MSC selbst oder deren Sekretom zukünftige Gewebeneubildung zusätzlich fördern.

ABBREVIATIONS

adipose derived MSC	ADSC
amniotic fluid	AF
amniotic fluid derived stem cell	AFSC
RAC-alpha serine/threonine-protein kinase	AKT1
allantoic fluid	AL
allantoic fluid derived stem cell	ALSC
angiopoietin	ANG
bone marrow mononuclear cell	BMMC
bone morphogenic protein	BMP
bone marrow derived MSC	BMSC
fibroblast colony forming cells	CFU-F
conditioned media	CM
cumulative population doubling	CPD
crown rump length	CRL
computed tomography	CT
chronic venous insufficiency	CVI
decellularized TEHV	dTEHV
endothelial cell	EC
extracellular matrix	ECM
endothelial-to-mesenchymal transformation	EMT
embryonic stem cell	ESC
food and drug administration	FDA
false discovery rate	FDR
fibroblast growth factor	FGF
fourier transform infrared spectroscopy	FTIR
good manufacturing practice	GMP
generation time	GT
graft-versus-host disease	GVHD
hematoxylin and eosin	H&E
hexfluoroispropanol	HFIP
hepatocyte growth factor	HGF
human leucocyte antigen-DR	HLA-DR
human peripheral mononuclear cells	hPBMC
human platelet lysate	hPL
human umbilical vein endothelial cells	HUVEC
interferon gamma	IFN-γ
insulin growth factor	IGF
interleukin	IL
induced pluripotent stem cell	iPSC
international society for cellular therapy	ISCT
lower control limit	LCL
monocyte chemoattractant protein	MCP
median fluorescence intensity	MFI
macrophage inflammatory protein	MIP
masson goldner	MG
matrix metalloproteinase	MMP
mass spectrometry	MS
mesenchymal stem cell	MSC
macrophage	MΦ
national institute of health	NIH
poly(4-hydroxybutyrate)	P4HB
phosphate buffer saline	PBS
poly(ε-caprolactone)	PCL
platelet-derived growth factor	PDGF
poly(ester urethane)ureas	PEUU
platelet factor 4	PF-4
poly(glycolic acid)	PGA
prostaglandin E2	PGE_2
poly(glycerol sebacate)	PGS
placental growth factor	PIGF
poly(lactic acid)	PLA
region of interest	ROI
stromal cell-derived growth factor	SDF
scanning electron microscopy	SEM
smooth muscle cell	SMC
tissue engineering	TE
tissue engineered heart valve	TEHV
tissue engineered venous valve	TEVV
transforming growth factor beta	TGF-β
tumor necrosis factor alpha	TNF-α
total protein	TP
thrombospondin-1	Tsp-1
upper control limit	UCL
vascular endothelial growth factor	VEGF
von giesson-elastin	VG-EL
valvular interstitial cell	VIC
von kossa	VK
Wharton's jelly derived MSC	WJSC
alpha smooth muscle actin	αSMA
β-tricalcium phosphate	β-TCP

1

General Introduction

The content of this chapter is based on:

Kehl D, Weber B, Hoerstrup SP. Bioengineered living cardiac and venous valve replacements: current status and future prospects. *Cardiovascular Pathology* 2016 Jul-Aug;25(4):300-5.
Copyright License No.: 4142361401206 (adapted)

Malheiro V, Enayati M, **Kehl D**, Bergmeister H, Weber B, Maniura-Weber K. Macrophage cellular crosstalk in the response to biomaterial implantation. *(under revision in eCells and Materials, 2016)*

CHAPTER 1.1

Bioengineered living cardiac and venous valve replacements: current status and future prospects

Debora Kehl[1], Benedikt Weber[1], Simon P. Hoerstrup[1]

[1] Institute for Regenerative Medicine (IREM), Center for Therapy Development and Good Manufacturing Practice, University of Zurich, 13 Moussonstrasse, Zurich, 8004, CH, Switzerland

Abstract

Valvular heart disease remains to be a major cause of death worldwide with increasing prevalence, mortality, and morbidity. Current heart valve replacements are associated with several limitations due to their nonviable nature. In this regard, heart valve tissue engineering has shown to represent a promising concept in order to overcome these limitations and replace diseased cardiac valves with living, autologous constructs. These bioengineered valves hold potential for *in situ* remodeling, growth, and repair throughout the patient's lifetime without the risk of thromboembolic complications and adverse immune responses. For the fabrication of tissue-engineered heart valves, several concepts have been established, the "classical" *in vitro* tissue engineering approach, the *in situ* tissue engineering approach, and alternative approaches including three-dimensional printing and electrospinning. Besides first attempts have been conducted in order to produce a tissue-engineered venous valve for the treatment of deep venous valve insufficiency. Here we review basic principals and current scientific status of valvular tissue engineering, including a critical discussion and outlook for the future.

Personal contribution:

Definition of article structure and content. Writing of all chapters within the manuscript: *1.1.1 Introduction; 1.1.2 Basic principle of heart valve tissue engineering; 1.1.2.1 In vitro heart valve tissue engineering – current status; 1.1.2.2 In situ heart valve tissue engineering – current status; 1.1.2.3 Alternative and adjunctive approaches for heart valve tissue engineering; 1.1.3 Basic principle of venous valve tissue engineering; 1.1.4 Limitations and future outlook;* including abstract and drafting of all figures 1-3. Correspondence with editorial office and responsible for revision process (R1 and R2).

Cardiovascular Pathology (published 2016)

1.1.1 INTRODUCTION

Valvular heart disease is responsible for a high disease load worldwide, affecting people of all ages and origins. In industrialized countries increasing aging of the population is the major cause of degenerative valve disease, while in developing countries the problem of rheumatic cardiac diseases is still prevalent, resulting in increased mortality and morbidity each year [1,2]. Although medical progress has been outstanding over the past few decades, the annual number of people requiring heart valve replacements is expected to triple globally from currently approximately 290,000 interventions per year to 850,000 in 2050 [2].

Surgical replacement of the insufficient valves is the most commonly used treatment for end stage valvular heart disease. Nowadays, either mechanical or biological prostheses are used for the replacement of dysfunctional valves. Although dramatically improving the life expectancy of the patients all currently available prostheses are associated with substantial limitations including the principal lack of growth, repair and remodeling capacities. The non-adaptive non-viable materials show substantial surface thrombogenicity (mechanical valves) and progressive calcific degeneration (bioprostheses). Lifelong anticoagulation therapies and repeated reoperations are therefore indispensable, especially for pediatric applications.

Besides also chronic venous insufficiency (CVI) represent a major global health problem with increasing prevalence, morbidity and socioeconomic impact [3]. Over long term, increased blood pressure within the lower extremities and venous return to the heart is impaired. This results from valvular incompetence, perforated veins, venous tributaries, venous obstruction or a combination of theses mechanisms [3]. Insufficient valves are associated with venous blood reflux, obstruction, stasis and distal venous hypertension [3]. As in the cardiac field current therapeutic applications are suboptimal with short lasting results using palliative conventional techniques and highly invasive vein reconstructions. Recently bioprosthesis have been investigated, so far with no success in long-term evaluations [4].

Taken together, current prostheses for valvular disease are suboptimal and new approaches need to be considered as alternative therapies. In this regard, tissue engineering has shown promising results by creating bioengineered, living autologous replacements with the ability for somatic growth, remodeling and repair.

1.1.2 BASIC PRINCIPLE OF HEART VALVE TISSUE ENGINEERING

Tissue engineering is an emerging field of research with the goal to improve and/or restore tissue/organ functionality via the development of engineered, living substitutes. Several strategies of heart valve tissue engineering have been followed: the *in vitro* and the *in situ* approach as well as alternative approaches including three-dimensional (3D) printing and electrospinning. For the traditional *in vitro* approach, autologous cells are isolated from individual patients, seeded onto biodegradable scaffolds, pre-conditioned and matured in a bioreactor system to induce native-analogous neo-tissue formation ex vivo, followed by implantation of a living, autologous engineered valve into the diseased patients. This strategy is referred to as *in vitro* tissue engineering and has been the principal experimental approach for heart valve tissue engineering over the last years. The second approach, referred to as *in situ* tissue engineering, aims at stimulating the bodies own regenerative capacity in order to induce tissue formation *in vivo* (*in situ*), instead of generating tissue ex vivo. Although the design of the scaffold and the potential seeding of isolated cells are still performed ex vivo, no extensive and regulatory complex *in vitro* cell expansion and conditioning in a bioreactor system are required prior to implantation. This approach is taking advantage of the intrinsic regenerative potential of the body itself inducing autologous host cell repopulation followed by tissue remodeling and potentially regeneration and growth. It represents a simplified strategy, without the need of extensive *in vitro* cell expansion techniques. Using this approach higher clinical feasibility of the tissue enginnered heart valve (TEHV) technology seems possible. Cell-mediated leaflet thickening, retraction and fibrosis induced by the mechanical conditioning of the seeded cells in the bioreactor might be circumvented and *in vitro* cellular manipulation reduced [5]. However it is of note that this approach substantially depends on the regenerative capacity of the host, which might be a critical issue in patients with metabolic diseases or immunologic defects. Therefore over the last years great effort has been made in the inclusion of bioactive compounds into the scaffolds to guide *in situ* tissue remodeling. In this regard the development of novel simplified and fast(er) technologies have been intensively studied. 3D-printing and electrospinnig with their different settings and modalities enable to approximate the constructs to the requirements of the ideal valvular substitute on the macro- to microscopic level – including an ideal heart valve anatomy and bioactivity. Ideally the release of bioactive molecules is coupled with the degradation of the polymer fibers, while new ECM is built *in situ*. However, *in vivo* studies will further need to evaluate these technologies for future TEHV.

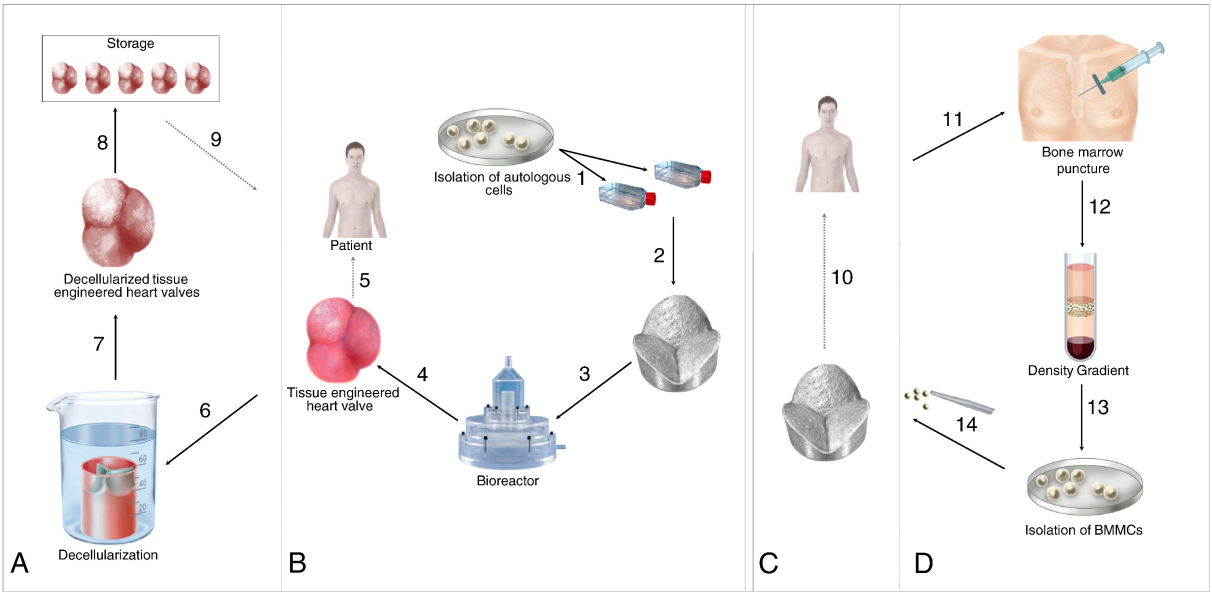

Figure 1: Main strategies of heart valve tissue engineering. (B) The concept of *in vitro* heart valve tissue engineering compromises the harvest of autologous cells from the patient which are subsequently expanded to high cell numbers *in vitro (1)*, seeded onto biodegradable scaffolds *(2)* and conditioned in a bioreactor system *(3)*. After 3-4 weeks new tissue has formed and the tissue engineered heart valves (TEHV) *(4)* can be implanted into the particular patient *(5)*. (A) In order to store TEHV, the concept of decellularization enables the removal of cellular components by detergent solutions *(6)* to create decellularized starter matrices *(7)* with long-term availability *(8).* These off-the-shelf constructs can subsequently be implanted *(9)* for the *in situ* host cell repopulation. (C) This concept of *in situ* tissue engineering takes advantage of the intrinsic remodeling capacity of the body. The implantation of starter matrices triggers autologous host cell recruitment, vascular remodeling and tissue formation *in vivo (10)*. (D) By seeding bone marrow mononuclear cells (BMMCs) onto such starter matrices the intrinsic remodeling capacity of the body can be further enhanced. Therefore, bone marrow is obtained by sternal puncture at the day of implantation *(11),* BMMCs are isolated by density gradient centrifugation *(12,13)* and seeded onto heart valve starter matrices *(14)*.

1.1.2.1 *IN VITRO* HEART VALVE T ISSUE ENGINEERING – CURRENT STATUS

The requirements for an *in vitro* tissue engineered heart valve compromise I) an autologous, easily accessible cell source, II) a biodegradable scaffold material, designed in the shape of a heart valve, and III) an *in vitro* bioreactor system for the mechanical and biochemical conditioning of the construct. The quality of the tissue depends highly on the individual cell source chosen. In the attempt to define the best suitable cell source, characteristics like their expansion potential, their capability to produce extracellular matrix (ECM) and their regenerative potential are of critical importance. Therefore, several promising cell sources isolated from different donor tissues have already been used for the *in vitro* generation of TEHV such as adipose tissue-derived cells [6], amniotic fluid-derived cells [7,8], bone marrow-derived cells [9-11], chorionic villi-derived cells [12], umbilical cord-derived cells [13,14] and dermal fibroblasts [15]. In particular, vascular myofibroblasts and endothelial cells (ECs) have been used for the fabrication of TEHV. After *in vitro* expansion of these cells to high numbers, myofibroblasts are seeded on fully degradable scaffold materials – either synthetic or natural – in its particular design. Ideally, scaffold materials must be biocompatible, supporting cellular ingrowth and interaction for the formation of a continuous tissue layer, and biodegradable, allowing for cellular expansion and matrix formation while the extrinsic material is gradually

degraded. Seeded scaffolds are firstly pre-incubated under static conditions before they are placed into a bioreactor system for mechanical conditioning through pulsatile flow and pressure gradients. These physiological conditions are responsible for the production of ECM from the seeded cells and therefore ultimately enhance neotissue formation *in vitro*. Finally the constructs are seeded with ECs to prevent thrombogenicity and resemble a native-like structure with a confluent luminal EC layer. At this point the constructs are ready for implantation. This technology has been investigated by several independent studies. Its principle feasibility has been demonstrated for the first time in 1995 with an *in vitro* engineered single pulmonary leaflet implanted into a lamb model [16]. Since then, the creation of a complete trileaflet TEHV based on synthetic scaffold material has shown to be feasible [17,18], with *in vivo* functionality up to 120 days [19] and the ability of *in vivo* growth and remodeling [20]. Significant increase in diameter and length demonstrated the ability of tissue-engineered constructs to grow [20]. Besides the use of vascular derived cells, several different stem cells have been investigated for their use in tissue engineering approaches. In particular, mesenchymal stem cells (MSCs) have shown to be an attractive alternative cell source due to their unique characteristics including I) multilineage differentiation potential, II) extensive *in vitro* proliferation, III) privileged immunological characteristics, and IV) paracrine mechanisms inducing host cell recruitment. In direct comparison to vascular derived cells there is no need to sacrifice intact vascular tissue. MSCs are easily accessible via low risk procedures in a wide variety of tissues, including tissues of fetal origin. This makes them suitable for pediatric *in vitro* heart valve tissue engineering that aims at the fabrication of an autologous, growing heart valve for the repair of congenital malformations prior to birth [21]. Besides the use of the most frequent synthetic biomaterials including poly(glycolic acid) (PGA), poly(lactic acid) (PLA), poly(ε-caprolactone) (PCL) and poly(4-hydroxybutyrate) (P4HB), also natural biomaterials such as collagen and fibrin have been widely used in TE applications. Fibrin-based heart valves seeded with ovine carotid artery-derived cells in an ovine model showed remarkable tissue remodeling [22,23]. Even augmented collagen production and enhanced retention of glycoaminoglycans within the developing ECM were detected by the use of fibrin in TEHV [24]. Recently, fibrin-based heart valve with a tubular leaflet design have been reported as an alternative to the conventional design of TEHV [25], including their principal feasibility for minimally invasive implantation techniques using self-expandable nitinol stents [26].

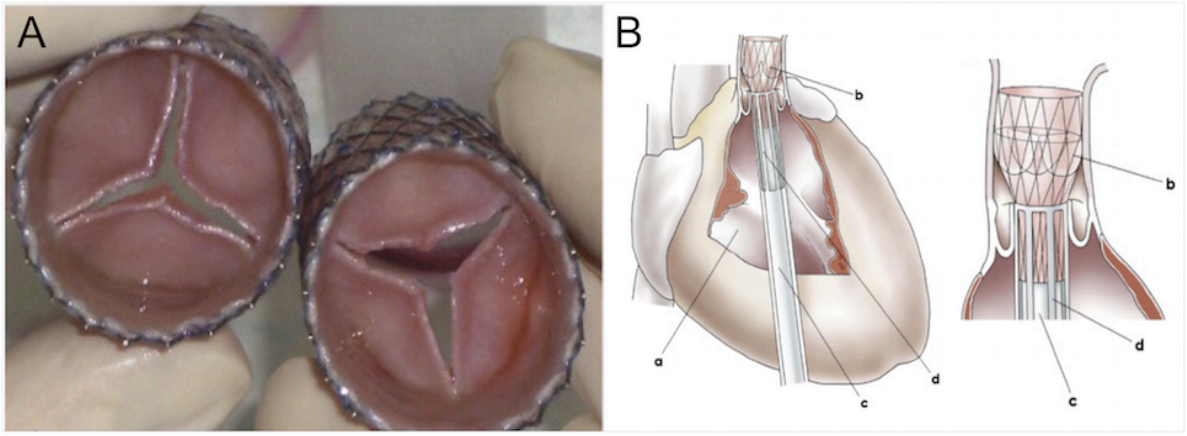

Figure 2: *In vitro* tissue engineered heart valves. (A) Distal view of a TEHV based on vascular-derived cells. (B) The crimped TEHV, integrated into a nitinol stent *(b)*, is loaded into the delivery system and inserted transapically into the right ventricle *(a)*. Deployment into the pulmonary position is conducted by slowly advancing the inner pusher *(c)* into the sheath system *(d)*. *Adapted and reprinted from Schmidt et al., 2010.*

However as the process of *in vitro* tissue engineering is logistically complex and highly time consuming, the establishment of new strategies where heart valves could be provided with unlimited supply at every required time point have been initiated. In this regard, the removal of cellular components by combinations of detergents and biological agents results in cell-derived starter matrices composed of ECM and proteins. Minimal criteria for effective decellularization consist of I) <50 ng dsDNA/mg ECM (dry weight), II) <200 bp DNA fragment length, and III) the lack of nuclear material in histological sections (e.g H&E and DAPI) [27].These homologous decellularized starter matrices are subsequently implanted for the *in situ* host cell repopulation. The decellularization process counteracts acute rejection of the implant by reducing the immune response. The use of allogeneic and xenogenic decellularized heart valves has been reported with long term animal models [28-30] and commercially available heart valve substitutes, including the allograft Cryolife's SynerGraft ® or xenografts AutoTissue GmbH Matrix P plus N™, with highly variable efficacy and outcomes. These initial investigations have led to the combination of *in vitro* tissue engineering strategies with decellularization techniques. Such decellularized TEHV (dTEHV) have shown principal feasibility in different animal models including non-human primate [31] and ovine models [15,32,33], either using synthetic PGA/P4HB [31,33] or natural fibrin gels in a tubular design [15,32]. Interestingly dTEHV have shown to exhibit reduced risk of insufficiency through leaflet retraction, cellular repopulation and matrix remodeling. Nevertheless, further enhancement/guidance of the leaflet recellularization seems crucial to prevent adverse remodeling and provide adequate long-term functionality of the constructs (see paragraph 2.2).

1.1.2.2 *IN SITU* HEART VALVE TISSUE ENGINEERING – CURRENT STATUS

In situ tissue engineering holds great promise due to the simplified fabrication protocols and reduced immunogenicity. As scaffolds are directly implanted without any prior *in vitro* incubation, this involves benefits such as no extensive *in vitro* cell expansion and manipulation as well as no conditioning of the constructs in a bioreactor requiring complex infrastructure and logistics (also involving time consuming regulatory approvals). The principal strategy of in situ tissue engineering aims at implantation of a cell-seeded 'starter matrix' that triggers autologous host cell recruitment with subsequent vascular remodeling/tissue formation *in vivo*.

In 1999, the *in situ* tissue engineering approach has been used for a first in-man trial for tissue engineered grafts, where human cells harvested from the peripheral vein were directly seeded on synthetic PCL reinforced with woven PGA and implanted successfully [34]. In 2011, clinical trials for tissue engineered vascular grafts have been initiated in the U.S. [35] using the *in situ* tissue engineering approach. This milestone in the field of cardiovascular tissue engineering raised great hope for the extrapolation of this concept to the more complex field of heart valve tissue engineering. At the same time, this procedure was introduced to the field of heart valve *in situ* tissue engineering. Its principal feasibility has been shown in a non-human primate model [34,36] as well as in the adult [37,38] and fetal [39] sheep model. In particular, scaffolds pre-seeded with autologous bone marrow mononuclear cells (BMMCs) have shown to enhance *in situ* remodeling. A higher cellularity indicative for an early cellular infiltration in the acute phase, followed by enhanced layered, endothelialized tissue formation on chronic survival have been reported using the bone marrow-derived mononuclear cell approach [36]. Similar results have been obtained in first investigations of the high-pressure system (aortic valve position) with acute and chronic survival [37,38].

As cell harvest and delivery can be performed within the same intervention using the *in situ* tissue engineering strategy, the combination with novel minimally invasive transcatheter-based implantation technologies could provide the opportunity of single-step minimally invasive procedures. In this regard, in a first large-scale ovine animal model, trileaflet heart valves have successfully been implanted using minimally invasive transapical procedures [40]. Furthermore, the prenatal minimally invasive implantation of autologous amniotic fluid stem cell-based TEHV in the ovine fetal model using an in-utero closed-heart hybrid single-step intervention has shown to be feasible [39]. This was performed in order to mimic the prenatal implantation of heart valves in fetuses with congenital heart valve malformations routinely detected by ultrasound examinations.

These results also uniquely exemplified that further characterization of the exact host remodeling cascade initiated by seeded BMMCs needs to be defined to guide *in situ* remodeling / tissue formation and to finally enable a clinical translation of the technology. Initially it was believed that

the seeded cells directly contribute to the formation of tissue [41]. However, recent studies have measured a rapid loss of the cells after implantation as the scaffold became repopulated by host-derived cells [42,43]. No integration of seeded cells into the scaffold could be detected, pointing towards the fact that the seeded cells do not directly contribute to the cellular infiltration and subsequent tissue formation. Nevertheless, seeded cells have shown to release paracrine factors initiating a cascade of tissue remodeling defined by an early monocyte/macrophage attraction (inflammation), followed by the recruitment of ECs and smooth muscle cells (SMCs) and finally leading to tissue formation *in vivo* [44,45]. The seeded cells therefore seem to create a microenvironment of cytokines and growth factors enhancing the intrinsic remodeling capacity of the body, in particular a healing response with a rapid influx of inflammatory cells. Using a novel rat model, where cellular ingrowth from the adjacent tissue is inhibited, the *in situ* regenerative potential of circulatory cells could be attributed to peripheral immune cells [46]. Infiltrating monocytes support this remodeling cascade by the additional release of multiple pro-angiogenic and immunomodulatory factors such as monocyte chemoattractant protein-1 (MCP-1), interleukin 6 (IL-6) and vascular endothelial growth factor (VEGF). Interestingly, a similar host cell response has been described when comparing unseeded scaffolds releasing MCP-1 with those seeded with BMMCs [45]. MCP-1 is suggested to burst/guide circulating host cells from the bloodstream for tissue formation, regeneration and angiogenesis [45-48]. Besides BMNCs, other cell sources have been investigated on their pro-angiogenic secretome for the use in TE applications, including MSCs [49], with first promising results. This implies that the cells could be replaced completely in the future. Fast degrading cell-free scaffolds by itself [50] or integrated with a drug delivery system releasing a specific composition and concentration of cytokines [51] might be a 'ready to use' solution for future tissue engineering approaches. Taken in mind that effective host remodeling is required for the success of any medical implant, further investigations will need to focus on the exact mechanical, structural and temporal window required.

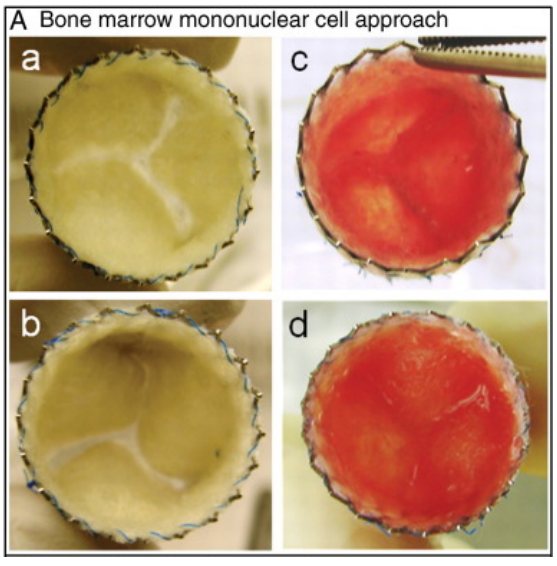

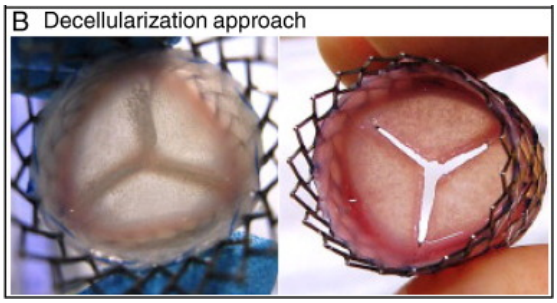

Figure 3: *In situ* tissue engineered heart valves. (A) Bone marrow-derived TEHV. Isolated bone marrow mononuclear cells were seeded on stented polyglycolic acid scaffold matrices *(a,b)* using fibrin as a cell carrier *(c,d)*. (B) Macroscopic view of a decellularized TEHV for implantation in a non-human primate model. *Adapted and reprinted from Weber et al., 2011 and 2013.*

1.1.2.3 ALTERNATIVE AND ADJUNCTIVE APPROACHES FOR HEART VALVE TISSUE ENGINEERING

Three-dimensional (3D) printing represents a rapid manufacturing technique that allows the construction of a fully customized TEHV with the patient's specific anatomy. Shortly, a 3D scan of the heart valve is acquired via X-ray or MRI, converted into a stereolithography file for the 3D printer and subsequently printed to generate either a cell-free or cell-encapsulated biological heart valve. In this regard, the group of Butcher has demonstrated that 3D hydrogel printing can fabricate anatomical heterogeneous valve conduits within 45min with accuracy up to 93% [52]. To better mimic the distinct mechanical properties between root and leaflets, different types of photocrosslinkable hydrogels were used accordingly [52]. The fabricated heart valve showed anatomically specific features, including the coronary ostium and sinuses [52]. By crosslinking different striped of PEG hydrogels, varying in stripe width and spacing, the anisotropic degree between the circumferential and radial orientation of a native valve leaflet could be mimic [53]. Furthermore, 3D printing allows to directly engineer heart valves with the desired cell types to promote *in situ* remodeling and deposition of ECM within the construct [54-56]. In particular, human aortic valvular interstitial cells (VICs) encapsulated within bioprint heart valves maintained cellular viability and promoted deposition of collagen and glycosaminoglycans [57]. Also the adhesion behavior, morphology, protein secretion and activation state of encapsulated VICs was modulated by specific bioactive peptides incorporated into the polymer networks [53].

Not only 3D printing but also electrospinning has raised great attention over the last years due to its simplified and fast manufacturing process. Electrospinning uses a high-voltage electrostatic field to generate fine fibers (micro to nano scale) through the ejection of the conductive polymer from a needle. Electrospun poly-(glycerol sebacate):poly(caprolactone) (PGS: PCL) scaffolds have shown to resemble the ECM of native heart valve leaflets and their mechanical properties [58,59]. While the PGS component of these hybrid polyester scaffolds accelerates the degradation rate of the scaffold, the seeded VICs remodel and deposit new ECM to consequently maintain the mechanical properties of the leaflet [60]. Native-like leaflet behaviour has also been described with electrospun PEGdma-PLA scaffolds seeded with VICs/ECs under physiological conditions in a bioreactor [61]. Besides electrospun scaffolds composed of poly(ester urethane)ureas (PEUU) have also the ability to mimic heart valve anisotrophic mechanical properties [62,63]. Besides, adjunctive approaches where multiple techniques are combined have been initiated for next generation TEHV. For instance, fibroblast cell sheets have been produced using the self-assembly method and subsequently assembled and molded to generate a stented TEHV [64,65]. Furthermore the combination of hydrogels with electrospinning might integrate the advantages of both technologies and improve the mechanical properties, scaffold composition, material strength and cellular compatibility of future TEHV [66,67].

1.1.3 BASIC PRINCIPLE OF VENOUS VALVE TISSUE ENGINEERING

In comparison to the field of heart valve tissue engineering only few attempts have been conducted in order to produce a tissue engineered venous valve (TEVV) for the treatment of deep venous valve insufficiency. So far only few clinical applications have been initiated for venous valves with either cryopreserved allografts [68] or glutaraldehyde-preserved xenografts [4]. In spite of initial good valvular performance, cryovalve insertion has been associated with high morbidity and high occlusion rates [68]. In a long-term follow-up, also the xenogenic glutaraldehyde-fixed valves resulted in valve incompetence and/or valvular stenosis related with excessive neo-intimal hyperplesia and fibrotic transformation [4]. Besides also surface thrombogenicity mainly owing to the low pressure and flow environment involving static flow phases in the venous circulation branch has been a major issue in valve implants. In summary, no durable and thrombus-resistant venous valvular replacements have been introduced to routine clinical use so far. A tissue engineered venous valve solution could overcome these limitations and mainly allow for autologous thromboresistant (endothelialized) implants. In a first experimental *in vitro* trial, tri- and bicuspid TEVVs have been generated based on the *in vitro* tissue engineering approach [69]. TEVVs were engineered from autologous bone marrow-derived MSCs and subsequently endothelialized showing layered tissue formation analogous to native valvular tissues [69]. The feasibility of using the tissue engineering technique for the generation of future TEVVs for the treatment of CVI has been demonstrated as part of this first study. However, future *in vivo* studies seem mandatory in order to evaluate their functionality in physiological conditions and their long-term durability.

1.1.4 LIMITATIONS AND FUTURE PERSPECTIVES

Even if still limited to the experimental phase, heart and venous valve tissue engineering has shown to be a potential future alternative therapeutic option for the replacement of diseased valves. Taking in consideration the demographic development, the prevalence of heart and venous valve disease will remain to be on the rise as the global population increases in age. Besides there is still no ideal therapy for congenital disease as the currently available prostheses lack the potential of growth. Since the introduction of vascular tissue engineering technologies, significant improvements have been made. First clinical trials on tissue-engineered vascular grafts have been initiated, the transition from animal models to the clinical reality on a broader scale seems within our grasp.

Nevertheless, several questions have to be addressed before a clinical application of tissue engineering will be feasible. For the *in vitro* tissue engineering approach the most favorable cell source needs to be defined. Therefore an exact characterization of the cells is indispensable, taking their proliferation capacity and cell survival in account. The impact of the ex vivo expansion on the

cells has to be defined, given that their ex vivo manipulation might result in adverse biochemical, genomic and immunological characteristics. In addition, xenogenic factors, such as fetal calf serum within the proliferation medium, need to be replaced for a safe clinical application. For the design of the valves, in all tissue engineering approaches, further adaptations will have to be considered in order to minimize radial shortening of the leaflets and central valvular regurgitation. In this regard TEHV need to better resemble the complex geometry of native heart valves, which includes sinuses, ostia, individual layers of valve leaflets (ventricularis, fibrosa and spongiosa) and a heterogeneous cellular composition [70]. Another important aspect concerns the scaffold material. Exact definition of degradation rates, mechanical properties, thrombogenicity and surface interaction with cells (cellular adhesion and ingrowth) need to be specified. Ultimately, cellular ECM production needs to be exactly timed with degradation of the actual scaffold to maintain structural integrity and counteract chronic inflammation, which might result in fibrosis and inappropriate functional behavior of the valve. This chronic inflammation is characterized by an accumulation of macrophages in the attempt to phagocytize the foreign biomaterial. Interestingly, the balance between M1 and M2 macrophages has shown to influence the remodeling capacity following implantation. In this regard several groups have established composite scaffolds for the controlled release of active biomolecules to influence macrophage phenotype. As to the *in situ* tissue engineering approach particular concerns have been raised given the highly heterogeneous *in vivo* remodeling responses among different individuals. This implies the definition of clinical guidelines for the use of tissue engineering technologies, where exact inclusion and exclusion criteria are of central importance. Moreover it requires an improved understanding of the cellular cascades evident throughout the *in vivo* remodeling phase. Summarized, improved outcomes for valve tissue engineering will require a systemic understanding of the multiple interacting factors to allow a safe clinical translation of such technologies in the future [70,71].

1.1.5 REFERENCES

1 Go, A. S. *et al.* Executive summary: heart disease and stroke statistics--2014 update: a report from the American Heart Association. *Circulation* **129**, 399-410, doi:10.1161/01.cir.0000442015.53336.12 (2014).

2 Yacoub, M. H. & Takkenberg, J. J. Will heart valve tissue engineering change the world? *Nat Clin Pract Cardiovasc Med* **2**, 60-61, doi:10.1038/ncpcardio0112 (2005).

3 Eberhardt, R. T. & Raffetto, J. D. Chronic venous insufficiency. *Circulation* **130**, 333-346, doi:10.1161/CIRCULATIONAHA.113.006898 (2014).

4 Zervides, C. & Giannoukas, A. D. Historical overview of venous valve prostheses for the treatment of deep venous valve insufficiency. *J Endovasc Ther* **19**, 281-290, doi:10.1583/11-3594MR.1 (2012).

5 Parvin Nejad, S., Blaser, M. C., Santerre, J. P., Caldarone, C. A. & Simmons, C. A. Biomechanical conditioning of tissue engineered heart valves: Too much of a good thing? *Adv Drug Deliv Rev* **96**, 161-175, doi:10.1016/j.addr.2015.11.003 (2016).

6 Colazzo, F. *et al.* Extracellular matrix production by adipose-derived stem cells: implications for heart valve tissue engineering. *Biomaterials* **32**, 119-127, doi:10.1016/j.biomaterials.2010.09.003 (2011).

7 Schmidt, D. *et al.* Prenatally fabricated autologous human living heart valves based on amniotic fluid derived progenitor cells as single cell source. *Circulation* **116**, I64-70, doi:10.1161/CIRCULATIONAHA.106.681494 (2007).

8 Schmidt, D. *et al.* Cryopreserved amniotic fluid-derived cells: a lifelong autologous fetal stem cell source for heart valve tissue engineering. *J Heart Valve Dis* **17**, 446-455; discussion 455 (2008).

9 Hoerstrup, S. P. *et al.* Tissue engineering of functional trileaflet heart valves from human marrow stromal cells. *Circulation* **106**, I143-150 (2002).

10 Sutherland, F. W. *et al.* From stem cells to viable autologous semilunar heart valve. *Circulation* **111**, 2783-2791, doi:10.1161/CIRCULATIONAHA.104.498378 (2005).

11 Gottlieb, D. *et al.* In vivo monitoring of function of autologous engineered pulmonary valve. *J Thorac Cardiovasc Surg* **139**, 723-731, doi:10.1016/j.jtcvs.2009.11.006 (2010).

12 Schmidt, D. *et al.* Living autologous heart valves engineered from human prenatally harvested progenitors. *Circulation* **114**, I125-131, doi:10.1161/CIRCULATIONAHA.105.001040 (2006).

13 Schmidt, D. *et al.* Engineering of biologically active living heart valve leaflets using human umbilical cord-derived progenitor cells. *Tissue Eng* **12**, 3223-3232, doi:10.1089/ten.2006.12.3223 (2006).

14 Sodian, R. *et al.* Tissue engineering of autologous human heart valves using cryopreserved vascular umbilical cord cells. *Ann Thorac Surg* **81**, 2207-2216, doi:10.1016/j.athoracsur.2005.12.073 (2006).

15 Syedain, Z. *et al.* 6-month aortic valve implantation of an off-the-shelf tissue-engineered valve in sheep. *Biomaterials* **73**, 175-184, doi:10.1016/j.biomaterials.2015.09.016 (2015).

16 Shinoka, T. *et al.* Tissue engineering heart valves: valve leaflet replacement study in a lamb model. *Ann Thorac Surg* **60**, S513-516 (1995).

17 Hoerstrup, S. P. *et al.* Functional living trileaflet heart valves grown in vitro. *Circulation* **102**, III44-49 (2000).

18 Sodian, R. *et al.* Tissue engineering of heart valves: in vitro experiences. *Ann Thorac Surg* **70**, 140-144 (2000).

19 Sodian, R. *et al.* Early in vivo experience with tissue-engineered trileaflet heart valves. *Circulation* **102**, III22-29 (2000).

20 Hoerstrup, S. P. *et al.* Functional growth in tissue-engineered living, vascular grafts: follow-up at 100 weeks in a large animal model. *Circulation* **114**, I159-166, doi:10.1161/CIRCULATIONAHA.105.001172 (2006).

21 Weber, B., Zeisberger, S. M. & Hoerstrup, S. P. Prenatally harvested cells for cardiovascular tissue engineering: fabrication of autologous implants prior to birth. *Placenta* **32 Suppl 4**, S316-319, doi:10.1016/j.placenta.2011.04.001 (2011).

22 Flanagan, T. C. *et al.* The in vitro development of autologous fibrin-based tissue-engineered heart valves through optimised dynamic conditioning. *Biomaterials* **28**, 3388-3397, doi:10.1016/j.biomaterials.2007.04.012 (2007).

23 Flanagan, T. C. *et al.* In vivo remodeling and structural characterization of fibrin-based tissue-engineered heart valves in the adult sheep model. *Tissue Eng Part A* **15**, 2965-2976, doi:10.1089/ten.TEA.2009.0018 (2009).

24 Alfonso, A. R. *et al.* Glycosaminoglycan entrapment by fibrin in engineered heart valve tissues. *Acta Biomater* **9**, 8149-8157, doi:10.1016/j.actbio.2013.06.009 (2013).

25 Weber, M. *et al.* Tissue-engineered fibrin-based heart valve with a tubular leaflet design. *Tissue Eng Part C Methods* **20**, 265-275, doi:10.1089/ten.TEC.2013.0258 (2014).

26 Moreira, R. *et al.* Tissue-engineered heart valve with a tubular leaflet design for minimally invasive transcatheter implantation. *Tissue Eng Part C Methods* **21**, 530-540, doi:10.1089/ten.TEC.2014.0214 (2015).

27 Crapo, P. M., Gilbert, T. W. & Badylak, S. F. An overview of tissue and whole organ decellularization processes. *Biomaterials* **32**, 3233-3243, doi:10.1016/j.biomaterials.2011.01.057 (2011).

28 Iop, L. *et al.* Decellularized allogeneic heart valves demonstrate self-regeneration potential after a long-term preclinical evaluation. *PLoS One* **9**, e99593, doi:10.1371/journal.pone.0099593 (2014).

29 Theodoridis, K. *et al.* Successful matrix guided tissue regeneration of decellularized pulmonary heart valve allografts in elderly sheep. *Biomaterials* **52**, 221-228, doi:10.1016/j.biomaterials.2015.02.023 (2015).

30 Gallo, M. *et al.* Physiological performance of a detergent decellularized heart valve implanted for 15 months in Vietnamese pigs: surgical procedure, follow-up, and explant inspection. *Artif Organs* **36**, E138-150, doi:10.1111/j.1525-1594.2012.01447.x (2012).

31 Weber, B. *et al.* Off-the-shelf human decellularized tissue-engineered heart valves in a non-human primate model. *Biomaterials* **34**, 7269-7280, doi:10.1016/j.biomaterials.2013.04.059 (2013).

32 Syedain, Z. H., Meier, L. A., Lahti, M. T., Johnson, S. L. & Tranquillo, R. T. Implantation of completely biological engineered grafts following decellularization into the sheep femoral artery. *Tissue Eng Part A* **20**, 1726-1734, doi:10.1089/ten.TEA.2013.0550 (2014).

33 Driessen-Mol, A. *et al.* Transcatheter implantation of homologous "off-the-shelf" tissue-engineered heart valves with self-repair capacity: long-term functionality and rapid in vivo remodeling in sheep. *J Am Coll Cardiol* **63**, 1320-1329, doi:10.1016/j.jacc.2013.09.082 (2014).

34 Shin'oka, T., Imai, Y. & Ikada, Y. Transplantation of a tissue-engineered pulmonary artery. *N Engl J Med* **344**, 532-533, doi:10.1056/NEJM200102153440717 (2001).

35 Vogel, G. Tissue engineering. Mending the youngest hearts. *Science* **333**, 1088-1089, doi:10.1126/science.333.6046.1088 (2011).

36 Weber, B. *et al.* Injectable living marrow stromal cell-based autologous tissue engineered heart valves: first experiences with a one-step intervention in primates. *Eur Heart J* **32**, 2830-2840, doi:10.1093/eurheartj/ehr059 (2011).

37 Emmert, M. Y. *et al.* Transapical aortic implantation of autologous marrow stromal cell-based tissue-engineered heart valves: first experiences in the systemic circulation. *JACC Cardiovasc Interv* **4**, 822-823, doi:10.1016/j.jcin.2011.02.020 (2011).

38 Emmert, M. Y. *et al.* Stem cell-based transcatheter aortic valve implantation: first experiences in a pre-clinical model. *JACC Cardiovasc Interv* **5**, 874-883, doi:10.1016/j.jcin.2012.04.010 (2012).

39 Weber, B. *et al.* Prenatally engineered autologous amniotic fluid stem cell-based heart valves in the fetal circulation. *Biomaterials* **33**, 4031-4043, doi:10.1016/j.biomaterials.2011.11.087 (2012).

40 Schmidt, D. *et al.* Minimally-invasive implantation of living tissue engineered heart valves: a comprehensive approach from autologous vascular cells to stem cells. *J Am Coll Cardiol* **56**, 510-520, doi:10.1016/j.jacc.2010.04.024 (2010).

41 Matsumura, G., Miyagawa-Tomita, S., Shin'oka, T., Ikada, Y. & Kurosawa, H. First evidence that bone marrow cells contribute to the construction of tissue-engineered vascular autografts in vivo. *Circulation* **108**, 1729-1734, doi:10.1161/01.CIR.0000092165.32213.61 (2003).

42 Harrington, J. K. *et al.* Determining the fate of seeded cells in venous tissue-engineered vascular grafts using serial MRI. *FASEB J* **25**, 4150-4161, doi:10.1096/fj.11-185140 (2011).

43 Hibino, N. *et al.* Tissue-engineered vascular grafts form neovessels that arise from regeneration of the adjacent blood vessel. *FASEB J* **25**, 2731-2739, doi:10.1096/fj.11-182246 (2011).

44 Hibino, N. *et al.* A critical role for macrophages in neovessel formation and the development of stenosis in tissue-engineered vascular grafts. *FASEB J* **25**, 4253-4263, doi:10.1096/fj.11-186585 (2011).

45 Roh, J. D. *et al.* Tissue-engineered vascular grafts transform into mature blood vessels via an inflammation-mediated process of vascular remodeling. *Proc Natl Acad Sci U S A* **107**, 4669-4674, doi:10.1073/pnas.0911465107 (2010).

46 Talacua, H. *et al.* In Situ Tissue Engineering of Functional Small-Diameter Blood Vessels by Host Circulating Cells Only. *Tissue Eng Part A* **21**, 2583-2594, doi:10.1089/ten.TEA.2015.0066 (2015).

47 Ballotta, V., Smits, A. I., Driessen-Mol, A., Bouten, C. V. & Baaijens, F. P. Synergistic protein secretion by mesenchymal stromal cells seeded in 3D scaffolds and circulating leukocytes in physiological flow. *Biomaterials* **35**, 9100-9113, doi:10.1016/j.biomaterials.2014.07.042 (2014).

48 Capoccia, B. J., Gregory, A. D. & Link, D. C. Recruitment of the inflammatory subset of monocytes to sites of ischemia induces angiogenesis in a monocyte chemoattractant protein-1-dependent fashion. *J Leukoc Biol* **84**, 760-768, doi:10.1189/jlb.1107756 (2008).

49 Smits, A. I., Ballotta, V., Driessen-Mol, A., Bouten, C. V. & Baaijens, F. P. Shear flow affects selective monocyte recruitment into MCP-1-loaded scaffolds. *J Cell Mol Med* **18**, 2176-2188, doi:10.1111/jcmm.12330 (2014).

50 Wu, W., Allen, R. A. & Wang, Y. Fast-degrading elastomer enables rapid remodeling of a cell-free synthetic graft into a neoartery. *Nat Med* **18**, 1148-1153, doi:10.1038/nm.2821 (2012).

51 Jana, S., Simari, R. D., Spoon, D. B. & Lerman, A. Drug delivery in aortic valve tissue engineering. *J Control Release* **196**, 307-323, doi:10.1016/j.jconrel.2014.10.009 (2014).

52 Hockaday, L. A. *et al.* Rapid 3D printing of anatomically accurate and mechanically heterogeneous aortic valve hydrogel scaffolds. *Biofabrication* **4**, 035005, doi:10.1088/1758-5082/4/3/035005 (2012).

53 Zhang, X. *et al.* Integrating valve-inspired design features into poly(ethylene glycol) hydrogel scaffolds for heart valve tissue engineering. *Acta Biomater* **14**, 11-21, doi:10.1016/j.actbio.2014.11.042 (2015).

54 Duan, B., Hockaday, L. A., Kapetanovic, E., Kang, K. H. & Butcher, J. T. Stiffness and adhesivity control aortic valve interstitial cell behavior within hyaluronic acid based hydrogels. *Acta Biomater* **9**, 7640-7650, doi:10.1016/j.actbio.2013.04.050 (2013).

55 Duan, B., Hockaday, L. A., Kang, K. H. & Butcher, J. T. 3D bioprinting of heterogeneous aortic valve conduits with alginate/gelatin hydrogels. *J Biomed Mater Res A* **101**, 1255-1264, doi:10.1002/jbm.a.34420 (2013).

56 Xu, T. *et al.* Complex heterogeneous tissue constructs containing multiple cell types prepared by inkjet printing technology. *Biomaterials* **34**, 130-139, doi:10.1016/j.biomaterials.2012.09.035 (2013).

57 Duan, B., Kapetanovic, E., Hockaday, L. A. & Butcher, J. T. Three-dimensional printed trileaflet valve conduits using biological hydrogels and human valve interstitial cells. *Acta Biomater* **10**, 1836-1846, doi:10.1016/j.actbio.2013.12.005 (2014).

58 Sant, S., Hwang, C. M., Lee, S. H. & Khademhosseini, A. Hybrid PGS-PCL microfibrous scaffolds with improved mechanical and biological properties. *J Tissue Eng Regen Med* **5**, 283-291, doi:10.1002/term.313 (2011).

59 Masoumi, N. *et al.* Electrospun PGS:PCL microfibers align human valvular interstitial cells and provide tunable scaffold anisotropy. *Adv Healthc Mater* **3**, 929-939, doi:10.1002/adhm.201300505 (2014).

60 Sant, S., Iyer, D., Gaharwar, A. K., Patel, A. & Khademhosseini, A. Effect of biodegradation and de novo matrix synthesis on the mechanical properties of valvular interstitial cell-seeded polyglycerol sebacate-polycaprolactone scaffolds. *Acta Biomater* **9**, 5963-5973, doi:10.1016/j.actbio.2012.11.014 (2013).

61 Hinderer, S. *et al.* Engineering of a bio-functionalized hybrid off-the-shelf heart valve. *Biomaterials* **35**, 2130-2139, doi:10.1016/j.biomaterials.2013.10.080 (2014).

62 Fan, R. *et al.* Optimal elastomeric scaffold leaflet shape for pulmonary heart valve leaflet replacement. *J Biomech* **46**, 662-669, doi:10.1016/j.jbiomech.2012.11.046 (2013).

63 Amoroso, N. J. *et al.* Microstructural manipulation of electrospun scaffolds for specific bending stiffness for heart valve tissue engineering. *Acta Biomater* **8**, 4268-4277, doi:10.1016/j.actbio.2012.08.002 (2012).

64 Dube, J. *et al.* Progress in developing a living human tissue-engineered tri-leaflet heart valve assembled from tissue produced by the self-assembly approach. *Acta Biomater* **10**, 3563-3570, doi:10.1016/j.actbio.2014.04.033 (2014).

65 Tremblay, C. *et al.* A new construction technique for tissue-engineered heart valves using the self-assembly method. *Tissue Eng Part C Methods* **20**, 905-915, doi:10.1089/ten.TEC.2013.0698 (2014).

66 Eslami, M. *et al.* Fiber-reinforced hydrogel scaffolds for heart valve tissue engineering. *J Biomater Appl* **29**, 399-410, doi:10.1177/0885328214530589 (2014).

67 Tseng, H. *et al.* Anisotropic poly(ethylene glycol)/polycaprolactone hydrogel-fiber composites for heart valve tissue engineering. *Tissue Eng Part A* **20**, 2634-2645, doi:10.1089/ten.TEA.2013.0397 (2014).

68 Neglen, P. & Raju, S. Venous reflux repair with cryopreserved vein valves. *J Vasc Surg* **37**, 552-557, doi:10.1067/mva.2003.93 (2003).

69 Weber, B. *et al.* Living-engineered valves for transcatheter venous valve repair. *Tissue Eng Part C Methods* **20**, 451-463, doi:10.1089/ten.TEC.2013.0187 (2014).

70 Cheung, D. Y., Duan, B. & Butcher, J. T. Current progress in tissue engineering of heart valves: multiscale problems, multiscale solutions. *Expert Opin Biol Ther* **15**, 1155-1172, doi:10.1517/14712598.2015.1051527 (2015).

71 Usprech, J., Chen, W. L. & Simmons, C. A. Heart valve regeneration: the need for systems approaches. *Wiley Interdiscip Rev Syst Biol Med* **8**, 169-182, doi:10.1002/wsbm.1329 (2016).

CHAPTER 1.2

Macrophage cellular crosstalk in the response to biomaterial implantation

Vera Malheiro[1], Marjan Enayati[2], **Debora Kehl**[3], Helga Bergmeister[2], Benedikt Weber[3], Katharina Maniura-Weber[1]

[1] Biointerfaces, EMPA, Swiss Federal Laboratories for Materials Science and Technology, St. Gallen, Switzerland
[2] Department of Biomedical Research, Medical University of Vienna, Vienna, Austria
[3] Institute for Regenerative Medicine (IREM), Center for Therapy Development and Good Manufacturing Practice, University of Zurich, Zurich, Switzerland

Abstract

The development of novel biomaterials for regenerative medicine applications requires improving our understanding of the underlying biological processes that occur after implantation. Identifying the multitude of biological interactions that take place during the different phases of the tissue response to a biomaterial is essential. The healing following implantation is a complex process in which effective tissue clearance, vascularization and matrix reconstruction are essential for achieving complete biomaterial integration. These dynamic events depend on the crosstalk between macrophages and other cells such as fibroblasts, endothelial cells and mesenchymal stem cells. In this review, we summarize the current knowledge of the interactions between macrophages and healing-associated cells. The impact of this crosstalk between cells on cell-material interaction, tissue regeneration and ultimate biomaterial integration are highlighted. The use of *in vitro* macrophage co-cultures and their potential role as a predictive tool/model for assessing host-biomaterial interactions and the functionality of tissue-engineered constructs are presented. Further, the benefits and challenges of such models are critically discussed.

Personal contribution:

Definition of article structure and content with collaborating partners, giving scientific input, adding sections/references and reviewing the complete manuscript during any stage of preparation and revision process (R1 and R2). Writing of chapters: 1.2.5 Endothelial cells and their role in healing; *1.2.5.1* M*Φ-EC crosstalk; 1.2.5.2* M*Φ-EC interaction with biomaterials*. Partial contribution to other chapters.

eCell and Materials (under revision 2016)

1.2.1 INTRODUCTION

The emerging field of biomaterials research has changed drastically over the last several years. Until recently, it was believed that a biomaterial should be inert and not interfere with body homeostasis. However, most contemporary efforts focus on developing bioactive biomaterial-based systems that promote and guide specific biological responses, such as tissue regeneration, remodeling or vascularization. The development of such biomaterials requires an in-depth understanding of the underlying biological processes that occur following biomaterial implantation, down to the cellular level. In this regard, *in vitro* models play a key role in biomaterials research by allowing the systematic study of the interactions of different cell types with a candidate biomaterial. However, while *in vitro* models provide excellent means to learn about principle molecular and cellular interactions, they cannot not accurately mimic the complexity of the native inflammatory response. The challenges in these studies include selection of the appropriate cell types, appropriate analytical tools as well as cultivation methodologies for the *in vitro* evaluation and development of novel candidate biomaterials.

Macrophages (MΦs) are one of the main cell types involved in the initial host-biomaterial interaction after implantation [1]. This interaction starts with the direct response of MΦs to the implant, followed by the recruitment of other cell types such as fibroblasts, endothelial cells (ECs) and mesenchymal stem cells (MSCs). Crosstalk among all of these cell types in living tissues will determine the future integration or rejection of the implanted biomaterial and therefore the development of predictive *in vitro* models to simulate and understand this response is highly relevant.

The aim of this review is to critically discuss the interactions between MΦs and fibroblasts, ECs and MSCs in both *in vivo* and *in vitro* models. The benefits, limitations and challenges of the currently used MΦ co-culture *in vitro* models are also discussed.

It is well established that cues presented by biomaterials play a determining role in modulating the response of cells. The implantation of any type of construct or biomaterial for tissue engineering (TE) invariably damages the tissue and its vasculature at the site of implantation. This tissue injury, affects the local environment of the foreign material and triggers the initial response to the material, which can be amplified or also dramatically altered by the characteristics of the material itself. Subsequently, a cascade of events is initiated that can be broadly divided into four distinct, but overlapping phases which have been originally described by Anderson [1] as shown in Figure 1: I) hemostasis, II) inflammation, III) proliferation and IV) repair.

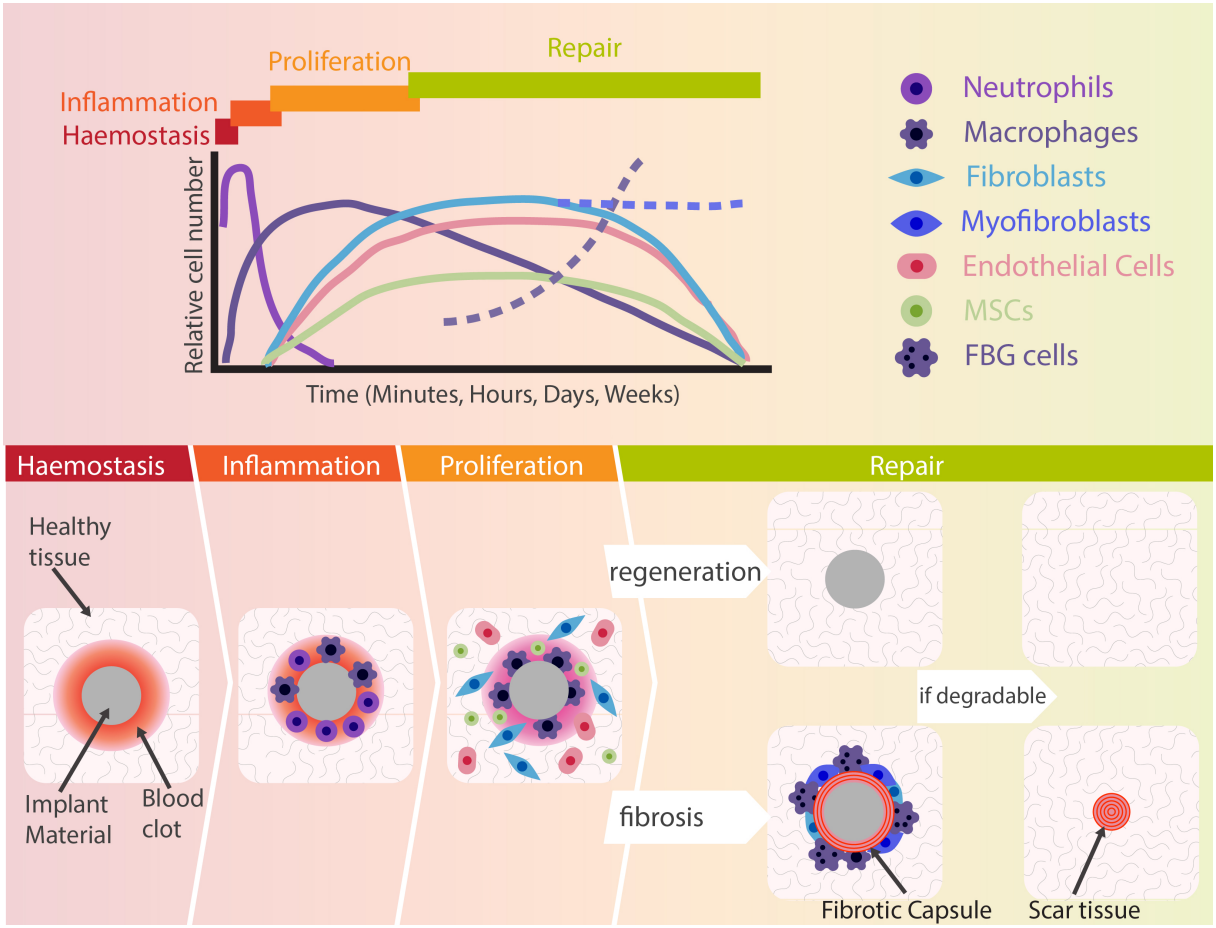

Figure 1. Graphic (top) and schematic (bottom) of the different healing stages and the respective cells involved in the foreign body response to a material. The intensity, time variables and repair mechanism (regeneration or fibrosis) developed depend on the extent of injury created during implantation and the size, shape, topography, and chemical, physical, and degradation properties of the implant material. Dashed lines in the graph represent situations leading to fibrosis, where an increasing and persistent number of myofibroblasts and foreign body giant (FBG) cells are typically found. Graph adapted from (Anderson, 1993).

Much progress has been made in understanding the interactions of somatic cells and stems cells with biomaterials [2], however, much less is known about the response of immune cells, especially macrophages, to biomaterial cues. Macrophages can either circulate in peripheral blood or reside in tissues; both types originate from different sources. It has been suggested that some tissue resident macrophages may arise *in utero* during embryological development [2,3]. Many examples have been reported in which tissue-specific factors steer very specific macrophage functions irrespective of their ontological origin, indicating a high degree of plasticity in the monocyte/macrophage system [4,5]. Organ-specific tissue-resident macrophages and circulating monocytes play essential roles in the mammalian response to injury in a number of organs such as liver, intestine, heart and skeletal muscle [5,6]. A recent review summarized the current knowledge on how dysregulated macrophage function impairs wound healing and contributes to the development of fibrosis in these tissues [5].

Bleeding at a wound site induces adhesion and degranulation of platelets and the rapid formation of a fibrin clot via various paths of activation of the blood coagulation cascade. This clot represents a

provisional matrix and is thought to constitute a major factor during the following inflammation phase [7]. Inflammatory cells initially populate this matrix: first neutrophils, and later, typically within 1–2 days after wounding, MΦs. During the subsequent proliferation phase, fibroblasts, MSCs, and ECs, together with other tissue-specific cell types, are recruited to the wound site. Under optimal conditions, these cells work in synchrony to regenerate the damaged tissue. However, the initial acute inflammation frequently develops into chronic inflammation in which activated MΦs accumulate at the implant surface in an attempt to phagocytize the foreign material. The persistent inflammatory state results in the fusion of the frustrated macrophages, giving rise to foreign body giant (FBG) cells [1]. Meanwhile, the fibroblasts continue to produce the extensive amounts of collagen that is often associated with their differentiation into the highly contractile myofibroblast phenotype [8]. Over time, this results in fibrotic encapsulation caused by the dense layer of collagenous connective tissue produced by the fibroblasts and, ultimately, the non-integration of the implant. It is thought that recruited monocytes, monocyte-derived macrophages and tissue-resident macrophages control cell number through cell proliferation [4]. It is unclear to what extend the presence of biomaterials interferes with the normal physiological process during healing. Recently, it was reported that FBG cells express both, markers classically described as inflammatory markers and markers associated with the healing state of macrophages [9]. This goes in line with recent studies that highlight that macrophages can present in a continuum of inflammatory/non-inflammatory stages, rather than in a clearly unidirectional state [10-14] (see also below section on macrophages).

TE strategies typically use degradable materials because the goal is for the material to degrade as neo-tissue formation proceeds. Ideally, this would result in the complete regeneration of the damaged tissue through regenerative mechanisms. However, scar tissue formation often occurs in real systems. The development of scar tissue can lead to interfacial problems because of the differences in the biomechanical properties between the healthy and the scar tissues. Furthermore, fibrotic encapsulation affects cell survival, the diffusion of bioactive molecules and the degradation rate of constructs for TE.

The type of implanted material influences the repair mechanisms initiated in the host. For example, biological degradable materials favor repair through regeneration. However, this is not always the case, and non-degradable synthetic materials do not always lead to severe fibrosis. Thus, the repair mechanism depends on a variety of both known and unknown factors. The manufacturing, macro-architecture and surface properties of the final implant can all alter the host response. For example, whereas decellularized extracellular matrix is one of the closest analogues to native tissue and is indeed in many ways an ideal biomaterial for regeneration, it can still elicit a severe foreign body response and the development of fibrosis [15] because of its immunogenicity or the manufacturing methodologies used (e.g., the use of crosslinking agents). Recent studies have reported that

crosslinking has an impact on the severity of the host response [16] which was reviewed by Aamodt and Grainger [17]. It has further been suggested that unnatural crosslinking leads to an increase of foreign body formation, probably due to the formation of difficult-to-break-down molecules [16].

In contrast, titanium implants applied directly in contact with bone often show impressive osseointegration without fibrosis or chronic inflammation [18]. However, osseointegration of biomaterials might be inflammation-triggered through an alternative pathway of host response involving neutrophils and prostaglandins [19].

Kzhyshkowska *et al.* even propose that the detailed understanding of the immune response from macrophages to biomaterials can help to develop personalized biomaterials through developing new materials and material coatings that allow, to some extend, immune engineering of a specific response [20]. A very recent study provides evidence that cytokine delivery systems might shift the early-stage macrophage response at the tissue-implant interface of a non-degradable material and suggests that modulation of the immune reaction at early stages of the host response [21]. This work demonstrated that the tuned release of IL-4 resulted in a reduced formation of fibrotic capsule surrounding the functional implant and that such immune engineering strategy may represent a feasible recipe for promoting biomaterial integration and success.

The detailed mechanisms determining the host response to a biomaterial following implantation have not been fully understood. Ultimately, this lack of information may lead to insufficient guidelines for the evaluation of new effective and safe biomaterials.

1.2.2 MACROPHAGES

Monocytes/macrophages (M/MΦ) are amongst the first responding cells after implantation of a biomaterial. They are attracted to the wound site by complement factors, transforming growth factor (TGF-β), platelet-derived growth factor (PDGF), platelet factor 4 (PF4), macrophage chemoattractant proteins 1-4 (MCP-1,2,3,4), RANTES, macrophage inflammatory protein 1a (MIP-1a) and MIP-1b [7,22-24]. Ubiquitous to most implantation sites, MΦs are responsible for the degree of the inflammatory response and tissue repair in the body. They are a terminally differentiated population of blood-circulating monocytes.

MΦs are monocyte-derived myeloid cells that develop from a common myeloid progenitor cell residing in the bone marrow; they are released into the blood stream upon maturation [11]. Circulating monocytes are generally non-proliferative, though some exceptions have been identified [25], with a short half-life of approximately 1–3 days. Here they are thought to provide a continuous source of MΦs in tissues by migrating across the endothelium and locally differentiating into functionally distinct MΦs (e.g. microglia cells in the brain, Kupffer cells in the liver and alveolar MΦs in the lung). While extravasation occurs as part of normal body homeostasis, their migration across the endothelium is enhanced in response to an inflammatory event. Recently, the role of tissue-resident macrophages in some organs has been highlighted in a review [4] and in this work it was emphasized that the relative contributions of tissue niche versus ontological origin to the regulation of macrophage function during steady state and healing/ inflammation will be of major interest for future studies.

Depending on the microenvironment encountered, MΦs may become activated and release proinflammatory factors and chemoattractants that recruit additional monocytes from the circulating blood, thus creating amplification loop of inflammation [11]. The MΦs recruited to the inflammatory site are a heterogeneous cell population with high plasticity, capable of acquiring distinct phenotypes. These phenotypes can be generally categorized into two major groups: I) classically activated, proinflammatory MΦs (M1-like) and II) alternatively activated immunomodulatory MΦs (M2-like) (Fig. 2).

The MΦ phenotype transition from M1-like to M2-like correlates with changes in the cytokine secretion profile of T cells, from type 1 (Th1) to type 2 (Th2). Indeed, the *in vitro* development of M1-like MΦs can be achieved by exposing naïve MΦs to interferon gamma (IFN-γ), the main Th1 cytokine, alone or in combination with lipopolysaccharide (LPS, endotoxin) or tumor necrosis factor alpha (TNFα), whereas M2-like MΦs are formed by exposure to interleukin-4 (IL-4), interleukin-13 (IL-13) or interleukin-10 (IL-10), which are typical Th2-type cytokines. M2-like MΦs encompass a range of well-recognized subtypes (M2a, M2b, and M2c), all of which have distinct inducers, markers and

functions. The inducers, markers and function of both, M1-like and M2-like MΦs, including the M2-subtypes, have been reviewed in detail elsewhere [13,26-28]. MΦs are capable of adjusting their cytokine release profile, metabolism and mobility in response to autologous and/or exogenous stimuli, allowing them to respond as needed in different stages of the healing or disease progression. For example, the binding of pathogen-associated molecular cues such as LPS to the cell membrane signals MΦs to the presence of invaders. This recognition of danger induces the activation of the hostile M1-like MΦ phenotype with the main function of stopping the threat. To do that, the cell employs mechanisms of pathogen clearance, such as increased release of inflammatory cytokines, reactive oxygen species and expression of complement-mediated phagocytic receptors, and prevents pathogen proliferation and growth by depleting iron from the extracellular matrix (ECM) by increasing their intracellular storage levels of ferritin. In contrast, in the absence of pathogens and presence of cytokines such as IL-4 or IL-13, MΦs can decrease inflammation and promote tissue regeneration. They release anti-inflammatory cytokines, iron, and endothelial and fibroblastic chemokines such as TGF-β and vascular endothelial growth factor (VEGF), all of which support cell proliferation, angiogenesis and matrix reconstruction.

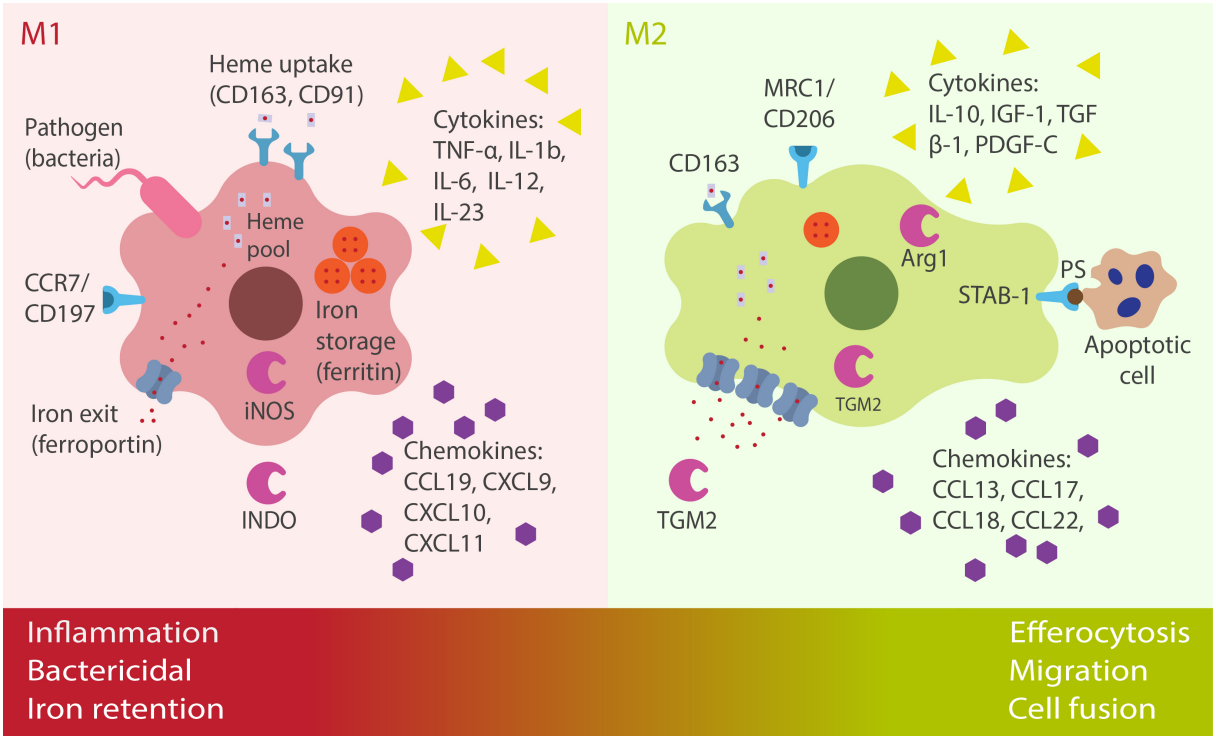

Figure 2. Schematic of the main specific markers and functions of M1 and M2 polarized macrophages. Note: Different sets of M2 markers are typical for different subsets of M2 macrophages. These markers are representative of human and murine species. Information retrieved from (Cairo *et al.*, 2011; Korns *et al.*, 2011; Mantovani *et al.*, 2004; Martinez *et al.*, 2006; Martinez *et al.*, 2009; Vogel *et al.*, 2014).

MΦs present dynamic and plastic phenotypes that continuously change with time and local microenvironmental signals [29-32]. Examination of the MΦ population at any given time point shows a mixture of MΦ phenotypes or MΦs in a state of transition that express marker subsets of both M1-like and M2-like phenotypes. In fact macrophages can present in a continuum of M1-like/M2-like stages [10-14].

Evidence suggests that the cell number ratio between M1-like and M2-like MΦs and with this the ratio of inflammatory/anti-inflammatory marker molecules significantly affect tissue remodeling following biomaterial implantation [11,33,34]. Cellular events such as inflammation, tissue clearance, cell recruitment and vascularization require an interplay between the different MΦ phenotypes. Because the behavior and recruitment of other cells from the surrounding tissue appear to be largely dependent on the environment created and sustained by the MΦs, a deeper understanding of the influence of MΦs on the behavior of the other cell types and on the host-biomaterial interaction is needed

1.2.3 MESENCHYMAL STEM CELLS AND THEIR ROLE IN HEALING

MSCs are a heterogeneous group of plastic adherent cells that exhibit self-renewal and multi-lineage differentiation capacities. They were first observed in the bone marrow by Friedenstein and colleagues in the 1970s [35]. Since then, MSCs have also been successfully isolated from alternative adult and fetal adnexal tissues. The commonly used definition for human MSCs described by the International Society for Cell Therapy [36] is based on their I) plastic adherence in standard culture conditions, II) *in vitro* tri-lineage differentiation potential into osteoblasts, adipocytes and chondrocytes and III) specific surface antigen expression positive for CD105, CD73 and CD90, but negative for CD45, CD34 and CD14; CD11b and CD79alpha; or CD19 and HLA-DR.

MSCs have been considered for a wide variety of clinical applications to promote healing, regeneration and remodeling of injured tissues by transplantation with or without a carrier for TE. On-going clinical trials are testing MSC treatments for autoimmune, cardiovascular, liver, graft-versus-host disease (GVHD) and neuronal diseases, as well as orthopedic injuries and cancer [37]. However, the underlying mechanisms involved in the functional restoration of diseased structures by MSCs have not yet been fully elucidated, largely because of the lack of a specific single marker that can be used to identify and trace them in the body. Alternative methods for studying MSC behavior *in vivo* involve the use of intravenously injected labeled cells. Although these methodologies involve certain technical challenges (reviewed in [38]), they have been successfully applied to demonstrate that MSCs are indeed actively recruited to sites of tissue injury where they contribute to an acceleration of the healing process [39,40]. In this regard, the release of anti-apoptotic and tropic factors by MSCs has been demonstrated to initiate cellular protection and repair through the recruitment of host cells. Furthermore, the role of MSCs in healing may be related to an immunomodulatory function (reviewed in [41]). Taken together, MSCs are considered to be a versatile cell source for regenerative medicine applications, either through direct administration/implantation as an element of a TE strategy or through their endogenous presence at wound sites.

1.2.3.1 MΦ-MSC CROSSTALK

Initially, interest in MSCs for clinical applications focused on their capability to replace damaged cells. However, that focus changed in 2004, when MSCs were considered for the treatment of acute GVHD because of their immunomodulatory potential [42]. The majority of the publications on the immunomodulatory function of MSCs that followed focused on their ability to inhibit T-cell proliferation. Conversely, in 2009, Nemeth *et al*. [43] demonstrated *in vivo* that MSC modulation following sepsis, a generalized and excessive inflammatory state, was not attributed to their role in T-cell inhibition, as demonstrated using mice genetically lacking mature T cells. Instead, they found

that depletion of M/MΦ eliminated the efficacy of MSC treatment on survival in the murine model. Furthermore, by combining *in vivo* and *in vitro* data, the authors showed that MSCs primed by the inflammatory environment increase their synthesis of prostaglandin E_2 (PGE_2), resulting in the induction of anti-inflammatory IL-10 production by MΦs. To test the mechanism of interaction, three different types of co-cultures were employed: I) direct culture in which MSCs and MΦs were seeded in a mixed monolayer allowing direct cell-cell physical contact; II) transwell cultures in which MSCs were seeded on the transwell membrane insert and MΦs were seeded on the well bottom, preventing direct cell contact; and III) conditioned medium (CM) co-culture experiments in which the culture media from the MSCs was mixed 1:1 into the MΦ culture media. Using these strategies, the authors were able to suggest that direct contact between the two cell types is necessary to stimulate IL-10 production. However, recent research has also reported MSC-mediated suppression of MΦ inflammation in transwell and CM experiments [44-46]. Taken together, while the exact signaling pathway between MSCs and M/MΦs has not yet been elucidated, their communication appears to be based on both direct contact and paracrine interactions.

Focusing on the paracrine mechanism, the effect of MSC-secreted factors on MΦs seems to be enabled by the release of PGE_2, in both murine and human MSCs, but the release of indoleamine 2,3-dioxygenase *in vitro* [47] and tumor necrosis factor-inducible gene 6 *in vitro* and *in vivo* [48] have also been implicated in the immunosuppressive effects of MSCs. Furthermore, the suppression and control of inflammation by MSCs is not only achieved by the release of selected cytokines, but also by their capacity to induce a shift in the macrophage phenotype from M1 towards M2 as reported by numerous papers in both direct and indirect cultures *in vitro* and *in vivo* [36,44-55]. However, it is important to understand that MSCs must be pre-exposed to a proinflammatory environment before becoming immunosuppressive [56], and thus depend on the immune cells themselves to exert their immunomodulatory functions.

MΦs are major contributors to the inflammatory microenvironment and, therefore, influence MSCs as much as they are influenced by MSCs. While the effects of MΦs on MSCs has not received the same attention as the reciprocal relationship, MΦs have been shown to influence not only the viability and growth of MSCs [57], but also their chondrogenic [58,59], osteogenic [38,60,61] and myogenic [62] differentiation potential. In general, the effects of MΦs appear to be dependent on the activation/polarization state of the MΦs. Accordingly, MΦs activated by IL-1β promote the differentiation of human adipose tissue-derived MSCs into smooth muscle cells [62], while M1 MΦs inhibit [58], whereas M2 MΦs promote [59], chondrogenesis. Furthermore, MΦs have been demonstrated to be essential for osteogenesis in general [63]. Contradictory data regarding the exact MΦ phenotype involved in osteogenic differentiation of MSCs have been published. Nicolaidou *et al*.

[61] claim that all M/MΦs possess the capability to induce osteogenesis, while other groups report that osteogenesis is only promoted by either M1-like [64] or M2-like [60] MΦs.

1.2.3.2 MΦ-MSC INTERACTIONS WITH BIOMATERIALS

The clinical interest in MSCs in the context of biomaterials research has grown drastically over the last decade because of their endogenous presence at the implantation site and their regenerative potential across a broad spectrum of therapeutic applications, including TE strategies. As mentioned in the previous section, MSCs both influence and are influenced by MΦs. This interaction affects the disease progression of sepsis and GVHD, for example. Therefore, the crosstalk between these cells can influence the body's healing process and also tissue remodeling in response to implanted biomaterials.

In a recent paper, Chen *et al*. [60] identified the advantages of using *in vitro* co-culture models to investigate β-tricalcium phosphate (β-TCP)-induced osseointegration. The osteoconductive nature of β-TCP is well recognized *in vivo*, but the mechanism behind the osteogenic potential of the material has not yet been fully explained. By exposing MSCs to CM from MΦs cultured in direct contact with β-TCP, the authors were able to correlate the detected osteogenic effect of β-TCP with a material-induced switch in MΦ polarization towards M2 and an activation of calcium-sensitive pathways. Other studies using both direct and transwell co-culture models have investigated the immunomodulatory characteristics of MSCs in TE strategies. MSCs encapsulated in polyethylene glycol (PEG) hydrogel induced a reduction in the amount of tumor necrosis factor alpha (TNF-α) released by MΦs in direct *in vitro* co-culture, which was further correlated *in vivo* to a reduced foreign body response to the implanted PEG gel [65]. This paracrine interaction was also described by Valles *et al*. [66], who monitored the effects of MSCs cultured either on two-dimensional (2D) or three-dimensional (3D) surfaces *in vitro* on the behavior of MΦs. Compared with conventional 2D cultivation, MSCs cultured on 3D substrates produced more anti-inflammatory PGE_2 and tumor necrosis factor-inducible gene 6, but less monocyte chemoattractant protein-1 (MCP-1) and IL-6. This resulted in a reduction in monocyte chemotaxis in response to CM from MSCs cultured on 3D substrates in an *in vitro* transwell assay. Taken together, the results of these studies highlight the role of the biomaterial in the overall cellular cascades involved in healing and suggest that further characterization of the MSC-MΦ interaction is essential for enhancing tissue formation and repair.

1.2.4 FIBROBLASTS AND THEIR ROLE IN HEALING

Fibroblasts are the majority cell type in connective tissue and are derived from primary mesenchymal cells. They are a heterogeneous dynamic cell population that displays phenotypic and functional diversity based on their anatomical origin. Fibroblasts play key roles in various processes, such as tissue regeneration, ECM production and inflammation [67]. However, their main functions are synthesizing and remodeling ECM molecules including collagen, glycosaminoglycans, glycoproteins and elastic fibers [68-70]. However, excessive deposition and synthesis of ECM molecules may lead to the formation of scar tissue or a fibrous capsule around an implant. This fibrotic process is caused by the inflammatory and immunological crosstalk between fibroblasts and the innate/adaptive immune system through the expression of various cytokines, growth factors and enzymes [71]. During this process, the resident fibroblasts in the tissue are activated and differentiated into myofibroblasts that synchronize angiogenesis and ECM formation. Thus, one major mediator of fibrotic tissue remodeling and wound healing is the activation of the ECM-producing myofibroblasts (Wynn *et al.* 2012, Klingberg *et al.* 2014). In the initial stage, the formation of fibrous tissue enhances the integration of the implant with the surrounding tissue. Further, it controls and modulates the inflammatory responses by isolating the damage caused by the implant. However, over-growth of the fibrous capsule can interfere with the functionality of the implant, which may lead to insufficient or deteriorating implant integration into the tissue and hence malfunction of the device.

1.2.4.1 MΦ-FIBROBLAST CROSSTALK

MΦs and fibroblasts concurrently synchronize and react to foreign materials. Crosstalk between fibroblasts and MΦs occurs via complex synergistic autocrine and paracrine, as well as juxtacrine, signaling [72]. These cells act cooperatively in various processes related to cell migration, implant degradation, fibrosis, healing and inflammation. Fibroblasts and MΦs secrete numerous enzymes, growth factors, ions, chemokines and cytokines to coordinate the host response to a foreign material [73]. Some of the most effective cytokine and chemokine inflammatory signals, which remain up-regulated in the presence of a foreign material, include TNF-α, IL-1, macrophage inflammatory proteins (MIP-1α, MIP-1β), MCP-1 and the Regulated on Activation, Normal T cell Expressed and Secreted (RANTES) chemokine [12,74-77]. Specifically, activated MΦs express IL-1, IL-4, IL-10, IL-13 and TNF-α, which leads to further fibroblast activation and overexpression of ECM molecules.

MΦs play a substantial role in remodeling and fibrosis. Signals from the recruited and locally resident MΦs promote ECM synthesis by fibroblasts [68-70]. Deposition and degradation of ECM requires an delicate balance between matrix metalloproteinases (MMPs) and tissue inhibitors of MMPs (TIMPs), which are expressed by MΦs [71]. For example, MMP9 is a dominant pro-fibrotic MMP; inhibiting

MMP9 can suppress fibrosis [78,79]. Besides MMPs, TGF-β is also produced mainly by MΦs and plays a fundamental pro-fibrotic role in chronic fibrotic disease [80]. TGF-β stimulates the expression of ECM genes and down regulates the expression of ECM degrading MMPs [81]. Overall, fibroblasts and MΦs induce both chemical and physical modifications to the microenvironment that regulate cell recruitment/proliferation and the production of ECM, proteins and enzymes [68,69,74]. Clarifying this intricate cross-communication between the fibroblasts and MΦs may assist in material selection for developing a fully functional implant.

The type of communication and signaling routes between fibroblasts and MΦs, as well as the source of the cells (primary or secondary), play key roles in models of the foreign body reaction *in vitro*. These cells communicate through various signaling routes including autocrine, paracrine (indirect cell-cell signaling) and juxtacrine (direct cell-cell signaling). Holt *et al*. [72] cultured both primary and secondary cells in mono- and co-culture formats to model different cell-cell communication conditions. The presence of both an inflammatory cell activator and an exogenous activating agent such as LPS, IFN-γ or phorbol esters are necessary to recreate the expressive cell inflammatory response. The morphologies of the primary and secondary cells under paracrine and juxtacrine co-culture conditions were both similar to their respective monocultures. However, the LPS-treated MΦs in mono- and co-culture displayed a highly activated morphology that normally results in the formation of FBG cells. LPS-stimulated MΦs expressed more inflammatory cytokines, such as IL-6 and TNF-α, compared with the non-stimulated cells, and this effect was more pronounced in primary cells. Other groups have reported that stimulated fibroblasts in monoculture express more IL-6 than non-stimulated fibroblasts [82].

Several cytokines and soluble factors, such as PGE2, released by fibroblasts can limit the release of MIP-1b, MIP-1a and TNF-α by MΦs [83,84]. Paracrine and juxtacrine co-culture systems showed a decrease in the expression of these cytokines compared with monocultures. However, it has been reported that IL-6 and RANTES are downregulated only in primary MΦ co-cultures, not in secondary MΦ co-cultures. This effect may be caused by mutual cytokine down-regulation that only occurs in primary cells [72]. Upregulation of TNF-α increases the expression of MCP-1, which is a mitogenic factor for fibroblasts [85]. Paracrine and juxtacrine signaling in co-cultured primary MΦs induced a large increase in MCP-1 expression compared with that in monocultures [72].

1.2.4.2 M*Φ*-FIBROBLAST INTERACTIONS WITH BIOMATERIALS

Together, MΦs and fibroblasts can orchestrate the degradation of natural biomaterials and native tissues, especially connective tissue. The first two innate events that occur in host-cell interactions are: 1) stimulation of MΦs, and 2) MΦ-enhanced fibroblast recruitment and their cooperative effects

on the implant [86]. Activated MΦs attach directly to a biomaterial and FBG cells secrete mediators, such as degradative enzymes, superoxide anions, oxygen free radicals and reactive oxygen intermediates, which facilitate the degradation of the biomaterial. The maximum concentration of these degradative agents is found at the implant-host interface. However, the chemical composition of the implant is the key determinant of the probability that an implant will degrade. For example, polyethylene and polypropylene polymers are susceptible to surface oxidation. Polyesters such as polycaprolactone, poly(glycolic acid) and poly(lactic acid) can be enzymatically degraded into small monomers that are metabolized through the Krebs' cycle. A few studies exist showing that fibroblasts are also capable of releasing hydrolases and, therefore, contribute to the degradation process through phagocyte-like functionality. After adhering to an implant, fibroblasts synthesize ECM. These ECM molecules stimulate the production of degradative enzymes, inducing hydrolytic reactions. They may also further increase the degradation of fibrous electrospun scaffolds by inducing stress on the structure after attachment. In addition, MΦs and fibroblasts synergistically facilitate the degradation of dextran-poly(lactic-co-glycolic acid) (PLGA) scaffolds [67]. Dextran-PLGA scaffolds seeded with MΦ-fibroblast co-cultures were degraded faster than scaffolds seeded with only one particular cell type. However, MΦs alone are more degradative than fibroblasts because they release a wider range of enzymes and oxidative agents [67].

Chronic inflammation typically results in damage to and degradation of connective tissue caused by the elimination of collagen or proteoglycans. The presence of MΦs and fibroblasts, along with T and B lymphocytes in the chronic inflammatory environment suggests that these cells play roles in the degradation of connective tissues, such as cartilage. Huybrechts-Godin *et al*. [87] reported that mitogen-stimulated and proteinase-secreting MΦs cooperate with fibroblasts and enhance their capacity for collagenase synthesis, subsequently leading to collagen degradation [87]. The addition of lymphocyte factors has been observed to increase the crosstalk between MΦs and fibroblasts in direct co-cultures, but has no direct effect on fibroblasts alone [87]. This finding confirms that the production of collagenase by fibroblasts is partially controlled by communication between fibroblasts and the various other cellular and humoral components of the immune system.

1.2.5 ENDOTHELIAL CELLS AND THEIR ROLE IN HEALING

Endothelial cells (ECs) line the entire vasculature, forming an inner cell layer that serves as a multifunctional barrier between the bloodstream and the surrounding tissues. Consequently, ECs are involved in a wide variety of different functions important for physiological homeostasis of the body. Being in direct contact with the blood, ECs function as a semi-permeable barrier that controls solute and macromolecule transfer through the endothelium. ECs have multifunctional paracrine and endocrine characteristics, including involvement in 1) immune and inflammatory reactions by regulating leukocyte migration into the tissue; 2) the formation of a non-thrombogenic vessel lumen by regulating thrombosis, coagulation, platelet adherence, fibrinolysis, vascular tone and blood flow; 3) angiogenesis, the sprouting of new blood vessels from pre-existing vascular tubes and 4) vasculogenesis, the formation of new blood vessels via the migration, assembly and maturation of ECs [88]. These last two EC functions, the formation and/or expansion of new functional blood vessels for tissue vascularization, regeneration and growth, are of particular interest to the field of biomaterials and the development of regenerative therapies, which includes wound healing, cell transplantation approaches and TE strategies. Angiogenesis at the implantation site is necessary to improve the integration of the scaffold into the native host tissue [89]. This process has long been understood to involve dynamic and bidirectional interactions between M/MΦs and ECs [90,91]. The expansion of blood vessels is divided into two phases: vessel sprouting and vessel anastomosis. Following an angiogenic stimulus, vessel sprouting occurs, which includes the transition of ECs from a quiescent to an active state and proteases are secreted to open the basal lamina and enable vascular growth [92]. Here, M/MΦs directly regulate the patterning of the local ECM degradation, consequently influencing the distribution of neovessel formation and their branch points [93] [94]. Anastomoses occur when two angiogenic sprouts meet and connect to form a new closed vascular tube. In this way, complex vascular networks can be assembled for the (re)vascularization of ischaemic tissue, wounds or biomaterials introduced for TE applications. It was shown that MΦs interact physically with ECs during the process of anastomosis formation to promote tip cell fusion during development [95,96]. Recent studies investigating materials for TE have further emphasized the important role of infiltrating inflammatory cells (primarily M/MΦs) for vascular host cell recruitment, tissue formation and maturation [97,98]. Consequently, MΦ depletion can inhibit neovessel formation, as demonstrated by the absence of cellular infiltration and incomplete endothelialisation. In summary, the interactions between M/MΦs and ECs during these angiogenic processes are based on direct bidirectional cell-cell interaction; the secretion of classic pro-angiogenic factors, including inflammatory cytokines and growth factors and the creation of a pro-angiogenic microenvironment.

1.2.5.1 MΦ-EC CROSSTALK

M/MΦs significantly support EC growth and proliferation when the cells are cultured in direct contact. Such direct co-culture of monocytes and human umbilical vein endothelial cells (HUVECs) revealed increased BrdU incorporation in HUVECs and a higher cell density in co-culture [99]. Increased proliferation also occurs with either a subset of pro-angiogenic CD14+, CD16+ and CD163+ M/MΦs [100] or VEGF-stimulated MΦs [101] co-cultured with dermal microvascular ECs. In most cases, a confluent monolayer of ECs can be found in the co-culture, but not monoculture, conditions [100,102]. In fact, the numerical ratio between the (co-)cultured cells significantly influences this proliferative effect. Further, monocytes also exhibit higher proliferation rates when exposed to HUVECs in direct co-culture conditions [103,104]. All of these findings highlight the positive correlation between the pro-angiogenic effects of MΦs and the actual number of ECs in the co-culture systems [101,104]. Similar results have been obtained from classic *in vitro* scratch/wound healing assays, in which a scratch is made on an EC monolayer to test and quantify EC migration into the denuded areas. The presence of monocytes in this assay accelerates the re-endothelialisation process [99]. Apart from this bidirectional proliferative effect, the time-dependent transformation of monocytes into endothelial-like cells has been described following their adherence to a pre-existing endothelium [105,106], interaction with biomaterials [107] and exposure to an angiogenic environment [108,109]. The ability of M/MΦs to promote angiogenesis has been associated with the secretion of classic pro-angiogenic factors as demonstrated with experiments using indirect co-culture systems, both through CM exposure and membranes filters that prevent direct cell contact. These co-culture systems are suitable tools for studying the expression of soluble factors such as VEGF, basic fibroblast growth factor (bFGF), placental growth factor (PIGF), angiopoietin (Ang-1, Ang-2) and IL-8. EC proliferation is enhanced by exposure to CM from activated monocytes in a concentration-dependent manner [110]. Indeed, neutralizing antibodies against bFGF, VEGF and IL-8 partially reverse this mitogenic effect [110]. The stimulating effects of bFGF and VEGF on the formation of capillary-like structures by ECs were larger if they were co-cultured with THP-1 monocytic cells [111]. Furthermore, pleiotrophin enhances both the migration and pro-angiogenic response of ECs and the expression of angiogenic molecules by monocytes [112].

Taken together, these data indicate that the bidirectional interaction between M/MΦs and ECs involves both the release of a broad spectrum of pro-angiogenic mediators, as well as the direct physical interaction of the two cell types.

1.2.5.2 MΦ-EC INTERACTION WITH BIOMATERIALS

There is very strong evidence that the composition of polymers in scaffolds alters the activation state of M/MΦs, which ultimately affects the angiogenic response to the biomaterial. In activated M/MΦs, the mRNA expression of angiogenic genes and the release of angiogenic mediators such as Ang-1, thrombospondin-1 (Tsp-1) and VEGF, are dependent on the polymer material used [113-115]. M/MΦs in direct contact with various polymeric materials, such as poly(L-lactic acid) and PLGA, exhibit a different release profile of inflammatory cytokines such as RANTES, TNF-α, IL-α/β, IL-3, IL-8 and IL-10 [114]. In addition, the medium conditioned by M/MΦs in contact with different polymeric materials may alter the proliferation, viability and capillary sprouting ability of ECs [113,114]. Significantly improved *in vitro* wound closure has been detected on EC monolayers using such CM in studies of different polymeric materials, pointing towards paracrine mediators as important signals for guiding regeneration [114]. Thus, vascularization and the long-term integration of implanted scaffolds with native tissue can be promoted by incorporating active paracrine agents [116]. For example, pro-angiogenic C16 peptides and anti-inflammatory Ac-SDKP peptides were incorporated into a collagen gel that was then loaded into porous scaffolds to evaluate their controlled release in HUVEC and M/MΦ co-cultures [116]. A high degree of interdependence between angiogenesis, assessed by the tubologenesis of the ECs, and inflammation, assessed by the phagocytic activity of the M/MΦs, was detected [116]. Furthermore, incorporation of the proinflammatory molecule fibrinogen into the chitosan biomaterial clearly decreased the expression of inflammatory cytokines while increasing the secretion of growth factors and mediators involved in wound healing and angiogenesis [115]. Several other studies have also reported enhanced vascularization and/or wound healing *in vitro* and/or *in vivo* by incorporating VEGF [117], PDGF-BB/FGF2 [118], laminin-5 [119], phytochemically-stabilized gold nanoparticles [120], bFGF [121] and calcium phosphate [122] into different biomaterials. The phenotype of the MΦs plays a key role in the induction of angiogenesis. Spiller *et al.* showed that not only the M2 phenotype, but also the coordinated transition from the M1 to M2 phenotype promotes angiogenesis in TE scaffolds [123]. For example, decellularized bone scaffolds that sequentially released the M1-promoting cytokine IFN-γ and then the M2-promoting cytokine IL-4, promoted sequential polarization from M1 to M2 as defined by their gene expression profile and cytokine release [124]. Interestingly, these scaffolds exhibited *in vivo* a higher vascularization capacity, suggesting that both M1 and M2 MΦs are necessary to achieve scaffold vascularization. That result is in agreement with the findings of Oliveira *et al*., who reported that the density of MΦs and not their polarization is responsible for improving *in vivo* angiogenesis [122].

In addition to polymer composition and exogenously incorporated mediators, the fiber, pore dimensions and size of the interconnected pores influence the resulting vascularization [125,126]. Polydioxanone scaffolds with larger pore sizes and fiber diameters induce higher expression of

angiogenic cytokines by MΦs co-cultured with the scaffolds. Further, this angiogenic cytokine secretion increased the length and density of the EC sprouts [125]. Taken together, all of these studies demonstrate that TE scaffolds can be designed to maximize the angiogenic response of the MΦs to the implanted biomaterial. However, it should be noted that a balanced expression of both pro- and anti-angiogenic factors is necessary to inhibit tumor growth and enable physiological performance of biomaterials in future TE applications.

1.2.6 MACROPHAGE CO-CULTURE MODELS: BENEFITS AND LIMITATIONS

Healing following implantation of a construct or biomaterial for TE is a complex event that involves the interplay between different cell types. Therefore, the current standard for evaluating graft-host interactions is the use of *in vivo* models. However, these investigations are expensive, raise several ethical questions and the results are not always fully predictive of the human physiology due to significant inter-species variability. The development of new drugs perfectly exemplifies the lack of consistency between animal and clinical studies. Clinical trials for new drugs are only conducted following substantial evidence for efficacy and safety in animals. However, in spite of their initial success in animal models, 85% of new drugs fail during early clinical trials and, of those that survive through to phase III, only half are approved for clinical use [127]. Creating predictive *in vitro* evaluation systems using human cells would reduce the need for *in vivo* animal experiments and may decrease the time for drug development. In addition, it may allow for mechanistic analyses and also reduce costs. However, there are also several limitations associated with the use of *in vitro* models. The majority of cell-based *in vitro* models are limited to the use of a single cell type, which does not correspond to the complex interactions that occur *in vivo* [72]. Therefore, co-culture models usually better capture the dynamic cellular interactions and biomaterial-associated signaling than mono-culture based assays. As previously mentioned, the presence of MΦs can modulate the behavior of various cell types including MSCs, ECs and fibroblasts during biomaterials evaluation testing. In this regards the development of an *in vitro* co-culture model including macrophages that successfully mimics the complex healing process evident *in vivo* still faces a series of challenges:

First, an appropriate *in vitro* model must be selected for each application. Various cells can be used for MΦ-based immunological studies (Table 1), and an appropriate cell type should be carefully selected based on the experimental setup. Although human cells are superior to murine models with regards to clinical translation a plethora of groups still use cells of murine origin, notably the transformed cell line RAW 264.7. Although the use of these murine lines is commonly accepted, substantial differences between the immunobiology of humans and mice have been clearly demonstrated [128]. In addition, significant variation has been observed between the responses of

primary versus transformed murine macrophages to biomaterials, which may lead to misleading conclusions [129]. Human cell lines, such as THP-1, do not entirely mimic the behavior of primary cells either, even if they are useful alternative models given their homogeneous genetic background. The consistent behavior of cell lines helps in the identification of mechanisms involved in the cellular response to particular culture conditions [130]. Compared with murine and human transformed cell lines, primary cells isolated from blood donors usually show high inter-patient variability and low proliferative potential *in vitro*. Furthermore, different isolation and culturing procedures may limit the experimental reproducibility and it would therefore be important to establish standardized cell cultivation and analytical protocols, which could facilitate comparability of different studies. The selection of primary MSCs poses similar challenges because of their inherent heterogeneity. In addition, the immunomodulatory capability of MSCs is also affected by the cell source [55], passage number [131] and exposure time [132]. Likewise, there are differences between ECs isolated from arterial, dermal microvascular, umbilical vein and pulmonary microvascular tissues.

Other factors limiting the utility of *in vitro* macrophage co-cultures are the absence of inflammatory stimulators, such as LPS, IFN-γ and TNF-α, and other inflammatory cells, such as T and B cells [75]. Exogenous inflammatory stimulators have been observed in the host-biomaterial interface and thus should be added to *in vitro* models. However, even the presence of these stimuli might not be sufficient to reproduce *in vivo* events. Several studies have shown that MΦs stimulated *in vitro* do not fully mimic the inflammatory behavior of cells stimulated *in vivo* [75]. For example, the expression of IL-6 was not responsive to LPS stimulation *in vitro,* whereas LPS stimulation *in vivo* increased the expression of TNF-α and other proinflammatory cytokines [133,134]. *In vitro* evaluations of biomaterial biocompatibility should also determine the effects of the biomaterial on the innate and acquired immune cells such as T cells, B cells, natural killer cells and granulocytes [69,135]. Consequently, *in vitro* models lacking these inflammatory cells are limited in their ability to accurately represent the *in vivo* cellular crosstalk. Together, the timing and microenvironment of cellular interactions between macrophages and other cell types define the final host response; *in vitro* models that fail to recapitulate the *in vivo* environment are of limited value for predicting the tissue response in vivo. For example, the immunomodulatory capacity of MSCs depends on the presence of the inflammatory environment created by MΦs, while the inflammatory state created by the MΦs is likewise affected by the presence of MSCs. Furthermore, the challenge of tracking MSCs and the plasticity of the MΦ phenotype makes it difficult to establish cause-and-effect timelines of their interactions *in vivo*. For example, one *in vitro* MΦ-MSC co-culture model failed to show that the degree of MSC differentiation when encapsulated in a PEG gel was linearly correlated with an increase in capsule formation *in vivo* [65]. This suggests that *in vitro* co-culture models alone are not yet sufficient for predicting the many possible outcomes following biomaterial implantation.

Another challenge for *in vitro* co-culture models is replicating the *in vivo* mechanical microenvironment. All tissues and organs within the body are exposed to continuous or pulsatile mechanical stimuli. Static *in vitro* co-culture models typically do not consider this biologically relevant aspect of tissue healing. The endothelium in the native environment in particular is exposed to shear stress and dynamic fluid flow. Therefore, investigations of monocyte extravasation and endothelial activation may find different results in static and dynamic cultures. In fact, static culture models do not induce the same EC phenotype as cultures under flow, and differences between steady and physiological pulsatile flow have been observed [136,137]. To address this, an increasing effort has been invested in creating vascularized grafts using TE technologies that more closely resemble native vessel structures. Microfluidic devices and bioreactors may enable more detailed examinations of the interplay between M/MΦs and ECs under flow conditions.

Overall, the use of *in vitro* co-culture models is indispensable to further understand and predict the tissue responses following biomaterial implantation. However, the culture conditions such as cell origin, the type of co-culture model and the cell culture protocols may limit the utility of the model and should be chosen carefully. Future work exploring and defining these limiting factors should be directed to further enable predictive *in vitro* experiments mimicking relevant steps in the cell-material response cascade. This might ultimately help to reduce the number of animal experiments as well as the time invested for the preclinical phase of research.

1.2.7 SUMMARY

The healing of tissues following implantation is a complex, dynamic and time-dependent process that involves a wide variety of different cell types. Successful healing depends on the interplay between inflammatory and regenerative mechanisms, including cell migration, angiogenesis, ECM production and remodeling. The present review has highlighted the multiple ways in which macrophages interact with endothelial cells, mesenchymal stem cells and fibroblasts during the healing process (Fig. 3). Specific molecules and signaling pathways that modulate the cellular responses and, consequently, the healing process have been described. However, further investigations are necessary to identify the precise cellular crosstalk between macrophages and MSCs, ECs, fibroblasts and biomaterials. In this regard, the development of more sophisticated *in vitro* co-culture models that better mimic the *in vivo* physiological environment would enable more precise studies of the complex healing process.

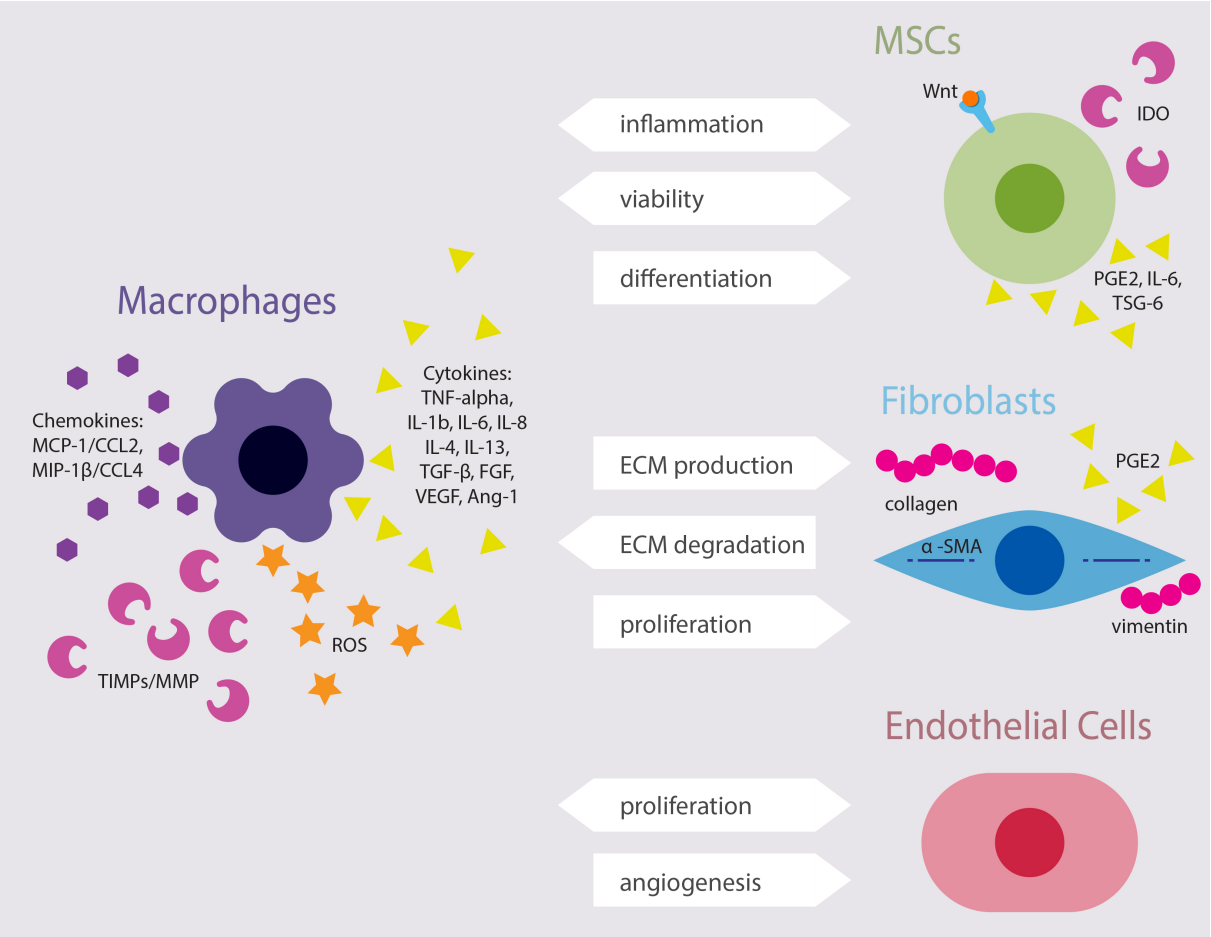

Figure 3. Schematic of macrophage crosstalk with MSCs, fibroblasts and ECs highlighting the processes and molecules that have been implicated in cell-cell interactions. Arrows show the cellular processes that are affected by cell-to-cell communication. Arrow direction points from affector to effector cell; e.g. macrophages affect the differentiation of MSCs, whereas fibroblasts affect the ECM degradation by macrophages.

1.2.8 REFERENCES

1 Anderson, J. M. Mechanisms of Inflammation and Infection with Implanted Devices. *Cardiovasc Pathol* **2**, S33-S41 (1993).

2 Sridharan, R., Cameron, A. R., Kelly, D. J., Kearney, C. J. & O'Brien, F. J. Biomaterial based modulation of macrophage polarization: a review and suggested design principles. *Materials Today* **18**, 313-325, doi:http://dx.doi.org/10.1016/j.mattod.2015.01.019 (2015).

3 Gordon, S. & Taylor, P. R. Monocyte and macrophage heterogeneity. *Nature reviews. Immunology* **5**, 953-964, doi:10.1038/nri1733 (2005).

4 Epelman, S., Lavine, K. J. & Randolph, G. J. Origin and functions of tissue macrophages. *Immunity* **41**, 21-35, doi:10.1016/j.immuni.2014.06.013 (2014).

5 Vannella, K. M. & Wynn, T. A. Mechanisms of Organ Injury and Repair by Macrophages. *Annual review of physiology*, doi:10.1146/annurev-physiol-022516-034356 (2016).

6 Gordon, S., Pluddemann, A. & Martinez Estrada, F. Macrophage heterogeneity in tissues: phenotypic diversity and functions. *Immunological reviews* **262**, 36-55, doi:10.1111/imr.12223 (2014).

7 Klopfleisch, R. & Jung, F. The pathology of the foreign body reaction against biomaterials. *J Biomed Mater Res A*, doi:10.1002/jbm.a.35958 (2016).

8 Wynn, T. A. Cellular and molecular mechanisms of fibrosis. *J Pathol* **214**, 199-210 (2008).

9 Moore, L. B., Sawyer, A. J., Charokopos, A., Skokos, E. A. & Kyriakides, T. R. Loss of monocyte chemoattractant protein-1 alters macrophage polarization and reduces NFkappaB activation in the foreign body response. *Acta Biomater* **11**, 37-47, doi:10.1016/j.actbio.2014.09.022 (2015).

10 Martinez, F. O. & Gordon, S. The M1 and M2 paradigm of macrophage activation: time for reassessment. *F1000prime reports* **6**, 13, doi:10.12703/p6-13 (2014).

11 Brown, B. N., Ratner, B. D., Goodman, S. B., Amar, S. & Badylak, S. F. Macrophage polarization: an opportunity for improved outcomes in biomaterials and regenerative medicine. *Biomaterials* **33**, 3792-3802, doi:10.1016/j.biomaterials.2012.02.034 (2012).

12 Mantovani, A., Biswas, S. K., Galdiero, M. R., Sica, A. & Locati, M. Macrophage plasticity and polarization in tissue repair and remodelling. *J Pathol* **229**, 176-185, doi:10.1002/path.4133 (2013).

13 Mosser, D. M. & Edwards, J. P. Exploring the full spectrum of macrophage activation. *Nature reviews. Immunology* **8**, 958-969, doi:10.1038/nri2448 (2008).

14 Mooney, J. E. *et al.* Transcriptional switching in macrophages associated with the peritoneal foreign body response. *Immunology and cell biology* **92**, 518-526, doi:10.1038/icb.2014.19 (2014).

15 Voges, I. *et al.* Adverse results of a decellularized tissue-engineered pulmonary valve in humans assessed with magnetic resonance imaging. *Eur J Cardio-Thorac* **44**, E272-E279 (2013).

16 Delgado, L. M., Bayon, Y., Pandit, A. & Zeugolis, D. I. To cross-link or not to cross-link? Cross-linking associated foreign body response of collagen-based devices. *Tissue engineering. Part B, Reviews* **21**, 298-313, doi:10.1089/ten.TEB.2014.0290 (2015).

17 Aamodt, J. M. & Grainger, D. W. Extracellular matrix-based biomaterial scaffolds and the host response. *Biomaterials* **86**, 68-82, doi:10.1016/j.biomaterials.2016.02.003 (2016).

18 Thomsen, P. *et al.* Structure of the interface between rabbit cortical bone and implants of gold, zirconium and titanium. *J Mater Sci-Mater M* **8**, 653-665 (1997).

19 Vitkov, L., Hartl, D. & Hannig, M. Is osseointegration inflammation-triggered? *Medical hypotheses* **93**, 1-4, doi:10.1016/j.mehy.2016.05.004 (2016).

20 Kzhyshkowska, J. *et al.* Macrophage responses to implants: prospects for personalized medicine. *J Leukoc Biol* **98**, 953-962, doi:10.1189/jlb.5VMR0415-166R (2015).

21 Hachim, D., LoPresti, S. T., Yates, C. C. & Brown, B. N. Shifts in macrophage phenotype at the biomaterial interface via IL-4 eluting coatings are associated with improved implant integration. *Biomaterials* **112**, 95-107, doi:10.1016/j.biomaterials.2016.10.019 (2017).

22 Zhao, O. H., Anderson, J. M., Hiltner, A., Lodoen, G. A. & Payet, C. R. Theoretical analysis on cell size distribution and kinetics of foreign-body giant cell formation in vivo on polyurethane elastomers. *Journal of biomedical materials research* **26**, 1019-1038, doi:10.1002/jbm.820260805 (1992).

23 McNally, A. K. & Anderson, J. M. Phenotypic expression in human monocyte-derived interleukin-4-induced foreign body giant cells and macrophages in vitro: dependence on material surface properties. *J Biomed Mater Res A* **103**, 1380-1390, doi:10.1002/jbm.a.35280 (2015).

24 McNally, A. K. & Anderson, J. M. Interleukin-4 induces foreign body giant cells from human monocytes/macrophages. Differential lymphokine regulation of macrophage fusion leads to morphological variants of multinucleated giant cells. *Am J Pathol* **147**, 1487-1499 (1995).

25 Clanchy, F. I. L., Holloway, A. C., Lari, R., Cameron, P. U. & Hamilton, J. A. Detection and properties of the human proliferative monocyte subpopulation *J Leukocyte Biol* **79**, 757-766 (2006).

26 Mantovani, A. *et al.* The chemokine system in diverse forms of macrophage activation and polarization. *Trends in immunology* **25**, 677-686, doi:10.1016/j.it.2004.09.015 (2004).

27 Gordon, S. Alternative activation of macrophages. *Nature reviews. Immunology* **3**, 23-35, doi:10.1038/nri978 (2003).

28 Murray, P. J. Macrophage Polarization. *Annual review of physiology*, doi:10.1146/annurev-physiol-022516-034339 (2016).

29 Stout, R. D. & Suttles, J. Immunosenescence and macrophage functional plasticity: dysregulation of macrophage function by age-associated microenvironmental changes. *Immunological reviews* **205**, 60-71, doi:10.1111/j.0105-2896.2005.00260.x (2005).

30 Stout, R. D. & Suttles, J. Functional plasticity of macrophages: reversible adaptation to changing microenvironments. *J Leukoc Biol* **76**, 509-513, doi:10.1189/jlb.0504272 (2004).

31 Porcheray, F. *et al.* Macrophage activation switching: an asset for the resolution of inflammation. *Clinical and experimental immunology* **142**, 481-489, doi:10.1111/j.1365-2249.2005.02934.x (2005).

32 El Kasmi, K. C. & Stenmark, K. R. Contribution of metabolic reprogramming to macrophage plasticity and function. *Seminars in immunology* **27**, 267-275, doi:10.1016/j.smim.2015.09.001 (2015).

33 Badylak, S. F., Valentin, J. E., Ravindra, A. K., McCabe, G. P. & Stewart-Akers, A. M. Macrophage phenotype as a determinant of biologic scaffold remodeling. *Tissue Engineering Part A* **14**, 1835-1842 (2008).

34 Sussman, E. M., Halpin, M. C., Muster, J., Moon, R. T. & Ratner, B. D. Porous Implants Modulate Healing and Induce Shifts in Local Macrophage Polarization in the Foreign Body Reaction. *Annals of biomedical engineering*, 1-9 (2013).

35 Friedenstein, A. J. Precursor Cells of Mechanocytes. *Int Rev Cytol* **47**, 327-359 (1976).

36 Dominici, M. *et al.* Minimal criteria for defining multipotent mesenchymal stromal cells. The International Society for Cellular Therapy position statement. *Cytotherapy* **8**, 315-317, doi:10.1080/14653240600855905 (2006).

37 Kim, N. & Cho, S. G. Clinical applications of mesenchymal stem cells. *The Korean journal of internal medicine* **28**, 387-402, doi:10.3904/kjim.2013.28.4.387 (2013).

38 Karp, J. M. & Leng Teo, G. S. in *Cell Stem Cell* Vol. 4 206-216 (2009).

39 Sasaki, M. *et al.* Mesenchymal Stem Cells Are Recruited into Wounded Skin and Contribute to Wound Repair by Transdifferentiation into Multiple Skin Cell Type. *The Journal of Immunology* **180** 2581-2587, doi:10.4049/jimmunol.180.4.2581 (2008).

40 Yeum, C. E., Park, E. Y., Lee, S. B., Chun, H. J. & Chae, G. T. Quantification of MSCs involved in wound healing: Use of SIS to transfer MSCs to wound site and quantification of MSCs involved in skin wound healing. *Journal of Tissue Engineering and Regenerative Medicine* **7**, 279-291, doi:10.1002/term.521 (2013).

41 Ma, S. *et al.* Immunobiology of mesenchymal stem cells. *Cell Death Differ* **21**, 216-225, doi:Doi 10.1038/Cdd.2013.158 (2014).

42 Le Blanc, K. *et al.* Treatment of severe acute graft-versus-host disease with third party haploidentical mesenchymal stem cells. *Lancet* **363**, 1439-1441, doi:10.1016/s0140-6736(04)16104-7 (2004).

43 Nemeth, K. *et al.* Bone marrow stromal cells attenuate sepsis via prostaglandin E-2-dependent reprogramming of host macrophages to increase their interleukin-10 production. *Nat Med* **15**, 42-49 (2009).

44 Cho, D. I. *et al.* Mesenchymal stem cells reciprocally regulate the M1/M2 balance in mouse bone marrow-derived macrophages. *Exp Mol Med* **46**, doi:ARTN e70 DOI 10.1038/emm.2013.135 (2014).

45 Maggini, J. *et al.* Mouse Bone Marrow-Derived Mesenchymal Stromal Cells Turn Activated Macrophages into a Regulatory-Like Profile. *Plos One* **5** (2010).

46 Zhang, Q. Z. *et al.* Human Gingiva-Derived Mesenchymal Stem Cells Elicit Polarization of M2 Macrophages and Enhance Cutaneous Wound Healing. *Stem Cells* **28**, 1856-1868, doi:Doi 10.1002/Stem.503 (2010).

47 Francois, M., Romieu-Mourez, R., Li, M. Y. & Galipeau, J. Human MSC Suppression Correlates With Cytokine Induction of Indoleamine 2,3-Dioxygenase and Bystander M2 Macrophage Differentiation. *Mol Ther* **20**, 187-195 (2012).

48 Qi, Y. *et al.* TSG-6 Released from Intradermally Injected Mesenchymal Stem Cells Accelerates Wound Healing and Reduces Tissue Fibrosis in Murine Full-Thickness Skin Wounds. *J Invest Dermatol* **134**, 526-537, doi:Doi 10.1038/Jid.2013.328 (2014).

49 Kim, J. & Hematti, P. Mesenchymal stem cell-educated macrophages: A novel type of alternatively activated macrophages. *Exp Hematol* **37**, 1445-1453, doi:DOI 10.1016/j.exphem.2009.09.004 (2009).

50 Choi, H., Lee, R. H., Bazhanov, N., Oh, J. Y. & Prockop, D. J. Anti-inflammatory protein TSG-6 secreted by activated MSCs attenuates zymosan-induced mouse peritonitis by decreasing TLR2/NF-kappa B signaling in resident macrophages. *Blood* **118**, 330-338, doi:DOI 10.1182/blood-2010-12-327353 (2011).

51 Ylostalo, J. H., Bartosh, T. J., Coble, K. & Prockop, D. J. Human Mesenchymal Stem/Stromal Cells Cultured as Spheroids are Self-activated to Produce Prostaglandin E2 that Directs Stimulated Macrophages into an Anti-inflammatory Phenotype. *Stem Cells* **30**, 2283-2296 (2012).

52 Abumaree, M. H. *et al.* Human Placental Mesenchymal Stem Cells (pMSCs) Play a Role as Immune Suppressive Cells by Shifting Macrophage Differentiation from Inflammatory M1 to Anti-inflammatory M2 Macrophages. *Stem Cell Rev Rep* **9**, 620-641, doi:DOI 10.1007/s12015-013-9455-2 (2013).

53 Melief, S. M., Geutskens, S. B., Fibbe, W. E. & Roelofs, H. Multipotent stromal cells skew monocytes towards an anti-inflammatory interleukin-10-producing phenotype by production of interleukin-6. *Haematologica* **98**, 888-895, doi:DOI 10.3324/haematol.2012.078055 (2013).

54 Geng, Y. Q. *et al.* Mesenchymal stem cells ameliorate rhabdomyolysis-induced acute kidney injury via the activation of M2 macrophages. *Stem Cell Res Ther* **5**, doi:Artn 80 Doi 10.1186/Scrt469 (2014).

55 Jin, H. J. *et al.* Comparative Analysis of Human Mesenchymal Stem Cells from Bone Marrow, Adipose Tissue, and Umbilical Cord Blood as Sources of Cell Therapy. *Int J Mol Sci* **14**, 17986-18001, doi:DOI 10.3390/ijms140917986 (2013).

56 Ren, G. W. *et al.* Mesenchymal stem cell-mediated immunosuppression occurs via concerted action of chemokines and nitric oxide. *Cell Stem Cell* **2**, 141-150, doi:DOI 10.1016/j.stem.2007.11.014 (2008).

57 Freytes, D. O., Kang, J. W., Marcos-Campos, I. & Vunjak-Novakovic, G. Macrophages modulate the viability and growth of human mesenchymal stem cells. *J Cell Biochem* **114**, 220-229, doi:Doi 10.1002/Jcb.24357 (2013).

58 Fahy, N. *et al.* Human osteoarthritic synovium impacts chondrogenic differentiation of mesenchymal stem cells via macrophage polarisation state. *Osteoarthr Cartilage* **22**, 1167-1175, doi:DOI 10.1016/j.joca.2014.05.021 (2014).

59 Sesia, S. B. *et al.* Anti-Inflammatory/Tissue Repair Macrophages Enhance the Cartilage-Forming Capacity of Human Bone Marrow-Derived Mesenchymal Stromal Cells. *J Cell Physiol* **230**, 1258-1269, doi:Doi 10.1002/Jcp.24861 (2015).

60 Chen, Z. T. *et al.* Osteogenic differentiation of bone marrow MSCs by beta-tricalcium phosphate stimulating macrophages via BMP2 signalling pathway. *Biomaterials* **35**, 1507-1518, doi:DOI 10.1016/j.biomaterials.2013.11.014 (2014).

61 Nicolaidou, V. *et al.* Monocytes Induce STAT3 Activation in Human Mesenchymal Stem Cells to Promote Osteoblast Formation. *Plos One* **7**, doi:ARTN e39871 DOI 10.1371/journal.pone.0039871 (2012).

62 Lee, M. J. *et al.* Macrophages Regulate Smooth Muscle Differentiation of Mesenchymal Stem Cells via a Prostaglandin F-2 alpha-Mediated Paracrine Mechanism. *Arterioscl Throm Vas* **32**, 2733-+, doi:Doi 10.1161/Atvbaha.112.300230 (2012).

63 Chang, M. K. *et al.* Osteal tissue macrophages are intercalated throughout human and mouse bone lining tissues and regulate osteoblast function in vitro and in vivo. *J Immunol* **181**, 1232-1244 (2008).

64 Guihard, P. *et al.* Induction of Osteogenesis in Mesenchymal Stem Cells by Activated Monocytes/Macrophages Depends on Oncostatin M Signaling. *Stem Cells* **30**, 762-772 (2012).

65 Swartzlander, M. D. *et al.* Immunomodulation by mesenchymal stem cells combats the foreign body response to cell-laden synthetic hydrogels. *Biomaterials* **41**, 79-88 (2015).

66 Valles, G. *et al.* Topographical cues regulate the crosstalk between MSCs and macrophages. *Biomaterials* **37**, 124-133, doi:DOI 10.1016/j.biomaterials.2014.10.028 (2015).

67 Pan, H., Jiang, H. & Chen, W. Interaction of dermal fibroblasts with electrospun composite polymer scaffolds prepared from dextran and poly lactide-co-glycolide. *Biomaterials* **27**, 3209-3220, doi:10.1016/j.biomaterials.2006.01.032 (2006).

68 Kelly, M., Kolb, M., Bonniaud, P. & Gauldie, J. Re-evaluation of fibrogenic cytokines in lung fibrosis. *Current pharmaceutical design* **9**, 39-49 (2003).

69 Anderson, J. M., Rodriguez, A. & Chang, D. T. Foreign body reaction to biomaterials. *Seminars in immunology* **20**, 86-100, doi:10.1016/j.smim.2007.11.004 (2008).

70 Ask, K. *et al.* Progressive pulmonary fibrosis is mediated by TGF-beta isoform 1 but not TGF-beta3. *The international journal of biochemistry & cell biology* **40**, 484-495, doi:10.1016/j.biocel.2007.08.016 (2008).

71 Van Linthout, S., Miteva, K. & Tschope, C. Crosstalk between fibroblasts and inflammatory cells. *Cardiovascular research* **102**, 258-269, doi:10.1093/cvr/cvu062 (2014).

72 Holt, D. J., Chamberlain, L. M. & Grainger, D. W. Cell-cell signaling in co-cultures of macrophages and fibroblasts. *Biomaterials* **31**, 9382-9394, doi:10.1016/j.biomaterials.2010.07.101 (2010).

73 Schmidt, D. R. & Kao, W. J. The interrelated role of fibronectin and interleukin-1 in biomaterial-modulated macrophage function. *Biomaterials* **28**, 371-382, doi:10.1016/j.biomaterials.2006.08.041 (2007).

74 Luttikhuizen, D. T., Harmsen, M. C. & Van Luyn, M. J. Cellular and molecular dynamics in the foreign body reaction. *Tissue engineering* **12**, 1955-1970, doi:10.1089/ten.2006.12.1955 (2006).

75 Schutte, R. J., Xie, L., Klitzman, B. & Reichert, W. M. In vivo cytokine-associated responses to biomaterials. *Biomaterials* **30**, 160-168, doi:10.1016/j.biomaterials.2008.09.026 (2009).

76 Volin, M. V. *et al.* RANTES expression and contribution to monocyte chemotaxis in arthritis. *Clinical immunology and immunopathology* **89**, 44-53 (1998).

77 Nath, A., Chattopadhya, S., Chattopadhyay, U. & Sharma, N. K. Macrophage inflammatory protein (MIP)1alpha and MIP1beta differentially regulate release of inflammatory cytokines and generation of tumoricidal monocytes in malignancy. *Cancer immunology, immunotherapy : CII* **55**, 1534-1541, doi:10.1007/s00262-006-0149-3 (2006).

78 Matsumoto, Y., Park, I. K. & Kohyama, K. Matrix metalloproteinase (MMP)-9, but not MMP-2, is involved in the development and progression of C protein-induced myocarditis and subsequent dilated cardiomyopathy. *J Immunol* **183**, 4773-4781, doi:10.4049/jimmunol.0900871 (2009).

79 Ducharme, A. *et al.* Targeted deletion of matrix metalloproteinase-9 attenuates left ventricular enlargement and collagen accumulation after experimental myocardial infarction. *The Journal of clinical investigation* **106**, 55-62, doi:10.1172/JCI8768 (2000).

80 Murray, L. A. *et al.* TGF-beta driven lung fibrosis is macrophage dependent and blocked by Serum amyloid P. *The international journal of biochemistry & cell biology* **43**, 154-162, doi:10.1016/j.biocel.2010.10.013 (2011).

81 Varga, J. & Jimenez, S. A. Stimulation of normal human fibroblast collagen production and processing by transforming growth factor-beta. *Biochemical and biophysical research communications* **138**, 974-980 (1986).

82 Isumi, Y. *et al.* Adrenomedullin stimulates interleukin-6 production in Swiss 3T3 cells. *Biochemical and biophysical research communications* **244**, 325-331, doi:10.1006/bbrc.1998.8261 (1998).

83 Oshikawa, K., Yamasawa, H. & Sugiyama, Y. Human lung fibroblasts inhibit macrophage inflammatory protein-1alpha production by lipopolysaccharide-stimulated macrophages. *Biochemical and biophysical research communications* **312**, 650-655, doi:10.1016/j.bbrc.2003.10.166 (2003).

84 Vancheri, C. *et al.* Human lung fibroblasts inhibit tumor necrosis factor-alpha production by LPS-activated monocytes. *American journal of respiratory cell and molecular biology* **15**, 460-466, doi:10.1165/ajrcmb.15.4.8879179 (1996).

85 Satriano, J. A. *et al.* Regulation of monocyte chemoattractant protein-1 and macrophage colony-stimulating factor-1 by IFN-gamma, tumor necrosis factor-alpha, IgG aggregates, and cAMP in mouse mesangial cells. *J Immunol* **150**, 1971-1978 (1993).

86 Zeng, Q. & Chen, W. The functional behavior of a macrophage/fibroblast co-culture model derived from normal and diabetic mice with a marine gelatin-oxidized alginate hydrogel. *Biomaterials* **31**, 5772-5781, doi:10.1016/j.biomaterials.2010.04.022 (2010).

87 Huybrechts-Godin, G., Hauser, P. & Vaes, G. Macrophage-fibroblast interactions in collagenase production and cartilage degradation. *The Biochemical journal* **184**, 643-650 (1979).

88 Feletou, M. in *The Endothelium: Part 1: Multiple Functions of the Endothelial Cells-Focus on Endothelium-Derived Vasoactive Mediators Integrated Systems Physiology: from Molecule to Function to Disease* (2011).

89 Yoo, S. Y. & Kwon, S. M. Angiogenesis and its therapeutic opportunities. *Mediators of inflammation* **2013**, 127170, doi:10.1155/2013/127170 (2013).

90 Nucera, S., Biziato, D. & De Palma, M. The interplay between macrophages and angiogenesis in development, tissue injury and regeneration. *The International journal of developmental biology* **55**, 495-503, doi:10.1387/ijdb.103227sn (2011).

91 Fung, E. & Helisch, A. Macrophages in collateral arteriogenesis. *Frontiers in physiology* **3**, 353, doi:10.3389/fphys.2012.00353 (2012).

92 Wacker, A. & Gerhardt, H. Endothelial development taking shape. *Current opinion in cell biology* **23**, 676-685, doi:10.1016/j.ceb.2011.10.002 (2011).

93 Anghelina, M., Krishnan, P., Moldovan, L. & Moldovan, N. I. Monocytes/macrophages cooperate with progenitor cells during neovascularization and tissue repair: conversion of cell columns into fibrovascular bundles. *Am J Pathol* **168**, 529-541, doi:10.2353/ajpath.2006.050255 (2006).

94 Anghelina, M., Moldovan, L., Zabuawala, T., Ostrowski, M. C. & Moldovan, N. I. A subpopulation of peritoneal macrophages form capillarylike lumens and branching patterns in vitro. *J Cell Mol Med* **10**, 708-715 (2006).

95 Fantin, A. *et al.* Tissue macrophages act as cellular chaperones for vascular anastomosis downstream of VEGF-mediated endothelial tip cell induction. *Blood* **116**, 829-840, doi:10.1182/blood-2009-12-257832 (2010).

96 Tammela, T. *et al.* VEGFR-3 controls tip to stalk conversion at vessel fusion sites by reinforcing Notch signalling. *Nature cell biology* **13**, 1202-1213, doi:10.1038/ncb2331 (2011).

97 Hibino, N. *et al.* A critical role for macrophages in neovessel formation and the development of stenosis in tissue-engineered vascular grafts. *FASEB J* **25**, 4253-4263, doi:10.1096/fj.11-186585 (2011).

98 Roh, J. D. *et al.* Tissue-engineered vascular grafts transform into mature blood vessels via an inflammation-mediated process of vascular remodeling. *Proc Natl Acad Sci U S A* **107**, 4669-4674, doi:10.1073/pnas.0911465107 (2010).

99 Schubert, S. Y., Benarroch, A., Ostvang, J. & Edelman, E. R. Regulation of endothelial cell proliferation by primary monocytes. *Arterioscler Thromb Vasc Biol* **28**, 97-104, doi:10.1161/ATVBAHA.107.157537 (2008).

100 Mayer, A., Hiebl, B., Lendlein, A. & Jung, F. Support of HUVEC proliferation by pro-angiogenic intermediate CD163+ monocytes/macrophages: a co-culture experiment. *Clin Hemorheol Microcirc* **49**, 423-430, doi:10.3233/CH-2011-1492 (2011).

101 Hiebl, B. *et al.* Influence of VEGF stimulated human macrophages on the proliferation of dermal microvascular endothelial cells: Coculture experiments. *Clin Hemorheol Microcirc* **46**, 211-216, doi:10.3233/CH-2010-1347 (2010).

102 Mayer, A., Roch, T., Kratz, K., Lendlein, A. & Jung, F. Pro-angiogenic CD14(++) CD16(+) CD163(+) monocytes accelerate the in vitro endothelialization of soft hydrophobic poly (n-butyl acrylate) networks. *Acta Biomater* **8**, 4253-4259, doi:10.1016/j.actbio.2012.08.011 (2012).

103 Clanchy, F. I. & Hamilton, J. A. HUVEC co-culture and haematopoietic growth factors modulate human proliferative monocyte activity. *Cytokine* **59**, 31-34, doi:10.1016/j.cyto.2012.03.029 (2012).

104 Pakala, R. & Benedict, C. R. Endothelial cells regulate the proliferation of monocytes in vitro. *Atherosclerosis* **147**, 25-32 (1999).

105 Tso, C., Rye, K. A. & Barter, P. Phenotypic and functional changes in blood monocytes following adherence to endothelium. *Plos One* **7**, e37091, doi:10.1371/journal.pone.0037091 (2012).

106 Thomas-Ecker, S. *et al.* Alteration in the gene expression pattern of primary monocytes after adhesion to endothelial cells. *Proc Natl Acad Sci U S A* **104**, 5539-5544, doi:10.1073/pnas.0700732104 (2007).

107 Krenning, G., Dankers, P. Y., Jovanovic, D., van Luyn, M. J. & Harmsen, M. C. Efficient differentiation of CD14+ monocytic cells into endothelial cells on degradable biomaterials. *Biomaterials* **28**, 1470-1479, doi:10.1016/j.biomaterials.2006.11.017 (2007).

108 Bellik, L., Musilli, C., Vinci, M. C., Ledda, F. & Parenti, A. Human mature endothelial cells modulate peripheral blood mononuclear cell differentiation toward an endothelial phenotype. *Exp Cell Res* **314**, 2965-2974, doi:10.1016/j.yexcr.2008.07.016 (2008).

109 Schmeisser, A. *et al.* Monocytes coexpress endothelial and macrophagocytic lineage markers and form cord-like structures in Matrigel under angiogenic conditions. *Cardiovascular research* **49**, 671-680 (2001).

110 Pakala, R., Watanabe, T. & Benedict, C. R. Induction of endothelial cell proliferation by angiogenic factors released by activated monocytes. *Cardiovasc Radiat Med* **3**, 95-101 (2002).

111 L'Vova T, Y. *et al.* Effect of Monocyte-Like THP-1 Cells on the Formation of Vascular Tubes by EA.Hy926s Endothelial Cells in the Presence of Cytokines. *Bull Exp Biol Med* **159**, 146-151, doi:10.1007/s10517-015-2911-z (2015).

112 Palmieri, D., Mura, M., Mambrini, S. & Palombo, D. Effects of Pleiotrophin on endothelial and inflammatory cells: Pro-angiogenic and anti-inflammatory properties and potential role for vascular bio-prosthesis endothelialization. *Adv Med Sci* **60**, 287-293, doi:10.1016/j.advms.2015.05.003 (2015).

113 Dagtekin, G., Schiffer, R., Klein, B., Jahnen-Dechent, W. & Zwadlo-Klarwasser, G. Modulation of angiogenic functions in human macrophages by biomaterials. *Biomaterials* **24**, 3395-3401 (2003).

114 Boccafoschi, F. *et al.* Biological evaluation of materials for cardiovascular application: the role of the short-term inflammatory response in endothelial regeneration. *J Biomed Mater Res A* **101**, 3131-3140, doi:10.1002/jbm.a.34630 (2013).

115 Maciel, J. *et al.* Adsorbed fibrinogen enhances production of bone- and angiogenic-related factors by monocytes/macrophages. *Tissue Eng Part A* **20**, 250-263, doi:10.1089/ten.TEA.2012.0439 (2014).

116 Zachman, A. L. *et al.* Pro-angiogenic and anti-inflammatory regulation by functional peptides loaded in polymeric implants for soft tissue regeneration. *Tissue Eng Part A* **19**, 437-447, doi:10.1089/ten.TEA.2012.0158 (2013).

117 Wernike, E. *et al.* VEGF incorporated into calcium phosphate ceramics promotes vascularisation and bone formation in vivo. *Eur Cell Mater* **19**, 30-40 (2010).

118 Hsu, C. W. *et al.* Improved Angiogenesis in Response to Localized Delivery of Macrophage-Recruiting Molecules. *Plos One* **10**, e0131643, doi:10.1371/journal.pone.0131643 (2015).

119 Kidd, K. R. *et al.* Stimulated endothelial cell adhesion and angiogenesis with laminin-5 modification of expanded polytetrafluoroethylene. *Tissue engineering* **11**, 1379-1391, doi:10.1089/ten.2005.11.1379 (2005).

120 Kim, J. E. *et al.* Accelerated healing of cutaneous wounds using phytochemically stabilized gold nanoparticle deposited hydrocolloid membranes. *Biomater Sci* **3**, 509-519, doi:10.1039/c4bm00390j (2015).

121 Liu, Q. *et al.* Acceleration of skin regeneration in full-thickness burns by incorporation of bFGF-loaded alginate microspheres into a CMCS-PVA hydrogel. *J Tissue Eng Regen Med*, doi:10.1002/term.2057 (2015).

122 Oliveira, H. *et al.* The proangiogenic potential of a novel calcium releasing biomaterial: Impact on cell recruitment. *Acta Biomater* **29**, 435-445, doi:10.1016/j.actbio.2015.10.003 (2016).

123 Spiller, K. L. *et al.* The role of macrophage phenotype in vascularization of tissue engineering scaffolds. *Biomaterials* **35**, 4477-4488, doi:10.1016/j.biomaterials.2014.02.012 (2014).

124 Spiller, K. L. *et al.* Sequential delivery of immunomodulatory cytokines to facilitate the M1-to-M2 transition of macrophages and enhance vascularization of bone scaffolds. *Biomaterials* **37**, 194-207, doi:10.1016/j.biomaterials.2014.10.017 (2015).

125 Garg, K., Pullen, N. A., Oskeritzian, C. A., Ryan, J. J. & Bowlin, G. L. Macrophage functional polarization (M1/M2) in response to varying fiber and pore dimensions of electrospun scaffolds. *Biomaterials* **34**, 4439-4451, doi:10.1016/j.biomaterials.2013.02.065 (2013).

126 Xiao, X. *et al.* The promotion of angiogenesis induced by three-dimensional porous beta-tricalcium phosphate scaffold with different interconnection sizes via activation of PI3K/Akt pathways. *Sci Rep* **5**, 9409, doi:10.1038/srep09409 (2015).

127 Mak, I. W. Y., Evaniew, N. & Ghert, M. Lost in translation: animal models and clinical trials in cancer treatment. *Am J Transl Res* **6**, 114-118 (2014).

128 Mestas, J. & Hughes, C. C. W. Of Mice and Not Men: Differences between Mouse and Human Immunology. *The Journal of Immunology* **172**, 2731-2738, doi:10.4049/jimmunol.172.5.2731 (2004).

129 Chamberlain, L. M., Godek, M. L., Gonzalez-Juarrero, M. & Grainger, D. W. Phenotypic non-equivalence of murine (monocyte-) macrophage cells in biomaterial and inflammatory models. *Journal of Biomedical Materials Research Part A* **88**, 858-871 (2009).

130 Chanput, W., Mes, J. J. & Wichers, H. J. THP-1 cell line: An in vitro cell model for immune modulation approach. *Int Immunopharmacol* **23**, 37-45 (2014).

131 Crisostomo, P. R. *et al.* High passage number of stem cells adversely affects stem cell activation and myocardial protection. *Shock* **26**, 575-580, doi:10.1097/01.shk.0000235087.45798.93 (2006).

132 Casiraghi, F. *et al.* Localization of Mesenchymal Stromal Cells Dictates Their Immune or Proinflammatory Effects in Kidney Transplantation. *Am J Transplant* **12**, 2373-2383 (2012).

133 Roumestan, C. *et al.* Anti-inflammatory properties of desipramine and fluoxetine. *Respiratory research* **8**, 35, doi:10.1186/1465-9921-8-35 (2007).

134 Schutte, R. J., Parisi-Amon, A. & Reichert, W. M. Cytokine profiling using monocytes/macrophages cultured on common biomaterials with a range of surface chemistries. *J Biomed Mater Res A* **88**, 128-139, doi:10.1002/jbm.a.31863 (2009).

135 Smith, M. J., Smith, D. C., White, K. L. & Bowlin, G. L. Immune Response Testing of Electrospun Polymers: An Important Consideration in the Evaluation of Biomaterials. *J Eng Fiber Fabr* **2**, 41-47 (2007).

136 Chien, S. Mechanotransduction and endothelial cell homeostasis: the wisdom of the cell. *American Journal of Physiology - Heart and Circulatory Physiology* **292**, H1209-H1224, doi:10.1152/ajpheart.01047.2006 (2007).

137 Uzarski, J. S., Scott, E. W. & McFetridge, P. S. Adaptation of Endothelial Cells to Physiologically-Modeled, Variable Shear Stress. *Plos One* **8**, e57004, doi:10.1371/journal.pone.0057004 (2013).

CHAPTER 1.3

Thesis outlook

A comprehensive overview of the state of art in cardiovascular tissue engineering is provided within this first introductory chapter **(Chapter 1.1)**. In addition, the importance of the host immune system – and its first cellular attraction of monocytes/macrophages – is pointed out in response to any implant for regenerative applications **(Chapter 1.2)**. In this regard, particularly MSCs have shown clinically and experimentally to support the *in situ* tissue remodeling after biomaterial implantation via an inflammation-mediated cellular cascade. Therefore, two chapters of this thesis are focusing on the characterization of MSCs from different tissue origins such as the bone marrow (BMSCs), adipose tissue (ADSCs), umbilical cord Wharton's jelly (WJSCs) and amniotic fluid (AFCs) **(Chapter 2 and 3)**, followed by a section on biodegradable scaffold matrixes for cardiovascular tissue engineering applications **(Chapter 4)**. Combining MSCs with certain polymer matrices may allow may allow for new delivery routes and specific tissue properties of bioengineered materials in the future.

Therefore, a better understanding of the phenotype, origin and underlying mechanisms of MSCs seems mandatory. Given that not the MSCs themselves but their secretome initiates first attraction of host cells to the transplant site, a systematic comparison of different therapeutically relevant MSCs enabled to define the most potent secretome composition for host immune cell attraction and angiogenesis **(Chapter 2.1)**. In the future these knowledge might be used to create "synthetic, non-cellular factors" that could be implemented within biodegradable scaffolds for *in situ* tissue engineering applications. AFCs were investigated in the standard ovine developmental model, which uniquely enables investigation of prenatally harvested fetal (stem) cells without any ethical and medical restrictions **(Chapter 3)**. Species differences were first evaluated to assure accurate MSC isolation from the anatomical different ovine fetal fluid cavities **(Chapter 3.1)**. Subsequently the "broadly multipotent" state of AFCs was investigated to exemplify that MSC origin influence expression levels of pluripotency related genes and ultimately cellular phenotype **(Chapter 3.2)**. In chapter 4, biodegradable scaffolds for the *in situ* tissue engineering approach were evaluated **(Chapter 4)**. The feasibility of a rapid and automated fabrication of extracellular matrix for *in situ* heart valve tissue engineering was tested *in vitro* and in the ovine animal model **(Chapter 4.1)**. At the end, the results of all studies are critically discussed with the focus on the clinical translation of MSCs **(Chapter 5)**.

2

Mesenchymal stem cells for inflammation-mediated angiogenesis

The content of this chapter is based on:

Kehl D, Mallone A, Generali M, Uldry AC, Heller M, Gantenbein B, Hoerstrup SP, Weber B. A proteomic approach: hWJSC secretome retains the highest inflammation-mediated angiogenesis potential. *(in preparation, 2017)*

CHAPTER 2.1

A proteomic approach: hWJSC secretome retains the highest inflammation-mediated angiogenesis potential

Debora Kehl[1], Anna Mallone[1], Melanie Generali[1], Anne-Christine Uldry[2], Manfred Heller[2], Benjamin Gantenbein[3,4], Simon P. Hoerstrup[1,3,5], Benedikt Weber[1,3,5]

[1] Institute for Regenerative Medicine (IREM), Center for Therapy Development and Good Manufacturing Practice, University of Zurich, Zurich, Switzerland
[2] Mass Spectrometry and Proteomics Core Facility, Department of Clinical Research, University of Bern, Bern, Switzerland
[3] Center for Applied Biotechnology and Molecular Medicine (CABMM), University of Zurich, Zurich, Switzerland
[4] Tissue and Organ Mechanobiology, Institute for Surgical Technology and Biomechanics, University of Bern, Switzerland
[5] Zurich Center for Integrative Human Physiology (ZHIP), University of Zurich, Zurich, Switzerland

Abstract

Mesenchymal stem cells (MSCs) secretome has shown to promote *in vivo* angiogenesis and endogenous regeneration in an inflammation dependent way. Recent studies emphasize that the secretome of MSC derived from different tissue sources have distinct profiles and ultimately functional responses. In this regard, the presented study systematically compares MSC secretomes from several donors from human adipose tissue (hADSCs), bone marrow (hBMSC) and umbilical cord Wharton's jelly (hWJSCs) on their chemoattractive and angiogenic potential. For this approach the MSC secretomes have been derived using a GMP-compliant protocol. LC/MS-MS analyses revealed that hBMSC and hWJSC secretomes possess a stronger pro-angiogenic and inflammatory profile compared to hADSCs secretome. In particular, hADSC secretome did not only lack crucial pro-angiogenic proteins (e.g AKT1 and FGF2), but also expressed most of the proteins to a significantly lower level compared to hBMSC and hWJSC. These results on the proteomic level were functionally confirmed *in vitro* by a significantly higher $CD14^{++}$ $CD16^{-}$ monocyte migration towards hBMSC and hWJSC secretome. Both secretomes also induced a marked pro-angiogenic phenotype of endothelial cells *in vitro* indicated by a significantly higher expression of CD105, CD202b, CD144, CD31. Matrigel plug assay did not found any differences *in vivo*. These results enable a broad overview of the angiogenic potential of human MSCs from different tissue sources and will allow for a direct comparison of the therapeutic potential of different MSC sources.

Personal contribution:

Experimental contributions (Kehl D only):
Isolation and expansion of all cell lines, including hADSC (n=5), hBMSC (n=5), hWJSC (n=5) and HUVEC (n=1). Characterization of MSC cell lines in terms of proliferation, trilineage differentiation potential into adipogenic, osteogenic and chondrogenic lineages and common MSC surface markers by flow cytometry. MSC conditioned media (CM) harvest and concentration for all cell lines. Isolation of hPBMCs for transmigration assay. Flow cytometric analysis of hPBMC migration and staining of the migratory subsets. Co-incubation of MSC CM on HUVEC and the subsequent flow cytometry analysis of pro-angiogenic surface markers. Protein elution and separation using gel electrophoresis.

Experimental contributions (Kehl D, together with co-authors)
Analysis of flow cytometry data using bidimensional tSNE and PhenoGraph algorithms. *In vivo* injection of MSC CM into mice and explant of matrigel plugs for evaluation of angiogenic response. Mass spectrometry analysis, identifying proteins/pathways of interest.

Non-experimental contributions (Kehl D only):
Study design and planning of the study. Acquiring funding and ethical licenses for the isolation of hMSCs from primary human material and the *in vivo* matrigel plug assay. Statistical analyses. Analyzing all results and drafting all figures. Writing the entire manuscript. Correspondence with collaborating partners.

Steps contained in the published work (without personal contribution of Kehl D)
Alcian Blue PAS staining for the determination of chondrogenic differentiation potential. Generation of bidimensional t-SNE maps from multidimensional flow cytometry data and application of PhenoGraph and FlowSOM algorithms. Mass spectrometry in collaboration with the Mass Spectrometry Facility Bern, Manfred Heller and Anne-Christine Uldry. Determination of serum leftover using multiplex particle-based flow cytometric cytokine assay (A. Urwyler, Cytolab).

In preparation (2017)

2.1.1 INTRODUCTION

Since the introduction of mesenchymal stem cells (MSCs) for the use in regenerative medicine, the number of pre-clinical and first clinical studies has constantly increased over the last decades (ClinicalTrials.gov). Initial MSC research focused on the multilineage differentiation of cells towards desired phenotypes, though it has become evident that functional benefits exerted by MSCs upon transplantation are rather due to the release of paracrine factors and biologically relevant molecules such as exosomes and microvesicles to the neighboring diseased or injured tissue [1,2]. The so-called MSC secretome or conditioned media (CM) influences the microenvironment following injury, promoting cytoprotection and endogenous regeneration of the injured tissue environment. These effects are particularly of interest for the treatment of ischemic diseases, where promoting vascularization and reinstalling perfusion of the ischemic tissues via angiogenesis is crucial for increasing the chances of tissue rescue and to prevent fibrosis.

Angiogenic factors produced by MSC include among others basic fibroblast growth factor (bFGF), vascular endothelial growth factor (VEGF), transforming growth factor beta (TGF-β), platelet-derived growth factor (PDGF), angiopoietin-1 (ANG-1), placental growth factor (PIGF), interleukin 6 (IL-6) ad monocyte chemoattractant protein 1 (MCP-1) [3]. The MSC secretome positively stimulated angiogenesis *in vitro* and *in vivo* [3] and the angiogenic activity can be significantly inhibited by neutralizing antibodies against VEGF, MCP-1 and IL-6 [4]. Exosomes may also mediate angiogenesis by transferring genetic material and pro-angiogenic molecules to the damaged areas and seem to be key factors for angiogenesis [5]. Additionally, inflammatory cells have shown to migrate towards MSC secretome and participate in the angiogenic process by secreting cytokines themselves that infuence endothelial cell (EC) function, including their activation, proliferation and migration [6]. Moreover, infiltrating monocytes/macrophages release proteases to regulate patterning and local degradation of the extracellular matrix (ECM), influencing the distribution of neovessel formation and their branch points [7,8].

Although most isolated secretomes from different MSC sources revealed angiogenesis-related proteins, the secreted factors seem to be distinct in composition and amount. In this regard, mass spectrometry analyses revealed higher secreted levels of hepatocyte growth factor (HGF), VEGF and IL-6 in rat adipose derived MSC (ADSCs), whereas rat bone marrow derived MSC (BMSCs) secreted higher amounts of cell migration-related chemokine stromal cell-derived factor 1 alpha (SDF-1α) [9]. On the other hand, human ADSCs expressed higher levels of insulin-like growth factor 1 (IGF-1), VEGF-D and IL-8 compared to human BMSCs, whereas other factor such as VEGF-A, bFGF, SDF-1 and angiogenin were expressed at similar levels without significant differences [10]. In the secretome of human Wharton's jelly derived MSCs (WJSCs) more secreted factors involved in angiogenesis were

found compared to human BMSCs, inducing better i*n vitro* microvasculature formation and endothelial cell migration [11]. Quantitative proteomics revealed an increased angiogenic profile within the secretome of MSC isolated from fetal rather than from adult skin [12]. Thus, these studies demonstrate that MSCs isolated from different tissue sources show dissimilarities with respect to their transcriptional, proteomic and functional profile. A systematic comparative analysis of the chemoattractive as well as angiogenic potential of MSC secretome isolated from different clinically relevant MSC sources has not been performed yet. Moreover, mostly targeted proteomic approaches have been used so far with only a fraction of angiogenic proteins identified.

Therefore, the presented study aimed to isolate and fully characterize MSCs secretomes from several donors from human adipose tissue (hADSCs), bone marrow (hBMSCs) and umbilical cord Wharton's jelly (hWJSCs) in order to systematically compare their chemoattractive and angiogenic potential. Importantly, MSC secretomes were obtained under standardized GMP-compliant culture protocols using human platelet lysate to replace xenogenic serum supplements. Firstly, we used high-resolution, two-dimensional liquid chromatography tandem mass spectrometry (LC-MS/MS) for a broad proteomic profile of human MSC secretomes, with focus on proteins related to inflammation and angiogenesis. Secondly, we differentially analyzed the functional response of MSC secretomes from different origins to define which MSC source possesses the highest potential for inducing inflammation mediated angiogenesis *in vitro* and *in vivo*.

2.1.2 MATERIAL AND METHODS

2.1.2.1 hMSC ISOLATION FROM DIFFERENT HUMAN TISSUES

All hMSC were isolated as described below and cultured in standard proliferation medium consisting of high-glucose DMEM supplemented with 10% human platelet lysate (hPL), 1% Glutamax (Gibco, USA), and an antibiotic-antimycotic solution (Sigma, Switzerland). hPL was obtained from platelet apheresis collection of donors compliant with local blood donation prerequisite (Center for Blood Donation Zurich, Switzerland). Medium changes for all cell sources were performed every third day and passaging was performed after reaching 80% confluence using Accustase (Innovative Cell Technologies Inc., USA).

HUMAN ADIPOSE DERIVED MESENCHYMAL STEM CELLS (hADSCs)

Adipose tissue (n=5) obtained from surgically performed liposuction procedure was used for the isolation of hADSCs approved by the cantonal ethics committee (KEK-ZH-2010-0476). Adipose tissue was digested using collagenase type A (Roche Diagnostics GmbH, Switzerland) at 37°C for 1h under constant gentle motion. The sample was filtered using a nylon cell strainer with 70µm mesh size (BD Bioscience, USA) and separated by histopaque-1077 density gradient centrifugation (Sigma, Switzerland) for 30min at 600g. The interphase was plated in standard proliferation medium for cellular attachment and growth.

HUMAN BONE MARROW DERIVED MESENCHYMAL STEM CELLS (hBMSCs)

Human bone marrow aspirate (n=5) was collected in sterile heparinized tubes (BD Bioscience, USA) after written informed consent from the patients. For isolation of hBMSCs the aspirate was separated by histopaque-1077 density gradient centrifugation for 25min at 800g. Subsequently, the mononuclear cell layer was collected, washed and plated in standard proliferation medium.

HUMAN WHARTON'S JELLY DERIVED MESENCHYMAL STEM CELLS (hWJSCs)

Human umbilical cords (n=5) were obtained after full-term births with written informed consent of the patient (KEK-ZH-2009-0095) and processed for isolation of hWJSC. Wharton's jelly was dissected from the umbilical cord and cut into small pieces (1mm^2). After letting the tissues adhere to the culture plate, standard proliferation medium was gently added. Tissue pieces were removed after a first cellular outgrowth could be detected and cells were harvested.

2.1.2.2 hMSC CHARACTERIZATION

DIFFERENTIATION POTENTIAL

Multillineage differentiation was assessed by inducing differentiation to osteocytes, adipocytes and chondrocytes. Therefore, hMSCs from adipose tissue (n=5), bone marrow (n=5) and Wharton's jelly (n=5) were either cultured in I) osteogenic medium: 10nM glycerol 2-phosphate (Sigma, Switzerland), 50µm L-ascorbic acid 2-phosphat (Sigma, Switzerland), 100nM dexamethasone (Sigma, Switzerland) and 2nM L-glutamine (Sigma, Switzerland) in low glucose DMEM (Sigma, Switzerland) with 10% hPL and an antibiotic-antimycotic solution, II) adipogenic medium (Gibco™, ThermoFisher Scientific, USA) or III) chondrogenic medium: 50µm L-ascorbic acid 2-phosphate, 0.5 ug/ml insulin (Sigma, Switzerland), 10 ng/ml transforming growth factor-beta1 (Preprotech, UK), 2 mM L-glutamine in high glucose DMEM with 1% hPL and an antibiotic-antimycotic solution. After 3 weeks, cells were fixed in 4% paraformaldehyde/PBS and subsequently stained with I) 2% Alzarin Red S (Sigma, Switzerland), II) 3mg/ml Oil Red O (Sigma, Switzerland) or III) Alcian Blue PAS.

PROLIFERATION PARAMETERS

Proliferation kinetics were assessed over 12 days for hADSC, hWJSC and hBMSC (n=5 per cell source). The amount of total cells after every third day was measured based on the absorbance of crystal violet. In brief, cells were fixed with methanol (Sigma, Switzerland) for 10min and subsequently stained with 0.1% crystal violet (Artechemis, Switzerland) for 5min. After washing and air-drying, absorbed crystal violet was solubilized with Na-deoxycholate (Sigma, Switzerland) while being heated at 60°C for 10min. The absorbance was recorded at 550nm using a standard ELISA reader Synergy HT (Bio TEK, USA). Quantitative data was obtained using a standard curve with serial dilutions. Cumulative population doubling (PD) rate and generation time (GT) were calculated according to previous described formula [13].

MSC MARKER EXPRESSION BY FLOW CYTOMETRY

Isolated hMSCs (n=5 per tissue source) were characterized for common MSC markers using flow cytometry. 2.5 x 10^5 MSCs were stained for 20min at 4°C according to standard procedures with the following antibodies: Pacific Blue mouse-anti human CD73 (clone AD2; Biolegend, USA), PerCP-Cy5.5 mouse anti-human CD90 (clone 5E10; BD Bioscience, USA), APC mouse anti-human CD105 (clone 266; BD Bioscience, USA), FITC mouse anti-human CD14 (clone MϕP; BD Bioscience, USA), PE mouse anti-human CD34 (clone 581; BD Bioscience, USA), BV605 mouse anti-human CD45 (clone HI30; BD Bioscience, USA) and Zombie Aqua fixable viability kit (Biolegend, USA). Antibodies have been used in

saturating conditions defined by serial dilutions. 50'000 events were acquired using a LSR Fortessa (BD Bioscience, USA) and the datasets were analyzed by FlowJo software (Tree Star, Inc., USA). Bidimensional t-SNE maps were generated from multidimensional flow cytometry data sets using the open source R platform and the Cytokit package (http://bioconductor.org). Firstly, 2000 events were randomly selected from the analyzed sample. Secondly, the selected events were clustered using PhenoGraph algorithm (k=42). PhenoGraph arranged all events in the multidimensional space according to similarities in surface marker expression levels and allowed to plot the data in two dimensions using bi-dimensional visual stochastic neighbor embedding (vi-SNE) graphs. We used the wi-SNE graphs to analyze and detect subset differences in MSC marker expression profile.

2.1.2.3 hMSC CONDITIONED MEDIA HARVEST

For hMSC conditioned media (CM) harvest, all hMSC lines (n=5 per tissue source) were cultured until 80% confluence in standard proliferation medium, washed with PBS and subsequently transferred to serum free conditions (basal medium only) for 16 hours. Collected CM was filtered using a 0.2µm filter, concentrated using centrifugal filter units with a 3-kDA cutoff at 4°C (Amicon Ultra Centrifugal filters, Millipore, USA) and stored at 80°C for further analysis. Exact number and viability of starved cells was obtained using a NucleoCounter NC-200 (CHemoMetec, Denmark). Aliquots of stored CM were always derived from $1x10^6$ cells in 200µl. Possible serum leftover of the primarily added hPL was assessed by quantitative evaluation of platelet factor 4 (PF-4) using a multiplex particle-based flow cytometric cytokine assay [14].

2.1.2.4 MASS SPECTROMETRY ANALYSIS

Proteins of MSC CM derived from $1x10^6$ cells (not concentrated with centrifugal filter units) were gained using 5µl Strata Clean resin beads per ml of CM (Agilent Technologies, USA). Beads were incubated for 30min by rotation at room temperature and subsequently centrifuged with 230g for 2min. Proteins were eluted from bead pellets by the addition of Laemmli buffer and boiling at 95°C for 5min. Eluted proteins of all MSC CM and their corresponding controls were loaded onto 12% SDS-Page gels (Sigma-Aldrich, Switzerland) and subsequently digested as described elsewhere [15]. An aliquot of 5µl peptide extract was analyzed by LC-MS/MS on an EASY-nLC1000 chromatograph connected to a QExactive HF mass spectrometer (ThermoFisher Scientific) using a Pepmap100 Trap C18 300 mm x 5 mm (Thermo Fisher Scientific) and a C18 separation column (3µm, 100 Å, 75µm x 15 cm, Nikkyo Technos, Tokyo, Japan) by applying a 40 min gradient as previously described [16].

LC-MS/MS data was processed with MaxQuant (version 1.5.4.1) using default settings for peak detection, strict trypsin cleavage rule allowing for up to three missed cleavages, variable oxidation on

methionine, deamidation of asparagine and glutamine, and acetylation of protein N-termini with strict carbamidomethylation of cysteines. Match between runs was used within each sample group with a retention time window of 1min. The fragment spectra were interpreted with the SwissProt Homo sapiens database (version 2016_04) accepting only protein identifications with at least two razor peptides at a 1% false discovery rate (FDR) cutoff.

2.1.2.5 IMMUNE CELL RESPONSE

Heparinized human peripheral blood was obtained from randomly selected healthy donors (n=3) (KEK-ZH-2014-0430). Human peripheral blood mononuclear cells (hPBMCs) were isolated according to standard protocols by ficoll density gradient centrifugation (Histopaque-1077; Sigma, Switzerland). Migration of $3x10^6$ hPBMCs in 300µl basal medium supplemented with 0.5% fetal calf serum (FCS) (Sigma, Switzerland) towards the lower compartment containing either I) 0.1ml MSC CM + 0.5% FCS (n=5 per tissue source), II) basal medium + 0.5% FCS or II) 5ng/ml monocyte chemoattractant protein 1 (MCP-1) + 0.5% FCS, was evaluated through a PET membrane with 3µm pores (Corning, USA) after 3 hours. The amount of migrated cells was determined by recording cell counts over 1 min on a FACSCanto II (BD Bioscience, USA). Monocyte subpopulations were differentiated by staining with FITC mouse-anti human CD14 (clone MϕP9, BD Bioscience, USA) and PerCP-Cy5.5 mouse-anti human CD16 (clone 3G8, BD Bioscience, Switzerland).

2.1.2.6 ENDOTHELIAL CELL RESPONSE

IN VITRO ENDOTHELIAL CELL ACTIVATION ASSAY

Endothelial cells were harvested from human umbilical cords with written informed consent of the patient (KEK-ZH-2009-0095). Briefly, human umbilical cord vein endothelial cells (HUVEC) were dissociated from the venous lumen by incubating a collagenase solution (2mg/ml collagenase type A, Roche Diagnostics GmBH, Switzerland) for 30min in a humidified incubator at 37°C and obtained in endothelial growth medium (EGM-2; Lonza, Switzerland). After several passages, HUVEC were starved in endothelial basal medium (EBM-2; Lonza, Switzerland) with 1% FCS for 4 hours and co-incubated for 16h with either I) 0.2ml MSC CM + 0.5% FCS (n=5 per MSC group), II) 0.2ml EGM-2 (n=5) or III) 0.2ml basal DMEM + 0.5% FCS (n=5) per 100’000 HUVEC. Harvested HUVEC were stained 20min at 4°C with the following surface antibodies: V450 mouse-anti human CD31 (clone WM59, BD Bioscience, USA), FITC mouse-anti human CD105 (clone 43A3, Biolegend, USA), PerCP-Cy5.5 mouse-anti human CD144 (clone 55-7H1, BD Bioscience, USA) and PE mouse-anti human CD202b (clone 33.1, Biolegend, USA). 50’000 events were acquired using a LSR Fortessa and the datasets were

analyzed by FlowJo software. Bidimensional t-SNE maps were generated from multidimensional flow cytometry (5000 events) and PhenoGraph algorithm employed as previously described.

IN VIVO MATRIGEL PLUG ASSAY

C57BL/l mice (female, 7-week old) were divided into four groups: control (n=5; basal medium), hADSC CM (n=5; derived from $1x10^6$ cells), hBMSC CM (n=5; derived from $1x10^6$ cells) and hWJSC CM (n=5; derived from $1x10^6$ cells). For each condition 0.2ml of medium was mixed with 0.3ml phenol red-free, growth factor reduced basement membrane matrix (Corning, USA). Media were injected subcutaneously into the left and right dorsal flank of mice (n=10 per group). After 14 days, mice were sacrificed and the matrigel plugs were harvested. For quantitative evaluation, matrigel plugs were weighed and homogenized in cold PBS using a tissue homogenizer. The homogenate was centrifuged at 6000g for 10min and the hemoglobin content of the supernatant measured using Drabkin's reagent kit 525 (Sigma-Aldrich, Switzerland). The absorbance was read at 540nm using a standard ELISA reader Synergy HT. All animal experiments were approved by the Cantonal Ethics Committee (State Veterinary Office of the Canton of Zurich, Switzerland; No. 105/2016).

2.1.2.7 STATISTICAL ANALYSIS

Quantitative data are presented as mean±standard deviation (GraphPad Prism; Graph Pad Software, Inc.). For statistical comparison either One-Way ANOVA with Tukey multiple comparison test or Two-Way ANOVA with Sidak's multiple comparisons test was used. P-values < 0.05 were considered statistically significant (*$p<0.05$, **$p<0.01$, ***$p<0.001$).

For MS data analysis, peptide feature intensities reported in the evidence file were group-wise median normalized and the intensities of the three most intense peptides summed to the protein intensity. When a group had at least one positive identification, missing values were imputed from the low end of the LOG2 transformed intensity distribution from each individual sample using Perseus (version 1.5.5.3) as suggested by Lazar et al. [17]. Proteins identified in any of the three platelet controls were not used for further statistical evaluations. With the remaining proteins, pairwise Students T-tests and a multi sample ANOVA test were performed, applying a permutation based FDR of 1% as an acceptation criteria for differentially expressed proteins and to correct for multiple testing. The results of the two-sample T-tests is used to identify proteins that are significantly over- or under-expressed in one group compared to another. Gene set enrichment analysis (GSEA) can be applied to the selected over- or under-expressed proteins in order to detect pathways that occur significantly more than they would by chance alone. In this study the GSEA tool SetRank [18] (open source R package) was applied in its unranked form to all pairs of samples. In order to avoid sample

source bias, the reference set of proteins was in each case the union of proteins of the two samples under consideration. Unlike many other GSEA algorithms, SetRank avoids false positive hits by taking into account gene sets overlap when calculating their significance. The decision whether a protein is significantly over- or under-expressed was made by applying a cut-off according to the FDR acceptation criteria [19]. Gene sets containing more than 100 genes were ignored in order to avoid generic, uninformative gene sets. The network analysis was performed with a p-value cut-off for gene sets of 0.01, and a false discovery rate cut-off of 0.05.

2.1.3 RESULTS

2.1.3.1 hMSC CHARACTERIZATION

All primary isolated MSC from human adipose tissue (n=5), bone marrow (n=5) and umbilical cord Wharton's jelly (n=5) were successfully cultured in xenofree GMP-compliant proliferation medium based on human platelet lysate (hPL). These conditions are necessary for all further analyses including immune cell activation and migration. hADSCs showed higher proliferation abilities compared to hBMSCs and hWJSCs (Figure 1B-C). In detail, hADSCs showed a significantly higher cumulative population doublings (CPD) and lower generation time compared to hBMSCs (Figure 1C). hBMSCs and hWJSCs showed similar proliferation, with significant higher GT compared to hADSC ($p<0.05$) and a tendency of lower CPD. Therefore, subsequent CM harvest was performed based on the exact amount of cells after serum free incubation.

Multipotent MSC nature of isolated cells was confirmed by trilineage differentiation into adipogenic, osteogenic and chondrogenic lineages positively staining with Oil Red O, Alzarin Red S and Alcian Blue PAS (Figure 1A). Overall no differences were detected in the differentiation potential of MSC from different tissue sources.

Multidimensional data from the flow cytometry analysis performed using common MSC markers (CD14, CD34, CD45, CD74, CD90 and CD105) were processed to generate bidimensional t-SNE maps (n=5 donors per cell source) (Figure 1D-E). The distribution of the recorded events within the t-SNE maps was visualized with cumulative density plots (Figure 1D). The expression profile of each marker within each t-SNE graph was described by cumulative marker expression level plots (Figure 1D). MSCs from all sources positively expressed CD73, CD90 and CD105, and only a minimal proportion of cells were positive for CD14, CD34 and CD45. Interestingly, hADSCs and hWJSCs showed similar event distribution in contrast to hBMSCs, which possesses a more condensed population. The recorded events were subdivided into three sectors to compare I) sector-dependent event density and II) sector-dependent median fluorescence intensity (MFI) of each particular marker. hBMSCs appeared to be significantly more abundant in sector 3 ($p<0.001$) and less abundant in sector 1 ($p<0.001$), whereas hADSCs and hWJSCs were distributed within all three sectors. Sector 3 is characterized by higher MFIs of CD73, CD90 and CD105 as visualized in Figure 1G compared to sector 1 and 2. Therefore, these results indicate that even if all MSC sources express CD73, CD90 and CD105, the amount of surface proteins is different among different cell sources and that hBMSCs have a stronger MSC phenotype compared to hADSCs and hWJSCs. No differences were found for hADSCs and hWJSCs.

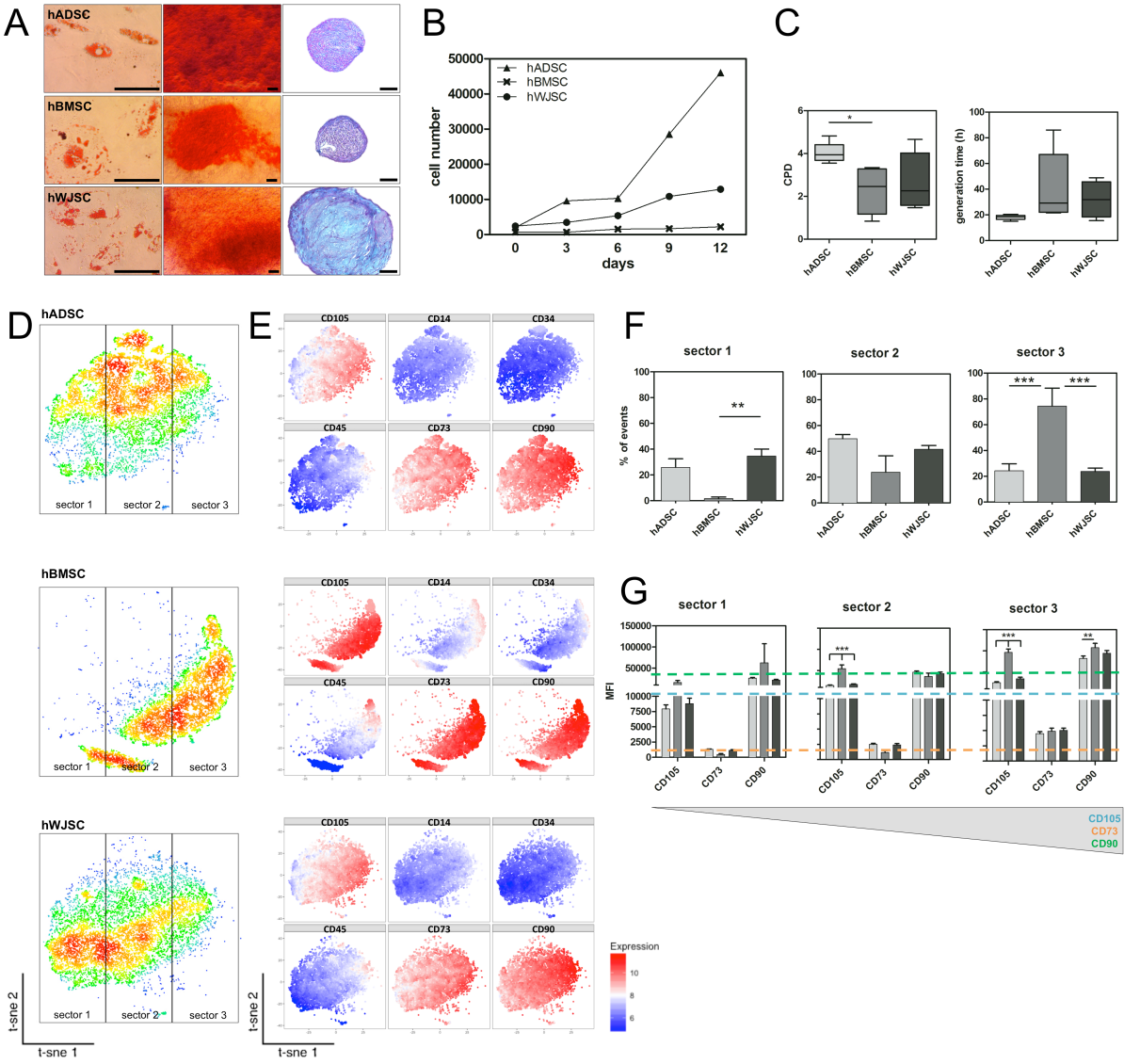

Figure 1: Characterization of hMSCs from adipose tissue, bone marrow and umbilical cord Wharton's jelly. (A) The capacity of hADSCs, hWJSCs and hBMSCs to differentiate into adipogenic (left), osteogenic (middle) and chondrogenic lineages (right) was demonstrated by positive staining with Oil Red O, Alzarin Red S and Alcian Blue PAS. Scale bar = 100µm. (B) Proliferation capacities between all hMSC sources were compared over 12 days by defining (F) the generation time (hours) and cumulative population doublings (CPD). (D-E) For phenotypic characterization, bidimensional t-SNE maps were generated from multidimensional flow cytometry data of common MSC markers CD73, CD90, CD105 and CD14, CD34, CD45. The cellular distribution of 5 donors per cell source is visualized with cumulative density plots (D), whereas the expression profile of each marker is described by marker expression level plots (red = expressed, blue = absent) (E). Recorded cells were distributed into three sectors to compare median fluorescence intensities (MFI). Percentage of events (F) and MFI (G) in each sector revealed that hBMSCs are significantly more abundant in sector 3, whereas hADSCs and hWJSCs are distributed within all three sectors. Sector 3 is defined by higher MFIs of CD73 (orange), CD90 (green) and CD105 (blue) as visualized by the mean lines of sector 1. No significant differences were detected between hADSCs and hWJSCs.

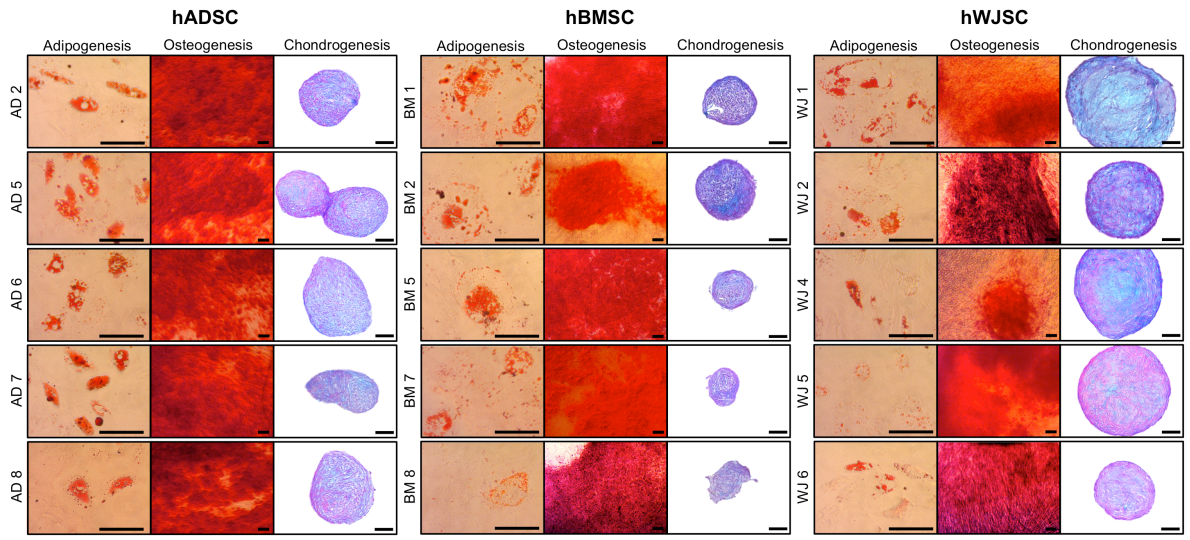

Supplementary Figure 1: Multilineage differentiation potential of hMSC from adipose tissue, bone marrow and umbilical cord Wharton's jelly. Differentiation of hADSC, hBMSC and hWJSC (n=5 per cell source) into adipogenic, osteogenic and chondrogenic lineages is visualized with Oil Red O, Alzarin Red S and Alcian Blue PAS. Scale bar = 100µm.

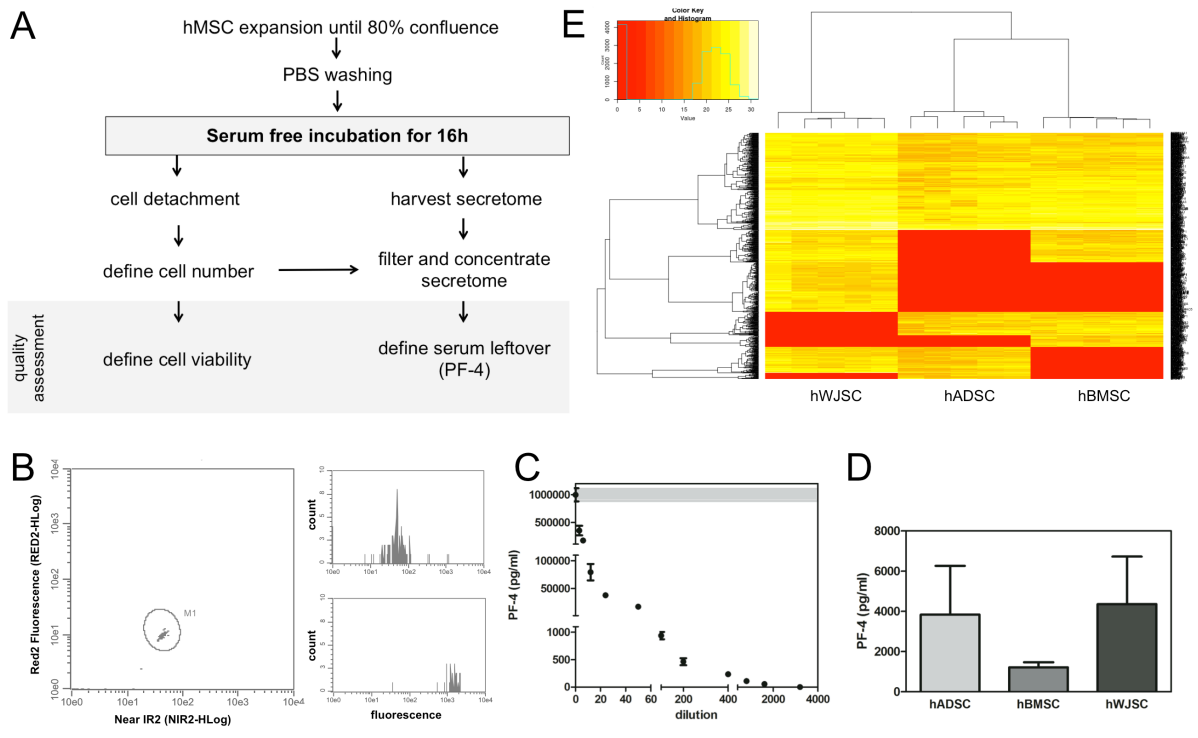

Figure 2: hMSC CM harvest. (A) Workflow for hMSC CM harvesting. Quality criteria have been defined, which consists of cellular viability and human platelet lysate (hPL) serum contamination, defined as platelet factor-4 (PF-4) leftover. (B-C) For the detection of serum contaminations, a serial dilution of 10% hPL in standard culture medium was performed using multiplexed particle-based flow cytometric cytokine assay. (B) Left panel displayed the gating of PF-4 and its quantification was done according to the right low and high standards. (C) At a dilution of 3200 no PF-4 could be detected, which demonstrates the baseline for subsequent functional assays and mass spectrometry analyses. (D) Concentrated secretoma (n=5 per cell source) revealed no significant differences in PF-4 leftover in all three MSC sources. (E) Proteins in the secretomes were relatively quantified by label-free proteomics approach. Red: protein not detected; Yellow: protein detected.

2.1.3.2 hMSC CM HARVEST

hMSC secretome, respectively conditioned media (CM) was harvested according to the workflow outlined in Figure 2A. Quality criteria were defined, which consisted of cellular viability after serum free incubation and remaining serum proteins in the incubating cells. Therefore, platelet factor 4 (PF-4), a protein of unique serum origin, was measured after incubation and further concentration of the harvested CM. Serial dilutions of human platelet lysate (figure 2B) allowed the comparison of the initial amount of hPL in normal proliferation medium (approximately 1ug/ml) with the one after the CM harvest procedure of hADSC (4360 ± 2371 pg/ml PF-4), hBMSC (1214 ± 254 pg/ml PF-4) and hWJSC (3840 ± 2429 pg/ml PF-4) (figure 2C). This data demonstrates that presented results on MSC CM are not biased by differences in leftover of hPL.

2.1.3.3 MASS SPECTROMETRY ANALYSIS

We focused on proteins involved in immune cell response (Figure 3) and angiogenesis (Figure 4) from the overall proteome and compared their intensities measured by LC/MS-MS. Proteins identified in any of the platelet lysate controls were excluded from the analysis, in order to assure that the proteins originated from the MSCs. Heat maps were generated according to protein intensities and significance displayed by pairwise student t-test. Location of the proteins was determined using the Uniprot.org database.

81 angiogenesis and endothelial cell function related proteins were detected in MSC secretome – 17 of these were cellular (meaning either intracellular or membrane bound, but not released or actively secreted into the extracellular space), 22 proteins were cellular with evidence of exosome and vesicle function, and 42 proteins were secreted into the extracellular space (Figure 4A). 7 of the proteins have been associated with a negative effect on angiogenesis according to literature (Figure 4A, proteins in red letter). According to the heat maps, 30 proteins showed significantly higher levels in hWJSC secretome compared to hBMSC and hADSC secretome. 10 proteins were significantly more abundant in hBMSC secretome compared to hWJSC and hADSC secretome. 13 were equally abundant in hBMSC and hWJSC secretome, but significantly higher than hADSCs. Only 3 proteins showed significantly higher levels in hADSC secretome compared to hBMSC and hWJSC secretome.

45 inflammation related proteins were detected in MSC secretome – 13 of these were cellular, 18 proteins were cellular with evidence of exosome and vesicle function, and 14 proteins were secreted into the extracellular space (Figure 3G). According to the heat maps, 18 showed significantly higher levels in hWJSC secretome, 2 in hBMSC secretome and 2 in hADSC secretome compared to the other sources. 7 were equally abundant in hBMSC and hWJSC secretome, but significantly higher than hADSCs.

To display protein interactions, all angiogenesis-related proteins were uploaded into String database and evaluated using Cytoscape. Figure 4B displays the interactions of all proteins related to angiogenesis, except of the ones not being part of any interaction (includes 18 proteins). Node size/color is based on the BetweennessCentrality defined by the combined score of String database. High ranked proteins are those, which possesses more interactions within the network. AKT1 and FGF2 were high ranked (blue in Figure 4B), followed by IL-6, PDGFRB, CTNNB1, PXN, VEGF-C, WNT5A, NOTCH3 (green in Figure 4B) and ENG, ANGPT1, TIMP2, PAX2, COL18A1, JAG1, EFNB2 (yellow in Figure 4C). Interestingly, out of this protein selection AKT1, FGF2, NOTCH3, ENG, ANGPT1, JAG1 and EFNB2 were not found in hADSC secretome, representing crucial angiogenic proteins within the network. Also hBMSC secretome showed lack of fundamental angiogenic proteins, missing AKT1 and EFNB2, whereas hWJSC secretome retained the more complete pro-angiogenic network by only missing NOTCH3. hWJSC secretome possessed not only a higher number of angiogenic proteins, but also specific pro-angiogenic proteins to a higher extent. Interestingly, similar highly ranked proteins such as AKT1, FGF2, IL6 and WNT5A were also found in the network related to inflammation and ranked accordingly (Figure 3H). Here 16 proteins were not part of any interaction and are not displayed.

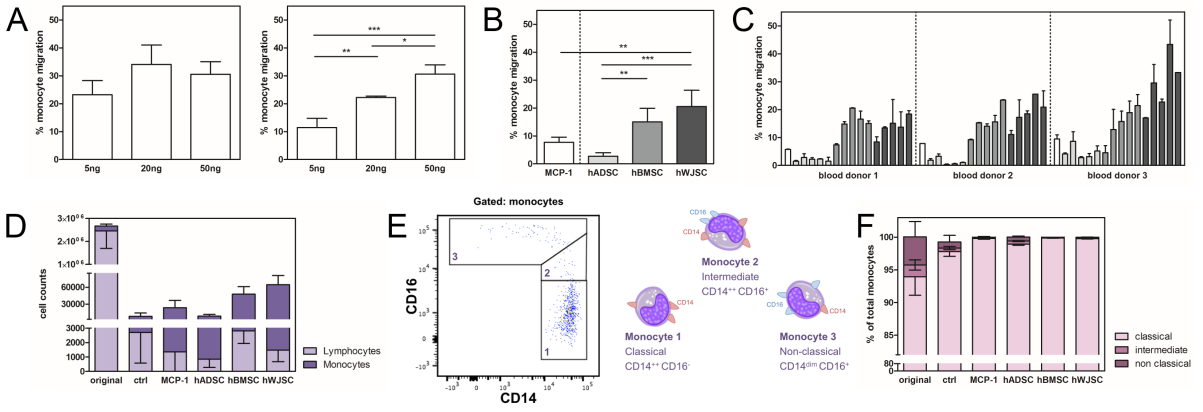

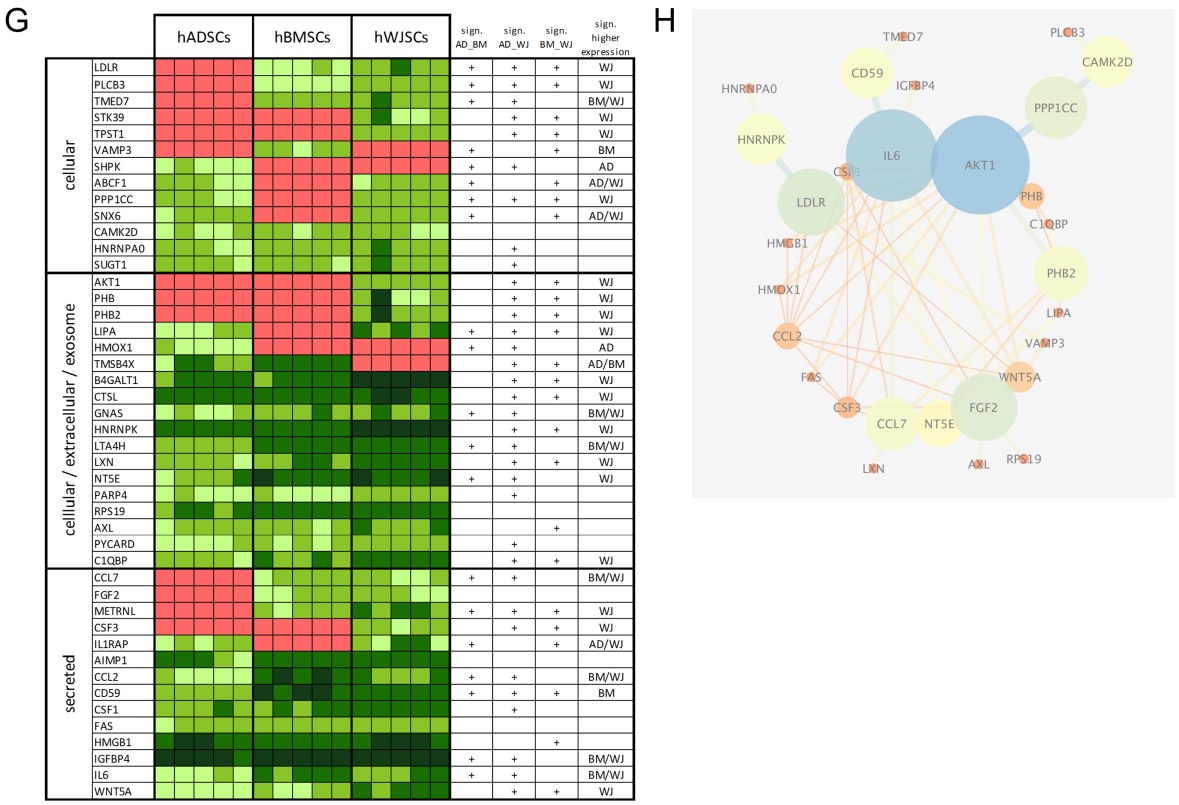

Figure 3: MSC CM induces immune cell response. (A) Concentration dependent migration of hPBMCs (n=3 healthy blood donors) through 3µm pores of a transwell insert was evaluated after 3hrs co-incubation with 5ng/ml, 20ng/ml and 50ng/ml MCP-1. Only at a starting amount of $3x10^6$ hPBMCs (right) and not of $1x10^6$ hPBMCs (left), significant differences in % of migration of total added monocytes could be detected. (B) Using $3x10^6$ hPBMCs, hMSC CM (n=5 per cell source) revealed enhanced migration of monocytes, with significantly higher migration of hBMSC CM and hWJSC CM in comparison to hADSC CM and 5ng/ml MCP-1 control. (C) Three individual healthy blood donors were used to define the chemoattractive potential of hMSC CM. (D) No essential lymphocyte migration (compared to initial population seeded) was detected. (E-F) MSC CM induced migration of mainly classical $CD14^{++}$ $CD16^{-}$ monocytes, but not of intermediate and non-classical monocytes, as revealed by a CD14 and CD16 staining. (G) MSC secretome proteins involved in immune cell response. Pairwise student t-test were performed to detect differences between secretomes obtained from hADSCs (AD), hBMSCs (BM) and hWJSCs (WJ) (n=5 per cell source). Significantly changed secretion is indicated by +. Heat map was generated based on protein intensities measured by LC/MS-MS (red = not detected, green = detected). (H) All identified proteins were uploaded into String database and evaluated using Cytoscape to define their interaction. Node size/color is based on the BetweennessCentrality defined by the combined score of String database, whereas low values are small size and orange (color code from low to high: orange – yellow – green – blue). The same principle was applied for map edge size/color. Proteins not being part of any interaction are not displayed.

2.1.3.4 IMMUNE CELL RESPONSE

The immune cell response induced by hMSC CM was tested by migration of hPBMCs from 3 independent healthy donors towards a transwell insert.

To assure concentration dependent migration of hPBMCs, the assay was established using 5ng/ml, 20ng/ml and 50ng/ml MCP-1. Only a starting amount of $3x10^6$ hPBMCs and not $1x10^6$ hPBMCs showed significant differences in percentage of migration of total added monocytes by flow cytometry (Figure 3A). All results are displayed with subtracted control migration of basal medium only. Using $3x10^6$ hPBMCs MSC CM enhanced migration of particularly monocytes (Figure 3B).

Significant higher monocyte migration to hBMSC CM ($p < 0.01$) and hWJSC CM ($p < 0.001$) compared to hADSC CM was found (n=5 per tissue source) (Figure 3B). No differences were detected between the CM of hBMSCs and hWJSC ($p = 0.14$). Monocyte migration of the three individual blood donors is displayed in figure 3C. Interestingly, no significant difference was detected in lymphocyte migration compared to the initial population seeded, supporting the immunomodulatory capacity of hMSC CM (Figure 3D). The original hPBMCs population consisted of 91.96 ± 2.02 % lymphocytes and 8.04 ± 2.02 % monocytes, when neglecting the small amount of dendritic cells (below 2 %). After migration, the following percentages of lymphocytes were found for hADSC CM 9.62 ± 7.53 %, hBMSC CM 5.89 ± 1.82 % and hWJSC CM 2.05 ± 1.24 % compared to basal medium only 24.58 ± 9.06 % and 5ng/ml MCP-1 3.34 ± 4.32 %, whereas the percentage of monocytes increased as followed for hADSC CM 90.38 ± 44.14 %, hBMSC CM 94.11 ± 27.93 % and hWJSC CM 97.95 ± 27.56 % compared to basal medium only 75.42 ± 83.84 % and 5ng/ml MCP-1 96.66 ± 53.83 %. To define the phenotype of migrated monocytes, a CD14 and CD16 staining enabled to classify the cells into three subgroups known as classical $CD14^{++}$ $CD16^{-}$ monocytes, intermediate $CD14^{++}$ $CD16^{+}$ monocytes and non-classical $CD14^{dim}$ $CD16^{+}$ monocytes (Figure 3E). The original seeded hPBMC population consisted of 93.50 ± 2.94 % classical, 2.04 ± 0.62 % intermediate and 4.51 ± 2.56 % non-classical monocytes of total monocytes analyzed (Figure 3E). After migration mainly classical hPBMCs prevailed with 98.99 ± 0.12 % classical, 0.47 ± 0.09 % intermediate and 0.54 ± 0.06 % non-classical for hADSC CM, 98.87 ± 0.02 % classical, 0.10 ± 0.02 % intermediate and 0.02 ± 0.01 % non-classical for hBMSC CM and 99.79 ± 0.07 % classical, 0.14 ± 0.05 % intermediate and 0.07 ± 0.03 % non-classical for hWJSC CM of total monocytes migrated. Whether monocyte phenotype change over migration or only classical monocytes migrate remains to be discussed.

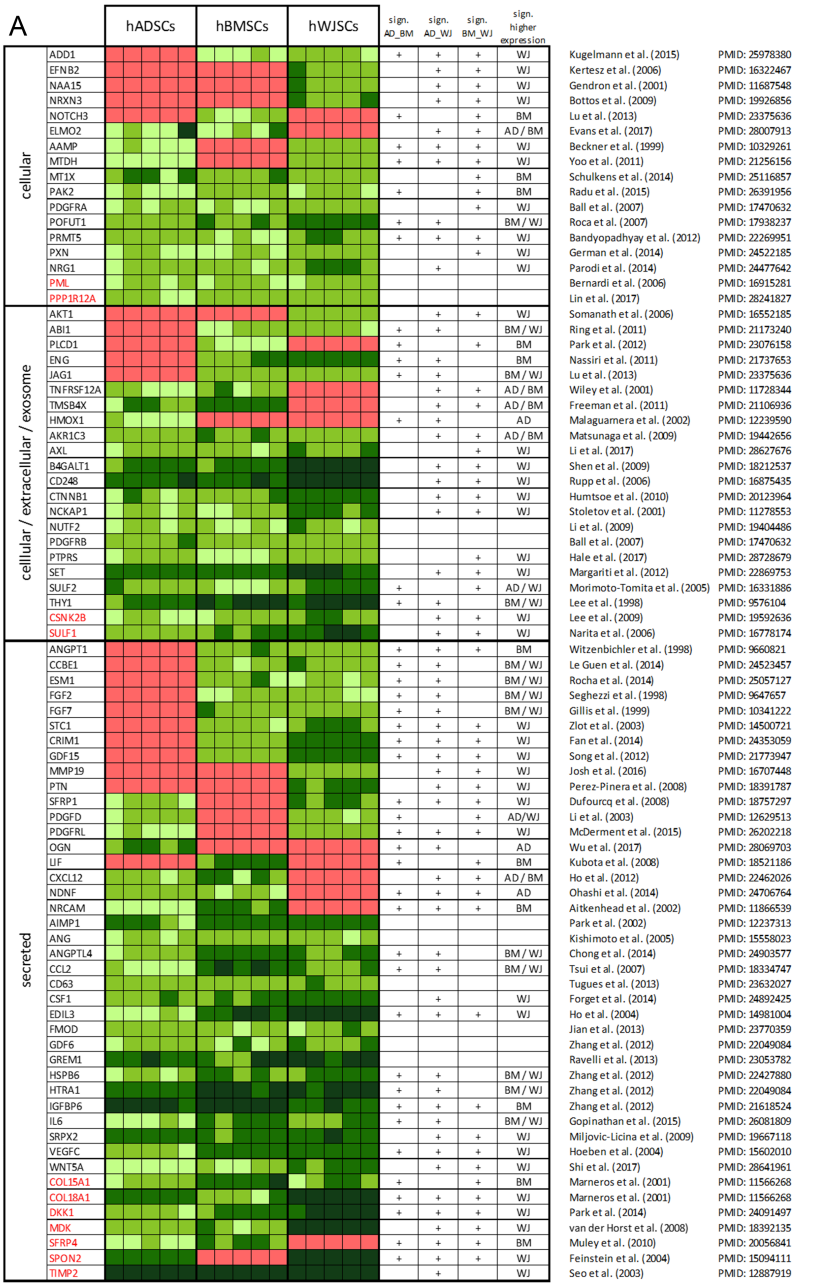
A
hADSCs
hBMSCs
hWJSCs
sign. AD_BM
sign. AD_WJ
sign. BM_WJ
sign. higher expression
cellular
ADD1 + + + WJ
EFNB2 + + WJ
NAA15 + + WJ
NRXN3 + + WJ
NOTCH3 + + BM
ELMO2 + + AD / BM
AAMP + + + WJ
MTDH + + + WJ
MT1X + BM
PAK2 + + BM
PDGFRA + WJ
POFUT1 + + BM / WJ
PRMT5 + + + WJ
PXN + WJ
NRG1 + WJ
PML
PPP1R12A
celllular / extracellular / exosome
AKT1 + + WJ
ABI1 + + BM / WJ
PLCD1 + + BM
ENG + + BM
JAG1 + + BM / WJ
TNFRSF12A + + AD / BM
TMSB4X + + AD / BM
HMOX1 + + AD
AKR1C3 + + AD / BM
AXL + WJ
B4GALT1 + + WJ
CD248 + + WJ
CTNNB1 + + WJ
NCKAP1 + + WJ
NUTF2
PDGFRB
PTPRS + WJ
SET + + WJ
SULF2 + + AD / WJ
THY1 + + BM / WJ
CSNK2B + + WJ
SULF1 + + WJ
secreted
ANGPT1 + + + BM
CCBE1 + + BM / WJ
ESM1 + + BM / WJ
FGF2 + + BM / WJ
FGF7 + + BM / WJ
STC1 + + + WJ
CRIM1 + + + WJ
GDF15 + + + WJ
MMP19 + + WJ
PTN + + WJ
SFRP1 + + + WJ
PDGFD + + AD/WJ
PDGFRL + + + WJ
OGN + + AD
LIF + BM
CXCL12 + + AD / BM
NDNF + + + AD
NRCAM + + + BM
AIMP1
ANG
ANGPTL4 + + BM / WJ
CCL2 + + BM / WJ
CD63
CSF1 + WJ
EDIL3 + + + WJ
FMOD
GDF6
GREM1
HSPB6 + + BM / WJ
HTRA1 + + BM / WJ
IGFBP6 + + + BM
IL6 + + BM / WJ
SRPX2 + + WJ
VEGFC + + + WJ
WNT5A + + WJ
COL15A1 + BM
COL18A1 + + WJ
DKK1 + + WJ
MDK + + WJ
SFRP4 + + BM
SPON2 + + + WJ
TIMP2 + WJ
Kugelmann et al. (2015) PMID: 25978380
Kertesz et al. (2006) PMID: 16322467
Gendron et al. (2001) PMID: 11687548
Bottos et al. (2009) PMID: 19926856
Lu et al. (2013) PMID: 23375636
Evans et al. (2017) PMID: 28007913
Beckner et al. (1999) PMID: 10329261
Yoo et al. (2011) PMID: 21256156
Schulkens et al. (2014) PMID: 25116857
Radu et al. (2015) PMID: 26391956
Ball et al. (2007) PMID: 17470632
Roca et al. (2007) PMID: 17938237
Bandyopadhyay et al. (2012) PMID: 22269951
German et al. (2014) PMID: 24522185
Parodi et al. (2014) PMID: 24477642
Bernardi et al. (2006) PMID: 16915281
Lin et al. (2017) PMID: 28241827
Somanath et al. (2006) PMID: 16552185
Ring et al. (2011) PMID: 21173240
Park et al. (2012) PMID: 23076158
Nassiri et al. (2011) PMID: 21737653
Lu et al. (2013) PMID: 23375636
Wiley et al. (2001) PMID: 11728344
Freeman et al. (2011) PMID: 21106936
Malaguarnera et al. (2002) PMID: 12239590
Matsunaga et al. (2009) PMID: 19442656
Li et al. (2017) PMID: 28627676
Shen et al. (2009) PMID: 18212537
Rupp et al. (2006) PMID: 16875435
Humtsoe et al. (2010) PMID: 20123964
Stoletov et al. (2001) PMID: 11278553
Li et al. (2009) PMID: 19404486
Ball et al. (2007) PMID: 17470632
Hale et al. (2017) PMID: 28728679
Margariti et al. (2012) PMID: 22869753
Morimoto-Tomita et al. (2005) PMID: 16331886
Lee et al. (1998) PMID: 9576104
Lee et al. (2009) PMID: 19592636
Narita et al. (2006) PMID: 16778174
Witzenbichler et al. (1998) PMID: 9660821
Le Guen et al. (2014) PMID: 24523457
Rocha et al. (2014) PMID: 25057127
Seghezzi et al. (1998) PMID: 9647657
Gillis et al. (1999) PMID: 10341222
Zlot et al. (2003) PMID: 14500721
Fan et al. (2014) PMID: 24353059
Song et al. (2012) PMID: 21773947
Josh et al. (2016) PMID: 16707448
Perez-Pinera et al. (2008) PMID: 18391787
Dufourcq et al. (2008) PMID: 18757297
Li et al. (2003) PMID: 12629513
McDerment et al. (2015) PMID: 26202218
Wu et al. (2017) PMID: 28069703
Kubota et al. (2008) PMID: 18521186
Ho et al. (2012) PMID: 22462026
Ohashi et al. (2014) PMID: 24706764
Aitkenhead et al. (2002) PMID: 11866539
Park et al. (2002) PMID: 12237313
Kishimoto et al. (2005) PMID: 15558023
Chong et al. (2014) PMID: 24903577
Tsui et al. (2007) PMID: 18334747
Tugues et al. (2013) PMID: 23632027
Forget et al. (2014) PMID: 24892425
Ho et al. (2004) PMID: 14981004
Jian et al. (2013) PMID: 23770359
Zhang et al. (2012) PMID: 22049084
Ravelli et al. (2013) PMID: 23053782
Zhang et al. (2012) PMID: 22427880
Zhang et al. (2012) PMID: 22049084
Zhang et al. (2012) PMID: 21618524
Gopinathan et al. (2015) PMID: 26081809
Miljovic-Licina et al. (2009) PMID: 19667118
Hoeben et al. (2004) PMID: 15602010
Shi et al. (2017) PMID: 28641961
Marneros et al. (2001) PMID: 11566268
Marneros et al. (2001) PMID: 11566268
Park et al. (2014) PMID: 24091497
van der Horst et al. (2008) PMID: 18392135
Muley et al. (2010) PMID: 20056841
Feinstein et al. (2004) PMID: 15094111
Seo et al. (2003) PMID: 12887919
B
C
hADSC
hBMSC
hWJSC

Figure 4: The pro-angiogenic proteome of hMSC secretome. (A) Proteins involved in angiogenesis and endothelial cell function in MSC secretomes. Pairwise student t-test were performed to detect differences between secretomes obtained from hADSCs (AD), hBMSCs (BM) and hWJSCs (WJ) (n=5 per cell source). Significant results are displayed by +. Heat map was generated based on protein intensities measured by LC/MS-MS (red = not detected, green = detected). For every protein related to angiogenesis, a reference has been added. Proteins in red letter are known to exhibit negative effects on angiogenesis, whereas proteins in black letter are known to be pro-angiogenic. (B) All identified proteins were uploaded into String database and evaluated using Cytoscape to define their interaction. Node size/color is based on the BetweennessCentrality defined by the combined score of String database, whereas low values are small size and orange (color code from low to high: orange – yellow – green – blue). The same principle was applied for map edge size/color. Proteins not being part of any interaction are not displayed (C) Proteins not found in the according secretome are displayed in red, demonstrating that central proteins are missing in hADSC secretome compare to hBMSC and hWJSC secretome.

2.1.3.5 ENDOTHELIAL CELL RESPONSE

To analyze the pro-angiogenic potential of hMSC CM *in vitro*, surface markers involved in angiogenesis such as angiopoietin-1 receptor (CD202b), endoglin (CD105), VE-cadherin (CD144) and PECAM-1 (CD31) were analyzed after co-incubation with either MSC CM, basal DMEM medium (negative control) or original EGM-2 medium (positive control). Bidimensional t-SNE density maps were generated from multidimensional data obtained flow cytometry and showed unequal event density distribution depending on the medium in which HUVEC were incubated (Figure 5A). Cumulative heat maps display scaled expression of the four surface markers (Figure 5B). In order to compare the effects of the different CM on HUVECs surface antigen profile, t-SNE maps were divided in three equal sectors. The % of events and the MFI was analyzed in each sector (Figure 5A). The three sectors were defined according to the MFI of all surface markers on HUVECs incubated under standard EGM-2 condition as following: Sector 1) $CD105^{medium}$, $CD202b^{low}$, $CD144^{medium}$, $CD31^{high}$; Sector 2) $CD105^{high}$, $CD202b^{high}$, $CD144^{high}$, $CD31^{medium}$; Sector 3) $CD105^{low}$, $CD202b^{low}$, $CD144^{low}$, $CD31^{low}$ (Figure 5C).

HUVECs treated with basal DMEM medium localize preferentially in sector 3, with the significant highest % of events ($p<0.001$) (Figure 5D). Importantly, sector 3 is characterized by the lowest expression all pro-angiogenic surface markers. When HUVECs were treated with MSC CM major event density shifts were observed. In detail, upon hBMSC and hWJSC CM treatment HUVECs localized mainly in sector 1 and 2; both sectors are characterized by higher surface expression level of pro-angiogenic surface markers. In particular, the CM-dependent event density shift towards sector 1 was significantly higher when HUVECs were treated with hBMSC CM and hWJSC CM compared to hADSC CM, basal DMEM medium and original EGM-2 medium ($p<0.001$) (Figure 5D). No differences among all MSC CM were found in sector 2 (Figure 5D). Overall these results demonstrate, that hBMSC CM and hWJSC CM induce a more angiogenic HUVEC phenotype *in vitro* compared to the pro-angiogenic induction triggered by hADSC CM and are closer to the phenotype obtained by treatment with original EGM-3 medium. Furthermore, the pro-angiogenic effects of MSC CM were tested *in vivo* angiogenesis by subcutaneously injection of matrigel mixed with MSC CM from different sources (Figure 6F). Vascularization of the matrigel plugs was quantitatively evaluated

measuring the hemoglobin content. Significantly higher hemoglobin content was detected in matrigels mixed with MSC CM compared to basal medium (Figure 6G). However no differences in angiogenic potential were detected between the three MSC sources *in vivo*.

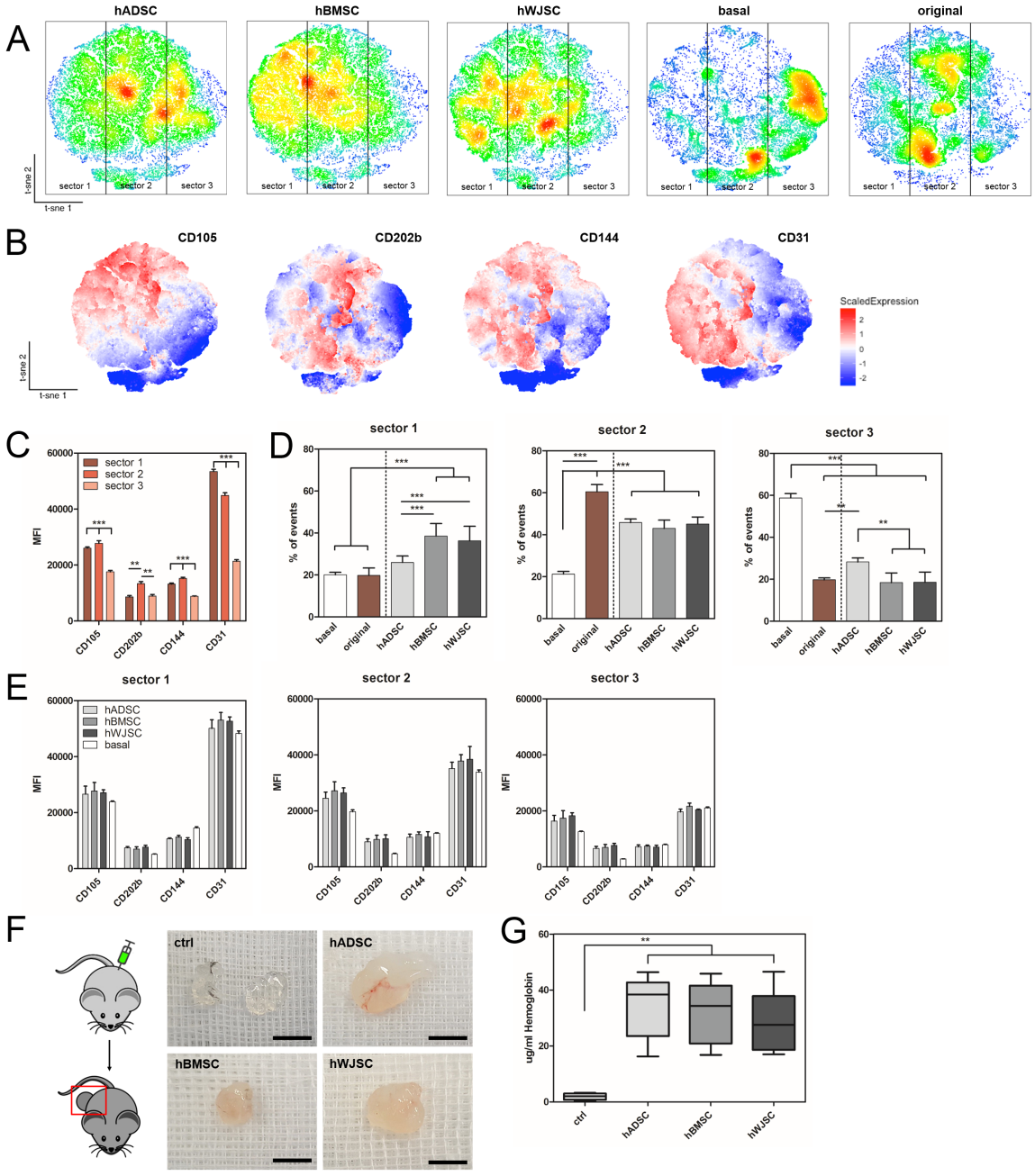

Figure 5: hMSC secretome is pro-angiogenic *in vitro* and *in vivo*. (A-E) Stimulation of HUVEC with MSC CM induces phenotypic changes *in vitro*, including the surface markers CD105, CD202b, CD144 and CD31. Bidimensional t-SNE maps show (A) unequal cellular distribution depending on the incubation medium (basal = basal DMEM; original = EGM-2) and (B) differences in expression pattern of surface markers. (C) Cells were therefore distributed into three sectors which are defined based on median fluorescence intensity (MFI) of surface markers of HUVEC under standard EGM-2 conditions. Sector 1) $CD105^{medium}$, $CD202b^{low}$, $CD144^{medium}$, $CD31^{high}$; Sector 2) $CD105^{high}$, $CD202b^{high}$, $CD144^{high}$, $CD31^{medium}$; Sector 3) $CD105^{low}$, $CD202b^{low}$, $CD144^{low}$, $CD31^{low}$. Percentage of events (D) and MFI (E) in each sector revealed that hBMSC CM and hWJSC CM induce a more angiogenic phenotype *in vitro* compared to hADSC CM. (F-G) *In vivo* matrigel plug assay demonstrated significantly increased vascularization when using hMSC CM compared to basal medium only, as visualized with the hemoglobin content in 60mg matrigel. Scale bar = 0.5 cm.

2.1.4 DISCUSSION

The current study demonstrates that MSCs derived from different clinically relevant tissue sources such as adipose tissue, bone marrow and umbilical cord Wharton's jelly have distinct chemoattractive and pro-angiogenic potential. In particular, hBMSC and hWJSC secretomes retained a higher inflammation mediated angiogenic profile and functional response compared to the hADSC secretome. Protein maps generated by high resolution LC/MS-MS demonstrated that angiogenic proteins with high betweenness centrality/interactions were primarily found in hBMSC and hWJSC secretome. These fundamental proteins, such as AKT1 and FGF2, have strong control over information flow within the pro-angiogenic network and related signaling pathways. Interestingly, these proteins not only influence the angiogenic process, but also mediate an inflammatory response. These observations also further support the close interaction between the primary inflammatory response and angiogenesis following tissue remodeling.

AKT1 has shown to promote angiogenic related functions of BMSCs *in vivo* [20] and its overexpression in MSCs of amniotic fluid [21] and bone marrow [22,23] supported the repair of ischemic heart tissue *in vivo*. Endothelial AKT1 enhances angiogenesis by phosphorylation of downstream angiogenic substrates [24] and was reported as a regulator in the acute inflammatory response [25]. On the other hand, FGF2 is a potent inducer of angiogenesis *in vitro* and *in vivo* [26] and synergistically potentiates inflammation mediated leukocyte recruitment [27]. Besides, the addition of FGF2 has shown to enhance the long-term angiogenic efficacy of transplanted hADSCs into ischemic tissue [28] and induce the production of MSC-derived extracellular vesicles for vessel stabilization [29]. Exosomes have even been proposed as key factors for angiogenesis, mediating through PDGFR, EGFR and NFkB pathways[30], given that MSC secretome depleted of exosomes exhibit an impaired pro-angiogenic function [5].

Thus, it is not surprising that hADSC secretome induced lower monocyte migration and angiogenic phenotype of HUVEC when considering the proteomic results. hADSC secretome did not only miss crucial pro-angiogenic proteins like AKT1 and FGF2, but also expressed most of the proteins to a significantly lower level compared to hBMSC and hWJSC secretome. Interestingly, surface marker expression was identical between hADSCs and hWJSCs, not allowing any anticipated conclusion about their functional response. Only hBMSCs demonstrated a different characterization profile with significant higher expression of CD73, CD90 and CD105, though did not exhibit better pro-angiogenic potential. However, hADSCs showed significant higher proliferation abilities compared to hBMSCs and hWJSCs. Previous studies have described hADSCs as genetical and morphological more stable in long-term culture with lower senescence and higher proliferative capacities [31]. Here, identical cellular

viability after secretome harvest was found, but higher proliferation might have influenced the pro-angiogenic potential of hADSCs.

Taken together, hWJSC secretome possesses a slightly more pro-inflammatory and pro-angiogenic secretome compared to the intermediate phenotype of hBMSC secretome even if our functional analyses failed to show statistically significant differences. In accordance to our study, recent comparative studies have shown that hWJSC secretome possesses more secreted factors involved in angiogenesis compared to hBMSC [11]. Ribeiro et al. proposed that hBMSC secretome might be most potent to reduce oxidative stress, while hWJSC and hADSC secretome seem more beneficial in the protection against excitotoxicity [32]. Furthermore, it was suggested that hWJSCs express more stemness and growth related genes, whereas hBMSCs express more genes involved in skeletal development [33].

We therefore propose hWJSCs – and the hWJSC derived secretome – as the most potent MSC source for clinical use. Prenatal hWJSCs can be obtained from healthy, young donors with minimal ethical concerns in high quantities and with no risk. On the contrary, the amount of hBMSC obtained from a bone marrow puncture is limited. hBMSCs are isolated from older patients, which are susceptible to aging factors such as the accumulation of cellular damage, cell death/senescence and loss of regenerative functions.

Nevertheless, patient variability has been detected in the presented study despite consistent isolation and characterization procedures. One has to emphasize that different donors among the tissue sources have been analyzed here, not allowing for direct comparison within one particular patient. Furthermore no restriction on donor age, gender and medical history are available in the current study. Therefore, 5 donors per cell source have been included into the study. However, patient variability did not enable to find any significant differences in this *in vivo* investigation conducted (Matrigel plug assay), in contrast to *in vitro* functional assays and mass spectrometry analyses; this might particularly also due to the additional variability in angiogenic response among different mice. Future studies will focus on a more reproducible *in vivo* angiogenic assay to confirm the presented differences among tissue sources.

Overall the establishment of clinical treatments based on MSC secretomes has clear advantages for clinical translation compared to autologous or homologous cells therapy, considering manufacturing costs and logistics. In addition, the unlimited supply of the MSC secretome off-the-shelf without the need for harvesting tissue from the affected patient would represent a major advantage over currently used experimental and clinical cell therapy approaches.

However, major challenge of *in vitro* secretome studies lies in discriminating proteins that are truly MSC-secreted from those that are artifacts from cell culture media components (such as serum

proteins) or derived from non-physiological stresses affecting the starving cells. In this regard, intracellular proteins can be detected in the secretome due to cellular death or leakage. However, there is now evidence that some of these proteins can also be released via nonclassical pathways via vesicles and exosomes and exert extracellular functions that seem to be different from their intracellular role [34]. Even if a subset of MSCs has entered apoptosis, it has been shown that factors released from apoptotic MSCs can contribute to regeneration of ischemic tissues [35,36]. In particular, Sun et al. highlighted the beneficial immunomodulatory roles of apoptotic stem cells by demonstrating that combined therapy with apoptotic and healthy ADSCs is superior to either alone [36]. Therefore, we believe that the complete secretome needs to be described in order to understand their interaction and *in vivo* function. Unlike pharmaceutical treatments that deliver a single agent, the MSC secretome provides several stimulatory and inhibitory bioactive factors at variable concentrations that might sustain physiological pharmacokinetics in the local microenvironment.

Besides, secretome harvest procedures allow for the attachment of serum proteins that can later be released into the MSC secretome [34]. This contamination with serum proteins might have been neglected in many previous in *vitro* and in *vivo* studies, which might lead to incorrect conclusions. Therefore, the presented work defined remaining serum proteins by the detection of PF-4, a cytokine uniquely released from activated platelets. No differences in PF-4 levels between the different MSC sources confirmed that the results are not biased by differences in serum leftover. Furthermore, serial dilutions allowed defining the detection limit of PF-4 and use this dilution, consisting of a 1:3200 dilution of standard proliferation medium, as a suitable control for subsequent MS analysis. In this way we could assure no culture medium artifacts within the presented data. However, some proteins might have been masked by this procedure as they can be derived from both, MSCs and hPL. Only by using standardized GMP-compliant culture protocols, with hPL instead of xenogenic components, we can increase *in vivo* safety for future clinical translation.

In conclusion, we have systematically compared MSC from hADSCs, hBMSCs and hWJSCs in order to determine which cell source possesses the highest potential for angiogenesis and endogenous regeneration. A GMP-compliant xenofree approach towards generating MSC secretome and enabling safe clinical translation has been established. MSC secretomes showed significant functional and proteomic differences in inflammation-mediated angiogenesis. Taken together, these results indicate that hWJSC secretome might represent the most potent MSC source for clinical angiogenesis induction. Compared with other tissue sources, hWJSCs have several advantages, such as their noninvasive collection procedure, fetal origin and unlimited supply as leftover materials, which emphasize their potential clinical utility for regenerative medicine in the future.

2.1.5 REFERENCES

1 Baraniak, P. R. & McDevitt, T. C. Stem cell paracrine actions and tissue regeneration. *Regen Med* **5**, 121-143, doi:10.2217/rme.09.74 (2010).

2 Murphy, M. B., Moncivais, K. & Caplan, A. I. Mesenchymal stem cells: environmentally responsive therapeutics for regenerative medicine. *Exp Mol Med* **45**, e54, doi:10.1038/emm.2013.94 (2013).

3 Tao, H., Han, Z., Han, Z. C. & Li, Z. Proangiogenic Features of Mesenchymal Stem Cells and Their Therapeutic Applications. *Stem Cells Int* **2016**, 1314709, doi:10.1155/2016/1314709 (2016).

4 Kwon, H. M. *et al.* Multiple paracrine factors secreted by mesenchymal stem cells contribute to angiogenesis. *Vascul Pharmacol* **63**, 19-28, doi:10.1016/j.vph.2014.06.004 (2014).

5 Shabbir, A., Cox, A., Rodriguez-Menocal, L., Salgado, M. & Van Badiavas, E. Mesenchymal Stem Cell Exosomes Induce Proliferation and Migration of Normal and Chronic Wound Fibroblasts, and Enhance Angiogenesis In Vitro. *Stem Cells Dev* **24**, 1635-1647, doi:10.1089/scd.2014.0316 (2015).

6 Naldini, A. & Carraro, F. Role of inflammatory mediators in angiogenesis. *Curr Drug Targets Inflamm Allergy* **4**, 3-8 (2005).

7 Anghelina, M., Krishnan, P., Moldovan, L. & Moldovan, N. I. Monocytes and macrophages form branched cell columns in matrigel: implications for a role in neovascularization. *Stem Cells Dev* **13**, 665-676, doi:10.1089/scd.2004.13.665 (2004).

8 Anghelina, M., Krishnan, P., Moldovan, L. & Moldovan, N. I. Monocytes/macrophages cooperate with progenitor cells during neovascularization and tissue repair: conversion of cell columns into fibrovascular bundles. *Am J Pathol* **168**, 529-541, doi:10.2353/ajpath.2006.050255 (2006).

9 Nakanishi, C. *et al.* Gene and protein expression analysis of mesenchymal stem cells derived from rat adipose tissue and bone marrow. *Circ J* **75**, 2260-2268 (2011).

10 Hsiao, S. T. *et al.* Comparative analysis of paracrine factor expression in human adult mesenchymal stem cells derived from bone marrow, adipose, and dermal tissue. *Stem Cells Dev* **21**, 2189-2203, doi:10.1089/scd.2011.0674 (2012).

11 Hsieh, J. Y. *et al.* Mesenchymal stem cells from human umbilical cord express preferentially secreted factors related to neuroprotection, neurogenesis, and angiogenesis. *PLoS One* **8**, e72604, doi:10.1371/journal.pone.0072604 (2013).

12 Gaetani, M. *et al.* Unbiased and quantitative proteomics reveals highly increased angiogenesis induction by the secretome of mesenchymal stromal cells isolated from fetal rather than adult skin. *J Tissue Eng Regen Med*, doi:10.1002/term.2417 (2017).

13 Bieback, K. *et al.* Human alternatives to fetal bovine serum for the expansion of mesenchymal stromal cells from bone marrow. *Stem Cells* **27**, 2331-2341, doi:10.1002/stem.139 (2009).

14 Svatek, R. S. *et al.* A multiplexed, particle-based flow cytometric assay identified plasma matrix metalloproteinase-7 to be associated with cancer-related death among patients with bladder cancer. *Cancer* **116**, 4513-4519, doi:10.1002/cncr.25401 (2010).

15 Gunasekera, K., Wuthrich, D., Braga-Lagache, S., Heller, M. & Ochsenreiter, T. Proteome remodelling during development from blood to insect-form Trypanosoma brucei quantified by SILAC and mass spectrometry. *Bmc Genomics* **13**, doi:Artn 556 10.1186/1471-2164-13-556 (2012).

16 Brugger, V. *et al.* Delaying histone deacetylase response to injury accelerates conversion into repair Schwann cells and nerve regeneration. *Nat Commun* **8**, 14272, doi:10.1038/ncomms14272 (2017).

17 Lazar, C., Gatto, L., Ferro, M., Bruley, C. & Burger, T. Accounting for the Multiple Natures of Missing Values in Label-Free Quantitative Proteomics Data Sets to Compare Imputation Strategies. *J Proteome Res* **15**, 1116-1125, doi:10.1021/acs.jproteome.5b00981 (2016).

18 Simillion, C., Liechti, R., Lischer, H. E. L., Ioannidis, V. & Bruggmann, R. Avoiding the pitfalls of gene set enrichment analysis with SetRank. *Bmc Bioinformatics* **18**, doi:ARTN 151 10.1186/s12859-017-1571-6 (2017).

19 Pan, K. H., Lih, C. J. & Cohen, S. N. Effects of threshold choice on biological conclusions reached during analysis of gene expression by DNA microarrays. *P Natl Acad Sci USA* **102**, 8961-8965, doi:10.1073/pnas.0502674102 (2005).

20 Shen, C. C. *et al.* The angiogenic related functions of bone marrow mesenchymal stem cells are promoted by CBDL rat serum via the Akt/Nrf2 pathway. *Exp Cell Res* **344**, 86-94, doi:10.1016/j.yexcr.2016.04.013 (2016).

21 Wang, Y. *et al.* The transplantation of Akt-overexpressing amniotic fluid-derived mesenchymal stem cells protects the heart against ischemia-reperfusion injury in rabbits. *Mol Med Rep* **14**, 234-242, doi:10.3892/mmr.2016.5212 (2016).

22 Gnecchi, M. *et al.* Early beneficial effects of bone marrow-derived mesenchymal stem cells overexpressing Akt on cardiac metabolism after myocardial infarction. *Stem Cells* **27**, 971-979, doi:10.1002/stem.12 (2009).

23 Kang, K. *et al.* Exosomes Secreted from CXCR4 Overexpressing Mesenchymal Stem Cells Promote Cardioprotection via Akt Signaling Pathway following Myocardial Infarction. *Stem Cells Int* **2015**, 659890, doi:10.1155/2015/659890 (2015).

24 Lee, M. Y. *et al.* Endothelial Akt1 mediates angiogenesis by phosphorylating multiple angiogenic substrates. *Proc Natl Acad Sci U S A* **111**, 12865-12870, doi:10.1073/pnas.1408472111 (2014).

25 Di Lorenzo, A., Fernandez-Hernando, C., Cirino, G. & Sessa, W. C. Akt1 is critical for acute inflammation and histamine-mediated vascular leakage. *Proc Natl Acad Sci U S A* **106**, 14552-14557, doi:10.1073/pnas.0904073106 (2009).

26 Seghezzi, G. *et al.* Fibroblast growth factor-2 (FGF-2) induces vascular endothelial growth factor (VEGF) expression in the endothelial cells of forming capillaries: an autocrine mechanism contributing to angiogenesis. *J Cell Biol* **141**, 1659-1673 (1998).

27 Zittermann, S. I. & Issekutz, A. C. Basic fibroblast growth factor (bFGF, FGF-2) potentiates leukocyte recruitment to inflammation by enhancing endothelial adhesion molecule expression. *Am J Pathol* **168**, 835-846, doi:10.2353/ajpath.2006.050479 (2006).

28 Lee, T. J. *et al.* Enhancement of long-term angiogenic efficacy of adipose stem cells by delivery of FGF2. *Microvasc Res* **84**, 1-8, doi:10.1016/j.mvr.2012.04.004 (2012).

29 Lopatina, T. *et al.* The Angiogenic Potential of Adipose Mesenchymal Stem Cell-derived Extracellular Vesicles is modulated by Basic Fibroblast Growth Factor. *J Stem Cell Res Ther* **4**, 245 (2014).

30 Anderson, J. D. *et al.* Comprehensive Proteomic Analysis of Mesenchymal Stem Cell Exosomes Reveals Modulation of Angiogenesis via Nuclear Factor-KappaB Signaling. *Stem Cells* **34**, 601-613, doi:10.1002/stem.2298 (2016).

31 Strioga, M., Viswanathan, S., Darinskas, A., Slaby, O. & Michalek, J. Same or not the same? Comparison of adipose tissue-derived versus bone marrow-derived mesenchymal stem and stromal cells. *Stem Cells Dev* **21**, 2724-2752, doi:10.1089/scd.2011.0722 (2012).

32 Pires, A. O. *et al.* Unveiling the Differences of Secretome of Human Bone Marrow Mesenchymal Stem Cells, Adipose Tissue-Derived Stem Cells, and Human Umbilical Cord Perivascular Cells: A Proteomic Analysis. *Stem Cells Dev* **25**, 1073-1083, doi:10.1089/scd.2016.0048 (2016).

33 Hsieh, J. Y., Fu, Y. S., Chang, S. J., Tsuang, Y. H. & Wang, H. W. Functional module analysis reveals differential osteogenic and stemness potentials in human mesenchymal stem cells from bone marrow and Wharton's jelly of umbilical cord. *Stem Cells Dev* **19**, 1895-1910, doi:10.1089/scd.2009.0485 (2010).

34 Brown, K. J. *et al.* Advances in the proteomic investigation of the cell secretome. *Expert Rev Proteomics* **9**, 337-345, doi:10.1586/epr.12.21 (2012).

35 Lee, R. H. *et al.* Intravenous hMSCs improve myocardial infarction in mice because cells embolized in lung are activated to secrete the anti-inflammatory protein TSG-6. *Cell Stem Cell* **5**, 54-63, doi:10.1016/j.stem.2009.05.003 (2009).

36 Sun, C. K. *et al.* Mixed serum-deprived and normal adipose-derived mesenchymal stem cells against acute lung ischemia-reperfusion injury in rats. *Am J Transl Res* **7**, 209-231 (2015).

3

The ovine model for the evaluation of therapeutic applications based on mesenchymal stem cells

The content of this chapter is based on:

Kehl D, Görtz S, Wang C, Hoerstrup SP, Bleul U*, Weber B*. Gestational age-dependent fetal fluid dynamics in the ovine developmental model. *(under revision in Reproduction, Fertility and Development, 2017)*

Kehl D°, Generali M°, Görtz S, Geering D, Slamecka J, Hoerstrup SP, Bleul U, Weber B. Amniotic fluid cells show higher pluripotency-related gene expression than allantoic fluid cells. *Stem Cell and Development,* 2017 Oct 1;26(19):1424-1437.

CHAPTER 3.1

Gestational age-dependent fetal fluid dynamics in the ovine developmental model

Debora Kehl[1], Sabrina Görtz[1], Craig Wang[2], Simon P. Hoerstrup[1,3,4], Ulrich Bleul[5*], Benedikt Weber[1,3,4*]

[*] These senior authors contributed equally

[1] Institute for Regenerative Medicine (IREM), Center for Therapy Development and Good Manufacturing Practice, University of Zurich, Zurich, Switzerland
[2] Department of Mathematics, University of Zurich, Zurich, Switzerland
[3] Center for Applied Biotechnology and Molecular Medicine (CABMM), University of Zurich, Zurich, Switzerland
[4] Zurich Center for Integrative Human Physiology (ZIHP), University of Zurich, Zurich, Switzerland
[5] Clinic of Reproductive Medicine, Department of Farm Animals, Vetsuisse-Faculty University of Zurich, Zurich, Switzerland

Abstract

The ovine developmental model represents the standard *in vivo* model for studies involving materno-fetal physiology, amniotic fluid research and fetal cell therapy prior to human clinical use. Although being close to the human fetal anatomy, it maintains two separate extraembryonic fluid compartments during gestation, known as the amnion and the allantois. A clear distinction between amniotic fluid (AF) versus allantoic fluid (AL) is therefore indispensable for correct scientific conclusions with regards to human translation. In the presented study, the biochemical composition of AF and AL was evaluated in ovine gravid uteri post mortem (n=31). Four parameters, consisting of Na^+, Cl^-, Mg^{2+} and total protein, have been found to allow for specific discrimination of the two fetal fluids and as potential surrogate parameters for gestational age. In addition, volumetric changes of the developing fetus and the two fetal fluid cavities were analyzed by contrast-enhanced computed tomography (n=12). AF showed a significant, linear volumetric increase over gestation, whereas AL volume maintained relatively static independent of gestational age. These results may provide a basis for future experimental studies in the ovine developmental model and may enable a more reliable and safe translation of obtained results to the human clinical situation.

Personal contribution:

Experimental contributions (Kehl D, together with co-authors)
Harvest of amniotic and allantoic fluid from gravid uteri post mortem. Electrolyte and total protein measurements with the Institute for Clinical Chemistry, University Hospital Zurich.

Non-experimental contributions (Kehl D only):
Study design and planning of the study. Acquiring funding for the entire project. Supervision and teaching of medical master students involved in the project. Analyzing all volumetric data and fluid parameters. Statistical analyses. Drafting all figures. Writing the entire manuscript. Submission and correspondence with editorial office.

Steps contained in the published work (without personal contribution of Kehl D)
Three-dimensional computed tomography (CT) of ovine anatomy and fetal fluid cavities, including injection of contrast agent.

Reproduction, Fertility and Development (under revision 2017)

3.1.1 INTRODUCTION

The ovine developmental model represents a standard *in vivo* model for the assessment of materno-fetal disease and fetal therapeutic applications prior to human clinical use. Even though it does not completely recapitulate human pregnancy, several scientific questions involving the entire duration of pregnancy cannot be addressed in the human situation given major ethical and medical restrictions. Consequently, the ovine model is well accepted and regularly used as part of preclinical fetal studies, such as fetal tracheal [1,2] and diaphragmatic [3-5] reconstruction, heart valve replacement [6], wound healing [7], materno-fetal interactions (placenta development/function) [8] or cell transplantations [9]. Also studies on ovine fetal adnexa-derived (stem) cells [10] or ovine amniotic fluid-derived (stem) cells [6,11] have been conducted revealing cellular phenotypes largely comparable to the human counterpart.

However, although being close to the human fetal anatomy, the ovine materno-fetal model maintains two separate extraembryonic fluid compartments during the entire gestation, which are known as the amnion and the allantois. In humans only a single cavity, known as the amniotic fluid cavity, is present after the 3rd to 5th week of conception where the transient allantoic fluid compartment is lost [12]. As a consequence, when dealing with studies mimicking the human physiology (such as fetal preclinical trials) this anatomical difference has to be appreciated. In particular in studies, which involve the amniotic fluid (or cells thereof), a clear distinction between amniotic versus allantoic fluid (AF vs. AL) harvest seems indispensable to allow for correct interpretation of the data. This is even more exemplified by recent studies showing significant differences in pluripotency-related gene expression of cells isolated from the ovine AF versus AL compartment [13] as well as proteomic analyses on both fluids [14]. Therefore, several groups have investigated the biochemical composition of the AF and AL showing differences in electrolyte and protein components between the two fetal fluids in mares [15], sheep [6,16,17] and feline [18]. These biochemical changes might be influenced by the fetal fluid metabolism and the significant volumetric changes of the ovine fetal fluid compartments over the course of gestation [16,19,20]. In spite of these first insights into the biochemical profiles and reports on the anatomical changes of the fetus in-utero, less is understood about the underlying mechanisms of fetal fluid regulation and solute exchange. The establishment of temporal relationships would therefore not only enable a better understanding of fetal fluid metabolism and gestational physiology for preclinical evaluations, but also facilitate a more reliable harvest of fetal fluids (and biochemical verification thereof) in the ovine animal model over gestation.

Therefore, the presented study analyzes volumetric changes of the fetus as well as the surrounding fetal fluid cavities by computed tomography (CT) and correlates these findings with the biochemical

profile obtained from both, the AF and AL, over the entire duration of ovine gestation. The analyses should enable a better comparison of fetal fluid dynamics in the ovine versus the human situation for future preclinical evaluations of materno-fetal disease and fetal therapeutic applications.

3.1.2 MATERIAL AND METHODS

3.1.2.1 HARVEST OF OVINE GRAVID UTERI

Ovine gravid uteri were provided post mortem by the slaughterhouse Hinwil, Switzerland (n=52). Crown rump length (CRL) of each fetus was determined in order to allocate it to one of the three gestational age groups according to previously published standards [21]. Gestational age group 1 is defined by a CRL ≤ 10, group 2 by a CRL > 10 ≤ 20 and group 3 by a CRL > 20. For CT examination (n=12), gravid uteri were directly stored at 4-8°C and measurements were performed within 48 hours. Both fetal fluids, AF and AL, were harvested from the same animal (n=40) as previously published [11]. In brief, the uterus and the fetal fluid cavities were opened surgically and the fetal fluids were aspirated with a 50ml syringe and a 10 Gauge needle under visual guidance. After centrifugation for 10 minutes at 1600 RPM, the supernatant was stored overnight at 4°C for the subsequent differential fluid analyses.

3.1.2.2 IMAGING OF OVINE GRAVID UTERI

For CT imaging the uteri were placed in a supine position. The imaging was performed using a multidetector CT scanner (Brilliance 16, Philips AG, Zurich, Switzerland). Transverse slices of the whole organs with a slice thickness of 2mm were made using a voltage peak of 120kVp and a current of 250mA. 2-20ml of contrast medium (Ioversol, Optiray 300, Guerbet, Switzerland) were injected into the amnion and allantois cavity under ultrasound guidance (MyLab One, Esaote, Maastricht, 8MHz Linear probe) depending on the particular size of the cavity. The fluid volumes were evaluated in a soft tissue and bone window with a window width (W) of 520 Hounsfield Units (HU), and a window level (L) of 100 HU.

3.1.2.3 VOLUMETRIC ASSESSEMENT OF OVINE FETAL FLUID CAVITIES

Volumetric measurements were performed with the Philips Intellispace Portal. Using the 3D Segmentation mode on the volume explorer, regions of interest (ROI) were selected according to the injected contrast medium. ROI were verified on all planes. Volumina were calculated by the software in cubic centimeter (cc) and the amount of injected contrast medium (ml) was subtracted from the obtained results. Separate measurements were conducted for AF and AL compartments for each animal. Fetal volume was determined by selecting the fetal body as ROI and calculating the corresponding fetal volume. Extremities were not selected given their poor recognition at early gestational ages.

3.1.2.4 DIFFERENTIAL OVINE FETAL FLUID ANALYSIS

To monitor gestational age differences in the composition of AF and AL, values of total protein (TP), Albumin, Sodium (Na^+), Chloride (Cl^-) and Magnesium (Mg^{2+}) were defined in harvested fetal fluids using the TP Gen.2 (Ref. 05171385190), the ISE indirect Na-K-Cl for Gen.2 (Ref. 108) and the Mg Gen.2 (Ref. 05171911190) of Roche/Hitachi Cobas analyzer (Roche Diagnostics, Switzerland).

3.1.2.5 STATISTICAL ANALYSIS

Quantitative data are presented as mean ± standard deviation (GraphPad Prism, GraphPad Software Inc., USA). Receiver operating characteristic curves (ROC) were generated for visualization of sensitivity (at a certain specificity) of parameters in the differential fetal fluid analysis (SPSS 21.0, IBM, USA). Differences in AF versus AL and gestational age groups were analyzed with Wilcoxon signed-rank test and p-values < 0.05 or z-values > ±1.96 were considered statistically significant. Correlations were analyzed with either the Pearson (ρ) or Spearman's Rank Correlation Coefficient (R) with the according significance level defined *p<0.05, **p<0.01, ***p<0.001, or additive Bayesian networks for dependency structure discovery using graphical modeling (R Version 3.3.3, Austria) [22]. Overall, for statistical analyses values below detection level were set to zero (in TP and partially Cl^-).

3.1.3 RESULTS

3.1.3.1 VOLUMETRIC ASSESSMENT OF OVINE FETAL FLUID CAVITIES – CORRELATION TO CRL

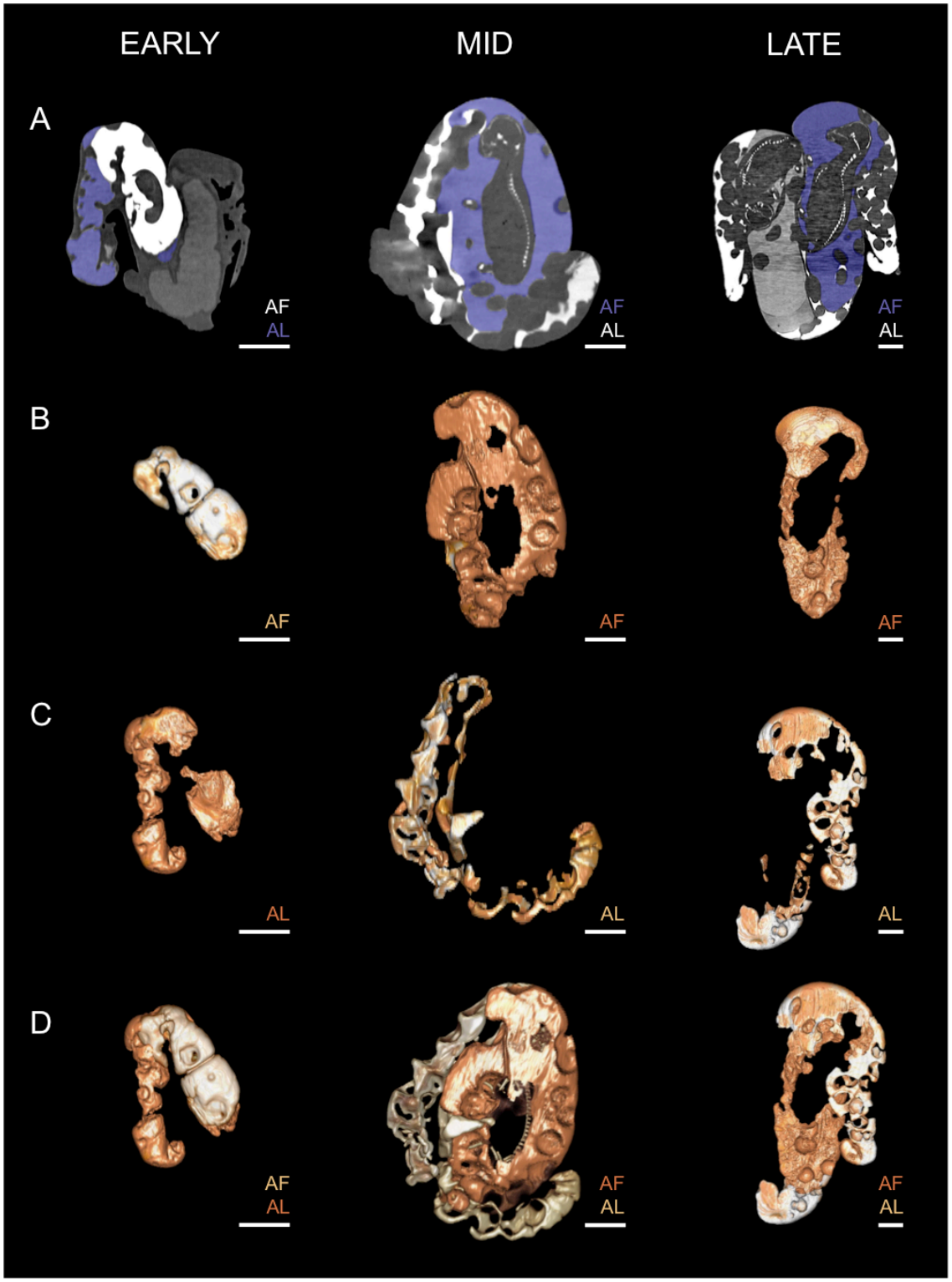

Figure 1: Computed tomography of ovine fetal fluid cavities over gestation. Computed tomography (CT) pictures of early, mid and late gestation were obtained to measure fetal fluid volumes of amniotic (AF) and allantoic (AL) fluid. (A) Contrast agent (Ioversol, Opitray 300) was used to visualize both cavities. Three-dimensional reconstruction of the ovine (B) amnion, (D) allantois and (D) merged, show *in vivo* architecture of the fetal fluid cavities during pregnancy. Scale bar = 4cm.

Volumetric measurements of the fetus by CT (Figure 1) revealed a significant correlation between the CRL and the fetal volume over gestation (R=0.98, $p < 0.001$) (Figure 2A). Given that CRL is defined as an indicator of the gestational age in this study, the volumetric assessment of the fetus further exemplifies the fetal development over time (Figure 2D). When analyzing the change of AF and AL over either the fetal volume or the CRL, identical results were found. AL volume maintained relatively static with a mean of 157 ± 77ml and no correlation to gestational age, respectively fetal volume (R=0.45, p=0.14) and CRL (R=0.46, p=0.13) (Figure 2B). AF represented the major fluid within the fetal cavity and significantly increased in a linear fashion over gestation, with positive correlations found for fetal volume (ρ=0.90, $p < 0.001$) and CRL (ρ=0.97, $p < 0.001$) (Figure 2B). Therefore, the total fetal fluid is mainly influenced by the increase in AF and also significantly correlates with the fetal volume (ρ=0.89, $p < 0.001$) and the CRL (ρ=0.95, $p < 0.001$). No significant differences were found in the amount of AF and AL at early gestation (p=0.81), whereas there are some evidence for differences at mid and late gestation (p=0.06 and p=0.06) (Figure 2C). The total fluid per fetal volume significantly decreases over gestation (R=-0.96, $p<0.001$) for AF (R=-0.90$p<0.001$) and AL (R=-0.90,$p<0.001$) (Figure 2E). In particular at early gestation (group 1) a much higher fluid volume to fetal size/volume was found, with equal amounts of AF and AL (group1: p=0.81). (Figure 2F). At mid and late gestation the fluid volume to fetal size/volume was found to be relatively static, however with weak evidence showing higher AF amount compared to AL (group 2: $p = 0.06$, group 3: p= 0.06) (Figure 2F). Correlation analyses (Figure 2G-H) revealed strong dependence between fetal size, amnion volume and fetal volume. However, correlation becomes independent when the effect of amnion is removed, further underlying that the major cavity increasing over time is based on AF. The independence of the allantois demonstrates its overall stable volume, not being in any relation with the course of gestation.

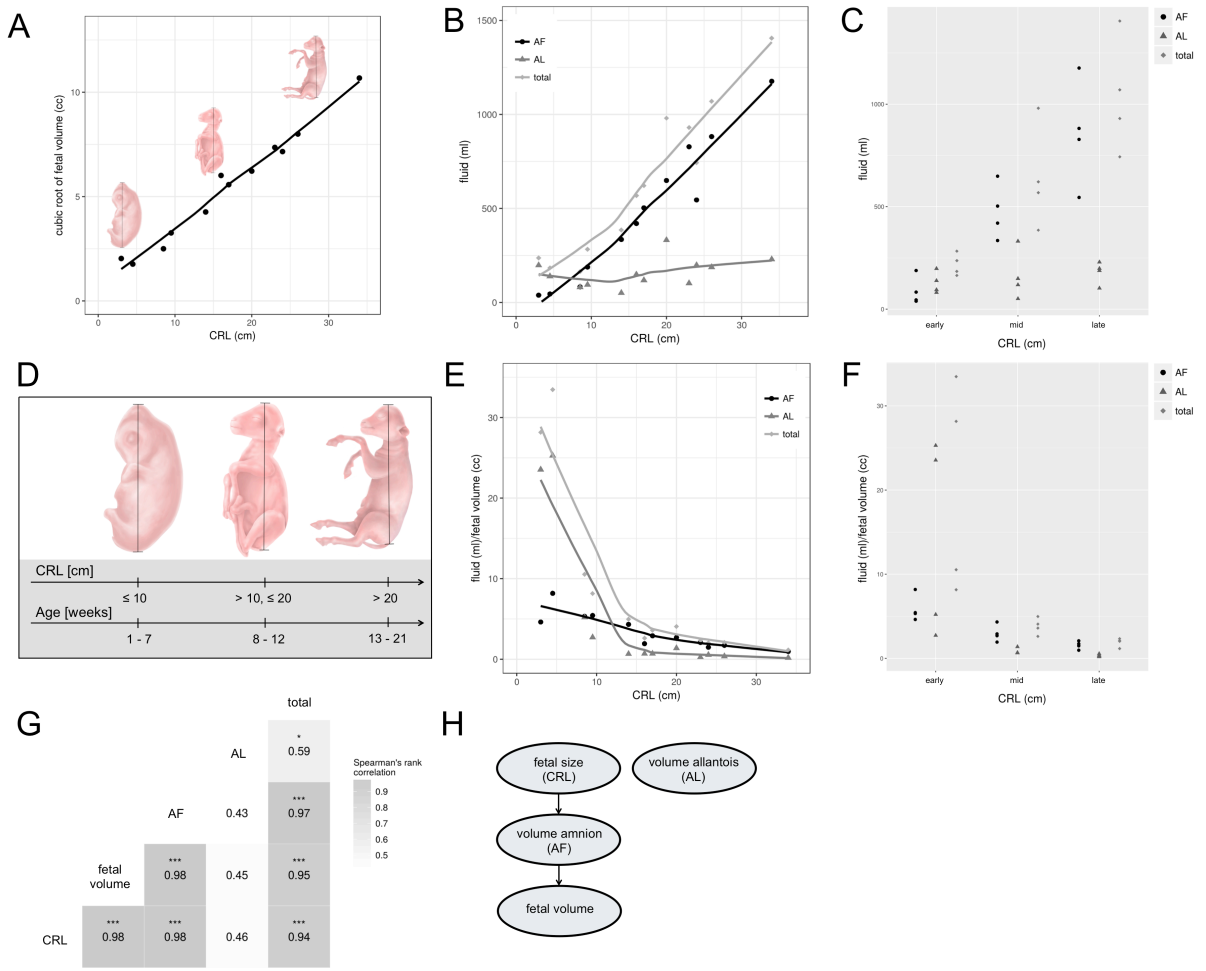

Figure 2: Volumetric assessment of ovine amniotic and allantoic fluid cavities over gestation. (A) Crown rump length (CRL) significantly correlates with fetal volume, (D) which is an indicator for gestational age. (B-C) The total fetal adnexal fluid is mainly influenced by AF over gestation increasing in a linear fashion, whereas AL maintains relatively static independent of gestational age. (E-F) Overall higher fetal adnexal fluid per fetal volume is found at early gestation. Over gestational time higher AF amount compared to AL are detected also in relation to fetal volume. (G) Spearman's rank correlation matrix display all correlation analyses conducted with each coefficient and the according significance level (*p<0.05, **p<0.01, ***p<0.001), (H) demonstrating with graphical modeling that there is a strong dependence between volume amnion and gestation, but not with volume allantois and gestation.

3.1.3.2 DIFFERENTIAL FETAL FLUID ANALYSIS

AF AND AL PURITY ASSESSMENT – CUT-OFF VALUES OF ELECTROLYTES AND TOTAL PROTEIN

Harvested ovine fetal fluids (n=40) were compared to reference values from an existing database [11], including TP, Albumin, Na^+, Cl^- and Mg^{2+}, in order to assess the purity of the fetal fluids and exclude possible collateral contamination. Using this reference pool [11], receiver operating characteristic curves (ROC) and cut-off values (for AF: Na^+-Cutoff ≥ 117.5 mmol/l, Cl^--Cutoff ≥ 95 mmol/l, Mg^{2+}-Cutoff ≤ 0.88 mmol/l, TP-Cutoff ≤ 1 g/l) were established (Figure 3A). At 100% sensitivity levels, the specificity values to detect inaccurate fluid harvest and contamination was 100% for TP, 90% for Na^+ and Cl^-, 86.7% for Mg^{2+}. TP (z = -4.646) and Mg^{2+} (z = -4.860) levels were significantly higher in the AL compared to the AF, which confirms that they detect AL contamination with high sensitivity. On the

other hand, Na^+ (z = -4.860) and Cl^- levels (z = -4.860) were significantly higher in the AF compared to the AL, suggesting that they detect AF contamination with high sensitivity. Consequently, AF samples with Mg^{2+} and TP values over the defined cut-off values and AL samples with Na^+ and Cl^- values over the defined cut-off values were excluded based on contamination according to our reference pool. Hemorrhagic contamination of the fetal fluids potentially causing the differences in the TP amount could be excluded by the lack of detection of albumin. If the amount of fetal fluid harvested was insufficient for the differential fluid analysis, the respective fetuses were excluded from further analyses (n=2). Taken together, 9/40 fetuses had to be excluded as their pure AF or AL origin could not be confirmed, whereas fetal fluid samples included into the study are displayed on the corresponding scatter plot (n=31) (Figure 3B).

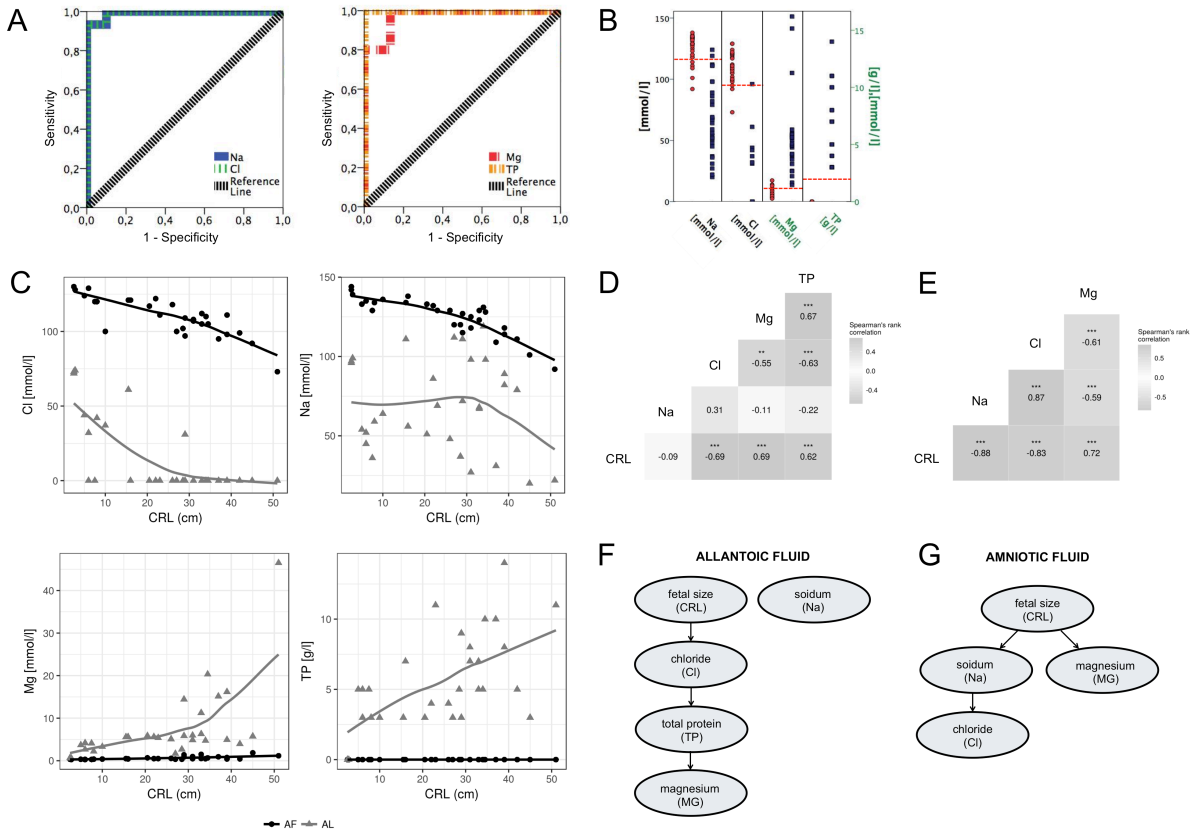

Figure 3: Differential analysis of ovine amniotic and allantoic fluid over gestation. (A) Receiver operating characteristic curve (ROC) show sensitivity levels to detect inaccurate fetal fluid harvest and contaminations, consisting of 100% for total protein (TP), 90% for sodium (Na) and chloride (Cl), 86.7% for magnesium (Mg). (B) Scatterplots of fetal fluid samples included into the study. The red line demonstrated cutoff values that have been established by the use of reference values from an existing database. (C) Photometric or colometric detection of Na^+, Cl^-, Mg^{2+} and TP of harvested fetal fluids showed increasing/decreasing values throughout gestation (CRL = crown rump length). Spearman's ranks correlation matrices for AL (D) and AF (E) display all correlation detected, graphical modeling results are displayed for AL (F) and AF (G).

CORRELATION – ELECTROLYTES AND TOTAL PROTEIN VS CRL

Measurements of AF and AL biochemical components from gravid uteri post mortem (n=31) showed several significant correlations with the CRL of the fetus (Figure 3C), representing a surrogate marker for the gestational age. Spearman's rank correlation matrices display correlations for each fluid, AL (Figure 3D) and AF (Figure 3E). While Na^+-levels of AF decreased significantly throughout pregnancy ($R=-0.88$, $p < 0.001$), no significant correlation could be detected in AL ($R=-0.09$, $p=0.64$). Cl^--levels of AF ($R=-0.83$, $p < 0.001$) and AL ($R=-0.69$, $p < 0.001$) decreased significantly throughout pregnancy. On the other hand, Mg^{2+} showed a significant increase in AF ($R=0.72$, $p < 0.001$) and AL ($R=0.69$, $p < 0.001$) fluid. TP levels only showed an increase in the AL throughout gestation ($R=0.62$, $p < 0.001$), while the values for AF were mostly below detection level (detection level: 2g/l).

Correlation analyses using graphical modeling revealed strong dependence between Na^+ and Cl^- levels in the amnion compartment, but not with Mg^{2+} levels when corrected for fetal size. In the allantois compartment, all measured electrolytes except for Na^+ depend on size. However, Mg^{2+} is independent of Cl^- given TP and independent of size given Cl^- and TP, whereas TP is independent of size given Cl^-.

3.1.4 DISCUSSION

Amniotic fluid is a highly dynamic compartment that changes in volume and composition during pregnancy. It not only provides mechanical cushioning, but also contains nutrients and growth factors for fetal growth and development. AF volume results from a balance between fetal fluid production (urination, expiration) and reabsorption (swallowing, intramembranous absorption) in a defined pattern through pregnancy [23]. In humans, AF volume increases linear to fetal size until mid gestation (~25 weeks), where AF volume is no longer increasing in a linear fashion given complete keratinization of the fetal skin. A plateau is reached near term gestation (~28 weeks) and thereafter its volume declines (~42 weeks) [23,24]. In the ovine model this AF plateau and decline has not been found in the presented study, consistent with previous reports [17]. In the ovine model AF showed a significant increase over time in a linear fashion, whereas AL maintained relatively static with smaller volumes compared to AF, as previously reported [17]. Interestingly, fluid dynamics described by Bazer et al. did show the same AL behavior with a small decrease around gestational week 7-10, followed by an increase afterwards [17]. These consistent findings suggest fluid control mechanisms in the allantois. Its function consists of collecting liquid waste from the embryo and gas exchange. There are also reports suggesting the allantois as a reservoir for nutrients, given its fusion with the chorion to form the chorioallantoic placenta during placentation [25]. This independence of the AL compartment has also been shown by the graphical modeling displayed in presented data, where a clear anatomical independence of this compartment was shown.

In the presented study, three electrolytes and TP were selected based on their clear discriminative potential between AF and AL. They represent hallmark biomarkers for the accurate isolation of fetal fluids in the ovine developmental model [11]. By this manner collateral contaminations can be easily excluded. This includes on one hand the evaluation of the fetal fluid function and composition during fetal interventions, and on the other hand well-defined isolation of fetal cells for cell based tissue regeneration. In this regard, the presented work shows that not only the mean values of each fluid show a sensitive and specific discrimination, but also changes over gestation still enable accurate discrimination of AF and AL. These evaluations extending the entire gestation are mandatory for future preclinical evaluations involving AF harvest in the ovine model and its translation into the human counterpart.

Average Cl^- and Na^+ levels were significantly higher in the AF and showed a significant decrease over pregnancy in the AF for both electrolytes but in the AL only for Cl^-. This is consistent with independent studies in mares [15], sheep [20,26] and feline [18]. The decrease in Na^+ and Cl^- in the AL is suggested to be based on the increasing reabsorption ability of the fetal kidneys by means of the Na^+-K^+-ATPase activity [18] and the increased renal responsiveness to plasma aldosterone [27]. In

humans, lower Na^+ concentrations are found by the end of pregnancy given an almost completely developed fetal kidney with Na^+ reabsorption of about 85-95% of the filtration load [28]. It has been shown that the origin of the AF in humans varies through pregnancy. During early gestation, AF is similar to fetal plasma and the production is due to diffusion of water and solutes between the fetus and the not-yet-keratinized fetal skin and the surfaces of the amnion, placenta and umbilical cord [23,29]. At late gestation, the majority of the fluid is produced by the fetus itself by secretion from the respiratory tract or by production of urine [23,29]. Thus at late gestation only 28% of ovine AL osmolality is based on electrolyte contribution, given major developmental changes in metabolic activity [30]. Interestingly, overall Na^+, K^+ and Cl^- concentrations have shown to account for a significant greater proportion of AF osmolality in humans (97%) as compared to ovine AF alone (86%) or hypothetically combined with ovine AL [31]. These results demonstrated increased concentration of nonelectrolyte solutes in the ovine model such as sugars and proteins compared to the human situation [31]. High TP values were found in the AL, with increasing values over time, whereas TP below detection level were measured for the AF. In pregnant sheep TP values only below 1g/l have been detected in the AF [15,20,32], which would be below the detection threshold of the method used in the presented study. In humans, AF proteins (0.2-7g/l) are mainly of maternal origin and its principal clearance mechanism is based on fetal swallowing [33]. Low level of TP in AF is necessary to maintain the osmotic pressure between AF and maternal blood [34]. Among these proteins, proteomic analysis revealed peptides involved in cellular movement, development of organs, cell-to-cell signaling, cellular growth and proliferation [35]. In humans, these proteins get into the AF by different routes such as the maternal uterine tissue, umbilical cord, AF cells, fetal urine, meconium and transudation through fetal skin [33]. Accordingly, AF is not the result of simple filtration from the maternal blood, but independently providing a pathway for the transport of regulatory proteins for fetal development [34]. However, one has to emphasize, that all the measured values itself might differ from physiological values due to post mortem harvest. As an example the meconium, which is usually retained in the fetus until after birth, can be expelled in certain cases into the fetal cavities. However, Na^+, K^+ and TP values detected in living sheep [17,31] covered the same range as described in the presented study, suggesting minimal compositional changes of the fetal fluids post mortem. Furthermore, Mg^{2+} levels in human and ovine AF were consistent, which has been hypothesized as an indicator for pregnancy complications such as preeclampsia and diabetes [36]. Overall, changes in the composition along gestation represent changes in metabolic and transport activity as well as different contributions of fetal and extra-embryonic tissues.

In summary, these results provide information on ovine fetal fluid dynamics and benchmark values for preclinical studies examining volumetric and compositional changes of the AF as well as the isolated cells thereof. Further this study highlights the necessity of a better characterization of the

physiology of currently used animal models for more accurate extrapolation of gained knowledge to the human situation, which also seems indispensable with regards to ethical principles in animal research.

3.1.5 REFERENCES

1 Kunisaki, S. M. *et al.*, D. O. Fetal tracheal reconstruction with cartilaginous grafts engineered from mesenchymal amniocytes. *J Pediatr Surg* **41**, 675-682; discussion 675-682, doi:10.1016/j.jpedsurg.2005.12.008 (2006).

2 Gray, F. L. *et al.* Prenatal tracheal reconstruction with a hybrid amniotic mesenchymal stem cells-engineered construct derived from decellularized airway. *J Pediatr Surg* **47**, 1072-1079, doi:10.1016/j.jpedsurg.2012.03.006 (2012).

3 Fuchs, J. R. *et al.* Diaphragmatic reconstruction with autologous tendon engineered from mesenchymal amniocytes. *J Pediatr Surg* **39**, 834-838; discussion 834-838 (2004).

4 Kunisaki, S. M. *et al.* Diaphragmatic repair through fetal tissue engineering: a comparison between mesenchymal amniocyte- and myoblast-based constructs. *J Pediatr Surg* **41**, 34-39; discussion 34-39, doi:10.1016/j.jpedsurg.2005.10.011 (2006).

5 Turner, C. G. *et al.* Preclinical regulatory validation of an engineered diaphragmatic tendon made with amniotic mesenchymal stem cells. *J Pediatr Surg* **46**, 57-61, doi:10.1016/j.jpedsurg.2010.09.063 (2011).

6 Weber, B. *et al.* Prenatally engineered autologous amniotic fluid stem cell-based heart valves in the fetal circulation. *Biomaterials* **33**, 4031-4043, doi:10.1016/j.biomaterials.2011.11.087 (2012).

7 Klein, J. D. *et al.* Amniotic mesenchymal stem cells enhance normal fetal wound healing. *Stem Cells Dev* **20**, 969-976, doi:10.1089/scd.2010.0379 (2011).

8 Barry, J. S. & Anthony, R. V. The pregnant sheep as a model for human pregnancy. *Theriogenology* **69**, 55-67 (2008).

9 Emmert, M. Y. *et al.* Intramyocardial transplantation and tracking of human mesenchymal stem cells in a novel intra-uterine pre-immune fetal sheep myocardial infarction model: a proof of concept study. *PLoS One* **8**, e57759, doi:10.1371/journal.pone.0057759 (2013).

10 Cremonesi, F. *et al.* Fetal adnexa derived stem cells from domestic animal: progress and perspectives. *Theriogenology* **75**, 1400-1415, doi:10.1016/j.theriogenology.2010.12.032 (2011).

11 Weber, B. *et al.* In vitro fabrication of autologous living tissue-engineered vascular grafts based on prenatally harvested ovine amniotic fluid-derived stem cells. *J Tissue Eng Regen Med* **10**, 52-70, doi:10.1002/term.1781 (2016).

12 Pansky, B. *Review of medical embryology*. (Macmillan New York, 1982).

13 Kehl, D. *et al.* Amniotic fluid cells show higher pluripotency-related gene expression than allantoic fluid cells. *Stem Cells and Development (under Revision 1, unpublished)* (2016).

14 Riding, G. A. *et al.* Proteomic analysis of bovine conceptus fluids during early pregnancy. *Proteomics* **8**, 160-177, doi:10.1002/pmic.200700465 (2008).

15 Zanella, L. F. *et al.* Biochemical profile of amniotic and allantoic fluid during different gestational phases in mares. *Journal of Equine Veterinary Science* **34**, 403-406 (2014).

16 Anitha, A., Thangavel, A. Biochemical profile of ovine amniotic and allantoic fluids. *Talminadu Journal Veterinary & Animal Sciences* **7**, 262-267 (2011).

17 Bazer, F. W. *et al.* Growth and development of the ovine conceptus. *J Anim Sci* **90**, 159-170, doi:10.2527/jas.2011-4180 (2012).

18 Fresno, L *et al.* Modulation of the biochemical composition of amniotic and allantoic fluids as a control mechanism of feline foetal development. *Placenta* **33**, 522-527, doi:10.1016/j.placenta.2012.03.002 (2012).

19 McCarty, R. C *et al.* Characterisation and developmental potential of ovine bone marrow derived mesenchymal stem cells. *J Cell Physiol* **219**, 324-333, doi:10.1002/jcp.21670 (2009).

20 Prestes, N. C. *et al.* Amniocentesis and biochemical evaluation of amniotic fluid in ewes at 70, 100 and 145 days of pregnancy. *Small Rumin Res* **39**, 277-281 (2001).

21 Sivachelvan, M. *et al.* Foetal age estimation in sheep and goats. *Small Ruminant Research* **19**, 69-76 (1996).

22 Kratzer, G. *et al.* abn: an R package for modelling multivariate data using additive Bayesian networks. *Technical Report* (2016).

23 Underwood, M. A. *et al.* Amniotic fluid: not just fetal urine anymore. *J Perinatol* **25**, 341-348, doi:10.1038/sj.jp.7211290 (2005).

24 Brace, R. A. & Wolf, E. J. Normal amniotic fluid volume changes throughout pregnancy. *Am J Obstet Gynecol* **161**, 382-388 (1989).

25 Bazer, F. W. Allantoic fluid: Regulation of volume and composition. *Fetal and Neonatal Body Fluids. R.A. Brace, ed. Perinatology Press, Cornell, NY*, 135-157 (1989).

26 Ross, M. G. *et al.* Ovine fetal urine contribution to amniotic and allantoic compartments. *Biol Neonate* **53**, 98-104 (1988).

27 Lingwood, B. *et al.*Effect of aldosterone on urine composition in the chronically cannulated ovine foetus. *J Endocrinol* **76**, 553-554 (1978).

28 Oliveira, F. R. *et al.* Biochemical profile of amniotic fluid for the assessment of fetal and renal development. *Braz J Med Biol Res* **35**, 215-222 (2002).

29 Parolini, O. *et al.* Amniotic membrane and amniotic fluid-derived cells: potential tools for regenerative medicine? *Regen Med* **4**, 275-291, doi:10.2217/17460751.4.2.275 (2009).

30 Wales, R. G. & Murdoch, R. N. Changes in the composition of sheep fetal fluids during early pregnancy. *J Reprod Fertil* **33**, 197-205 (1973).

31 Albuquerque, C. A. *et al.* Human and ovine amniotic fluid composition differences: implications for fluid dynamics. *J Matern Fetal Med* **8**, 123-129, doi:10.1002/(SICI)1520-6661(199905/06)8:3<123::AID-MFM10>3.0.CO;2-# (1999).

32 Tangalakis, K. *et al.* Effect of maternal glucocorticoid treatment on ovine fetal fluids at 0.6 gestation. *Reprod Fertil Dev* **7**, 1595-1598 (1995).

33 Tisi, D. K. *et al.* Total protein concentration in human amniotic fluid is negatively associated with infant birth weight. *J Nutr* **134**, 1754-1758 (2004).

34 Tong, X. L. *et al.* Potential function of amniotic fluid in fetal development---novel insights by comparing the composition of human amniotic fluid with umbilical cord and maternal serum at mid and late gestation. *J Chin Med Assoc* **72**, 368-373, doi:10.1016/S1726-4901(09)70389-2 (2009).

35 Cho, C. K. *et al.* Proteomics analysis of human amniotic fluid. *Mol Cell Proteomics* **6**, 1406-1415, doi:10.1074/mcp.M700090-MCP200 (2007).

36 Bocos Terraz, J. P. *et al.* Magnesium concentration in amniotic fluid in the early weeks of the second trimester of pregnancy. *BMC Res Notes* **4**, 185, doi:10.1186/1756-0500-4-185 (2011).

CHAPTER 3.2

Amniotic fluid cells show higher pluripotency-related gene expression than allantoic fluid cells

Debora Kehl[1°], Melanie Generali[1°], Sabrina Görtz[1], Diego Geering[1], Jaroslav Slamecka[2], Simon P. Hoerstrup[1,3,4], Ulrich Bleul[5], Benedikt Weber[1,3,4]

° These authors contributed equally
[1] Institute for Regenerative Medicine (IREM), Center for Therapy Development and Good Manufacturing Practice, University of Zurich, Zurich, Switzerland
[2] Mitchell Cancer Institute, University of South Alabama, Alabama, USA
[3] Center for Applied Biotechnology and Molecular Medicine (CABMM), University of Zurich, Zurich, Switzerland
[4] Zurich Center for Integrative Human Physiology (ZIHP), University of Zurich, Zurich, Switzerland
[5] Clinic of Reproductive Medicine, Department of Farm Animals, Vetsuisse-Faculty University of Zurich, Zurich, Switzerland

Abstract

Amniotic fluid represents an abundant source of multipotent stem cells, referred as broadly multipotent given their differentiation potential and expression of pluripotency-related genes. However, the origin of this broadly multipotent cellular fraction is not fully understood. Several sources have been proposed so far, including embryonic and extra-embryonic tissues. In this regard, the ovine developmental model uniquely allows for direct comparison of fetal fluid-derived cells from two separate fetal fluid cavities, the allantois and the amnion, over the entire duration of gestation. As allantoic fluid mainly collects fetal urine, cells originating from the efferent urinary tract can directly be compared to cells deriving from the extra-embryonic amniotic tissues and the fetus. This study shows isolation of cells from the amniotic (oAFCs) and allantoic fluid (oALCs) in a strictly paired fashion with oAFCs and oALCs derived from the same fetus. Both cell types showed cellular phenotypes comparable to standard mesenchymal stem cells (MSC), with trilineage differentiation potential and expression of common ovine MSC markers. However, the expression of MSC markers per single cell was higher in oAFCSs as measured by flow cytometry. oAFCs exhibited higher proliferative capacities and showed significantly higher expression of pluripotency-related genes *OCT4, STAT3, NANOG* AND *REX1* by qRT-PCR compared to paired oALCs. No significant decrease of pluripotency-related gene expression was noted over gestation, implying that cells with high differentiation potential may be isolated at the end of pregnancy. In conclusion, this study suggests that cells with highest stem cell characteristics may originate from the fetus itself or the amniotic fetal adnexa rather than from the efferent urinary tract or the allantoic fetal adnexa.

Personal contribution:

Experimental contributions (Kehl D only):
Flow cytometry analysis of MSC markers in oAFCs, oALCs and oBMSCs. Differentiation of all three cell types into adipogenic, osteogenic and chondrogenic lineages. Primer design and establishment.

Experimental contributions (Kehl D, together with co-authors)
Harvest of amniotic and allantoic fluid from gravid uteri post mortem. Isolation, expansion and freezing of oAFCs, oALCs and oBMSCs. Phenotyping all cell types by immunohistochemistry for common MSC and pluripotency-related markers.

Non-experimental contributions (Kehl D only):
Study design and planning of the study. Acquiring funding for the entire project. Supervision and teaching of two medical master students involved in the project. Analyzing all raw data. Statistical analysis. Drafting all figures. Writing the entire manuscript. Submission and correspondence with editorial office, including revision (R1).

Steps contained in the published work (without personal contribution of Kehl D)
qPCR of pluripotency-related markers. Three-dimensional computed tomography (CT) of ovine anatomy and fetal fluid cavities, including injection of contrast agent.

Stem Cell and Development (published 2017)

3.2.1 INTRODUCTION

Amniotic fluid represents an abundant source of multipotent stem cells, which are currently being explored as a versatile cell source for autologous cell-based therapies. These amniotic fluid-derived stem cells (AFSCs) have a phenotype similar to bone marrow-derived (multipotent) mesenchymal stem cells (BMSCs) [37]. However, human AFSCs are often referred to as "broadly multipotent" given the expression of factors involved in the maintenance of pluripotency in embryonic stem cells (ESCs), such as *OCT4*, *NANOG* and *SSEA-4* [38,39]. AFSCs have also been differentiated into cell types of all three germ layers, including adipogenic, osteogenic, myogenic, hepatic, neuronal and endothelial lineages [40], either using an unselected or a small pre-selected population of c-kit (CD117) positive cells [38]. These characteristics make AFSCs highly amenable to reprogramming, which further supports their higher "stemness" compared to postnatal multipotent stem cell sources [41-44].

So far, the origin of human AFSCs during intrauterine development in general as well as the origin of this broadly multipotent cellular fraction in particular is not fully understood yet. AFSCs represent a heterogeneous population of cells and ultimately several sources of origin have been proposed, including embryonic (such as the urinary tract, the skin, the urogenital, respiratory or gastrointestinal tract) as well as extra-embryonic tissues (such as the placental tissue or the amniotic fetal adnexa) [45]. Also the origin of the amniotic fluid itself varies with increasing gestational age, while at the beginning the production is mainly due to active water and electrolyte transport across the amniochorionic membrane and fetal skin, in the second half of gestation most of the fluid is produced by the fetus itself, either by secretion from the respiratory tract or by production of urine [23,29]. This further suggests that the origin of cells may also vary with different stages of gestation. However, anatomical and ethical limitations prevent further studies concerning the origin of AFSCs in humans.

On the contrary, the ovine developmental model uniquely enables investigation of prenatal extraembryonic (stem) cell compartments [11]. Although being structurally and ontogenetically similar to the human fetal anatomy [8] and thus, serving as a standard *in vivo* animal model for several fetal therapeutic interventions involving AFSCs [1-7,11,46], it maintains two separate extraembryonic fluid compartments over the entire duration of pregnancy, the allantoic and the amniotic fluid cavities (Figure 1). In human embryogenesis the allantois is only present in the first 3 to 5 weeks after conception and afterwards it involutes to form the the intraembryonic urachus [12]. Interestingly, in sheep the allantoic fluid compartment mainly collects fetal urine, which is drained from the urinary bladder via the urachus [8]. It therefore represents a model that allows for a direct comparison of fetal fluid-derived cells originating from the efferent urinary tract and the allantoic fetal adnexa with cells derived from the fetus itself and amniotic fetal adnexa directly surrounding the fetus. A

comparison of the pluripotency-related gene expression of fetal fluid-derived cells from different compartments would shed some first light on the actual origin of the (broadly) multipotent cellular component of human amniotic fluid cells, in particular on whether these cells seem to originate from efferent urinary tissues or not.

Therefore, the present study compares the expression of pluripotency-related genes between cells isolated from the amniotic versus the allantoic fluid cavity in the ovine developmental model over gestation in a strictly paired fashion.

3.2.2 MATERIAL AND METHODS

3.2.2.1 POST MORTEM HARVEST OF OVINE FETAL FLUIDS

Ovine amniotic and allantoic fluids were harvested from gravid uteri post mortem from the local slaughterhouse Zurich/Hinwil, Switzerland (n=9). The fetuses were selected according to crown rump length (CRL) and allocated to three corresponding gestational age groups – group 1: CRL ≤ 15 cm; group 2: >15 cm, ≤ 30 cm CRL; group 3: > 30 cm CRL [21]. For illustration purposes of the ovine fluid cavities, a computer tomography (CT) (Brilliance 16, Philips AG, Zurich, Switzerland) examination was performed with different concentrations of contrast medium injected into each fluid cavity (Ioversol, Optiray 300, Guerbet, Switzerland) (Figure 1).

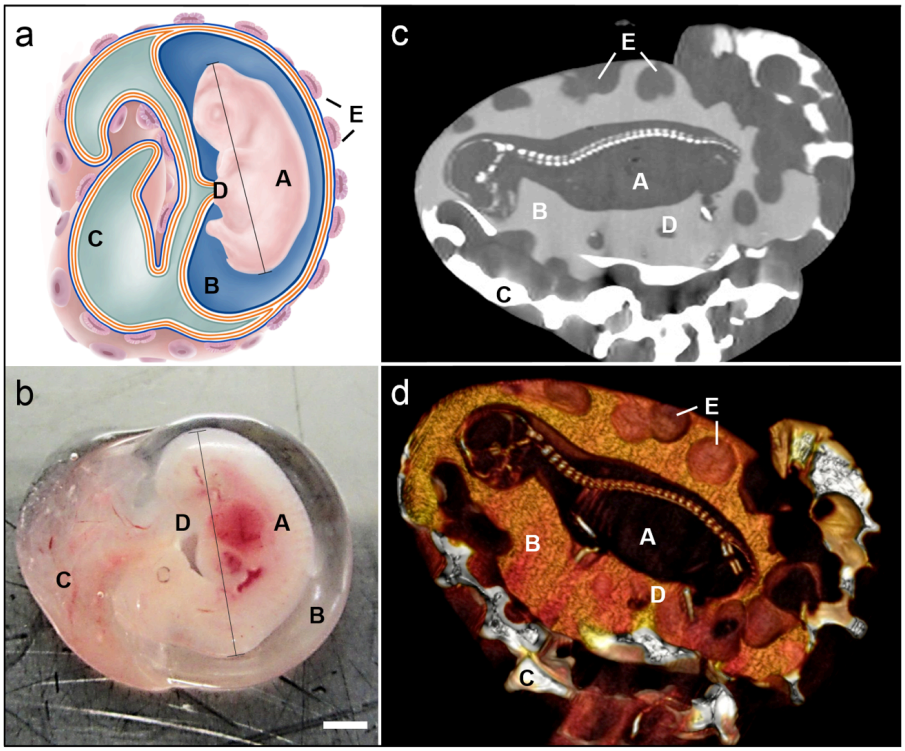

Figure 1: The ovine developmental model and its corresponding fetal fluid cavities. (a-b) The ovine fetus (A) is surrounded by the inner amniotic fluid cavity (B), which is separated from the outer allantoic fluid cavity (C) drained via the umbilical cord (D). The fetal fluid cavities are surrounded by the uterine wall, which is covered by single placentoma units (E). (c-d) Three-dimensional computed tomography (CT) reconstruction of the ovine anatomy and the fetal fluid volumina (by the use of 10ml Optiray 300 for amniotic fluid and 20ml Optiray for allantoic fluid) show *in vivo* architecture of the ovine fetal fluid compartments as previously described in the schematic. Scale bar = 0.5 cm.

For the harvest of ovine fetal fluid, the uterus and the fetal fluid cavities were opened surgically and the fetal fluids were aspirated with a 50ml syringe and a 10 Gauge needle under visual guidance as previously published [11]. In case of inaccurate surgical puncture or blood contamination, isolated samples were excluded from the study. Following centrifugation for 10 minutes at 300g, residual cells were separated from their corresponding fetal fluid. For each animal, one aliquot of harvested supernatant was stored overnight at 4°C to verify the accuracy of fetal fluid harvest (and

consequently accurate cell isolation) according to previous studies [11]. Therefore, values of total protein, Albumin, Sodium, Chloride and Magnesium were compared to reference values from an existing database previously published [11]. These parameters revealed a high discriminative power to distinguish between the two fetal fluids. If selected values deviate from the reference values, isolated cells were excluded from subsequent analysis, as their pure origin could not be proven.

3.2.2.2 ISOLATION AND EXPANSION OF CELLS

oAFCs AND oALCs

Ovine amniotic fluid cells (oAFCs; n=9) and allantoic fluid cells (oALCs; n=9) were isolated by centrifugation of the fetal fluids at 300g. The obtained cell pellet was seeded into standard culture flasks and incubated in a humidified incubator at 5% CO_2 at 37 °C. The proliferation medium consisted of endothelial basal medium (EBM™; Lonza, Switzerland) supplemented with 10% fetal calf serum (FCS, Sigma-Aldrich, Switzerland), and growth factors (recombinant long-insulin-like growth factor-1 (R3-IGF-1), human fibroblast growth factor (rhFGF-B), human epidermal growth factor (rhEGF) and ascorbic acid, as well as an antibiotic-antimycotic solution containing 100 U/ml penicillin, 100 µg/ml streptomycin and 25 ng/ml amphotericin B.

This medium has been used in previous studies [11,41,47,48] and demonstrated to prevent pre-differentiation of isolated fetal cells and maintain their stem cell phenotype over *in vitro* passaging. Non-adherent cells were removed by replacing the medium 72-96 hours following the seeding procedure. At 80% confluency, cells were split using Accutase (Gibco™, ThermoFisher Scientific, USA) or Trypsin-EDTA Solution (Sigma-Aldrich, Switzerland). Cellular viability was assessed using a 0.4% trypan blue exclusion staining (Gibco™, ThermoFisher Scientific, USA). A stock of frozen cells at every passage was stored in liquid nitrogen (10% DMSO in FCS, Sigma-Aldrich, Switzerland) until further analysis.

CONTROL oBMSCs

The isolation of ovine bone marrow-derived mesenchymal stem cells (oBMSCs; n=3) as control cells was performed according to standard procedures. In brief, bone marrow aspirate was obtained from the sternum or iliac crest of an adult sheep in oblique supine position under general aesthesia according to the cantonal ethical permission No. 9/14. Int. 25040. Bone marrow aspirate was diluted 1:2 with PBS for a histopaque (Histopaque-1077, Sigma-Aldrich, Switzerland) density gradient centrifugation at 400G for 30min. The obtained mononuclear cell layer was washed with PBS and seeded in above mentioned proliferation medium for further expansion. A stock of frozen cells at every passage was stored in liquid nitrogen (10% DMSO in FCS) for further analysis.

3.2.2.3 PHENOTYPIC CHARACTERIZATION OF oAFCs, oALCs AND CONTROL oBMSCs

ANTIBODIES

Primary antibodies used were specific against CD11b (clone CC126, AbDSerotec, UK), CD29 (A.Zannettino, Adelaide, Australia) [19], CD44 (clone MAC329, LifeSpan BioSciences, USA; sc-59758, Santa Cruz Biotech, USA), CD166 (clone 3A6, Biolegend, USA), STRO-4 (A.Zannettino, Adelaide, Australia) [49], Desmin (clone D33, Dako, Denmark), Vimentin (clone Vim3B4, Dako, Denmark), α-smooth muscle actin (αSMA) (clone 1A4, Dako, Denmark), NANOG (hNanog.2, eBioscience, USA), OCT3/4 (H-134, Santa Cruz, USA) and STAT3 (BD Transduction Laboratories, USA). All stainings were accompanied by isotype controls for IgG1 (clone MOPC-21, Biolegend, USA) and IgG2a (clone MOPC-173, Biolegend, USA or AbDSerotec, UK), IgG2b (clone C.SW IgG_{2b}, k, BD Pharmingen^{TM}, USA) as well as secondary antibody-only control stainings. For immunofluorescence stainings, primary antibodies were detected with secondary goat-anti-mouse Cyanine-2-conjugated antibodies (Alexafluor 488, Jackson-ImmunoResearch or Life Technologies, USA), donkey-anti-rat Cyanine-2-conjugated antibodies (Alexafluor 488, Jackson-ImmunoResearch, USA) or goat-anti-rabbit Cyanine-2-conjugated antibodies (Alexafluor 488, Life Technologies, USA), phalloidin (AlexaFluor 546, Invitrogen, ThermoFisher Scientific, USA) and DAPI (Sigma-Aldrich, Switzerland). For flow cytometry, primary antibodies were detected with either a FITC-conjugated goat-anti-mouse antibody (BD Bioscience, USA) or a FITC-conjugated goat-anti-rat antibody (Biolegend, USA).

IMMUNOFLUORESCENCE STAINING

For immunofluorescence stainings, oAFCs (n=3), oALC (n=3) and oBMSC (n=3) were washed with PBS and fixed with 4% parafolmaldehyde/PBS for 10min. Following a second washing step with PBS, cells were permeabilized with 0.2% Triton X-100/PBS (Sigma-Aldrich, Switzerland) for 10min at room temperature. After blocking with 5% goat serum in 1% BSA/PBS for 30min at room temperature, primary antibodies (diluted in 5% goat serum/1% BSA/PBS) were added and incubated for 1h or overnight at room temperature. Cells were washed three times for 5min with PBS and incubated with the secondary antibodies for 45min at room temperature. Again, three washing steps with PBS were performed (3x 5min) and samples were mounted with Aqua-Poly/Mount (Polysciences, Inc., USA). Stained cells were visualized using an inverted fluorescence microscope equipped with a CCD camera (Zeiss Axiovert II; Zeiss, Germany and Leica DM6000B).

FLOW CYTOMETRY ANALYSIS

For flow cytometry analysis, 2 x 10^5 oAFCs (n=3), oALC (n=3) and oBMSC (n=3) were used per primary antibody staining, each diluted in FACS-buffer (2% FCS/PBS, 5mM EDTA) and incubated for 30min at

4°C. After two washing steps with FACS-buffer, the cells were incubated for another 30min at 4°C with secondary FITC-conjugated antibodies. Again, two washing steps with FACS-buffer were performed. Between 50'000 to 100'000 events were acquired using a FACSCanto II (BD Bioscience, USA) and the datasets were analyzed with FlowJo software (Tree Star, Inc., USA). Median fluorescence intensity ratio (MFIR) was calculated relative to the unstained controls. Specificity of the antibodies was verified using the corresponding isotype controls.

3.2.2.4 CELL PROLIFERATION KINETICS

Proliferation kinetics were monitored over the complete expansion period for every isolated fetal fluid. Only paired cell lines were integrated into the analysis, meaning that oAFCs (n=9) and oALCs (n=9) from the same fetus were expanded and compared. The population doubling (PD) rate was determined by integrating the harvested viable cell number (following a trypan blue exclusion staining) into the mentioned formula below [50]. N_1 is defined as the plated and N_H the harvested cell number.

$$X = \frac{[\log_{10}(N_H) - \log_{10}(N_1)]}{\log_{10}(2)}$$

To define the absolute number of times each cell has doubled since their first isolation *in vitro*, the cumulative population doublings (CPD) were calculated up to passage 3. Therefore, the PD of each passage was summed up to the PD of the previous one. The generation time (average time between two cell doublings) was calculated at all three passages using the following formula [50]:

$$X = \frac{\log_{10}(2) \cdot \Delta t}{\log(N_H) - \log\,(N_1)}$$

3.2.2.5 TRILINEAGE DIFFERENTIATION POTENTIAL

Multilineage differentiation was assessed by inducing differentiation of oAFCs (n=3), oALCs (n=3) and oBMSCs (n=3) to osteogenic, adipogenic and chondrogenic lineages according to standard protocols. Briefly, ovine cells were cultured in either I) osteogenic medium: 10nM glycerol 2-phosphat (Sigma, Switzerland), 50um L-ascorbic acid 2-phosphat (Sigma, Switzerland), 100nM dexamethasone (Sigma, Switzerland) and 2nM L-glutamine (Sigma, Switzerland) in low glucose Dulbecco's Modified Eagle Medium (DMEM; Sigma, Switzerland) with 10% FCS and an antibiotic-antimycotic solution, II) adipogenic medium (Gibco™, ThermoFisher Scientific, USA) or chondrogenic medium: 50um L-ascorbic acid 2-phosphat, 0.5 ug/ml insulin (Sigma, Switzerland), 10 ng/ml transforming growth factor-beta1 (Preprotech, UK), 2 mM L-glutamin in high glucose DMEM with 1% FCS and an

antibiotic-antimycotic solution. After 3 weeks, ovine cells were fixed in 4% paraformaldehyde/PBS and subsequently stained with either I) 2% Alzarin Red S (Sigma, Switzerland), II) 3mg/ml Oil Red O (Sigma, Switzerland) or III) Alcian Blue PAS.

3.2.2.6 PLURIPOTENCY-RELATED GENE EXPRESSION

Total RNA was extracted using RNeasy Mini Kits (Qiagen, Switzerland) and reverse transcription was carried out using Superscript III RT (Invitrogen, Switzerland) according to the manufacturer's instructions. Quantitative real-time PCR (qRT-PCR) was performed using Rotor-Gene SYBR Green PCR Kit SYBR (Qiagen, Switzerland) and ovine pluripotent stem cell primers (Microsynth, Switzerland) for *OCT4, STAT3, NANOG, SOX2* and *REX1* (Table 1). Primers have been established and evaluated by the use of a previously published ovine induced pluripotent stem cell (iPSC) line kindly provided by Paul Verma and Jun Liu of the Stem Cell and Genetic Engineering Group, Monash University, Clayton, Australia [51]. The expression levels were analysed twice in triplicates using standard conditions on a Rotor-Gene Q (Qiagen, Switzerland) for n=9 oAFCs, n=9 oALCs and n=3 oBMSCs. GAPDH served as housekeeping gene to quantify relative stemness expression levels using the ΔCT threshold cycle method. Expression levels were calculated with 2^{-dCT} and a multiplication factor of 100.

Gene	Forward primer	Reverse primer
OCT4	GTCACTGCTTGATCGTTTGC	GTGAGAGGCAACCTGGAGAG
STAT3	GACTGGAAGAGGCGACAACA	CGTTGCTGGGCCCTGAG
NANOG	TGCAGAGGAGAGCACAGAGA	CGTTGCTGGGCCCTGAG
SOX2	ACCAGCTCGCAGACCTACAT	GGTAGTGCTGGGACATGTGA
REX1	CAAGGCAAGGAGGCGGAG	AGCCGGCTGACTCCCT
GAPDH	GCGTGGACAGTGGTCATAAGT	TGGCAAAGTGGACATCGTTG

Table 1. Ovine primer sequences for quantitative real-time polymerase chain reaction analysis of pluripotencyy-related gene expression in ovine amniotic fluid cells and ovine allantoic fluid cells

3.2.2.7 STATISTICAL ANALYSIS

Quantitative data are presented as mean ± standard deviation (GraphPad Prism, GraphPad Software Inc., USA). For statistical comparison of the paired results on oAFCs and oALCs paired students-t-test were performed and p-values < 0.05 were considered statistically significant. Saphiro-Wilk normality test proved that the datasets were normally distributed ($p > 0.05$). Grubbs' test determined whether one of the data points represented a significant outlier from the rest ($p < 0.05$).

3.2.3 RESULTS

3.2.3.1 CELL ISOLATION, PROLIFERATION AND PHENOTYPIC CELL CHARACTERIZATION

After harvest of fetal fluids, the origin and purity of the fetal fluids was verified using a biochemical differential fluid analysis according to previously published protocols [11] prior to inclusion of the samples into the present study. Cellular yield, cell attachment and phenotypes were analyzed using light microscopy and compared between oAFCs (n=9), oALCs (n=9) and control oBMSCs (n=3) (Figure 2). Bacterial contamination and premature senescence, defined by stagnation of proliferation, high granularity of the cells and cellular detachment, was equally distributed between oAFCs and oALCs. Compared to oBMSCs, the oAFCs and oALCs showed a more heterogeneous intra- and inter-patient phenotypic variability, including cell size and phenotype.

Three morphological cell types (Figure 2a-h) were predominantly evident in both oAFCs (Figure 2a-d) and oALCs (Figure 2e-h): I) small spindle-shaped cells (Figure 2a-b and 2e-f), II) cobblestone-like cells, resembling epithelioid cells (Figure 2d, 2h), and III) larger flattened fibroblastic cells (Figure 2c, 2g). After direct plating, a highly heterogeneous population of cells was observed, whereas with passaging, the cell population became more homogenous with either phenotype I or III. At higher passages, a higher senescence rate was found with morphological changes of the cells and stagnated proliferation. Concerning proliferation (Figure 2j-k), oAFCs showed a tendency for lower generation times (GT) and higher cumulative population doublings (CPD) when compared to oALCs derived from the same mother animal and fetus (n=9 per source). Significant differences where predominantly found at passage 3 ($p < 0.05$). No differences in proliferation parameters were detected when cells derived from different gestational ages were compared to each other.

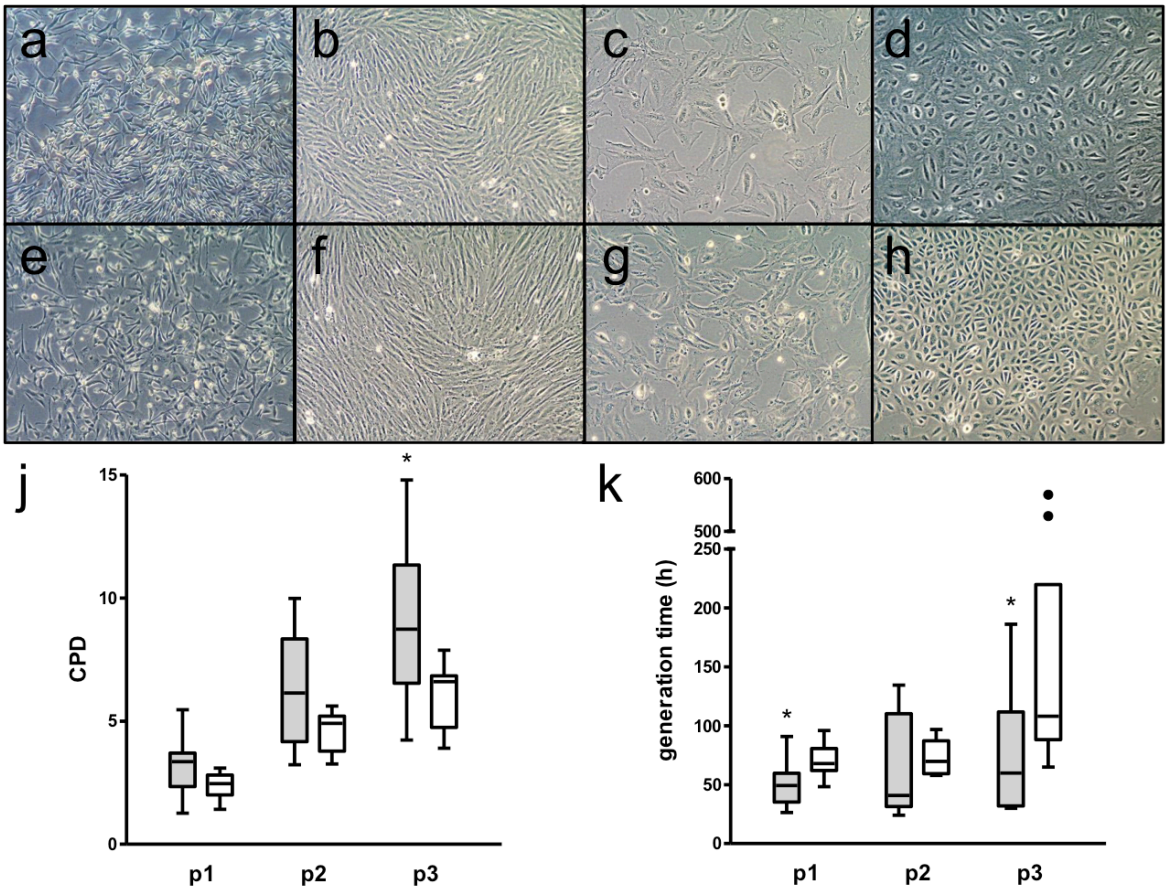

Figure 2: Morphology and proliferation capacity of isolated oAFCs and oALCs. Isolated oAFCs (n=9) (a-d) and oALCs (n=9) (e-h) showed similar initial heterogeneous cell phenotypes, including small spindle-shaped cells (a, b, e, f), larger flattened fibroblastic cells (c, g) and cobblestone-like cells, resembling epithelioid cells (d, h). After longer cultivation periods, a more homogenous cell population of mostly spindle-shaped and fibroblast-like cells prevailed. oAFCs (grey whiskers) exhibit a higher proliferation capacity then oALCs (white whiskers), given (j) the higher cumulative population doublings (CPD) and (k) the lower generation times. * = $p<0.05$

3.2.3.2 MSC SURFACE MARKER EXPRESSION AND TRILINEAGE DIFFERENTIATION OF oAFCs VERSUS oALCs

Immunofluorescence stainings (passage 3-5) of representative paired oAFCs (n=3) and oALCs (n=3) from the same fetus revealed a positive expression of common ovine MSC markers CD29, CD44, STRO-4 as well as Vimentin and alpha-smooth muscle actin (α-SMA) (Figure 3). A myogenic, mesodermal phenotype is supported by the positive expression of the intermediate filament Vimentin and α-SMA. Partial positivity was detected in CD166 and αSMA in both oAFCs and oALCs. Isotype control staining did not produce any signals. Overall no differences between oAFCs, oALCs and oBMSCs (n=3) could be detected by immunohistochemical analyses on a qualitative level.

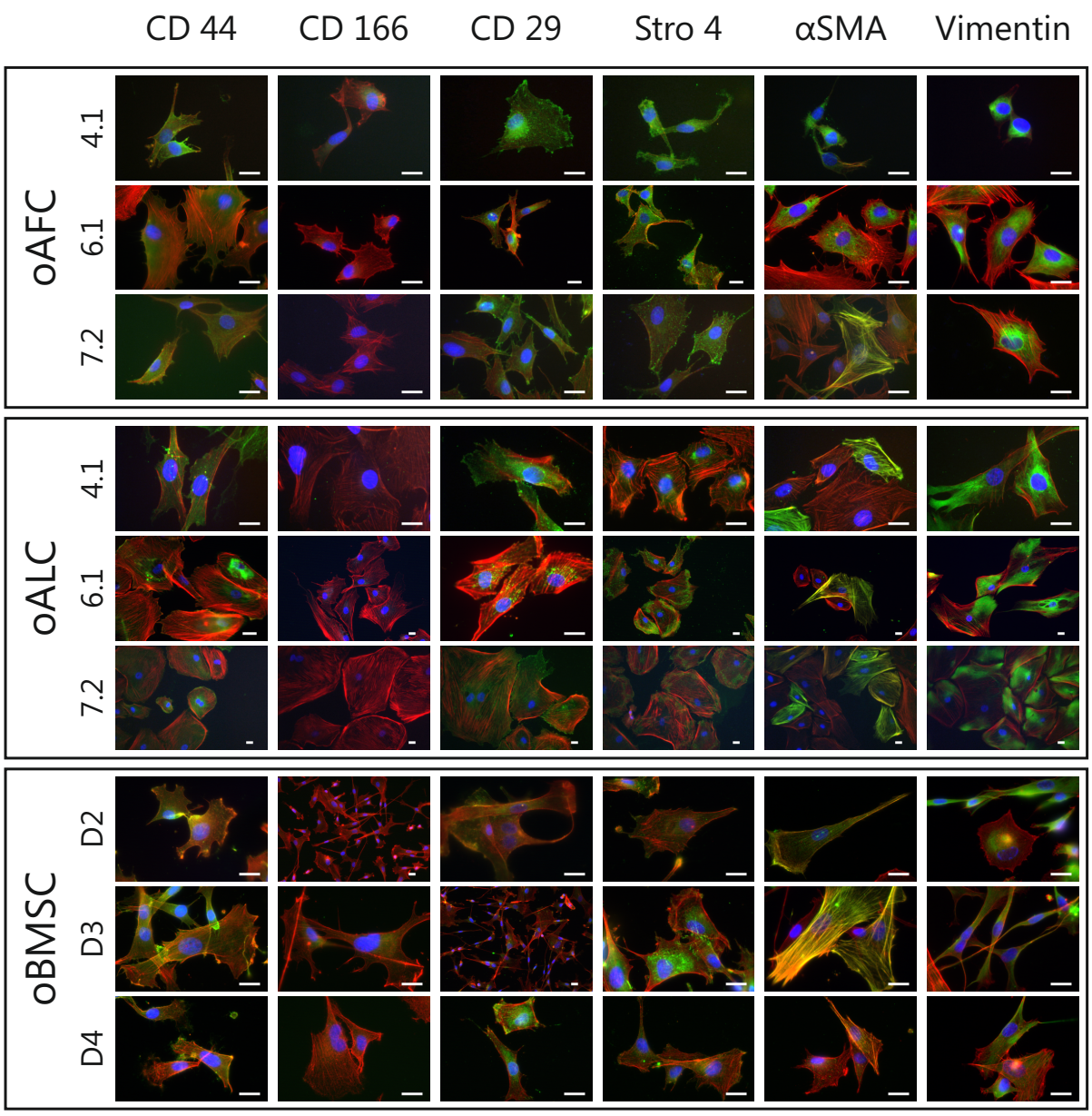

Figure 3: Phenotypic characterization of isolated oAFCs and oALCs. Immunohistological analyses of representative paired oAFCs (n=3; animal 4.1, 6.1 and 7.2) and oALCs (n=3; animal 4.1, 6.1 and 7.2) revealed positive expression of common MSC markers CD29, CD44, Stro4 and partial expression of CD166 (Phalloidin in red, Dapi in blue and respective antibody in green). Positive expression of Vimentin and αSMA show a myogenic, mesodermal phenotype of the cells. No phenotypic differences to standard oBMSCs (n=3; animal D2, D3 and D4) were detected. Scale bar = 10 µm.

Therefore, in order to further quantify MSC stem cell marker expression levels and to also detect differences between the three cell sources quantitatively, flow cytometry analyses for the same set of markers were conducted at passage 3-4 (Figure 4). Again positive expression of CD29, CD44, CD166 and STRO-4 was found in oAFCs (n=3), oALCs (n=3) and control oBMSCs (n=3) (with no expression of CD11b) (Figure 4a). Notably, oAFCs and oALCs were paired and derived from the same fetus for flow cytometry analyses. No statistically significant differences in the percentage of positive cells concerning the expression of CD11b, CD29, CD44 and STRO-4 could be detected between the three cell sources (Figure 4b, all P's >0.05). CD166 positive cells were more abundant in the fetal cell

sources (oAFCs and oALCs) than in adult oBMSC control cells. In contrast median fluorescence intensity ratios (MFIR) of the common MSC markers showed high heterogeneity between the three paired animal samples analyzed (Figure 4c). However, a reduced MFIR of common MSC markers was observed in oALCs when compared to oAFCs from the same mother animal and fetus (Figure 4d). This could be better appreciated when calculating the ratio of MFIR of oAFC/oALC samples for the following ovine MSC markers CD29 (mean ratio=2.4), CD44 (mean ratio=1.4) and STRO-4 (mean ratio=3) (Figure 4e).

These results demonstrate a higher expression of MSC surface markers per single cell in oAFC compared to paired oALC samples (even if the overall percentages of cell populations with MSC marker expression were equal in oAFCs and oALCs). Contrary to human cells, positive expression of the following established set of markers – CD29, CD44, CD166 and STRO-4 – defines MSC origin in the ovine animal model [19,49].

In addition, trilineage differentiation into the adipogenic, osteogenic and chondrogenic lineages was proven for oAFCs (n=3), oALCs (n=3) and oBMSCs (n=3). However, high inter-individual variances were evident and successful differentiation had to be assessed by direct comparison to the control set-up (Figure 5). In particular, osteogenic differentiation resulted in a weak Alzarin Red staining even if clear different to the control set-up.

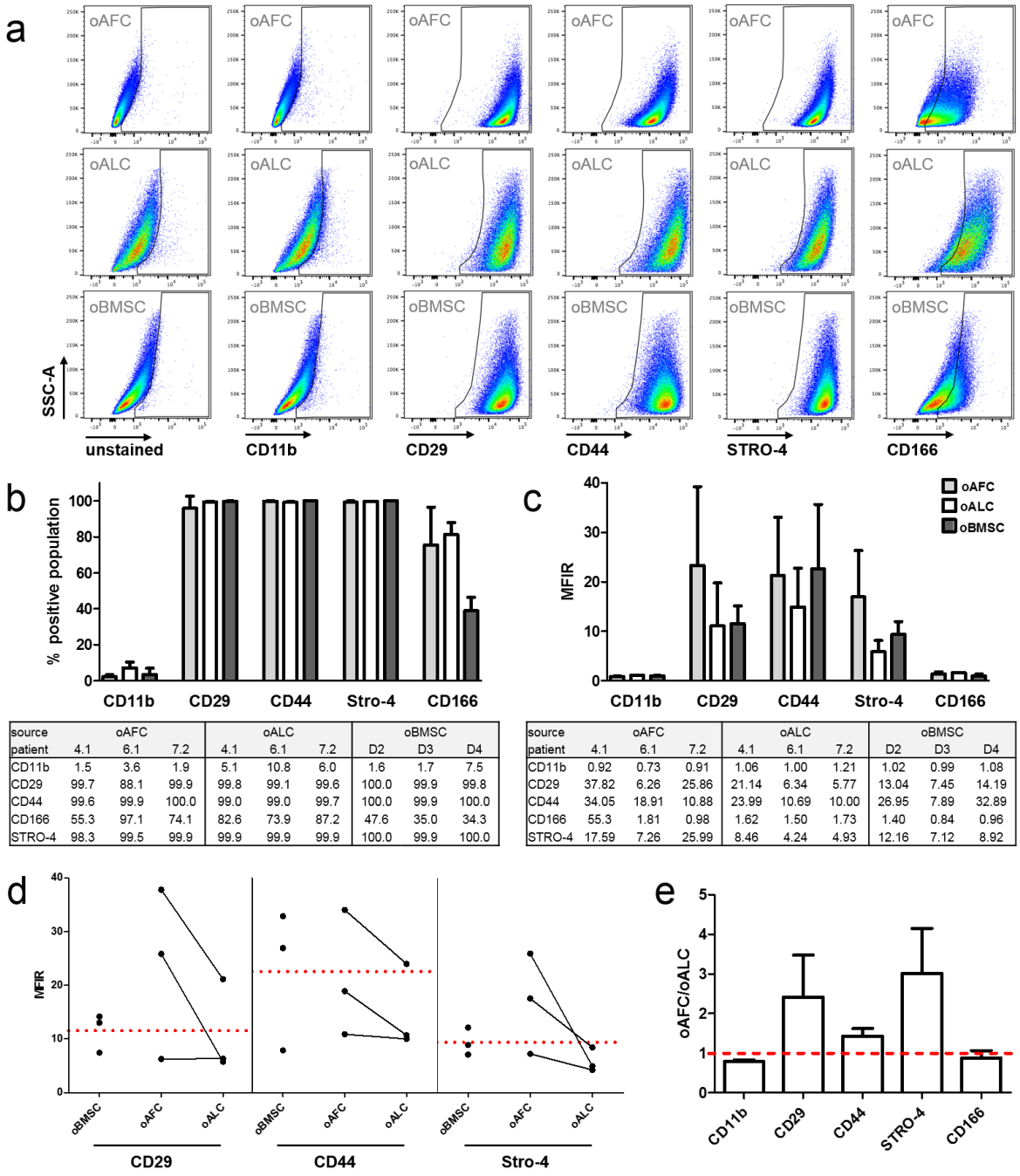

source	oAFC			oALC			oBMSC		
patient	4.1	6.1	7.2	4.1	6.1	7.2	D2	D3	D4
CD11b	1.5	3.6	1.9	5.1	10.8	6.0	1.6	1.7	7.5
CD29	99.7	88.1	99.9	99.8	99.1	99.6	100.0	99.9	99.8
CD44	99.6	99.9	100.0	99.0	99.0	99.7	100.0	99.9	100.0
CD166	55.3	97.1	74.1	82.6	73.9	87.2	47.6	35.0	34.3
STRO-4	98.3	99.5	99.9	99.9	99.9	99.9	100.0	99.9	100.0

source	oAFC			oALC			oBMSC		
patient	4.1	6.1	7.2	4.1	6.1	7.2	D2	D3	D4
CD11b	0.92	0.73	0.91	1.06	1.00	1.21	1.02	0.99	1.08
CD29	37.82	6.26	25.86	21.14	6.34	5.77	13.04	7.45	14.19
CD44	34.05	18.91	10.88	23.99	10.69	10.00	26.95	7.89	32.89
CD166	55.3	1.81	0.98	1.62	1.50	1.73	1.40	0.84	0.96
STRO-4	17.59	7.26	25.99	8.46	4.24	4.93	12.16	7.12	8.92

Figure 4: Mesenchymal stem cell marker expression of isolated oAFCs and oALCs. Expression of common ovine MSC markers was confirmed by flow cytometry with positive expression of CD29, CD44, and STRO-4, partial expression of CD166 and no expression of CD11b in paired oAFCs (n=3; animal 4.1, 6.1 and 7.2) and oALCs (n=3; animal 4.1, 6.1 and 7.2). oBMSCs served as a control cell source (n=3; animal D2, D3 and D4). (a) Flow cytometry gating strategy after exclusion of dead cells. No differences could be detected between oAFCs, oALCs and control oBMSCs (b) in the percentage of positive cells of all analyzed surface markers as well as (c) the median fluorescence intensity ratio (MFIR) due to high interpatient differences. (d) However, a reduced MFIR was observed in oALCs compared to paired oAFCs from the same fetus. Dotted red line displays the mean of control oBMSCs. (e) The ratio >1 of oAFC/oALC underlines the higher expression of MSC markers in oAFCs.

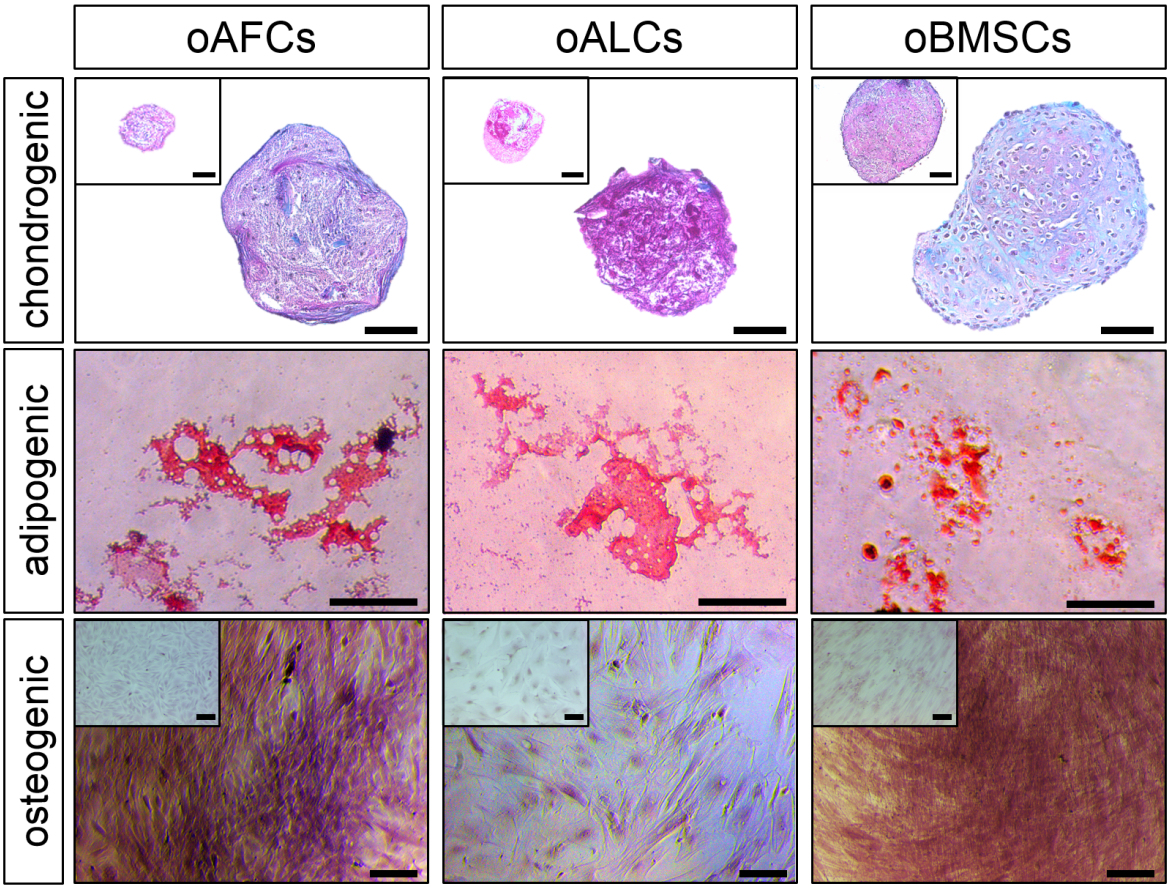

Figure 5: Multilineage differentiation potential of isolated oAFCs and oALCs. The capacity of oAFCs (n=3), oALCs (n=3) and oBMSCs (n=3) to differentiate into adipogenic, osteogenic and chondrogenic lineages was demonstrated by positive staining with Oil Red O, Alzarin Red S and Alcian Blue PAS. The upper squares represent stained controls. Scale bar = 100 µm.

3.2.3.3 PLURIPOTENCY-RELATED GENE EXPRESSION OF oAFCs versus oALCs

The expression of OCT4, STAT3 and NANOG was qualitatively shown with immunofluorescence stainings of representative cell lines of each cell group (Figure 6). Higher expression of all pluripotency-related markers has been detected for fetal oAFCs (n=3) and oALCs (n=3) in direct comparison to control oBMSCs (n=3). Ovine endothelial cells (oECs) served as control cells to verify the specificity of the particular staining and did not express any of the analyzed pluripotency-related markers (data not shown).

To quantify the differences in expression of genes involved in the maintenance of pluripotency, qRT-PCR analyses for *OCT4, STAT3, NANOG, SOX2* and *REX1*, at early (p1 = passage 1) and late (p4 = passage 4) passages, were performed (Figure 7). Significantly higher expression ($p < 0.05$) of *OCT4, STAT3, NANOG* and *REX1* was found in oAFCs (n=9) compared to oALCs (n=9) from the same offspring at p4 (Figure 7a, d, g, j, m). No significant difference was detected for *SOX2* (p=0.09). At p1, only a tendency of higher expression in oAFCs could be observed for *OCT4, STAT3, NANOG* and *SOX2*, but with no statistically significant differences (Figure 7a, d, g, j, m). Given these results with no

significant differences at p1, the observation of a decreasing heterogeneity of cell populations following further expansion might be of particular interest. *REX1* revealed a tendency of higher expression in oALCs in p1 (p=0.07), which could reflect a substantially higher expression of Rex1 at early gestational ages (gestational age group 1). Unpaired standard oBMSCs (n=3) served as a baseline MSC source for direct comparison.

By pairing each oAFC cell line with the corresponding oALC cell line from the same offspring, a significantly reduced expression of pluripotency-related genes in oALCs becomes evident at p4 (Figure 7b, e, h, k, n). To further analyze the gestational age dependency of pluripotency-related gene expression, three gestational age groups have been established based on the CRL (n=3 per group). However, qRT-PCR revealed no gestational age dependency in the expression of *OCT4, STAT3, NANOG* and *SOX2* (Figure 7c, f, i, l, o). Interestingly, higher *REX1* expression levels were observed in oALCs at gestational age group 1 compared to gestational age group 2 and 3.

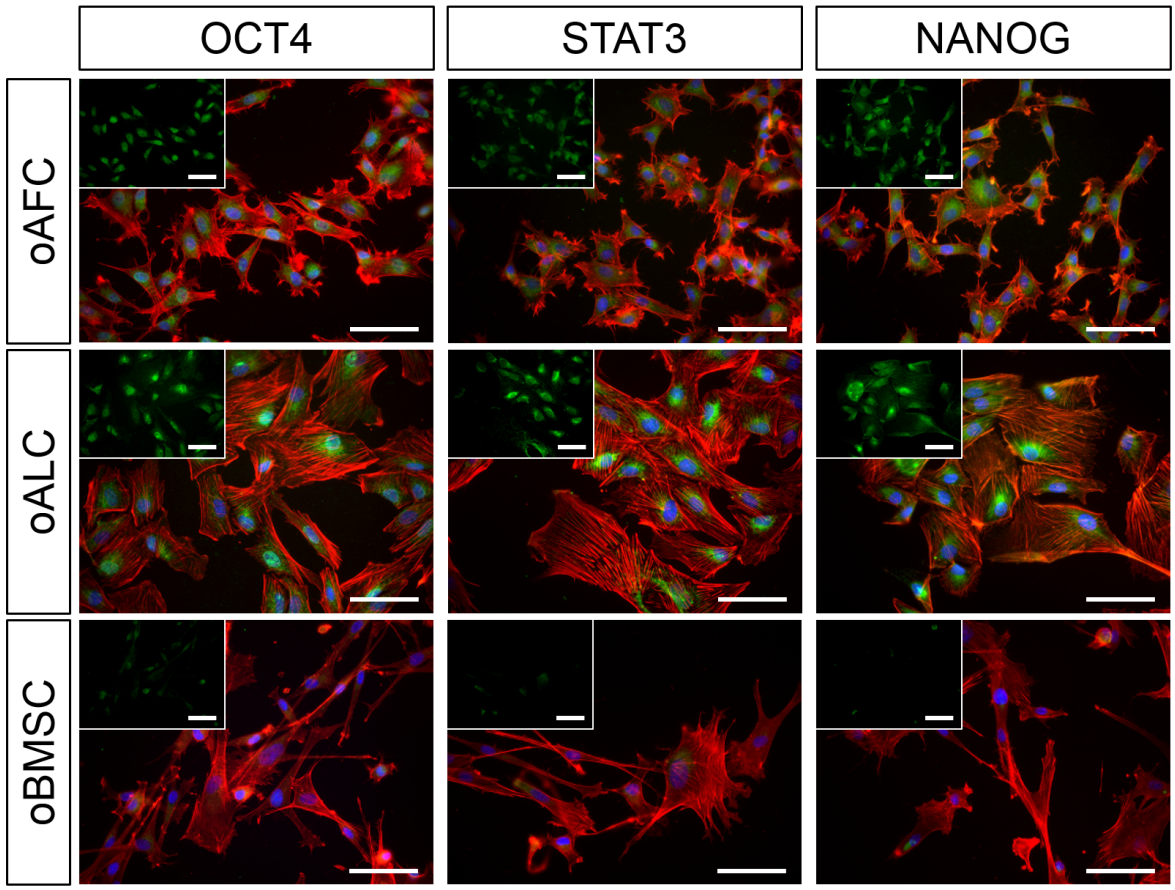

Figure 6: Phenotypic characterization of pluripotency-related stem cell markers of isolated oAFCs and oALCs. Immunohistological analyses of representative paired oAFCs (n=3) and oALCs (n=3) (Phalloidin in red, Dapi in blue and respective antibody in green) revealed positive expression of the pluripotency-related markers OCT4, STAT3 and NANOG. In direct comparison to oBMSCs (n=3) higher expression has been detected in fetal cells. Scale bar = 100 µm.

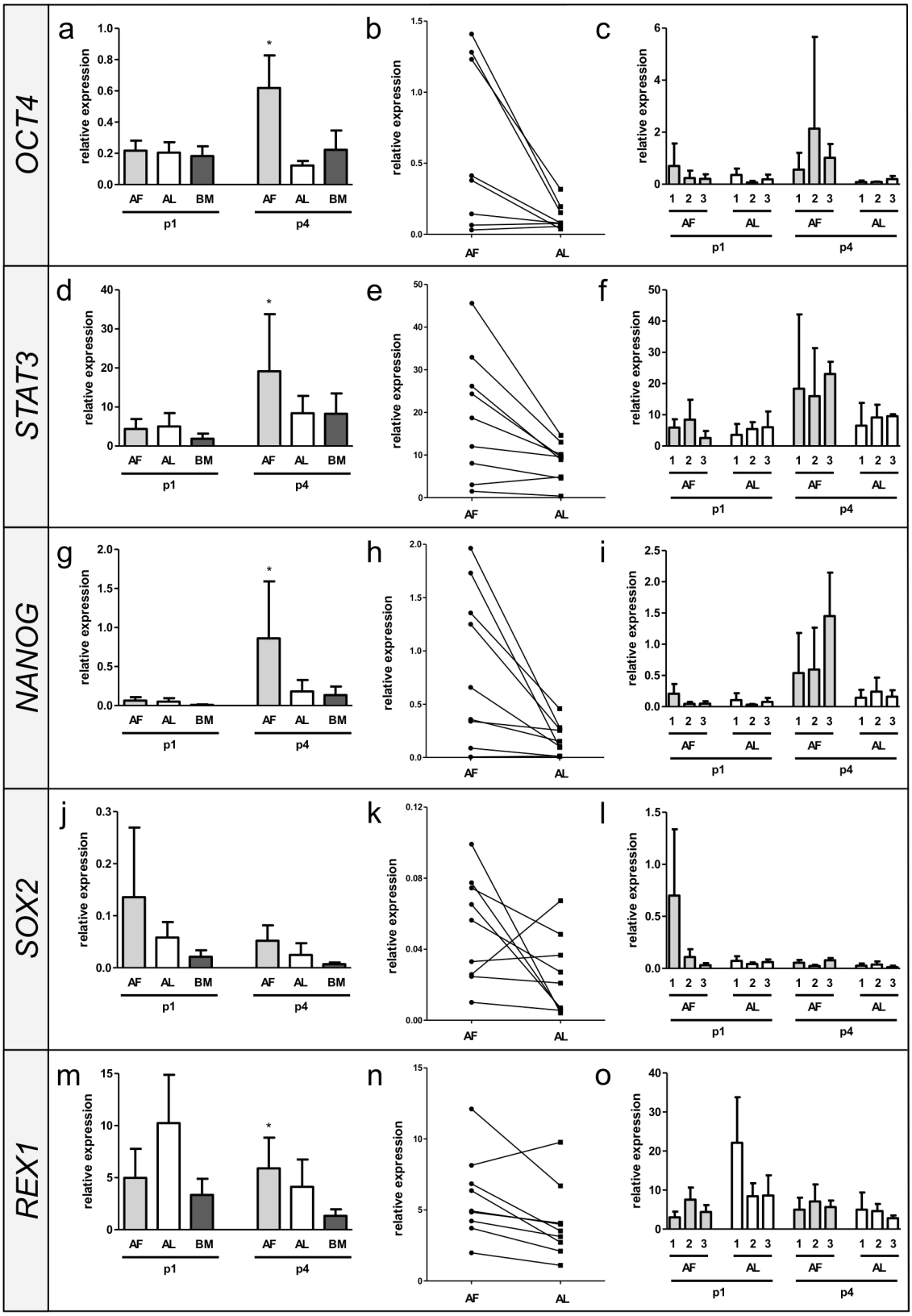

Figure 7: Quantitative real time PCR of pluripotency-related stem cell markers of isolated oAFCs and oALCs. Genes involved in the maintenance of pluripotency, including *OCT4* (a), *STAT3* (d), *NANOG* (g), *SOX2* (j) and *REX1* (m), revealed positive expression at early (p1) and late (p4) passages in paired oAFCs (n=9) and oALCs (n=9). Significant higher expression was detected in oAFCs at p4 in *OCT4*, *STAT3*, *NANOG* and *REX1* (a, e, h, n) ($p<0.05$), given a more heterogenous cell population than shortly after harvest (p1). Unpaired standard oBMSCs (n=3) served as a source of standard MSCs for direct comparison. An interpatient reduced expression in oALCs compared to paired oAFCs was detected (b, e, h, k, n). No gestational age dependency in the expression of pluripotent stem cell markers was found for all analyzed genes (c, f, i, l, o) (1: gestational age group 1; 2: gestational age group 2; 3: gestational age group 3) (n=3 per cell source for each gestational age). * = $p<0.05$

3.2.4 DISCUSSION

The present study aimed at addressing the origin of the broadly multipotent stem cell fraction in amniotic fluid by the use of the ovine developmental model, which is frequently used as an *in vivo* model for studying prenatal disease and fetal therapeutic applications prior to human clinical use. However, one major difference to the human anatomy is the retention of an allantoic fluid cavity, which enabled us to derive samples of fetal fluid and cells from two separate extraembryonic fluid compartments from the same animal. In this manner cells deriving from the efferent urinary tract and the allantoic fetal adnexa (released into the allantoic fluid compartment) can directly be compared to those deriving from the fetal skin, gastrointestinal, respiratory tracts and amniotic fetal adnexa (released into the amniotic fluid compartment). In the light of several pre-clinical studies also investigating amniotic fluid stem cell-based therapies in this animal model [1-6,46], these differences may have to be taken into account in future trials focusing on a pure harvest of amniotic fluid only. However, in the presented study, this embryological difference enabled us to derive samples of fetal fluids and cells from both extraembryonic fluid cavities from the same animal and compare the expression of pluripotency-related markers between both cell types, including oAFCs and oALCs, over the entire duration of gestation.

In this regard the present strictly paired analyses of ovine fetal fluid-derived cells, revealed significantly higher pluripotency-related gene expression in oAFCs than in oALCs, though showing similar cellular phenotypes. Significantly higher expression has been detected by qRT-PCR for *OCT4, STAT3, NANOG* and *REX1*, whereas only a tendency for higher *SOX2* was found. Interestingly, *SOX2* expression has been associated with neural induction and enhanced neural differentiation [52], even in preselected *SOX2* expressing AFSC [53], implying that in the present study only a small portion of neural progenitor cells have been detected in both fetal fluids analyzed. In the ovine preclinical model the expression of several pluripotency-related genes has been reported in amniotic fluid-derived cells, including *NANOG* [6,11,46,54-56], *SOX2* [6,46,54-56], *OCT4* [6,46,55-57], *TERT* [46,54-57] and *STAT3* [11], and further underlines that the ovine broadly multipotent cell compartment shows a similar expression pattern to the human counterpart [38,39,53,58-64].

In humans, AFSC genes being involved in the undifferentiated state of cells have received major attention given that AFSCs are thought to represent an “intermediate stage” between pluripotent stem cells and lineage-restricted adult stem cells and ultimately can reacquire pluripotency through reprogramming more easily [41-44]. AFSCs can form three-dimensional embryoid bodies, which were positive for alkaline phosphatase and expressed specific genes of ESCs [59]. Therefore, the presented results suggest that the cells with higher expression of selected markers representing hallmark genes of pluripotency, and thus broad(er) differentiation potential, originate rather from the fetus itself

(including skin, respiratory and gastrointestinal tract) or the extra-embryonic amniotic tissues. The allantoic fluid cavity, being mainly composed of fetal urine, seems to contain a cell compartment with significantly lower pluripotency-related gene expression suggesting that the urogenitary tract may not be the primary source of broadly multipotent cells, contrary to the speculation of previous reports [65-67].

In humans, urine becomes evident in the amniotic fluid at week 8 of gestation, given that the urethra is fully developed and the fetal kidneys became functional [23]. In the second half of gestation (~25 weeks) the production of amniotic fluid is predominately based on fetal urine (~300ml/kg fetal weight/day or 600-1200ml/day near term) and secretion of oral, nasal, tracheal as well as pulmonary fluids (~60 to 100ml/kg fetal weight/day) [23]. Consequently, urine represents a possible abundant source of stem cells. A population of stem cell-like cells has also been recently described in human adult urine displaying MSC markers [68] and feasibility of using these cells for tissue engineering applications has been demonstrated [69-71]. Previous studies described a heterogeneous cell population in amniotic fluid where ultimately a wide spectrum of different cellular origins has been proposed, in particular the fetal skin, urinary, gastrointestinal and respiratory tracts as well as extra-embryonic membranes. Few studies have described subpopulations of progenitor cells committed to specific lineages or prone to differentiate easily under appropriate culture conditions, including renal- [65-67], pancreatic- [72] and neuronal- [73] progenitors. In particular, renal/podocyte precursors are suggesting the urogenital tract as the possible source of amniotic fluid (stem) cells [65-67]. On the other hand human AFSCs derived from early gestational periods have shown to express ubiquitously Keratin-8, suggesting an epithelial origin of the cells [53]. However, conclusive evidence is missing so far and further research is necessary to investigate the origin of broadly multipotent stem cell component in particular.

Besides, the higher expression of pluripotency-related genes, oAFCs also exhibit a higher proliferative capacity in a direct, paired comparison to oALCs, which would be in line with their higher stem cell characteristics reported above. Particularly at higher passages increased proliferation capacities of oAFCs were observed, where ultimately a more morphologically homogenous cell population became evident in both cell types analyzed, in agreement with previous studies [74]. The authors suggest that stem cell-like cells are enriched over progressive passaging through selected proliferation medium towards a more homogenous population, which further underlines the higher pluripotency-related gene expression pattern at later passages (p4) compared to early passages (p1) reported here. Immunofluorescence and flow cytometry stainings verified a mesodermal, myogenic phenotype of isolated fetal cells, with higher expression of common MSC markers per single cell (measured with MFIR) in oAFCs compared to oALCs. Selected MSC markers differ from the ones used with human MSCs given interspecies differences. They have previously been described to uniquely

characterize ovine BMSCs for future translational studies involving this animal model [19,49]. Besides, one needs to emphasize the limited amount of well established markers in the ovine model and the necessity for better standardized protocols for future clinical studies implying the ovine developmental model. This interspecies difficulty was also observed in the multilineage differentiation of ovine fetal cells, even if their multilineage differentiation potential could be positively confirmed. Nevertheless, this study for the first time uniquely provides I) a systematic comparative analysis of fetal fluid cells from both cavities, the amnion and the allantois, II) paired analysis of AFCs and ALCs from the same offspring, and III) quantitative information on the pluripotency-related gene expression over gestation. Initial studies on the isolation of fetal fluid cells have been performed in canine [75] and feline [76] models, proving the principal feasibility of ALC isolation with a differentiation potential and surface marker expression equivalent to multipotent MSCs from the amniotic fluid. However, oALCs have not been broadly characterized so far and solid evidence for their stem cell nature is missing. In particular, the expression of pluripotency-related genes has not been analyzed. Furthermore, strictly paired quantitative analyses between AFCs and ALCs were missing and non-paired analyses may neglect the substantial inter-individual variances also detected in the present study.

In spite of the differences between oAFCs and oALCs, the present study did not find any gestational age dependent differences of cellular phenotype, proliferation and the expression of pluripotency-related markers. So far most studies on human AFSCs used cells from the second trimester of gestation, as routine amniocenteses in human are usually performed between 14 and 26 weeks of pregnancy [77]. Nevertheless, several studies have demonstrated that human AFSCs can also be successfully isolated at first [42,60] and third [61,78] trimester of gestation. In agreement with our results, comparable cellular phenotypes have been observed in human AFSCs isolated in the second or third trimester of gestation, including expression of *OCT4* and *NANOG* [61,78].

However, Moschidou et al. illustrated that cells isolated from the first trimester of gestation express a larger number of organ specific genes, suggesting a more undifferentiated state of cells [60]. As development proceeds, cells from the second trimester do not express the complete pattern of pluripotent factors anymore and become more committed with a limited differentiation potential [42,60,61]. Also when isolating circulating CD34+ hematopoietic progenitors cells and multipotent stem cells from the human umbilical cord blood, the frequency and immature pool of cells showed a decrease towards the later stages of pregnancy [79,80]. However, in the present study, the complete pattern of pluripotency-related genes, including *OCT4, NANOG, STAT3, SOX2* and *REX1*, showed a consistent expression independent of the developmental stage at which cells were harvested. In addition, also no morphological phenotype tendency could be assigned to a certain gestational age,

all three morphological phenotypes were equally distributed and abundant at every stage of fetal development.

These results suggest that cells with high pluripotency-related gene expression seem to be equally abundant within the amniotic fluid over the entire duration of gestation. Consequently, amniotic fluid harvest for regenerative applications may also be performed shortly before or directly at birth, to minimize any risk of amniocentesis for the fetus in cases were no diagnostic amniocentesis is necessary. A single study focusing on the analysis of human amniotic fluid obtained at the time of elective cesarean delivery also reported expression of Oct-4, however the analysis was limited to this single pluripotency-related factor only [81]. Further research on human amniotic fluid samples pre- and perinatally seems mandatory to confirm these findings and to establish amniotic fluid as a potential perinatal cell source.

In conclusion, the presented data suggest that the expression of pluripotency-related genes of cells derived from the fluid directly surrounding the fetus is substantially higher than the one of cells derived from the efferent urinary tract. These findings suggest that the cells expressing the highest stem cell characteristics may originate from the fetus itself (e.g. the fetal skin, the respiratory or the gastrointestinal tract). Interestingly, contrary to previous reports on human cord blood [79,80], no significant decrease of the pluripotency-related gene expression was noted over pregnancy, implying that even at the end of pregnancy, AFSCs with high differentiation potential may be isolated. These findings will have to be confirmed by future studies in humans, at least as far as the major ethical and medical restrictions allow for it. However, if confirmed, these findings may have major implications for harvesting, banking and usage of AFSCs for future therapeutic applications.

3.2.5 REFERENCES

1 In 't Anker, P. S. *et al.* Amniotic fluid as a novel source of mesenchymal stem cells for therapeutic transplantation. *Blood* **102**, 1548-1549, doi:10.1182/blood-2003-04-1291 (2003).

2 De Coppi, P. *et al.* Isolation of amniotic stem cell lines with potential for therapy. *Nat Biotechnol* **25**, 100-106, doi:10.1038/nbt1274 (2007).

3 Roubelakis, M. G. *et al.* Molecular and proteomic characterization of human mesenchymal stem cells derived from amniotic fluid: comparison to bone marrow mesenchymal stem cells. *Stem Cells Dev* **16**, 931-952, doi:10.1089/scd.2007.0036 (2007).

4 Antonucci, I. *et al.* Amniotic fluid stem cells: a promising therapeutic resource for cell-based regenerative therapy. *Curr Pharm Des* **18**, 1846-1863 (2012).

5 Slamecka, J. *et al.* Non-integrating episomal plasmid-based reprogramming of human amniotic fluid stem cells into induced pluripotent stem cells in chemically defined conditions. *Cell Cycle* **15**, 234-249, doi:10.1080/15384101.2015.1121332 (2016).

6 Moschidou, D. *et al.* Valproic acid confers functional pluripotency to human amniotic fluid stem cells in a transgene-free approach. *Mol Ther* **20**, 1953-1967, doi:10.1038/mt.2012.117 (2012).

7 Jiang, G. *et al.* Human transgene-free amniotic-fluid-derived induced pluripotent stem cells for autologous cell therapy. *Stem Cells Dev* **23**, 2613-2625, doi:10.1089/scd.2014.0110 (2014).

8 Li, Q. *et al.* Generation of induced pluripotent stem cells from human amniotic fluid cells by reprogramming with two factors in feeder-free conditions. *J Reprod Dev* **59**, 72-77 (2013).

9 Prusa, A. R. & Hengstschlager, M. Amniotic fluid cells and human stem cell research: a new connection. *Med Sci Monit* **8**, RA253-257 (2002).

10 Parolini, O. *et al*. Amniotic membrane and amniotic fluid-derived cells: potential tools for regenerative medicine? *Regen Med* **4**, 275-291, doi:10.2217/17460751.4.2.275 (2009).

11 Underwood, M. A. *et al.* Amniotic fluid: not just fetal urine anymore. *J Perinatol* **25**, 341-348, doi:10.1038/sj.jp.7211290 (2005).

12 Weber, B. *et al.* In vitro fabrication of autologous living tissue-engineered vascular grafts based on prenatally harvested ovine amniotic fluid-derived stem cells. *J Tissue Eng Regen Med* **10**, 52-70, doi:10.1002/term.1781 (2016).

13 Barry, J. S. & Anthony, R. V. The pregnant sheep as a model for human pregnancy. *Theriogenology* **69**, 55-67 (2008).

14 Klein, J. D. *et al.* Amniotic mesenchymal stem cells enhance normal fetal wound healing. *Stem Cells Dev* **20**, 969-976, doi:10.1089/scd.2010.0379 (2011).

15 Weber, B. *et al.* Prenatally engineered autologous amniotic fluid stem cell-based heart valves in the fetal circulation. *Biomaterials* **33**, 4031-4043, doi:10.1016/j.biomaterials.2011.11.087 (2012).

16 Colosimo, A. *et al.* Characterization, GFP gene Nucleofection, and allotransplantation in injured tendons of ovine amniotic fluid-derived stem cells. *Cell Transplant* **22**, 99-117, doi:10.3727/096368912X638883 (2013).

17 Turner, C. G. *et al.* Preclinical regulatory validation of an engineered diaphragmatic tendon made with amniotic mesenchymal stem cells. *J Pediatr Surg* **46**, 57-61, doi:10.1016/j.jpedsurg.2010.09.063 (2011).

18 Kunisaki, S. M. *et al.* Fetal tracheal reconstruction with cartilaginous grafts engineered from mesenchymal amniocytes. *J Pediatr Surg* **41**, 675-682; discussion 675-682, doi:10.1016/j.jpedsurg.2005.12.008 (2006).

19 Kunisaki, S. M. *et al.* Diaphragmatic repair through fetal tissue engineering: a comparison between mesenchymal amniocyte- and myoblast-based constructs. *J Pediatr Surg* **41**, 34-39; discussion 34-39, doi:10.1016/j.jpedsurg.2005.10.011 (2006).

20 Fuchs, J. R. *et al.* Diaphragmatic reconstruction with autologous tendon engineered from mesenchymal amniocytes. *J Pediatr Surg* **39**, 834-838; discussion 834-838 (2004).

21 Gray, F. L. *et al.* Prenatal tracheal reconstruction with a hybrid amniotic mesenchymal stem cells-engineered construct derived from decellularized airway. *J Pediatr Surg* **47**, 1072-1079, doi:10.1016/j.jpedsurg.2012.03.006 (2012).

22 Pansky, B. *Review of medical embryology*. Macmillan New York, (1982).

23 Sivachelvan, M *et al*. Foetal age estimation in sheep and goats. *Small Ruminant Research* **19**, 69-76 (1996).

24 Schmidt, D. *et al.* Cryopreserved amniotic fluid-derived cells: a lifelong autologous fetal stem cell source for heart valve tissue engineering. *J Heart Valve Dis* **17**, 446-455; discussion 455 (2008).

25 Schmidt, D. *et al.* Prenatally fabricated autologous human living heart valves based on amniotic fluid derived progenitor cells as single cell source. *Circulation* **116**, I64-70, doi:10.1161/CIRCULATIONAHA.106.681494 (2007).

26 McCarty, R. C. *et al.* Characterisation and developmental potential of ovine bone marrow derived mesenchymal stem cells. *J Cell Physiol* **219**, 324-333, doi:10.1002/jcp.21670 (2009).

27 Gronthos, S. *et al.* Heat shock protein-90 beta is expressed at the surface of multipotential mesenchymal precursor cells: generation of a novel monoclonal antibody, STRO-4, with specificity for mesenchymal precursor cells from human and ovine tissues. *Stem Cells Dev* **18**, 1253-1262, doi:10.1089/scd.2008.0400 (2009).

28 Bieback, K. *et al.* Human alternatives to fetal bovine serum for the expansion of mesenchymal stromal cells from bone marrow. *Stem Cells* **27**, 2331-2341, doi:10.1002/stem.139 (2009).

29 Liu, J. *et al.* Generation and characterization of reprogrammed sheep induced pluripotent stem cells. *Theriogenology* **77**, 338-346 e331, doi:10.1016/j.theriogenology.2011.08.006 (2012).

30 Zhang, S. & Cui, W. Sox2, a key factor in the regulation of pluripotency and neural differentiation. *World J Stem Cells* **6**, 305-311, doi:10.4252/wjsc.v6.i3.305 (2014).

31 Jezierski, A. *et al.* Probing stemness and neural commitment in human amniotic fluid cells. *Stem Cell Rev* **6**, 199-214, doi:10.1007/s12015-010-9116-7 (2010).

32 Colosimo, A. *et al.* Prolonged in vitro expansion partially affects phenotypic features and osteogenic potential of ovine amniotic fluid-derived mesenchymal stromal cells. *Cytotherapy* **15**, 930-950, doi:10.1016/j.jcyt.2013.03.014 (2013).

33 Di Tomo, P. *et al.* Calcium sensing receptor expression in ovine amniotic fluid mesenchymal stem cells and the potential role of R-568 during osteogenic differentiation. *PLoS One* **8**, e73816, doi:10.1371/journal.pone.0073816 (2013).

34 Berardinelli, P. *et al.* Role of amniotic fluid mesenchymal cells engineered on MgHA/collagen-based scaffold allotransplanted on an experimental animal study of sinus augmentation. *Clin Oral Investig* **17**, 1661-1675, doi:10.1007/s00784-012-0857-3 (2013).

35 Mauro, A. *et al.* Isolation, characterization, and in vitro differentiation of ovine amniotic stem cells. *Vet Res Commun* **34 Suppl 1**, S25-28, doi:10.1007/s11259-010-9393-2 (2010).

36 Spinelli, V. *et al*. Induced pluripotent stem (iPS) cells from human fetal stem cells (hFSCs). *Organogenesis* **9**, 101-110, doi:10.4161/org.25197 (2013).

37 Antonucci, I. *et al.* Human second trimester amniotic fluid cells are able to create embryoid body-like structures in vitro and to show typical expression profiles of embryonic and primordial germ cells. *Cell Transplant* **23**, 1501-1515, doi:10.3727/096368914X678553 (2014).

38 Moschidou, D. *et al.* Molecular signature of human amniotic fluid stem cells during fetal development. *Curr Stem Cell Res Ther* **8**, 73-81 (2013).

39 Savickiene, J. *et al.* Human Amniotic Fluid Mesenchymal Stem Cells from Second- and Third-Trimester Amniocentesis: Differentiation Potential, Molecular Signature, and Proteome Analysis. *Stem Cells Int* **2015**, 319238, doi:10.1155/2015/319238 (2015).

40 Pipino, C. *et al.* Molecular and phenotypic characterization of human amniotic fluid-derived cells: a morphological and proteomic approach. *Stem Cells Dev* **24**, 1415-1428, doi:10.1089/scd.2014.0453 (2015).

41 Bossolasco, P. *et al.* Molecular and phenotypic characterization of human amniotic fluid cells and their differentiation potential. *Cell Res* **16**, 329-336, doi:10.1038/sj.cr.7310043 (2006).

42 Karlmark, K. R. *et al.* Activation of ectopic Oct-4 and Rex-1 promoters in human amniotic fluid cells. *Int J Mol Med* **16**, 987-992 (2005).

43 Da Sacco, S. *et al.* Human amniotic fluid as a potential new source of organ specific precursor cells for future regenerative medicine applications. *J Urol* **183**, 1193-1200, doi:10.1016/j.juro.2009.11.006 (2010).

44 Da Sacco, S. *et al.* A novel source of cultured podocytes. *PLoS One* **8**, e81812, doi:10.1371/journal.pone.0081812 (2013).

45 Monteiro Carvalho Mori da Cunha, M. G. *et al.* Amniotic Fluid Derived Stem Cells with a Renal Progenitor Phenotype Inhibit Interstitial Fibrosis in Renal Ischemia and Reperfusion Injury in Rats. *PLoS One* **10**, e0136145, doi:10.1371/journal.pone.0136145 (2015).

46 Zhang, Y. *et al.* Urine derived cells are a potential source for urological tissue reconstruction. *J Urol* **180**, 2226-2233, doi:10.1016/j.juro.2008.07.023 (2008).

47 Wu, S *et al*. Human urine-derived stem cells seeded in a modified 3D porous small intestinal submucosa scaffold for urethral tissue engineering. *Biomaterials* **32**, 1317-1326, doi:10.1016/j.biomaterials.2010.10.006 (2011).

48 Bodin, A. *et al.* Tissue-engineered conduit using urine-derived stem cells seeded bacterial cellulose polymer in urinary reconstruction and diversion. *Biomaterials* **31**, 8889-8901, doi:10.1016/j.biomaterials.2010.07.108 (2010).

49 Wu, S. *et al.* Implantation of autologous urine derived stem cells expressing vascular endothelial growth factor for potential use in genitourinary reconstruction. *J Urol* **186**, 640-647, doi:10.1016/j.juro.2011.03.152 (2011).

50 Zou, G. *et al.* Induction of pancreatic beta-cell-like cells from CD44+/CD105+ human amniotic fluids via epigenetic regulation of the pancreatic and duodenal homeobox factor 1 promoter. *DNA Cell Biol* **30**, 739-748, doi:10.1089/dna.2010.1144 (2011).

51 Prusa, A. R. *et al.* Neurogenic cells in human amniotic fluid. *Am J Obstet Gynecol* **191**, 309-314, doi:10.1016/j.ajog.2003.12.014 (2004).

52 Kim, J. *et al.* Human amniotic fluid-derived stem cells have characteristics of multipotent stem cells. *Cell Prolif* **40**, 75-90, doi:10.1111/j.1365-2184.2007.00414.x (2007).

53 Fernandes, R. A. *et al*. Derivation and characterization of progenitor stem cells from canine allantois and amniotic fluids at the third trimester of gestation. *Placenta* **33**, 640-644, doi:10.1016/j.placenta.2012.03.009 (2012).

54 Iacono, E. *et al.* Could fetal fluid and membranes be an alternative source for mesenchymal stem cells (MSCs) in the feline species? A preliminary study. *Vet Res Commun* **36**, 107-118, doi:10.1007/s11259-012-9520-3 (2012).

55 Bajek, A. *et al.* High Quality Independent From a Donor: Human Amniotic Fluid Derived Stem Cells-A Practical Analysis Based on 165 Clinical Cases. *J Cell Biochem*, doi:10.1002/jcb.25618 (2016).

56 Schiavo, A. A. *et al.* Endothelial properties of third-trimester amniotic fluid stem cells cultured in hypoxia. *Stem Cell Res Ther* **6**, 209, doi:10.1186/s13287-015-0204-0 (2015).

57 Gasparoni, A. *et al.* Immunophenotypic changes of fetal cord blood hematopoietic progenitor cells during gestation. *Pediatr Res* **47**, 825-829 (2000).

58 Shields, L. E. & Andrews, R. G. Gestational age changes in circulating CD34+ hematopoietic stem/progenitor cells in fetal cord blood. *Am J Obstet Gynecol* **178**, 931-937 (1998).

59 You, Q. *et al.* The biological characteristics of human third trimester amniotic fluid stem cells. *J Int Med Res* **37**, 105-112 (2009).

4

Biodegradable scaffolds for cardiovascular tissue engineering

The content of this chapter is based on:

Capulli AK, Emmert MY, Pasqualini FS, **Kehl D**, Caliskan E, Lind JU, Sheehy SP, Park SJ, Ahn S, Weber B, Goss JA, Hoerstrup SP, Parker KK. JetValve: Rapid manufacturing of biohybrid scaffolds for biomimetic heart valve replacements. Biomaterials 2017 Jul 133:229-241.
Copyright License No.: 4141250446890

Combined with:
Kehl D, Capulli AK, Emmert MY, Weber B, Parker KK[+], Hoerstrup SP[+]. Long term *in vivo* follow-up of biohybrid jetspun heart valve replacements. *(unpublished data)*

CHAPTER 4.1

JetValve: Rapid manufacturing of biohybrid scaffolds for biomimetic heart valve replacements

Andrew K. Capulli[1], Maximillian Y. Emmert[1,2,3], Francesco S. Pasqualini[1,2], **Debora Kehl**[2], Etem Caliskan[2], Johan U. Lind[1], Sean P. Sheehy[1], Sung Jin Park[1], Seungkuk Ahn[1], Benedikt Weber[1,2], Josue A. Gross[1], Simon P. Hoerstrup[1,2], Kevin Kit Parker[1]

[1] Disease Biophysics Group, Wyss Institute for Biologically Inspired Engineering, John A. Paulson School of Engineering and Applied Sciences, Harvard University, 29 Oxford St, Pierce Hall 321, Cambridge, MA 02138, USA
[2] Institute for Regenerative Medicine (IREM), Center for Therapy Development and Good Manufacturing Practice, University of Zurich, 13 Moussonstrasse, Zurich, 8004, CH, Switzerland
[3] Clinic for Cardiac Surgery, University Hospital Zurich, 100 Ramistrasse, Zurich, 8091, CH, Switzerland

Abstract

Tissue engineered scaffolds have emerged as a promising solution for heart valve replacement because of their potential for regeneration. However, traditional heart valve tissue engineering has relied on resource-intensive, cell-based manufacturing, which increases cost and hinders clinical translation. To overcome these limitations, *in situ* tissue engineering approaches aim to develop scaffold materials and manufacturing processes that elicit endogenous tissue remodeling and repair. Yet despite recent advances in synthetic materials manufacturing, there remains a lack of cell-free, automated approaches for rapidly producing biomimetic heart valve scaffolds. Here, we designed a jet spinning process for the rapid and automated fabrication of fibrous heart valve scaffolds. The composition, multiscale architecture, and mechanical properties of the scaffolds were tailored to mimic that of the native leaflet fibrosa and assembled into three dimensional, semilunar valve structures. We demonstrated controlled modulation of these scaffold parameters and show initial biocompatibility and functionality *in vitro.* Valves were minimally-invasively deployed via transapical access to the pulmonary valve position in an ovine model and shown to be functional for 15 h. Long-term follow up of 1-month *in vivo* revealed low cellular infiltration into the heart valve scaffolds and limited endogenous tissue.

Personal contribution:

Experimental contributions (Kehl D only):
Establishment of suture layout, storage conditions and sterilization of valves for *in vivo* implantation. Integration of electrospun valves into self-expandable nitinol stent and suturing under sterile conditions. Adaptation of the crimping procedure and subsequent crimping analysis of the valves (suture retention, macroscopic valve geometry). Preparation and coordination of JetValve scaffolds for *in vivo* implantation and explanation. Crimping of heart valves before *in vivo* implantation into minimal invasive delivery device. Post mortem macroscopic analysis of engineered valves, including explant photography, paraffin embedding, microtome cutting and microscope histological analysis (such as H&E, Masson Trichom etc.). Isolation of native ovine pulmonary heart valve and their characterization for comparative analyses. Evaluate cellular infiltration and *in vivo* functionality of implanted heart valves based on histological analyses and *in vivo* echocardiography.

Experimental contributions (Kehl D, together with co-authors)
Design input for building automated spinning process and storage evaluation. Evaluation of *in vivo* functionality of implanted heart valves based on echocardiography.

Non-experimental contributions (Kehl D only):
Coordination of *in vivo* implantation procedures. Amendment of ethical permission for *in vivo* implantation. Maintaining data exchange with collaborating partners in Boston by writing and summarizing *in vivo* findings/data. Reviewing manuscript.

Steps contained in the published work (without personal contribution of Kehl D)
Design of jet spinning process for the mandrel-based manufacturing of heart valve scaffolds. Mandrel scaling and customization. Definition of composition (fiber diameter and orientation, scaffold porosity), multiscale architecture and mechanical properties of electrospun heart valves. Scaffold batch process capability based on scaffold stiffness and biohybrid composition. *In vitro* cellular infiltration studies of valvular interstitial cells into heart valve leaflet and conduit scaffold. *In vitro* functional testing of engineered heart valves in a pulse duplicator system. *In vivo* implantation of engineered heart valves into anesthetized animals. Submission and revision of manuscript. Statistical analyses.

Biomaterials (published 2017)

4.1.1 INTRODUCTION

Historically, heart valve tissue engineering has relied on cell-based manufacturing to build living tissues *in vitro* [1]. In this approach, cells are seeded onto scaffolds and conditioned in bioreactors that mimic the physiological conditions (pressures and flows) of the native valve [2,3]. The conditioned cells remodel the scaffold in order to produce a microenvironment that mimics the complex spatial organization, mechanical properties, and biochemical composition of the native leaflet extracellular matrix (ECM) [4]. These scaffold/tissue constructs are complex biomaterials designed to elicit immunological mechanisms that drive tissue regeneration [5]. In recent attempts to improve translation of tissue engineered valvular scaffolds, storage has been made possible by decellularizing [6-8] conditioned scaffolds, which can be recellularized prior to [9] or after implantation [10]. Although this strategy has shown promise as both a functional and regenerative approach, these "off-the-shelf" valvular scaffolds can take months and cost thousands of dollars to produce using manual and non-standardized manufacturing techniques. Fabrication steps including cell sourcing/isolation [11] and cell/scaffold conditioning [12,13] in heavily regulated GMP environments are complex and may require the patient to take immunosuppressive therapies if foreign biologics [14] or non-degradable materials are used. As a result of the manufacturing time, cost, and inherent potential for product material variability [15], the translation of tissue engineered heart valves to the clinic remains limited [16,17].

In situ heart valve tissue engineering is a simplified method for permanent, regenerative valve replacement [18]. In this approach, the scaffold is designed to promote endogenous mechanisms that drive tissue formation and remodeling once implanted [10,17]. The manufacturing process must therefore be capable of producing scaffolds that both modulate the direction of blood flow in the heart immediately upon implantation and recapitulate aspects of the microenvironment of the native valve ECM with the goal of promoting endogenous remodeling [19]. To achieve this, numerous materials fabrication techniques such as fiber electrospinning [20] and force spinning [21], hydrogel molding [22], and 3D/bioprinting [23] have been developed to fabricate biomimetic valvular scaffolds, each with unique building advantages. The nanoscale resolution of fiber production systems, the simplicity of hydrogel material properties manipulation, and the customizable global designs achievable with 3D printing each recapitulate central of aspects of valvular architecture. However, new biomaterials manufacturing techniques achieving both high resolution and degree of customization remain needed to mimic 1) the anisotropic architecture of the valvular ECM, 2) the stiffness of the leaflet to withstand systolic and diastolic loading, and 3) incorporate native ECM proteins to allow for cellular attachment and infiltration [13,24]. Easy manipulation of these manufacturing parameters will be necessary to tailor the complex, and still yet to be fully understood, remodeling response over time.

In this study, we introduce a cell-free manufacturing technique for the rapid production of biomimetic semilunar heart valvular scaffolds (JetValves). JetValves were manufactured in a two-step mandrel collection process which enabled facile shape and size customization. By varying the biohybrid composition and manufacturing collection parameters of JetValves, the multiscale architecture, mechanical properties and biochemistry of the scaffold fibers were engineered to recapitulate those of the native valve leaflet fibrosal ECM (ovine). The controlled and automated fabrication of JetValves enabled seamless and rapid production (minutes from raw material to product) allowing for the implementation of quality control standards to ensure scaffold consistency prior to use. JetValves demonstrated acute durability and basic functionality *in vitro* as well as biocompatibility/competency *in vivo* upon minimally invasive implantation into an ovine pulmonary valve model. The JetValve fabrication process may thus provide a versatile platform for the rapid production of tissue engineered heart valve scaffolds.

4.1.2 MATERIAL AND METHODS

4.1.2.1 JETVALVE MANDREL-BASED MANUFACTURIN PROCESS

Tri-leaflet valvular scaffolds (JetValves) were three-dimensionally manufactured by the cumulative collection of force-extruded fibers onto custom sized mandrels. A two-step collection process was used via automation of the Rotary Jet Spinning system (aRJS, Fig. 1a) [21,25] controlled by a customized LabVIEW interface for the first time (National Instruments, v12.0.1f4). First, the leaflet cusps were spun by the collection of fibers onto a rotating semilunar valve leaflet shaped mandrel (male-mandrel) cyclically translating through the fiber extrusion plane. Leaflets were subsequently separated by the removal excess fiber accumulation on the top of the leaflet shaped mandrel with a scalpel. By the addition of a shielding mandrel (female-mandrel) over the leaflet mandrel and further fiber deposition, the leaflets were seamlessly spun into a fibrous conduit to produce the semilunar valve within a vessel structure (Fig. 1b, Supplemental video 1). Once dried, removal of Teflon or 3D printed, Teflon-coated collection mandrels from either end of the fibrous conduit was possible without disrupting its structure.

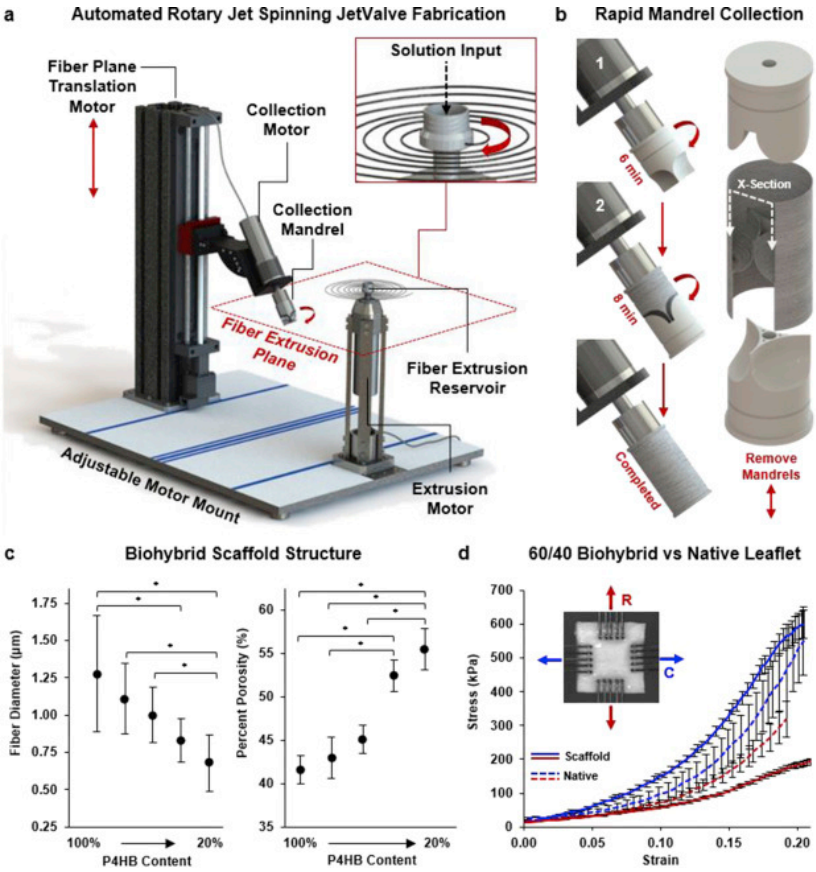

Figure 1: Main Automated Rotary Jet Spinning of JetValves. (a) CAD representation of the automated Rotary Jet Spinning system (aRJS). (b) A two-step mandrel collection system was used consisting of (1) a leaflet mandrel and (2) shielding mandrel. (c) At a 30 k RPM fiber extrusion rate, 4% w/v P4HB/Gelatin biohybrid solutions had decreased fiber diameter but increased percent scaffold porosity as a function of decreasing polymer content (N = 6 production runs per condition, $*p < 0.5$). (d) Stress vs strain plots of 60/40 P4HB/Gelatin blends compared to native leaflet cusps up to 20% strain (blue circumferential (C), red radial (R) fiber alignment; N = 6 production runs per condition, N = 5 native leaflets; $*p < 0.5$).

4.1.2.2 JETVALVE FABRICATION FOR STRUCTURAL AND FUNCTIONAL TESTING

Poly-4-hydroxybutyrate (P4HB, Tepha Inc., TephaFLEX)/gelatin (from porcine skin, strength 300; Sigma, G2500) "biohybrid" (synthetic-polymer/protein) solutions of varied composition (P4HB/Gelatin; 100/0, 80/20, 60/40, 40/60, and 20/80) were stirred for 12 hr at 4% w/v in hexfluoroispropanol (HFIP, Oakwood Chemical, 003409). A small amount, 0.2% w/v, of polyglycolide (PGA, Sigma, 457620) was added to each solution for compositional comparison to previously published valvular scaffolds [6,7,9]; the effect of PGA on scaffold mechanics and structure were assumed to be negligible, therefore compositions are henceforth referred to as P4HB/Gelatin. After mixing, solutions were individually pumped into the rotating reservoir of the aRJS at 5.0 ml/min through polyfluoroalkoxy alkane tubing (Saint-Gobain, TSPF35-0125-031-50) using an automated syringe pump (Harvard Apparatus, 703007). The reservoir of the aRJS was machined from stainless steel to ensure structural stability at high speeds and rotated at 30k RPM (motor: Nakanishi, EM-3080J) to extrude solution jets within a horizontal "fiber extrusion plane." Solution jets were extruded from two 360 µm diameter orifices drilled horizontally into the bottom of the reservoir. Fibers ranging in diameter, porosity and stiffness were produced by varying the biohybrid solution (Fig. 1c and Fig, 1d), similar to previous RJS hybrid materials [25], and collected onto semilunar valve shaped rotating mandrels as described above. Mandrels were rotated at 3k RPM at 0º, 22.5º, or 45º relative to the horizontal as they vertically translated through the fiber extrusion plane at 10 cm/s (linear motor: Misumi, LX20). JetValve scaffolds manufactured for ovine implantation were 30 mm in diameter and composed of 60/40 P4HB/Gelatin; 30 ml of solution were spun to form the leaflets and 40 ml were spun to form the remainder of the conduit. 8 mm wide sample strips were cut from either end of each JetValve scaffold for measuring batch process capability of JetValves prepared for implantation.

4.1.2.3 MANDREL SCALING AND CUSTOMIZATION

JetValve mandrels were custom-drawn and scaled using computer aided design software (Solidworks, 2015) and milled from Teflon for implantation (Proto Labs) or 3D printed in Rigid Opaque photopolymer for rapid scaling (Blue, Stratasys, Object30 Printer). Leaflet and shielding mandrels were readily scaled from 30 mm (ovine, implantation model used in this study) to 3 mm to produce JetValves of various sizes; 750 µm in diameter (~mouse sized) mandrels could also be 3D printed and spun onto to form miniature JetValves. (Fig. 2a). Sinuses were added to the shielding mandrel to produce aortic valve relevant geometries using the same, two-step mandrel spinning method of fabrication described above. A "Sinus Cylinder" for housing "Sinus Cartridges" comprised the shielding-female mandrel and allowed for seamless sinus bulge incorporation into the JetValve with easy mandrel removal via breakdown of the cylinder-cartridge assembly once dried (Fig. 2b).

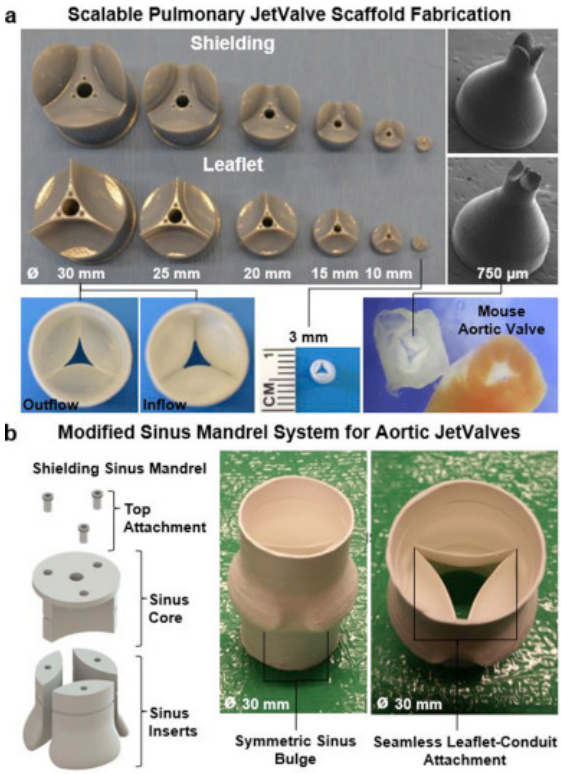

Figure 2: JetValve mandrel scaling and customization. (a) Digital photograph, (left) of 3D printed shielding (upper row) and leaflet (lower row) JetValve mandrels and scaffolds ranging from 30 mm to 3 mm in diameter. Scanning electron microscope images, (right) of miniaturized JetValve mandrels and scaffold, 750 µm in diameter. (b) Shielding mandrel modification for JetValve scaffolds with sinus bulges. The shielding mandrel was compartmentalized into individual, symmetric sinus component "inserts" which could be fixed to a housing sinus "core," (left). Mandrels were removed from scaffolds without disrupting the structure, digital photographs (right), by removing the connections of the core and inserts.

4.1.2.4 FIBER DIAMETER AND SCAFFOLD POROSITY

Scanning electron microscopy (SEM) and ImageJ software (NIH, v1.48s) were used to measure the fiber diameter and percentage porosity of JetValve scaffolds of varied biohybrid composition (P4HB/Gelatin; 100/0, 80/20, 60/40, 40/60, and 20/80; n=6 production runs per biohybrid condition). Samples were sputter coated in 5 nm of platinum/palladium (Quorum Technologies, EMS 300TD) to avoid charge accumulation and scaffold deformation/melting during SEM imaging. A field emitting electron microscope was used to image samples (Zeiss, FESEM Ultra Plus) at 15 kV with a high efficiency secondary electron detector, 1.75k magnification for fiber diameter and 1k magnification for porosity images. Using ImageJ, 10 fiber diameter regions of interest (ROIs) were taken per sample using the linear measuring tool and one porosity ROI was taken per sample using thresholding percentage (percent porosity: fiber vs. non-fiber).

4.1.2.5 SCAFFOLD AND TISSUE BIAXIAL MECHANICAL PROPERTIES

JetValve scaffolds of varied biohybrid composition (P4HB/Gelatin; 100/0, 80/20, 60/40, 40/60, and 20/80) were equibiaxially loaded to determine low (0-10%) and high (10-20%) strain stiffness measurements in comparison to freshly harvested ovine pulmonary leaflets. 8x8 mm scaffold samples (n=6 production runs per biohybrid condition) and 8x8 mm native leaflet samples (n=5, cut from cusp centers) were loaded onto 5x5 mm mounting tines of a biaxial tensile tester equipped with

2.5 N load cells (CellScale, BioTester) [26]. Loaded samples were submerged in a phosphate buffer saline (PBS, Thermo Fisher, 10010023) bath at 37ºC to simulate hydration and temperature conditions *in vivo*. Each sample was first preconditioned equibiaxially at a strain rate of 5% per second to 2% strain 4 times to ensure complete hydration of the scaffold or tissue. Next, each sample was loaded equibiaxially at a strain rate of 5% per second to 20% strain 4 times. Force/displacement measurements and images were recorded throughout the test at 15 Hz; stress vs. strain plots were then generated from these measurements and the original dimensions of the samples (i.e. thickness/length in each direction, parallel and perpendicular to fiber/ECM orientation). Stiffness moduli were calculated as the slope to the stress vs. strain curves in the respective low and high strain regimes. To test the effect of collection angle on both conduit and leaflet stiffnesses, 60/40 blends were collected at 0˚, 22.5˚, and 45˚ (n=6 from 3 production runs per angle) and biaxially tested as described above.

4.1.2.6 SCAFFOLD FIBER AND TISSUE ORIENTATION

The fiber orientation of 60/40 P4HB/Gelatin JetValve leaflet and conduit samples collected at 0º, 22.5º, or 45º (n=3 production runs per condition) were compared to that of decellularized ovine pulmonary valve leaflets (n=7 leaflets). Freshly harvested pulmonary leaflets were decellularized in 1% sodium dodecyl sulfate (SDS, Sigma, L6026) for 4 days. After decellularization, leaflets were rinsed in ultra-pure water (Thermo Fisher, 10977-015) then dehydrated in serial ethanol washes (30%, 50%, 70%, 90%, 3x 100%) for 5 min each (EtOH, VWR, 64-17-5). Dehydrated leaflets were then dried using a critical point drier (Tousimis, 931 Series SAMDRI) and sputter coated. SEM images of scaffolds and decellularized tissue were taken as described above from five regions encompassing the whole area of the leaflet (scaffold and native) and five regions along the length of the conduit. SEM images were analyzed with custom made ImageJ and Matlab software to calculate the orientational order parameter (OOP), a quantitative measure of the degree of fiber orientation within a scaffold/tissue. In brief, foreground pixels were assigned the orientation of the local neighborhood using a structure tensor method; then, the set of all orientations was summed assuming they represented the directions of vectors of unit magnitude. The result is a number that goes from 0, for perfectly random set of orientations, to 1 for perfectly aligned foreground pixels [27,28].

4.1.2.7 SCAFFOLD SHELF LIFE

X-ray photoelectron spectrometry (XPS, Thermo Scientific, K-Alpha XPS,) was used to evaluate freshly-spun and hydrated JetValve scaffold composition in time. 8x8 mm pieces of 60/40 P4HB/Gelatin scaffolds were hydrated in 1 L of ultra-pure water and stored in an incubator at 37ºC

for up to 1 week. Hydrated samples were removed from the water bath every 24 hr with sterile forceps and were dried for 12 hr under vacuum, after which their composition was evaluated using the XPS system (n=3 production runs/XPS measurements per time point, 0-7 days). Briefly, each sample was etched for 30 seconds at 500 eV (medium) to remove any surface debris that may have accumulated during sample preparation and was survey scanned over a 400 µm2 spot size. Gelatin ratiometric content was estimated based upon the measured presence of nitrogen in the sample and the amount of solvent (HFIP) was estimated based upon the measured presence of fluorine, each normalized to the element's percentage within the respective molecule. Under the assumption that sample purity was maintained throughout the hydration, drying, and etching process, P4HB content was estimated as the remaining scaffold percentage non-gelatin or solvent. Additionally, 8x8 mm pieces of 60/40 scaffolds incubated under the same conditions (n=3 production runs) were biaxially tested as described above to directly determine changes in stiffness due to the same hydrated storage conditions.

4.1.2.8 CELLULAR INFILTRATION STUDIES

In vitro cellular infiltration studies using porcine valvular interstitial cells (VICs) were conducted to determine the potential of JetValve scaffolds to support tissue growth as defined by cell penetration. Porcine VICs were isolated and statically grown on 60/40 P4HB/Gelatin scaffolds for 48hr as recently described [29], 1 week, and 2 weeks to determine the degree of cellular infiltration in time. 60/40 leaflet and conduit scaffolds (n=6 production runs per condition) were produced as above with the addition of 5 µl/ml of 0.2 µm red fluorescent FluoSpheres (Invitrogen, F8810) added to the pre-spun solution for scaffold visualization during microscopy. VICs were isolated from freshly harvested porcine hearts using collagenase (Blood Farms Inc., Groton, MA; in compliance with FDA guidelines) and seeded onto 8x8 mm sections of leaflet and conduit scaffolds at 200k cells/cm2. At each time point, scaffold/VIC tissues were fixed in 4% paraformaldehyde (Electron Microscopy Sciences, 15710) and 0.5% Triton 100-X(Sigma, T8787) in PBS for 15 min. Samples were then rinsed 3x in PBS for 10 min each and stored at 4˚C. To prepare for imaging, samples were incubated for 1 hr with 5 µl/ml of 4',6-Diamidino-2-Phenylindole, Dihydrochloride (DAPI, Invitrogen, D1306) in PBS to stain the VIC nuclei. Samples were then rinsed with PBS 3x for 15 min each to remove residual DAPI stain and mounted between 25 mm diameter coverslips. 200x200 µm z-stacks from the surface of the scaffold, identified by coplanar-focused FluorSpheres and DAPI stained nuclei, to the center of the deepest penetrating nuclei within the scaffold were taken using a Zeiss LSM 7 LIVE confocal microscope. The distance from the surface of the scaffold to the deepest penetrating nuclei, i.e. thickness of the z-stack, was used to measure cell infiltration depth and visualized using Zen lite 2.3 software (Zeiss, SP1).

4.1.2.9 SCAFFOLD BATCH PROCESS CAPABILITY

The Batch Process Capability [30] (±3 times the variance) was used to evaluate the manufacturing accuracy and precision of aRJS produced 60/40 P4HB/Gelatin JetValves (n=16 valves) for implantation. For fiber diameter, the upper control limit (UCL) was set at 1.2 µm and the lower control limit (LCL) was set at 0.8 µm based upon previously published tissue engineered scaffolds [6,7,9]. As scaffold porosity is a function of fiber diameter using the aRJS manufacturing technique and JetValve input materials, the UCL was set at 50% and the LCL was set at 30% given the achievable range and reproducibility of the manufacturing process. All stiffness measurement control limits were based upon the measured stiffnesses of freshly harvested pulmonary leaflets: low strain stiffness in the parallel fiber direction control limits ranged from 0-10 MPa, low strain stiffness in the perpendicular fiber direction control limits ranged from 0-1 MPa, and high strain stiffness in the parallel and perpendicular fiber directions control limits ranged from 0-20 MPa. For scaffold thickness, sample strip thicknesses ULC was set at 600 µm and the LCL was set at 250 µm to ensure scaffolds were thin enough to be crimped consistently but not too thin as to lose structure once crimped and/or loaded *in vivo*. Protein content was taken as the relative amount of P4HB to gelatin in the scaffold as measured by comparing the peak height of the carbonyl stretch peak at 1720 cm-1 (indicative of P4HB) to the amide I peak at 1645 cm-1 (indicative of gelatin) using Fourier Transform Infrared Spectroscopy (FTIR) [25]; the protein content UCL was set at 2.5 and the LCL set at 0.5. The scaffold fiber orientation was measured using the OOP based upon the OOP measured in decellularized native tissue as described above; the OOP UCL was set at 0.8 and the LCL was set at 0.375.

4.1.2.10 *IN VITRO* FUNCTIONAL TESTING

Preliminary evaluation of JetValve functionality using an *in vitro* pulse duplicator system (Vivitro Labs, Pulse Duplicator) was conducted to ensure the integrity of the scaffold leaflet design under physiologic pressures and flows [31]. 60/40 JetValves were anchored into 30 mm diameter nitinol stents with 5-0 suture (Ethicon, black monofilament) and continuously loaded for 48 hr under pulmonary pressure conditions (n=3 JetValve flow trials). A FDA waveform at 70 beats per minute was applied to the pulse duplicator's 150 ml silicon ventricle; distal compliance chambers were adjusted to achieve pulmonary-like pressures across the JetValve during diastole with a cardiac output of 2.2 L/min (valve diameter, beat rate, and cardiac output within the ranges of previously reported ovine measurements [7,32]). Ventricular (proximal to the JetValve) and arterial (distal to the JetValve) pressures and intravalvular volumetric flow rates were measured at 48 hr at a sampling rate of 256 samples per cycle.

4.1.2.11 *IN VIVO* IMPLANTATION DEPLOYMENT AND FUNCTIONAL TESTING

60/40 JetValves were implanted into the orthotopic pulmonary valve position of ovine models for deployment and acute functional testing via transapical access (Fig. 3a), a delivery technique recently shown to be a viable implantation method for tissue engineered heart valves [7]. The ethics committee (ZH151_2013, Zürich, Switzerland) approved the study in compliance with the Guide for the Care and Use of Laboratory Animals, published by the National Institutes of Health (NIH publication No. 85-23). After a right sided thoracotomy, the pericardium was opened and the right ventricle (RV) was exposed, before it was punctured using needle through purse-string sutures. Next, a guide wire was introduced into the RV and placed into the main pulmonary artery under fluoroscopic control. The scaffold loaded implantation catheter was introduced into the RV over the wire and placed over the native pulmonary valve. Optimal positioning was controlled by contrast angiography, before the scaffold was delivered under fluoroscopic control. After full delivery of the scaffold a final contrast angiography was done to ensure optimal positioning, instant functionality and complete exclusion of the native pulmonary valve (Supplemental videos 2 and 3). The delivery device was removed, the RV was closed with the purse-string, and the thoracotomy was closed. Finally trans-esophageal echocardiographic assessment was performed postoperatively to evaluate valve functionality.

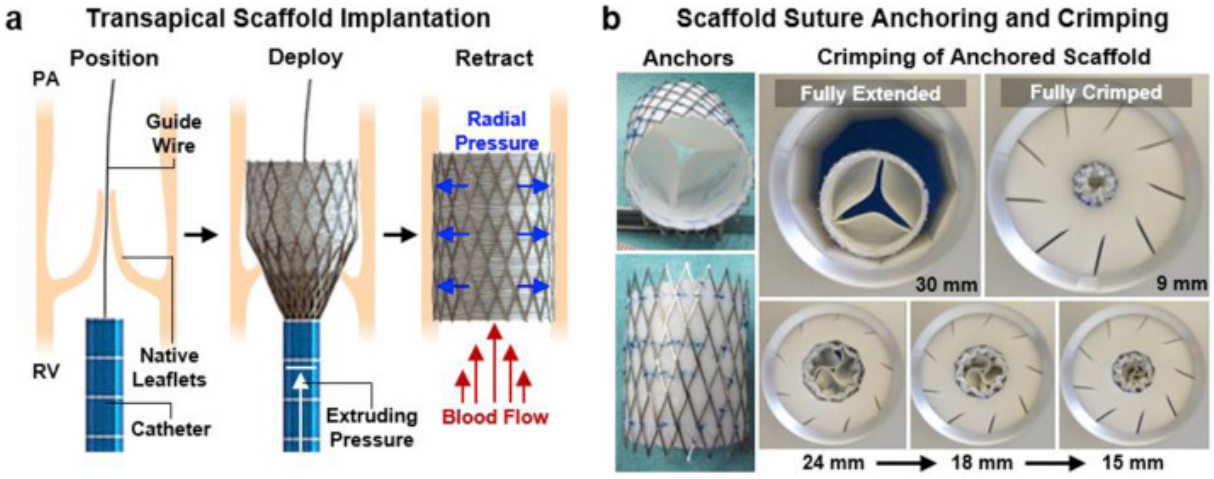

Figure 3: JetValve catheter-based deployment and crimping. (a) Transcatheter delivery involved fixing the scaffold in a self-expanding nitinol stent, transapical placement via entry through the right ventricle (RV), positioning via a guide wire system, deployment of the stented scaffold over the native leaflets, and retraction of the catheter through the ventricle. Radial pressure of the released stent held the valve scaffold in place between the RV and pulmonary artery (PA), over the native valve leaflets. (b) Crimping of anchored JetValves from the 30 mm fully extended conformation to the fully crimped 9 mm conformation to accommodate implantation.

For the acute situation (n=4), functionality measurements were taken after 15 hr *in vivo* and valves were subsequently explanted for visual inspection of structural integrity and H&E staining. The 15 hr evaluation time point was used to test the stability of valve functionality after the stresses of

minimally invasive delivery on the JetValve/stent construct. For the chronic situation (n=3), functionality measurements were taken after 1 month *in vivo*. The scope of this study was to determine if the JetValve manufacturing technique and biohybrid materials introduced here could produce a scaffold able to sustain the rigors of a minimally invasive implantation method and enable host cellular infiltration.

For minimally invasive deployment, JetValves were crimped from 30 mm in diameter to 9 mm in diameter and loaded into the implantation catheter. Stress minimization during crimping was a critical design concern because of the non-woven micro-structure of the scaffold and resulting potential susceptibility to suture and shear-induced tearing. To test capacity for crimping, JetValves were anchored into nitinol stents via suture and pneumatically crimped from 30 mm (fully extended, adult ovine size) to 9 mm (fully crimped) at 45 psi. Leaflet shape and thickness were optimized to ensure a “swirling” fold during the crimping process that minimized the stresses on the leaflets and leaflet-conduit sutured anchor points (Fig. 3b).

4.1.2.12 STATISTICAL ANALYSES

All statistical analyses of data were done using SigmaPlot software (v12.0, Systat Software Inc.); the sample size “n” used for statistical analyses are reported in the respective methods sections 2.3-2.10 above. Data analyses of variance were done using the One-Way ANOVA test (for fiber diameter, porosity, stiffness, and cell infiltration depth) or the Two-Way ANOVA test (for scaffold fiber anisotropy ‘OOP’). Pairwise multiple comparison procedures

4.1.3 RESULTS

4.1.3.1 JETVALVE BIOHYBRID STRUCTURE AND MECHANICS

Fiber diameter and porosity [33,34] are structural scaffold parameters that contribute to the degree of endogenous cellular attachment and infiltration during the remodeling process. To control these parameters, scaffolds were composed of biohybrid blends of poly-4-hydroxybutyrate (P4HB) and gelatin, i.e. denatured collagen, which is the primary structural component of valve leaflets. By varying the biohybrid concentration within the scaffold, fiber diameter [25] and alignment could be controlled to approximate that of the native valve ECM. We mixed high molecular weight P4HB (MW ~450 kDa) with gelatin (MW ~50-100 kDa) to control solution viscosity and consequently fiber diameter [21,35]. By decreasing P4HB content, fiber diameter could be reduced (range: 100/0 1.28 ± 0.39 µm to 20/80 680 ± 0.19 nm) to achieve a higher porosity (range: 100/0 41.59 ± 1.58% to 20/80 55.51 ± 2.38%) within the construct (Fig. 1c).

As in the native valve structural fibrosa, fibers were primarily oriented in the circumferential direction of the scaffold leaflets to withstand transvalvular loading during diastole while the high Mw of the P4HB and non-woven mesh structure would allow for elastic, radial stretching during systole. The continuous deposition of fibers onto mandrels angled 0˚, 22.5˚, and 45° relative to the fiber extrusion plane produced circumferential alignment within JetValve ECM [29] (native OOP: 0.49 ± 0.06, 0˚ JetValve Leaflet OOP: 0.51 ± 0.03, 22.5˚ JetValve Leaflet OOP: 0.57 ± 0.03, 45˚ JetValve Leaflet OOP: 0.53 ± 0.04, Fig. 4a). However, fiber anisotropy within the conduit portions of the JetValve constructs was significantly reduced although consistent for all angles of collection (0˚ JetValve Conduit OOP: 0.25 ± 0.04, 22.5˚ JetValve Conduit OOP: 0.23 ± 0.04, 45˚ JetValve Conduit OOP: 0.25 ± 0.04, Fig. 4a). Because fiber anisotropy varied spatially within JetValves, we asked how collection angle influenced scaffold packing density or porosity in the leaflet versus conduit portions of the constructs. For JetValve leaflets, increasing collection angle decreased scaffold porosity, a trend that was observed for JetValve conduits as well, although not statistical (Fig. 4b). For 0˚ and 22.5˚ collection angles, leaflet porosities were increased by ~10% compared to conduit porosities of leaflets, recapitulating the load bearing, collagen-rich fibrosa layer of the native valve the same angle; however, leaflet and conduit porosities reached similar values when scaffolds were collected at 45˚.

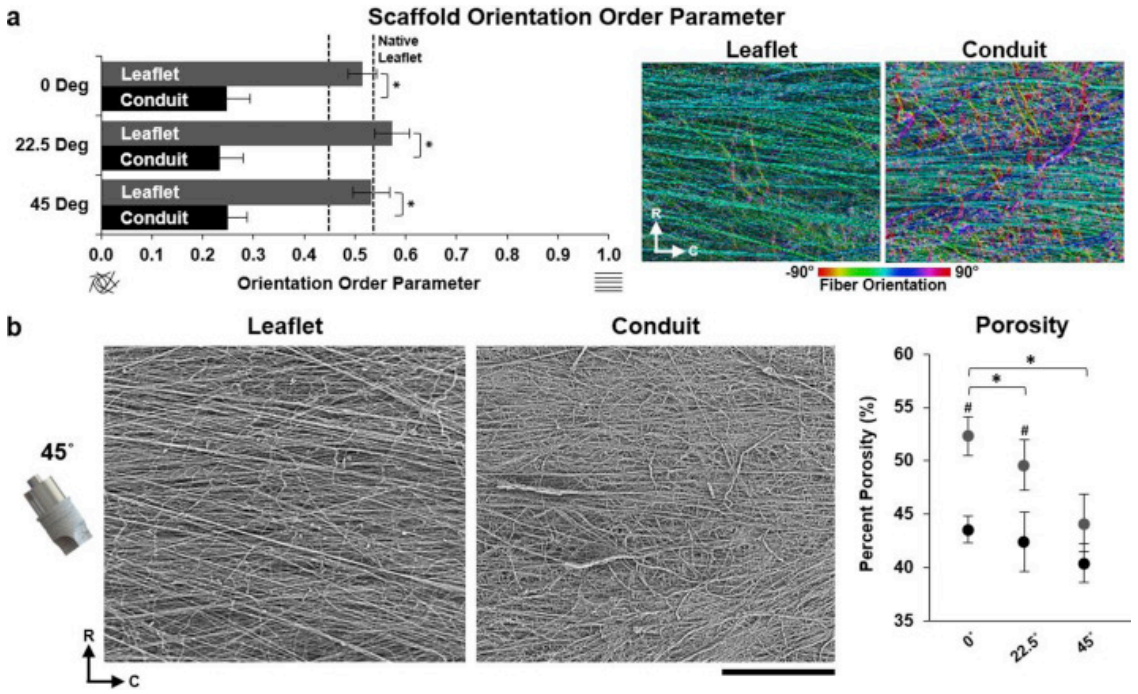

Figure 4: JetValve leaflet/conduit anisotropy and porosity. (a) JetValve leaflet anisotropy was comparable to native anisotropy, as indicated by OOP, and was significantly more anisotropic than the conduit for each collection angle. Colorized SEM images, right, indicate local fiber direction, (R) indicates radial direction and (C) indicates circumferential direction (N = 3 production runs per condition and N = 7 native leaflets, $*p < 0.5$ comparing leaflet vs. conduit). (b) Representative SEM images of JetValve leaflet and conduit scaffold collected at 45° (scale bar 500 µm). Porosity of leaflets and conduits as a function of collection angles (N = 3 production runs per condition, $*p < 0.5$ comparing angles and $^{\#}p < 0.5$ comparing leaflet vs conduit for a given angle). Data presented as mean ± s.e.m.

Recapitulating the bulk anisotropy of the native leaflet fibrosa and varying fiber biohybrid composition allowed for control of the bulk biaxial stiffness of the JetValve leaflets. The mechanical properties of the valvular leaflets determines the stress and strain fields within the tissue during the cardiac cycle, ultimately enabling their functionality [34,36]. Accordingly, elastic, fibrous scaffolds such as JetValves should be designed to mimic these mechanical properties to ensure optimal functionality in flow [37]. We therefore designed the stretch-dependent, biaxial stiffness of our scaffolds to recapitulate that of the native leaflet ECM. The P4HB/Gelatin ratio of fibers governed the biaxial stiffness of the bulk scaffold at both low (0-10%) and high (10-20%) strains (Fig. 5a). At low strain, in the primary (circumferential) axis of fiber alignment, scaffold stiffness ranged from 505.52 ± 61.72 kPa (40/60) to 5.12 ± 0.82 MPa (100/0) vs. 643.23 ± 215.76 kPa (native); in the perpendicular (radial) axis of fiber alignment, scaffold stiffness ranged from 211.91 ± 31.32 kPa (40/60) to 4.33 ± 0.16 MPa (100/0) vs. 501.41 ± 74.72 kPa (native). At high strain, in the primary (circumferential) axis of fiber alignment, scaffold stiffness ranged from 1.16 ± 0.11 MPa (40/60) to 34.47 ± 1.54 MPa (100/0) vs. 3.33 ± 0.45 MPa (native); in the perpendicular (radial) axis of fiber alignment scaffold stiffness ranged from 338.38 ± 44.31 kPa (40/60) to 13.89 ± 0.75 MPa (100/0) vs. 1.49 ± 0.40 MPa (native). Only when the P4HB/Gelatin ratio of fibers was reduced to 60/40 or 40/60 did scaffold stiffness approximate that of the native leaflet in both strain regimes in the primary and perpendicular axes of fiber alignment. JetValves were not crosslinked resulting in scaffold fibers that

began to stick to mandrels at ≥60% gelatin content; we therefore used 60/40 P4HB/Gelatin blends for further functional testing. Because collection angle spatially affected scaffold anisotropy and porosity, we asked if stiffness values were also influenced by collection angle. Biaxial stiffness values generally decreased as a function of increasing collection angle (Fig. 5b and Supplemental Fig. 1). Likely due to increased packing during fiber collection, conduit stiffnesses were found to be higher than corresponding collection angle leaflet stiffnesses in both the circumferential and radial directions.

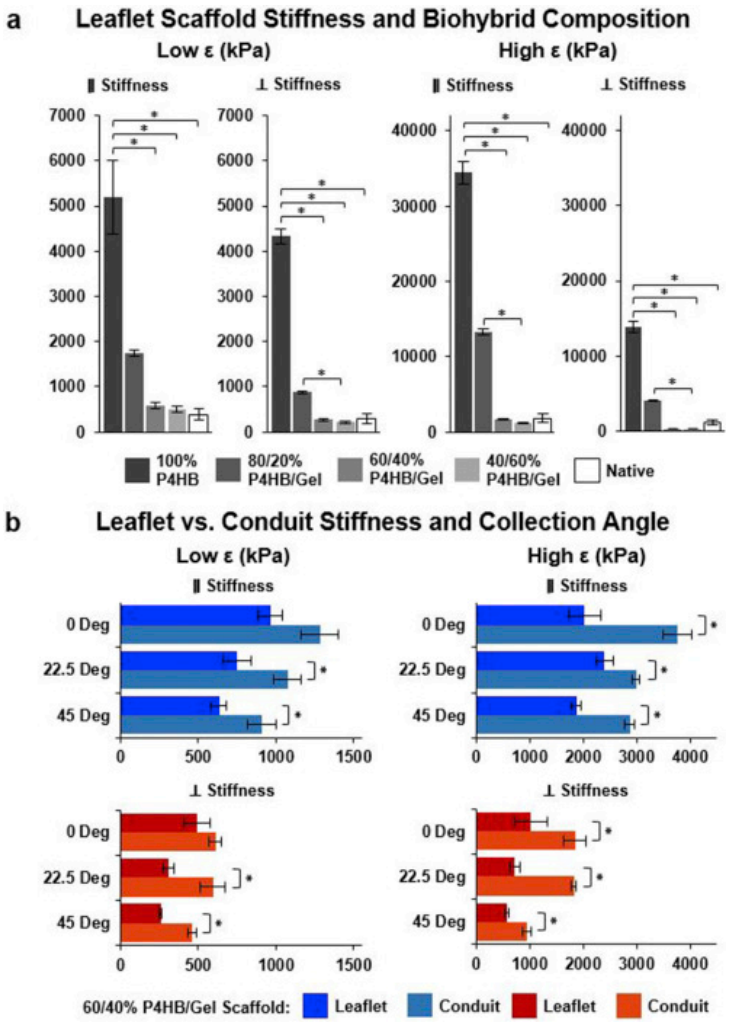

Figure 5: JetValve biaxial stiffness as a function of biohybrid composition, collection angle, and location. (a) Increasing protein percentage within the biohybrid ratio of spun scaffolds decreased the low strain (0–10%) and high strain (10–20%) biaxial global stiffness of scaffolds (N = 6 production runs per condition, N = 5 native leaflets; *p < 0.5, data presented as mean ± s.e.m. (b) Conduit samples comprised of 60/40 P4HB/Gelatin blends were stiffer than corresponding collection angle leaflet samples for both low and high strains (N = 6 production runs per conditions; *p < 0.5 between leaflet and conduit stiffness for the same collection angle, data presented as mean ± s.e.m.).

4.1.3.2 JETVALVE SURFACE BIOCHEMISTRY AND HYDRATED SHELF LIFE

Because JetValve biohybrid scaffolds were physically blended, the compositional effects of not crosslinking and hydrating of the scaffold were further analyzed due to the time required for minimally invasive surgical delivery preparation. To prepare for stent anchoring and crimping, JetValves were hydrated resulting in more pliable fibers. Because the scaffold protein content was not crosslinked, once hydrated the shelf-life of the scaffold would be limited due to passive gelatin

diffusion from the surface of the fibers. Using FTIR, initial relative protein content within JetValves was measured by comparing the height of the carbonyl stretch peak (1720 cm-1, indicative of P4HB) with those of the amide I and amide II peaks (1645 and 1535 cm-1 respectively, indicative of gelatin, Fig. 6a) [25]. The 60/40 P4HB/Gelatin scaffold blend was chosen as it most closely mimicked the leaflet structural and mechanical design criteria described above while maintaining constant polymer crystallinity and therefore a predictable degradation profile over a range of manufacturing spinning speeds (Fig. 6b).

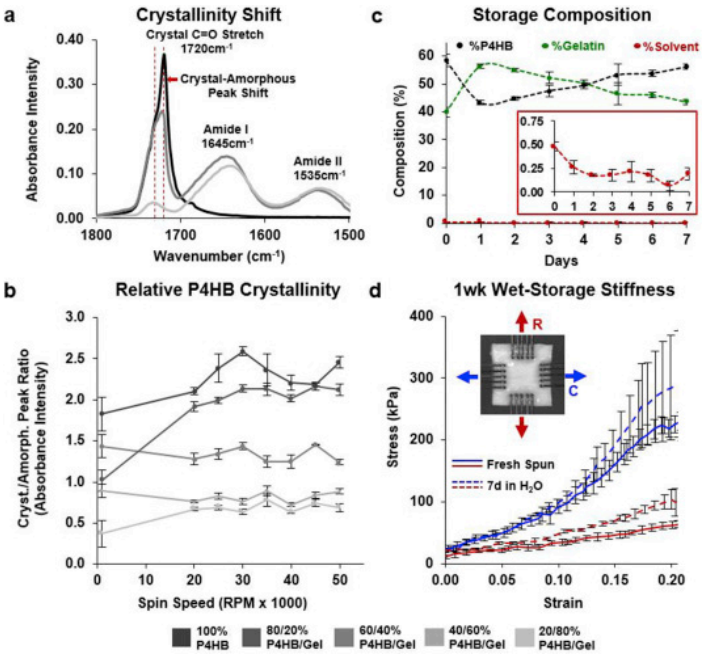

Figure 6: Shelf life composition and stiffness of JetValves. (a) Initial protein content and P4HB crystallinity was measured by comparing carbonyl stretch and amide FTIR absorbency peak heights. (b) Neither protein content nor polymer crystallinity were affected by fiber extrusion spin speed; Biohybrid blends of 60/40 P4HB/Gelatin exhibited stable relative crystallinity for all spin speeds compared to compositions with higher synthetic polymer content (N = 3 production runs per condition). (c) Ratiometric (XPS) hydrated scaffold content over the course of 1 week. Inset: trace amounts of bound HFIP solvent were detected upon hydration (N = 3 production runs). (d) The biaxial mechanical properties of 1 week hydrated scaffolds compared to those of fresh-spun scaffolds (N = 3 production runs per condition; blue represents circumferential (C), red represents radial (R) fiber alignment; data presented as mean ± s.e.m.).

The as-spun, dry composition of the 60/40 JetValve blend was measured to be 58.43 ± 2.30% P4HB, 39.85 ± 1.86% gelatin, and 0.44 ± 0.4% HFIP. Once hydrated, the surface gelatin composition of the scaffold increased to 56.42 ± 0.81% but returned to 43.48 ± 0.89% after 7 days in pure water (XPS, Fig. 6c). As fibers within the scaffold were hydrated, uncrosslinked and therefore chemically unbound gelatin first diffused to the fiber surface, then into the surrounding water. Additionally, the HFIP content decreased by nearly half (0.26 ± 0.07%) after 1 day in water suggesting that the residual, bound solvent was only present in trace amounts once hydrated. The shelf life of the hydrated 60/40 JetValves was therefore approximatively 1 week, the timeframe within which JetValve composition stayed within 60/40 to 40/60 P4HB/Gelatin composition with stiffness similar to as-spun scaffolds (Fig. 6d) as recorded above.

4.1.3.3 *IN VITRO* CELLULAR INFILTRATION

JetValve composition was designed to be an approximation of previously published, tissue engineered valves that exhibited cellular infiltration and extensive regeneration via endogenous repair mechanisms [6,7,9,33,38]. Although composed of similar materials to those tissue engineered products previously investigated, we asked if the rapid and non-biological manufacturing of JetValve scaffolds allowed for cellular infiltration and if this integration varied spatially throughout the construct. Primary harvest porcine VICs infiltrated leaflet portions of 60/40 JetValve scaffold faster than conduit portions of the scaffold by one week in culture (Fig 7a; infiltration depth Leaflet: 14.52 ± 1.16 µm compared to Conduit: 11.09 ± 0.81 µm). However, by two weeks in culture, infiltration depth for leaflet and conduit sections were similar (Leaflet: 27.17 ± 3.56 µm compared to Conduit: 25.68 ± 2.90 µm) although leaflet tissues appeared more densely populated (Fig. 7b).

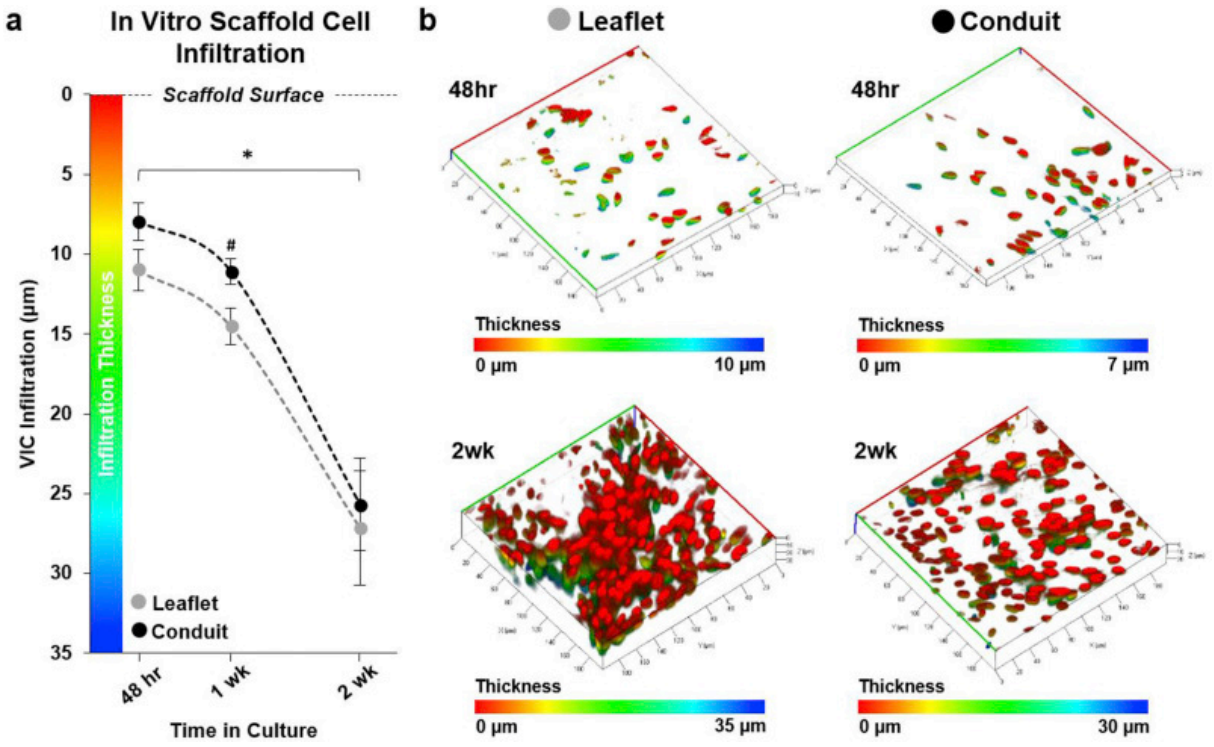

Figure 7: *In vitro* valvular interstitial cell (VIC) infiltration. (a) VICs infiltrated the JetValve leaflet portion of scaffolds in greater abundance than conduit portions by 1 week; by 2 weeks, infiltration depth evened at ~25–26 µm from the scaffold surface (N = 6 production runs/tissues per condition, *p < 0.5 between like scaffold areas in time, #p < 0.5 between leaflet and conduit at the same time point; data presented as mean ± s.e.m) (b) Representative three dimensional reconstructions of VIC nuclei within the JetValve scaffold (red indicates nuclei of cells on the scaffold surface, while blue indicates the nuclei of cells that have penetrated into the scaffold, all images in isometric 3D view, 40,000 µm^2 area).

4.1.3.4 aRJS MANUFACTURED JETVALVE BATCH PROCESS CAPABILITY

In order to evaluate scaffold quality and fabrication reproducibility, essential for eventual clinical translation [15], we implemented standard industrial manufacturing process controls based upon the JetValve design criteria described above. We accomplished this by analyzing the structural, mechanical, and biochemical batch process capability (CP) of each scaffold as a measure of both manufacturing accuracy and precision [30]. Batch CP specifications were held to standard precision values of ±3 times the batch parameter variance, ensuring that over 99% of scaffolds within a passing batch were within specification. Despite laboratory-scale batch sizes (≤4), manufacturing achieved higher than 70% batch acceptance rate, which was increased to 100% with the addition of small batch correction factors [39].

4.1.3.5 *IN VITRO* AND *IN VIVO* JETVALVE FUNCTIONAL TESTING

JetValve functionality was evaluated both *in vitro* and *in vivo*. Preliminary evaluation of scaffold function using an *in vitro* pulse duplicator system was conducted to ensure the integrity of the scaffold leaflets under physiologic pressures and flows. JetValves were continuously loaded for 48 hr under pulmonary-like conditions, maintaining scaffold structural integrity and exhibiting a regurgitant fraction of 30.24 ± 2.07% during diastolic closing (Fig. 8a). *In vivo* studies were then conducted to determine if 1) JetValve scaffolds could be delivered using a minimally invasive method, 2) if the as-spun, acellular scaffolds would be immediately functional upon implantation, and 3) if the scaffold design was biocompatible (i.e. non-thrombogenic). JetValves were delivered transapically into the native pulmonary valve position in an ovine model for 15 hr as a proof-of-concept. Implanted scaffolds revealed acute functionality as sufficient leaflet motion and good coaptation area were observed with non/minor regurgitation fraction on echocardiography. Transvalvular pressure gradients across the valve, <2mmHg, were also comparable to native leaflets during systole (Fig. 8b, Echo: Supplemental videos 4 and 5; Doppler: Supplemental videos 6 and 7). Gross examination and histological analyses done at the time of explantation revealed competent valves with pliable and intact leaflets. No/minor thrombus formation and initial, what appears to be neutrophil infiltration on the scaffold surface were observed (Supplemental Fig. 3) indicative of the acute safety and compatibility of JetValve scaffolds.

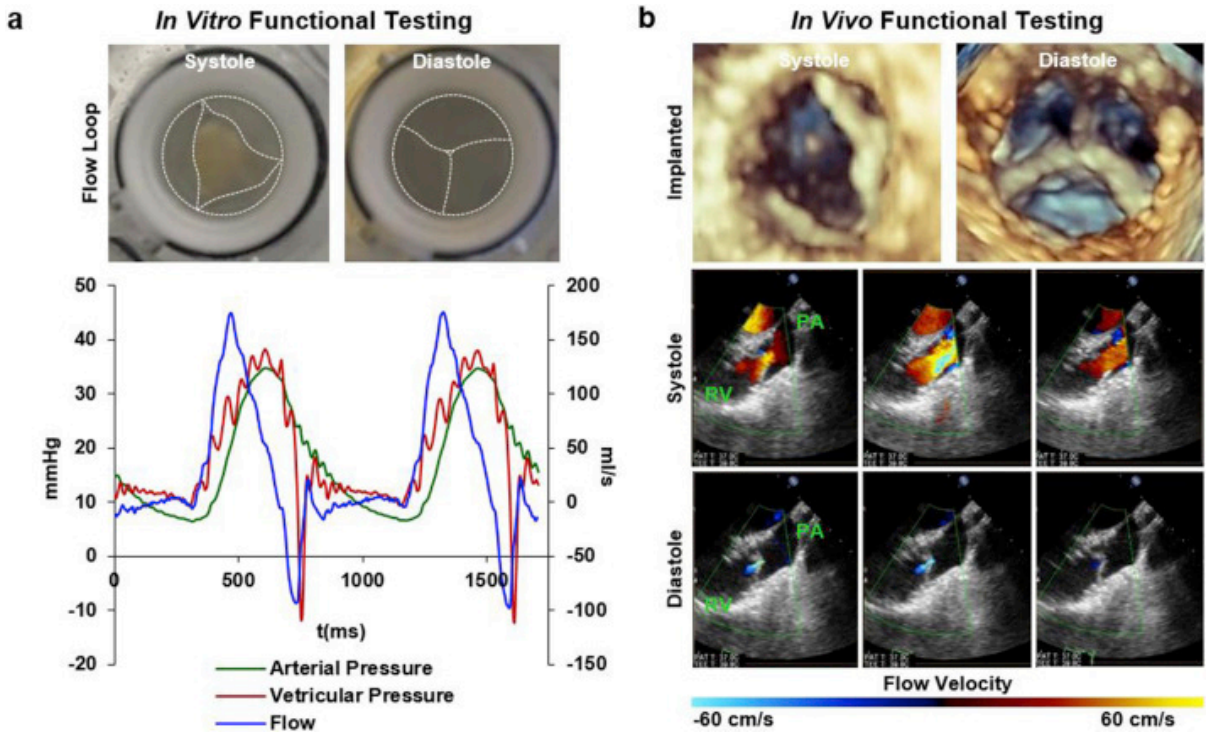

Figure 8: *In vitro* and *in vivo* functionality. (a) Top: digital photographs from arterial view of mounted JetValves during systole and diastole at 48 h (dotted lines highlight the JetValve leaflet and conduit edges). Bottom: flow through the JetValve reached ~175 ml/s during peak systole with complete valve closure during diastole (~30% regurgitant fraction, ~10 mmHg transvalvular pressure). (b) Top: distal three-dimensional echocardiography revealed complete leaflet opening and closing during systole and diastole respectively at 15 h. Bottom: Doppler imaging showed unrestricted blood flow through the JetValve leaflets during systole and complete closure with minor regurgitation fraction during diastole (RV: right ventricle, PA: pulmonary artery).

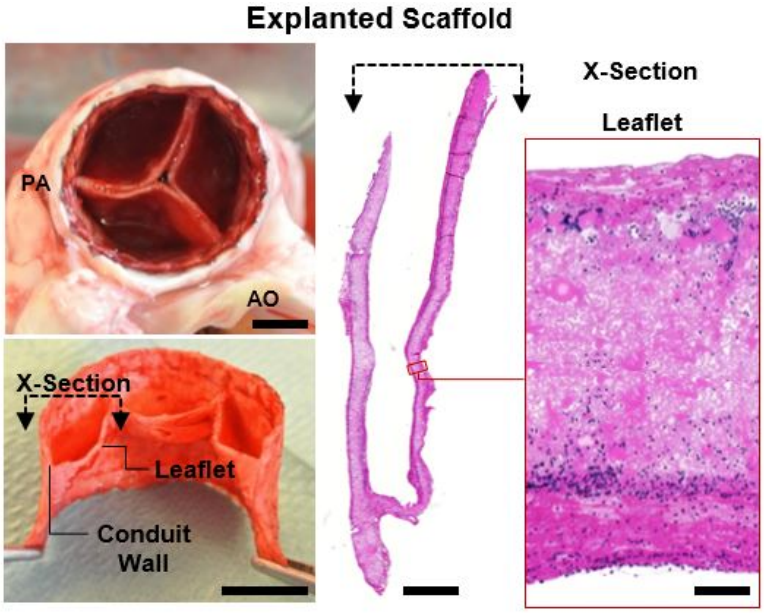

Supplemental Figure 3: Histological examination of explanted JetValves at 15 hr post-implantation. JetValves explanted 15 hr after implantation revealed no/minor thrombus formation on the intact leaflets. Hematoxylin and eosin (H&E) staining of explanted JetValves showed limited scaffold infiltration of circulating immune cells (scale bars: 10 mm pulmonary view, 20 mm cross sectional view, 2 mm cross sectional histology, and 100 µm histology inset)

Long-term *in vivo* implantation of 1 month revealed several complications as to the suture retention (n=1) and migration of the stent (n=2). Migration was due to either size-mismatch of the ovine pulmonary annulus with the implanted stent size or inaccurate placing during the implantation procedure due to the implantation device. This unintentional migration enabled functionality of the native ovine valves, consequently leading to less/no loading of the implanted heart valve scaffolds. Leaflet motion was limited to single loaded leaflets, resulting in no coaptation and overall functionality of implanted scaffolds (Fig. unpublished 1). Hemodynamic loaded leaflets were thin and pliable, whereas no loading resulted in thickening of the scaffold by tissue accumulation and leaflet attachment to the vessel wall. Therefore, only hemodynamic loaded leaflets of two implantations were evaluated on cellular infiltration and endogenous tissue formation by cross examination and histological analysis after 4 weeks *in vivo*.

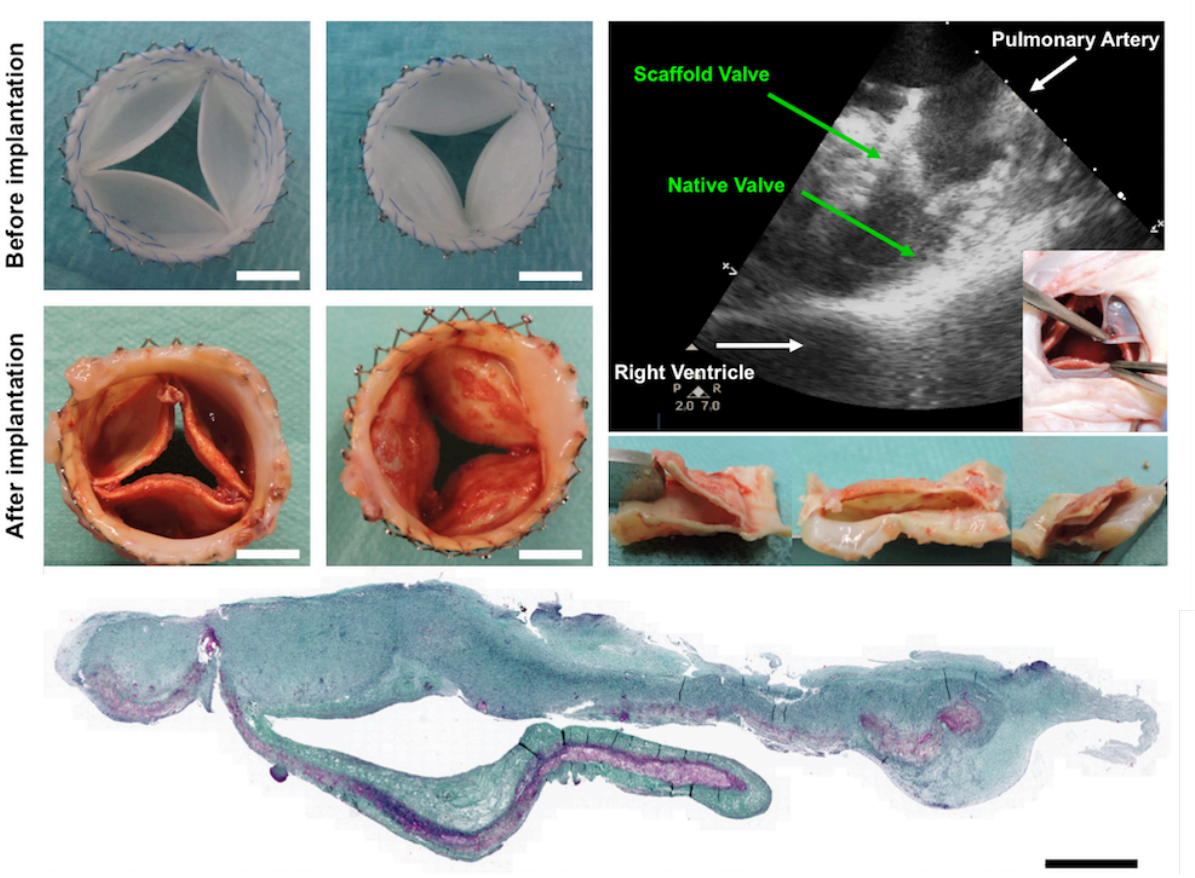

Unpublished figure 1: Evaluation of explanted Jetvalves after 1 month post-implantation. JetValves revealed no functionality and coaptation of the heart valve leaflets *in vivo* given functional native leaflets on top. Hemodynamic loaded leaflets were thin and pliable with regular motion as detected by echocardiography. Endogenous tissue formation (green) was found on the surface of implanted material (violet) with limited integration as demonstrated by Masson Goldner staining. (scale bars: 1cm in cross examination pictures of implanted valves, XY in cross sectional histology)

In comparison to native ovine heart valve leaflets, recruitment of host cells was limited to the surface layer of the hemodynamic loaded leaflet scaffolds (Fig. unpublished 2). Low degree of repopulation was also found in the hinge and wall regions of all implanted scaffolds, which usually is repopulated faster and independently from hemodynamic loading. Overall implanted leaflet scaffolds did not possess an endothelial cell layer (CD31 positive cells), which is essential for an anti-thrombotic behavior of the scaffold. No elastic fibers (Von Giesson-Elastin, VG-EL), intermediate filaments (Vimentin, Vim) and collagen depositions (Masson Goldner, MG) were found in the central region of the implanted scaffolds. Calcifications (Von Kossa, VK) and enhanced attraction of alpha-smooth muscle actin positive cells (αSMA) were not detected. A portion of endogenous tissue was found on the surface of hemodynamic loaded scaffolds, however its integration with the implanted material was low and resulted in easy delamination (Fig. unpublished 1). This accumulation of tissue resulted in an overall valve thickness extending the original material implanted. Histological analyses at the time of explantation further revealed low degradation of electrospun scaffold in comparison to the originally implanted 60/40 P4HB/Gelatin scaffold.

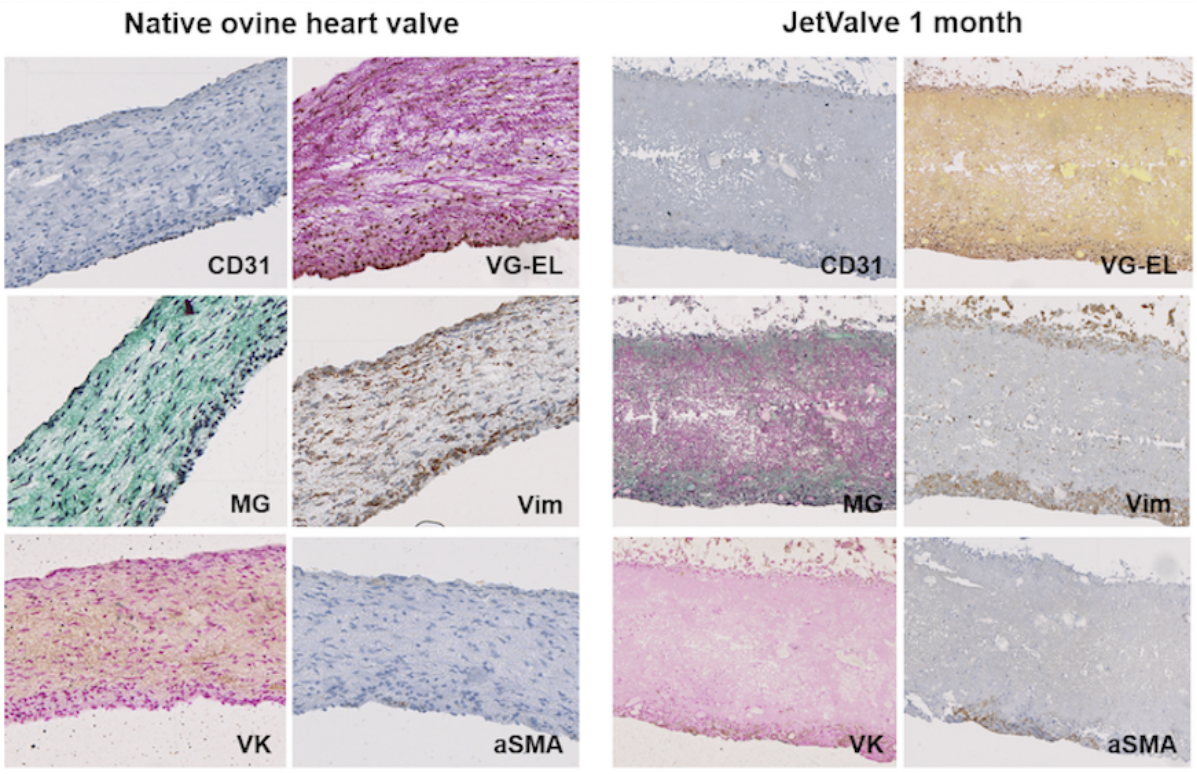

Unpublished figure 2: Histological examination of explanted JetValves at 1 month post-implantation. Explanted JetValve leaflets revealed limited recruitment of host cells with low endogenous tissue formation compared to native ovine leaflets. Infiltrating cells were only found on the surface layer of implanted scaffold (CD31 = platelet endothelial cell adhesion molecule; VG-EL = Von-Giesson Elastin; MG = Masson Goldner; Vim = Vimentin; VK = Von Kossa; aSMA = alpha-smooth muscle actin).

4.1.4 DISCUSSION

In this study, we present a novel method of manufacturing valve replacements containing leaflets with fibrosal-like fiber alignment and global semilunar valve structure in minutes. This level of throughput is an improvement in time to manufacture relative to previously reported mandrel-based, fibrous valve fabrication techniques [40,41]. Slow solution infusion rates (≤2 ml/hr) and grounded-mandrel collection speeds (≤1 RPM) have resulted in production times ranging from 1.5 hr [40] to over 3.5 hr [41] per scaffold using comparable electrospinning methods. By increasing infusion and fiber collection rates by two and three orders of magnitude respectively, we were able to produce 30 mm diameter JetValves in less than fifteen minutes. JetValve production times can be compared to those achievable with 3D printing techniques [42,43]; however, 3D printing still remains unable to produce the spatial resolution of nano/micro-fiber production platforms. Similarly, hydrogel and soft-polymer molding and patterning techniques for engineering heart valves have been limited to feature resolutions within tens to hundreds of microns [44-47] and often require hours to days for fabrication due to gelation/layer bonding times. In comparison, we were able to achieve fiber resolution ranging from hundreds of nanometers to microns by varying solution composition and collection in order to rapidly recapitulate the size scale and anisotropy of the native fibrosa ECM layer of the valve.

Scaffold biochemical and mechanical properties are critical for guiding tissue regeneration and macro-scale leaflet functionality [48,49]. Accordingly, the bulk, biaxial stiffness of JetValve leaflets was engineered to match that of native tissue similar to previously reported 'off-the-shelf' cell-based manufactured valve scaffolds [7,9] but without the need for long culture and *in vitro* conditioning. JetValve stiffness values were an order of magnitude smaller than previously reported, as-spun off-the-shelf fibrous scaffolds [50] and commercially available 'stiff' bioprosthetic valves (single versus tens of megapascals) [51]. This was made possible by the inclusion of uncrosslinked gelatin in the biohybrid JetValve fibers and varying the collection angle on the aRJS system. Despite not crosslinking JetValves, exposure of biohybrid fibers to water for up to 1 week did not significantly change the stiffness of the scaffold. During this period, P4HB/Gelatin content remained within compositional range for mimicking the measured native tissue stiffness values. This length of hydrated shelf life is comparable to recent fiber/gel valvular scaffold composites [52] and is well in excess of the time required for pre-implantation procedures: on the order of hours for stent fixation, crimping, and surgical delivery preparation.

While recent studies have begun to apply defined standards (e.g. ISO) for the assessment of tissue engineered heart valve functional performance [52,53], little work has been done to establish industrial-style quality control standards for tissue engineering manufacturing processes and products [54].

Therefore the structural, mechanical, and compositional scaffold design parameters discussed above were measured and evaluated for each JetValve prepared for implantation as a factor of safety for the animal models used. The automated method of JetValve assembly and simplicity of manufacturing customization enabled straightforward implementation of multi-parameter process capability metrics [55,56]. Our group has developed similar multi-parameter quality assessment indices for stem cell manufacturing [27,57] and suggest that the same can and should be done for tissue engineered products [19]. We envision batch process capability and other quality control metrics may likewise be applied to future JetValve designs and similar automated *in situ* tissue engineered scaffold processes to ensure patient or model safety prior to functional testing.

Restoration of valvular functionality upon implantation is the immediate goal of regenerative scaffolds. As-manufactured JetValves showed potential as functioning and biocompatible valves both *in vitro* and *in vivo* after crimping and minimally invasive delivery. Scaffold stiffness plays a critical role in leaflet kinematics and the development of transvalvular pressure gradients during systole [58,59]. As in previously proposed Polymer/Gelatin composite models for achieving native tissue-like stiffnesses [60], the biohybrid JetValve scaffold composition was tuned to mimic native ECM leaflet stiffness. As a result, transvalvular pressure gradients of <2 mmHg were observed *in vivo* which is equivalent to recently published human and ovine tissue engineered heart valve (<5 mmHg) [31,53]. However, *in vitro* pulse duplicator testing did reveal a regurgitant fraction of approximately 30% which is above ISO standards of similarly sized heart valves [52]. These data did not appear, though, to fully predict JetValve functionality *in vivo* where rapid and complete leaflet coaptation and minimal closing jet were observed with echo/doppler imaging. JetValves were mounted in the pulse duplicator system in the absence of radial loading which is normally applied *in vivo* by the surrounding tissue (pulmonary artery and valve annulus). This resulted in full expansion of the stent and may explain the level of measured regurgitation *in vitro*. While these data do not necessarily give indication as to the regenerative capacity or long-term functionality of JetValves, they do support the manufacturing method as viable. These time points, 48 hr *in vitro* and 15 hr *in vivo*, indicate that the JetValve manufacturing technique can be used to produce a working, semilunar valve structure amenable to minimally invasive implantation with acute safety. Future iterations of the JetValve scaffold will reveal which compositions and spinning/collection parameters will be necessary for long-term functionality and tissue regeneration.

In addition to restoring function, the long-term goal of all regenerative, *in situ* tissue engineered scaffolds is to promote both full regeneration and adaptive growth of the target tissue. Such scaffolds should serve as resorbable platforms onto and into which the body can “auto-engineer” its own replacement tissue that, ideally, perfectly matches healthy native tissue. This requires intricate engineering design of scaffold architectural, mechanical, and biochemical properties [50] to control

time-dependent biological processes including cellular recruitment, inflammation, and scaffold remodeling [61]. Here, we showed that 60/40, as-spun JetValves supported progressive VIC infiltration and tissue growth at least *in vitro*, suggestive of their potential for serving as scaffolds for long-term endogenous tissue formation *in vivo*. However, these studies are limited and it is likely that that inclusion of anti-inflammatory agents and/or growth factors may be necessary for endogenous repair mechanism to be activated. Inclusion of these factors as dopants is possible using the JetValve manufacturing method without significant modification to the technique or time to production. Growth factors associated with development such as transforming growth factor-β1 (TGF-β1), bone morphogenic proteins (BMPs), and/or platelet-derived growth factors (PDGFs) may be incorporated into scaffolds to elicit endothelial-to-mesenchymal transformation (EMT), for example, in order to populate and remodel the scaffold [55,62,63]. Additionally, recently reported hybrid-manufacturing techniques for the production of more complex, tri-layered scaffolds have been developed in an effort to better mimic this anisotropic, stratified structure of the valvular ECM for optimal hemodynamic performance and tissue regeneration [52,64-66]. The JetValve production platform is amenable to fabrication of similarly layered scaffolds while maintaining industrial-like scaffold production rates [67-69] due to its additive nature. By successively spinning fibrosa, spongiosa, and ventricularis-like layers of biohybrid materials with mechanical properties and biochemistry tailored to the specific ECM layers of the valve, stratified JetValve production could be possible.

We further propose that this method can be valuable for the fabrication or other fibrous replacement organ scaffolds or for production of customized scaffolds given the specific age, size, and organ or organ-part needs of a patient [19]. Fibrous, vascularized tissue such as myocardium or branching blood vessels may incorporate vascular endothelial growth factors (VEGFs), angiopoietins, or ephrins to elicit neovascularization within the scaffold [70]. Although precise growth factor combinations and amounts needed to recruit tissue specific cell progenitors remains to be identified [15,71], the flexibility of the JetValve manufacturing process described here would allow for easy incorporation of multiple factors into scaffolds to promote homing and assembly of endogenous cells and tissues. Furthermore, because mandrels can be 3D printed in any shape, scaffolds of customized anatomy may be spun using this technique: combining the JetValve mandrel-based spinning process with the idea of 3D printing patient specific organ geometries [43,72-74]. The manufacturing process we present here is well suited to rapidly and iteratively study the properties and compositions needed for fibrous scaffold-based endogenous tissue repair and is amenable to patient-specific customization.

In conclusion, we have introduced a manufacturing process for the rapid fabrication of fibrous, semilunar heart valve scaffolds. By varying manufacturing parameters such as solution composition, extrusion speed, and mandrel size or collection angle, functional scaffolds were built to model basic

native valvular ECM. This method is amenable to further customization by tuning the same multiscale structural, mechanical, and biochemical scaffold parameters to potentially match the anatomy of specific patients and/or determine which values of these parameters will elicit an ideal remodeling response once implanted. Because scaffolds were fabricated three-dimensionally, they could easily be incorporated into stents and implanted minimally invasively as-spun, without the need for post processing or *in vitro* preconditioning. The simplicity and control of this scaffold manufacturing process offers a viable, cell-free and clinically translatable alternative for the fabrication of heart valves and possibly other fibrous organs. Therefore, first long term *in vivo* functionality of electrospun heart valves is necessary before safe clinical translation.

In this regard, a follow up study for the long-term *in vivo* evaluation has been initiated. Despite initial success in the acute situation, recruitment of host cells was limited to the surface layer of the valve scaffold after 1-month post-implantation. It appeared that cells could not infiltrate the implanted scaffold to form endogenous tissue. In contrast, previous studies demonstrated fast cellular repopulation of decellularized tissue engineered heart valves after 1-month implantation, with comparable cellularity of the leaflets to that of native leaflets [6]. Although *in vitro* infiltration of VIC could be demonstrated in the presented study, one has to emphasize that the *in vitro* cellular infiltration was limited to ~25 µm, which overall only represents a small portion of the surface scaffold in comparison of the overall thickness of the JetValve scaffold with a UCL of 600 µm and a LCL of 250 µm. Reasons as to the limited host cell infiltration might be scaffold composition, porosity and/or pore sizes. Host cells interact primarily with chemical functional groups on the material surface, which are produced in natural extracellular materials but not in synthetic materials such as P4HB [75]. Too small pore sizes result in a high cellular density at the scaffold surface, whereas too large pore sizes decrease surface area and limit cellular attachment [76]. Optimal pore size varies on the tissue being engineered, its required mechanical properties and the different cell types infiltrating it. Inclusion of bioactive substances has shown to activate endogenous tissue remodeling by enhancing cell attraction and binding. As an example, the local release of inflammatory cytokines and chemokines has shown to increase host cell recruitment via an inflammatory process and determine the fate of implanted scaffold towards functional tissue [77]. Like that the balance between tissue formation and scaffold degradation could be improved. Degradation of implanted scaffold material after 1 month *in vivo* was limited in the presented study. Therefore exact degradation rates of electrospun material need to be further defined, given its biohybrid compositon 60/40 P4HB/Gelatin and a negligible amount of PGA. Complete resorption of P4HB occurs between 12 and 18 month *in vivo* [78], whereas gelatin degradation alone occurs rapidly. Overall further studies are mandatory to elucidate the exact underlying mechanisms of tissue remodeling and scaffold

degradation involved. In particular, the precise role of engineered scaffolds with respect to their chemo-attraction of host cells and tissue formation has to be assessed.

Besides further optimization of scaffold composition for better recellularization and remodeling capacities, adaptations of the heart valve design are required. The presented valve geometry represents a simplified flat version with sharp transition areas from the heart valve belly to the wall region. Integration of sinuses would enable better biomechanical load of the leaflets and ultimately support leaflet movement and durability, while functioning as a washout mechanism to prevent blood stagnation and thrombosis [79]. Therefore, first studies are recapitulating the native heart valve anatomy by including bioengineered sinus of Valsalve and demonstrating initial *in vivo* functionality in the aortic position [80]. However another anatomical structure never incorporated into engineered heart valves are ventricular papillary muscles and its chordea tendineae, which prevent valve inversion or prolapse during ventricular contraction. Ultimately future studies will need to evaluate the necessity and advantages of such anatomical structures in the functionality and translation of engineered heart valves.

4.1.5 REFERENCES

1 Chaikof, E. L. The development of prosthetic heart valves--lessons in form and function. *N Engl J Med* **357**, 1368-1371, doi:10.1056/NEJMp078175 (2007).

2 Jana, S., Tranquillo, R. T. & Lerman, A. Cells for tissue engineering of cardiac valves. *J Tissue Eng Regen Med* **10**, 804-824, doi:10.1002/term.2010 (2016).

3 Robinson, P. S., Johnson, S. L., Evans, M. C., Barocas, V. H. & Tranquillo, R. T. Functional tissue-engineered valves from cell-remodeled fibrin with commissural alignment of cell-produced collagen. *Tissue Eng Part A* **14**, 83-95, doi:10.1089/ten.a.2007.0148 (2008).

4 Jana, S., Tefft, B. J., Spoon, D. B. & Simari, R. D. Scaffolds for tissue engineering of cardiac valves. *Acta Biomater* **10**, 2877-2893, doi:10.1016/j.actbio.2014.03.014 (2014).

5 Badylak, S. F. TISSUE REGENERATION. A scaffold immune microenvironment. *Science* **352**, 298, doi:10.1126/science.aaf7587 (2016).

6 Weber, B. *et al.* Off-the-shelf human decellularized tissue-engineered heart valves in a non-human primate model. *Biomaterials* **34**, 7269-7280, doi:10.1016/j.biomaterials.2013.04.059 (2013).

7 Driessen-Mol, A. *et al.* Transcatheter implantation of homologous "off-the-shelf" tissue-engineered heart valves with self-repair capacity: long-term functionality and rapid in vivo remodeling in sheep. *J Am Coll Cardiol* **63**, 1320-1329, doi:10.1016/j.jacc.2013.09.082 (2014).

8 Syedain, Z. H., Bradee, A. R., Kren, S., Taylor, D. A. & Tranquillo, R. T. Decellularized tissue-engineered heart valve leaflets with recellularization potential. *Tissue Eng Part A* **19**, 759-769, doi:10.1089/ten.TEA.2012.0365 (2013).

9 Dijkman, P. E., Driessen-Mol, A., Frese, L., Hoerstrup, S. P. & Baaijens, F. P. Decellularized homologous tissue-engineered heart valves as off-the-shelf alternatives to xeno- and homografts. *Biomaterials* **33**, 4545-4554, doi:10.1016/j.biomaterials.2012.03.015 (2012).

10 Sengupta, D., Waldman, S. D. & Li, S. From in vitro to in situ tissue engineering. *Ann Biomed Eng* **42**, 1537-1545, doi:10.1007/s10439-014-1022-8 (2014).

11 Schaefermeier, P. K. *et al.* Potential cell sources for tissue engineering of heart valves in comparison with human pulmonary valve cells. *ASAIO J* **55**, 86-92, doi:10.1097/MAT.0b013e31818f54e4 (2009).

12 Emmert, M. Y. & Hoerstrup, S. P. Tissue engineered heart valves: moving towards clinical translation. *Expert Rev Med Devices* **13**, 417-419, doi:10.1586/17434440.2016.1171709 (2016).

13 Archer, R. & Williams, D. J. Why tissue engineering needs process engineering. *Nat Biotechnol* **23**, 1353-1355, doi:10.1038/nbt1105-1353 (2005).

14 Christians, U., Klawitter, J., Klawitter, J., Brunner, N. & Schmitz, V. Biomarkers of immunosuppressant organ toxicity after transplantation: status, concepts and misconceptions. *Expert Opin Drug Metab Toxicol* **7**, 175-200, doi:10.1517/17425255.2011.544249 (2011).

15 Schoen, F. J. Heart valve tissue engineering: quo vadis? *Curr Opin Biotechnol* **22**, 698-705, doi:10.1016/j.copbio.2011.01.004 (2011).

16 Webber, M. J., Khan, O. F., Sydlik, S. A., Tang, B. C. & Langer, R. A perspective on the clinical translation of scaffolds for tissue engineering. *Ann Biomed Eng* **43**, 641-656, doi:10.1007/s10439-014-1104-7 (2015).

17 Place, E. S., Evans, N. D. & Stevens, M. M. Complexity in biomaterials for tissue engineering. *Nat Mater* **8**, 457-470, doi:10.1038/nmat2441 (2009).

18 Dijkman, P. E., Fioretta, E. S., Frese, L., Pasqualini, F. S. & Hoerstrup, S. P. Heart Valve Replacements with Regenerative Capacity. *Transfus Med Hemother* **43**, 282-290, doi:10.1159/000448181 (2016).

19 Capulli, A. K., MacQueen, L. A., Sheehy, S. P. & Parker, K. K. Fibrous scaffolds for building hearts and heart parts. *Adv Drug Deliv Rev* **96**, 83-102, doi:10.1016/j.addr.2015.11.020 (2016).

20 Szentivanyi, A., Chakradeo, T., Zernetsch, H. & Glasmacher, B. Electrospun cellular microenvironments: Understanding controlled release and scaffold structure. *Adv Drug Deliv Rev* **63**, 209-220, doi:10.1016/j.addr.2010.12.002 (2011).

21 Badrossamay, M. R., McIlwee, H. A., Goss, J. A. & Parker, K. K. Nanofiber assembly by rotary jet-spinning. *Nano Lett* **10**, 2257-2261, doi:10.1021/nl101355x (2010).

22 Zhang, X. *et al.* Application of hydrogels in heart valve tissue engineering. *J Long Term Eff Med Implants* **25**, 105-134 (2015).

23 Jana, S. & Lerman, A. Bioprinting a cardiac valve. *Biotechnol Adv* **33**, 1503-1521, doi:10.1016/j.biotechadv.2015.07.006 (2015).

24 Cheung, D. Y., Duan, B. & Butcher, J. T. Current progress in tissue engineering of heart valves: multiscale problems, multiscale solutions. *Expert Opin Biol Ther* **15**, 1155-1172, doi:10.1517/14712598.2015.1051527 (2015).

25 Badrossamay, M. R. *et al.* Engineering hybrid polymer-protein super-aligned nanofibers via rotary jet spinning. *Biomaterials* **35**, 3188-3197, doi:10.1016/j.biomaterials.2013.12.072 (2014).

26 Barbour, K., Huang, H. Y. S. & Huang, H. S. The stress relacation behaviours of diseased heart valve tissue.

27 Pasqualini, F. S., Sheehy, S. P., Agarwal, A., Aratyn-Schaus, Y. & Parker, K. K. Structural phenotyping of stem cell-derived cardiomyocytes. *Stem Cell Reports* **4**, 340-347, doi:10.1016/j.stemcr.2015.01.020 (2015).

28 Rezakhaniha, R. *et al.* Experimental investigation of collagen waviness and orientation in the arterial adventitia using confocal laser scanning microscopy. *Biomech Model Mechanobiol* **11**, 461-473, doi:10.1007/s10237-011-0325-z (2012).

29 Capulli, A. K., MacQueen, L. A., O'Connor, B. B., Dauth, S. & Parker, K. K. Acute pergolide exposure stiffens engineered valve interstitial cell tissues and reduces contractility in vitro. *Cardiovasc Pathol* **25**, 316-324, doi:10.1016/j.carpath.2016.04.004 (2016).

30 Lipták, B. G. Process Control: Instrument engineers' handbook. *Butterworth-Heinemann* (2013).

31 Reimer, J. M., Syedain, Z. H., Haynie, B. H. & Tranquillo, R. T. Pediatric tubular pulmonary heart valve from decellularized engineered tissue tubes. *Biomaterials* **62**, 88-94, doi:10.1016/j.biomaterials.2015.05.009 (2015).

32 Yelderman, M., Quinn, M. D., McKown, R. C., Eberhart, R. C. & Dollar, M. L. Continuous thermodilution cardiac output measurement in sheep. *J Thorac Cardiovasc Surg* **104**, 315-320 (1992).

33 Balguid, A. *et al.* Tailoring fiber diameter in electrospun poly(epsilon-caprolactone) scaffolds for optimal cellular infiltration in cardiovascular tissue engineering. *Tissue Eng Part A* **15**, 437-444, doi:10.1089/ten.tea.2007.0294 (2009).

34 Sacks, M. S., Schoen, F. J. & Mayer, J. E. Bioengineering challenges for heart valve tissue engineering. *Annu Rev Biomed Eng* **11**, 289-313, doi:10.1146/annurev-bioeng-061008-124903 (2009).

35 Mellado, P. *et al.* A simple model for nanofiber formation by rotary jet-spinning. *Appl Phys Lett* **99** (2011).
36 Aggarwal, A. & Sacks, M. S. A framework for determination of heart valves' mechanical properties using inverse-modeling approach. *International Conference on Functional Imaging and Modeling of the Heart, Springer*, 285–294 (2015).
37 Hobson, C. M. *et al.* Fabrication of elastomeric scaffolds with curvilinear fibrous structures for heart valve leaflet engineering. *J Biomed Mater Res A* **103**, 3101-3106, doi:10.1002/jbm.a.35450 (2015).
38 Hoerstrup, S. P. *et al.* Functional living trileaflet heart valves grown in vitro. *Circulation* **102**, III44-49 (2000).
39 Yu, T. & Wang, G. The process quality control of single-piece and small-batch products in advanced manufacturing environment. *Industrial Engineering and Engineering Management, 2009. IE&EM'09. 16th International Conference on, IEEE*, 306–310 (2009).
40 Del Gaudio, C., Bianco, A. & Grigioni, M. Electrospun bioresorbable trileaflet heart valve prosthesis for tissue engineering: in vitro functional assessment of a pulmonary cardiac valve design. *Ann Ist Super Sanita* **44**, 178-186 (2008).
41 van Lieshout, M. I., Vaz, C. M., Rutten, M. C., Peters, G. W. & Baaijens, F. P. Electrospinning versus knitting: two scaffolds for tissue engineering of the aortic valve. *J Biomater Sci Polym Ed* **17**, 77-89 (2006).
42 Lueders, C., Jastram, B., Hetzer, R. & Schwandt, H. Rapid manufacturing techniques for the tissue engineering of human heart valves. *Eur J Cardiothorac Surg* **46**, 593-601, doi:10.1093/ejcts/ezt510 (2014).
43 Hockaday, L. A. *et al.* Rapid 3D printing of anatomically accurate and mechanically heterogeneous aortic valve hydrogel scaffolds. *Biofabrication* **4**, 035005, doi:10.1088/1758-5082/4/3/035005 (2012).
44 Masoumi, N., Johnson, K. L., Howell, M. C. & Engelmayr, G. C., Jr. Valvular interstitial cell seeded poly(glycerol sebacate) scaffolds: toward a biomimetic in vitro model for heart valve tissue engineering. *Acta Biomater* **9**, 5974-5988, doi:10.1016/j.actbio.2013.01.001 (2013).
45 Kolewe, M. E. *et al.* 3D structural patterns in scalable, elastomeric scaffolds guide engineered tissue architecture. *Adv Mater* **25**, 4459-4465, doi:10.1002/adma.201301016 (2013).
46 Zhang, X. *et al.* Integrating valve-inspired design features into poly(ethylene glycol) hydrogel scaffolds for heart valve tissue engineering. *Acta Biomater* **14**, 11-21, doi:10.1016/j.actbio.2014.11.042 (2015).
47 Chen, Q., Bruyneel, A., Clarke, K., Carr, C. & Czernuszka, J. Collagen-based scaffolds for potential application of heart valve tissue engineering. *J. Tissue Sci. Eng.* (2013).
48 Bouten, C. V. *et al.* Substrates for cardiovascular tissue engineering. *Adv Drug Deliv Rev* **63**, 221-241, doi:10.1016/j.addr.2011.01.007 (2011).
49 Liu, W., Thomopoulos, S. & Xia, Y. Electrospun nanofibers for regenerative medicine. *Adv Healthc Mater* **1**, 10-25, doi:10.1002/adhm.201100021 (2012).
50 Hinderer, S. *et al.* Engineering of a bio-functionalized hybrid off-the-shelf heart valve. *Biomaterials* **35**, 2130-2139, doi:10.1016/j.biomaterials.2013.10.080 (2014).
51 Kalejs, M. *et al.* St Jude Epic heart valve bioprostheses versus native human and porcine aortic valves - comparison of mechanical properties. *Interact Cardiovasc Thorac Surg* **8**, 553-556, doi:10.1510/icvts.2008.196220 (2009).
52 Moreira, R. *et al.* Tissue-Engineered Fibrin-Based Heart Valve with Bio-Inspired Textile Reinforcement. *Adv Healthc Mater* **5**, 2113-2121, doi:10.1002/adhm.201600300 (2016).
53 Syedain, Z. *et al.* 6-Month aortic valve implantation of an off-the-shelf tissue-engineered valve in sheep. *Biomaterials* **73**, 175-184, doi:10.1016/j.biomaterials.2015.09.016 (2015).
54 Melchels, F. P. *et al.* Additive manufacturing of tissues and organs. *Prog. Polym. Sci.* **37**, 1079-1104 (2012).
55 Hasan, A. *et al.* Micro and nanotechnologies in heart valve tissue engineering. *Biomaterials* **103**, 278-292, doi:10.1016/j.biomaterials.2016.07.001 (2016).
56 Sanz-Garcia, A. *et al.* Heart valve tissue engineering: how far is the bedside from the bench? *Expert Rev Mol Med* **17**, e16, doi:10.1017/erm.2015.15 (2015).
57 Sheehy, S. P. *et al.* Quality metrics for stem cell-derived cardiac myocytes. *Stem Cell Reports* **2**, 282-294, doi:10.1016/j.stemcr.2014.01.015 (2014).
58 Duan, B., Kapetanovic, E., Hockaday, L. A. & Butcher, J. T. Three-dimensional printed trileaflet valve conduits using biological hydrogels and human valve interstitial cells. *Acta Biomater* **10**, 1836-1846, doi:10.1016/j.actbio.2013.12.005 (2014).
59 Merryman, W. D. *et al.* Correlation between heart valve interstitial cell stiffness and transvalvular pressure: implications for collagen biosynthesis. *Am J Physiol Heart Circ Physiol* **290**, H224-231, doi:10.1152/ajpheart.00521.2005 (2006).
60 Stradins, P. *et al.* Polymer nanofiber materials matching mechanical properties of native aortic valve. *Science Proceedings, Heart Valve Biol. Tissue Eng. 2012* (2013).
61 Bouten, C. V., Driessen-Mol, A. & Baaijens, F. P. In situ heart valve tissue engineering: simple devices, smart materials, complex knowledge. *Expert Rev Med Devices* **9**, 453-455, doi:10.1586/erd.12.43 (2012).
62 Schroeder, J. A., Jackson, L. F., Lee, D. C. & Camenisch, T. D. Form and function of developing heart valves: coordination by extracellular matrix and growth factor signaling. *J Mol Med (Berl)* **81**, 392-403, doi:10.1007/s00109-003-0456-5 (2003).
63 Sewell-Loftin, M. K., Chun, Y. W., Khademhosseini, A. & Merryman, W. D. EMT-inducing biomaterials for heart valve engineering: taking cues from developmental biology. *J Cardiovasc Transl Res* **4**, 658-671, doi:10.1007/s12265-011-9300-4 (2011).
64 Masoumi, N. *et al.* Tri-layered elastomeric scaffolds for engineering heart valve leaflets. *Biomaterials* **35**, 7774-7785, doi:10.1016/j.biomaterials.2014.04.039 (2014).
65 Eslami, M. *et al.* Fiber-reinforced hydrogel scaffolds for heart valve tissue engineering. *J Biomater Appl* **29**, 399-410, doi:10.1177/0885328214530589 (2014).
66 Puperi, D. S. *et al.* Electrospun polyurethane and hydrogel composite scaffolds as biomechanical mimics for aortic valve tissue engineering. *ACS Biomater. Sci. Eng.* **2**, 1546-1558 (2016).
67 Tamayol, A. *et al.* Fiber-based tissue engineering: Progress, challenges, and opportunities. *Biotechnol Adv* **31**, 669-687, doi:10.1016/j.biotechadv.2012.11.007 (2013).
68 Peltola, S. M., Melchels, F. P., Grijpma, D. W. & Kellomaki, M. A review of rapid prototyping techniques for tissue engineering purposes. *Ann Med* **40**, 268-280, doi:10.1080/07853890701881788 (2008).
69 Yeong, W. Y., Chua, C. K., Leong, K. F. & Chandrasekaran, M. Rapid prototyping in tissue engineering: challenges and potential. *Trends Biotechnol* **22**, 643-652, doi:10.1016/j.tibtech.2004.10.004 (2004).
70 Yancopoulos, G. D. *et al.* Vascular-specific growth factors and blood vessel formation. *Nature* **407**, 242-248, doi:10.1038/35025215 (2000).
71 Mendelson, K. & Schoen, F. J. Heart valve tissue engineering: concepts, approaches, progress, and challenges. *Ann Biomed Eng* **34**, 1799-1819, doi:10.1007/s10439-006-9163-z (2006).

72 Rengier, F. *et al.* 3D printing based on imaging data: review of medical applications. *Int J Comput Assist Radiol Surg* **5**, 335-341, doi:10.1007/s11548-010-0476-x (2010).

73 Lee, J. Y., Choi, B., Wu, B. & Lee, M. Customized biomimetic scaffolds created by indirect three-dimensional printing for tissue engineering. *Biofabrication* **5**, 045003, doi:10.1088/1758-5082/5/4/045003 (2013).

74 Murphy, S. V. & Atala, A. 3D bioprinting of tissues and organs. *Nat Biotechnol* **32**, 773-785, doi:10.1038/nbt.2958 (2014).

75 O'Brien, B. J. Biomaterials and scaffolds for tissue engineering. *Materials Today* **13** (2011).

76 Murphy, C. M. & O'Brien, F. J. Understanding the effect of mean pore size on cell activity in collagen-glycosaminoglycan scaffolds. *Cell Adh Migr* **4**, 377-381 (2010).

77 Roh, J. D. *et al.* Tissue-engineered vascular grafts transform into mature blood vessels via an inflammation-mediated process of vascular remodeling. *Proc Natl Acad Sci U S A* **107**, 4669-4674, doi:10.1073/pnas.0911465107 (2010).

78 Williams, S. F., Rizk, S. & Martin, D. P. Poly-4-hydroxybutyrate (P4HB): a new generation of resorbable medical devices for tissue repair and regeneration. *Biomed Tech (Berl)* **58**, 439-452, doi:10.1515/bmt-2013-0009 (2013).

79 Katayama, S., Umetani, N., Sugiura, S. & Hisada, T. The sinus of Valsalva relieves abnormal stress on aortic valve leaflets by facilitating smooth closure. *J Thorac Cardiovasc Surg* **136**, 1528-1535, 1535 e1521, doi:10.1016/j.jtcvs.2008.05.054 (2008).

80 Nakayama, Y. *et al.* In-body tissue-engineered aortic valve (Biovalve type VII) architecture based on 3D printer molding. *J Biomed Mater Res B Appl Biomater* **103**, 1-11, doi:10.1002/jbm.b.33186 (2015).

5

General discussion

5.1 MSC HYPE OR HOPE?

Adult MSCs were first identified by Friedstein et al. in the 1960s and 1970s, when observing a group of cells within the bone marrow that developed into fibroblastic colony forming cells (CFU-F) and could differentiate *in vitro* into several mesenchymal lineage cells such as chondrocytes, adipocytes, myoblasts and osteoblasts [1]. Since then, MSCs have been isolated form almost all adult tissues. This includes among others the bone marrow [2], adipose tissue [3], dental tissue [4], skin and foreskin [5], peripheral blood [6] and vessels [7]. Besides MSCs are also found in fetal tissues and fluids, such as the amniotic fluid [8] and membrane [9], placenta [10] and fetal membrane [10] and umbilical cord Wharton's jelly [11].

The interest in MSCs for clinical applications has constantly increased since the last decade. The advantages of MSC include their easy accessibility, extensive *in vitro* expansion, their multilineage differentiation potential, immunomodulation and secretion of trophic factors initiating tissue remodeling. In preclinical studies, MSCs have therefore shown the potential for the treatment of many chronic diseases such as neurodegenerative, cardiovascular, autoimmune and wound healing diseases. More then 20 years ago Lazarus et al. conducted the first clinical trial using BMSCs for lymphomas [12]. Since then, the efficacy and feasibility of MSC-based cell therapy has been tested in several different settings and patients suffering congenital or acquired diseases. Currently, there are 619 studies found for "Mesenchymal Stem Cells" in different clinical phases throughout the world [13]. The amount of MSC-based clinical trials has even triplet since the study number described by Wang et al. 2012 [14]. Among 619 registered trials, 33 have been either suspended, terminated or withdrawn. 539 of the studies are in early study phases, including early phase I, phase I and phase II. Only a small portion is registered as clinical phase III or IV. Clinical trials conducted with MSCs did only show mild adverse effects, given evidence that MSC-based therapies are well tolerated and safe. Potential late-side effects, such as MSC tumorigenic potential, will be evaluated in the future with longer follow-up times. However, the overall effectiveness of MSC is currently limited to graft versus host diseases and hematological bone and cartilage diseases [15]. It seems as if beneficial effects of MSC-based therapies are related to the immunomodulation and regenerative potential of these cells [15]. Nevertheless, inflammation is a key event in a lot of pathologies and therefore beneficial effects of MSC-based therapies are also expected in other diseases.

Before clinical translation the following points need to be addressed. **First**, there is still not a single characterization of MSC available limiting comparison of different studies conducted and their results (see paragraph 5.2). We are still far from defining a molecular signature for MSC from different tissue sources. **Secondly**, the mechanism of action of MSCs is still not fully elucidated yet. It has been postulated to be based on the secretion of cytokines and biologically relevant molecules rather than

direct effect of MSC (see paragraph 5.3). Processes such as MSC survival after transplantation, modulation of the host immune system and MSC phenotype after *in vivo* translation remain unknown. **Thirdly**, suitable animal models are necessary to enable more accurate extrapolation of gained knowledge to the human situation and finally, also different delivery routes have to be critically evaluated (see paragraph 5.4).

5.2 MSC CHARACTERIZATION PARAMETERS

MSC are isolated, cultured and characterized differently among laboratories. Even if cultured in different culture media supplemented with varying concentration of serum and oxygen, all MSCs exhibit the minimum criteria proposed in 2006 by the International Society for Cellular Therapy (ISCT)[16]. According to them, isolated cells need I) to be plastic adherent under standard culture conditions, II) to possess specific set of cell surface markers, i.e expression of cluster of differentiation (CD)105, CD90 and CD73 and lack of expression of CD14, CD34, CD45 and human leucocyte antigen-DR (HLA-DR), and III) to differentiate *in vitro* into osteocytes, chondrocytes and adipocytes [16]. The goal of these ISCT guidelines was to offer a quality control for researcher in the field of MSCs and to decrease possible experimental variability and increase transparency of published data.

However, these criteria still enable a mixed population of cells and neglect the tissue origin of isolated cells. Tissue-specific differences can be maintained under *in vitro* culture conditions and markers may vary depending on the MSC tissue source. Furthermore, ISCT criteria do not improve the purification of MSCs after isolation but produce heterogeneous, non-clonal cultures of stromal cells containing stem cells with different multipotent properties, committed progenitors and differentiated cells [15]. In particular, in the situation were MSC are present in low quantities, such as the bone marrow with only 0.01% to 0.001% [17]. In an attempt to further increase purity of isolated MSCs, positive and negative selection markers have been tested. Even if there are some concerns over using such isolation strategies due to cross-linking of antigens altering cellular phenotypes and potentially activating signaling pathways, increased clonogenicity compared to cells isolated based on plastic adhesion has been reported [18,19]. Clonogenicity is also not assumed in currently used trilineage differentiation assays to assess MSC plasticity. Differentiation into adipogenic, osteogenic and chondrogenic lineages can be initiated by single (precursor) cells within the heterogeneous and mixed cell population. Furthermore, *in vitro* culturing of MSCs has shown to decrease differentiation potential [20], emphasizing the need to verify MSC multipotency not only after isolation, but also after been passaged several times. In the presented thesis, multipotency has therefore been evaluated at passage 3-4 after isolation in all donors and at the same passage as other assays have been

performed, such as conditioned media harvest and MSC characterization (see chapter 2 and 3). Like that culture differences were minimized. However besides the decline in their multipotency, also increased probability of malignant transformation [21], decrease telomerase activity [22] and changed cellular morphology have been described on long-term culture. In this regard, also markers to monitor senescent-associated changes have been suggested for a better MSC characterization over passaging.

In addition to previously described concerns about ISCT guidelines, quantitative information about the expression of MSC surface markers of analyzed cells is not obtained. This is essential when comparing MSC lines from different donors and tissue sources. Therefore, the present thesis analyzed all surface markers using multicolor flow cytometry (described in chapter 2), enabling phenotypic single cells instead of percentages within the overall population. Median fluorescence intensity ratios (MFIR) allowed quantification of different subsets of MSCs. In the future, specific subpopulation might be even enriched using fluorescence-activated cell sorting. A potential side effect of sorting might be the cross-linking of surface antigens or other molecules [23]. Also embryonic stem cell (ESC) markers are used to characterize MSCs. Expression of ESC markers such as Oct4, Nanog, Sox2 and SSEA-4 have been found in so called “broadly multipotent” MSCs from fetal sources such as the amniotic fluid (described in chapter 3.2). These markers have also been qualitatively detected in MSC from the bone marrow, adipose tissue and dermis [24]. Nevertheless, fetal MSCs exhibit higher plasticity, faster proliferation and senesced later in culture than their adult counterparts [25]. In the future quantifiable characterization parameters are therefore necessary to compare the primitive state of MSCs between different groups, isolation protocols, tissue sources and donors. It seems not enough to have certain markers expressed without any prove for higher plasticity and possible related cellular features.

MSCs have also been isolated form several animal models such as mice, pig and sheep and are used for preclinical studies before human translation. In contrary to the human situation, there are no established minimal criteria for the identification of MSCs in non-humans. Not available species-specific antibodies and a different set of surface markers limit the accurate comparison to the human situation (described in chapter 3). This would not only enable better predictions of safety and efficacy using MSC-based therapies, but also open novel treatment strategies for the veterinarian clinic.

Taken together, further research in this field will not only enable a better defined MSC population, but also less variability between documented results in the literature and ultimately less contradictory data and a better clinical translation.

5.3 MSC SECRETOME VERSUS CELLS

Published research has pointed out the broad *in vitro* differentiation potential of MSC from different sources into all three lineages including not only adipocytes, osteocytes and chondrocytes, but also cardiomyocytes, pancreatic cells, neuronal cells and hepatocytes [26]. However, the question whether *in vivo* differentiation of MSC is required for beneficial effects in treated patients remains debated. Initially, stem cell research focused on the direct differentiation of MSCs into intended phenotypes. Some functional improvements were found with MSC transplantation and could directly be attributed to *in vivo* homing and cell differentiation [26]. However, it has become evident that functional benefits found in animal models and treated patients may be due to paracrine actions of introduced MSCs rather than cell differentiation. Cytokines and biologically relevant molecules secreted by MSCs exert potent effects on other cell types *in vitro* and *in vivo* as demonstrated by a number of studies utilizing conditioned media (CM) collected from different MSC sources [27]. Paracrine factors have been postulated to influence the microenvironment following injury by recruiting host cells enabling cytoprotection, angiogenesis and endogenous regeneration of injured environment in an inflammation mediated cellular cascade (see chapter 1.2).

Considering clinical translation, MSC CM can provide several advantages over using the cell itself. No cells means there is no risk of inadequate differentiation of MSCs in a certain tissue environment, as shown by undesired ectopic bone within the heart of MSC-treated mouse in a model of myocardial infarction [28]. Further, long-term *in vitro* culturing of MSC are not necessary which involves high costs for a regulated GMP-compliant facilities to expand high numbers of cells. MSC CM can be manufactured, freeze-dried and transported more easily. Even if controversially debated and more evidence is still needed, several studies have suggested chromosomal aberrations during long-term culturing of MSC, which subsequently enable malignant neoplastic transformation [29,30]. This would mean patient treated with MSCs could potentially promote growth of new or preexisting tumors [31]. Moreover, by using MSC CM there is no need to match the donor and the recipient to avoid any adverse immunological responses, although MSC are unable to bring substantial alloreactivity by protecting them against natural killer cell lysis [32]. However, certain limitations exist with the use of MSC CM, such as its contamination by animal products used in the serum. Serum proteins can easily bind to the surface of cells and subsequently be part of the CM harvested. Therefore, the presented thesis (described in chapter 2) established culturing conditions without any xenogenic factor involved. This not only enables *in vitro* experiments with human immune cells, but also increases safety for possible clinical evaluation. The use of fetal bovine and calf serum has raised some concerns given the possibility to induce host immune reactions and transmission of unidentified zoonose and prions. By using autologous or allogeneic human platelet lysate as serum substitute

(described in chapter 2) for *in vitro* expansion such risks could be avoided. Finally, the relative amount of secreted factors and the effective functional response *in vivo* need to be evaluated depending on the harvest procedure and clinical application. This is often neglected in preclinical studies where different concentrations of MSC CM or amount of MSC itself are used depending on the experimental assay, rather than equalizing it. The study in chapter 2 has therefore harvested MSC CM based on the amount of incubated cells. This enables comparison of different MSCs even with different proliferation capacities. Hence, it seems important to consider that MSC CM offers a cocktail of both stimulatory and inhibitory factors and that the interaction of several cytokines and biologically relevant molecules might sustain physiological pharmocokinetics compare to the deliver of single factors (described in chapter 2). In ischemic heart diseases, single cytokine therapy trials have not met expectations underlying that processes such as regeneration may need simultaneous administration of multiple factors at different concentrations to act synergistically [33]. To high dosages of single factors can lead to the formation of aberrant and leaky vessels, hypotension and tumor angiogenesis [33].

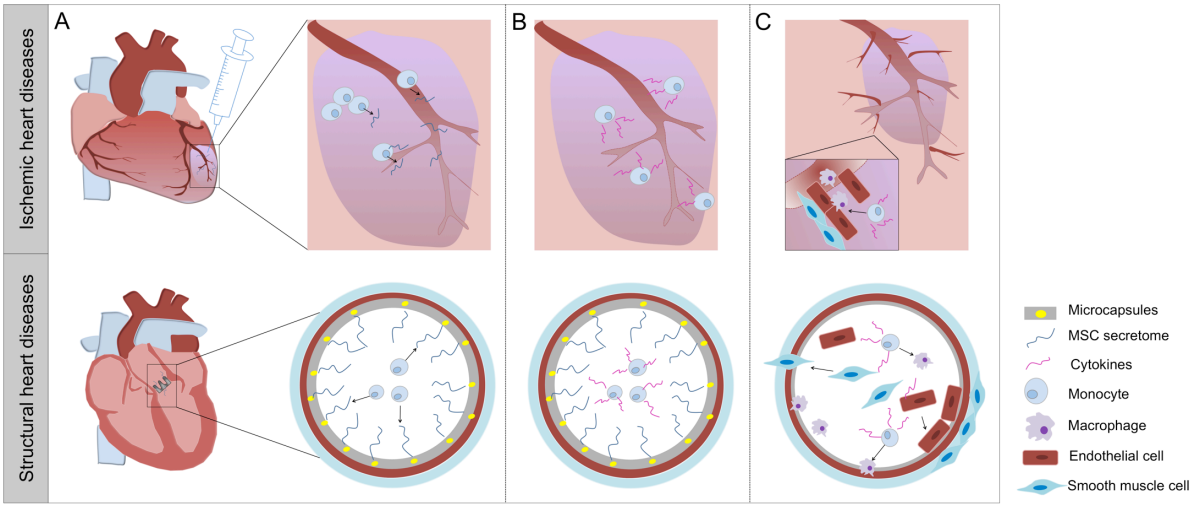

Unpublished figure 1: Delivery routes for MSC CM in ischemic heart diseases (e.g myocardial infarction) and structural heart diseases (e.g heart valve diseases). Intramyocardial or systemic injections is predominantly described for ischemic heart diseases, where the replacement of diseased heart valves is focusing on the in situ tissue engineering approach, including so called microcapsules for defined MSC CM release. Both delivery routes induce an inflammation-mediated cellular cascade of vascular remodeling, defined by a first monocyte attraction followed by a second vascular cell attraction (smooth muscle cells / endothelial cells). These events result in reperfused tissue (promotion of angiogenesis) and tissue formation (promotion of extracellular matrix production).

5.4 MSC DELIVERY ROUTE FOR CLINICAL APPLICATIONS

The route of MSCs administrations varies between local (e.g intramuscular or subcutaneous) and systemic (e.g intravenous or intraarterial) injections or by the use of synthetic and natural scaffold materials as a carrier. In this regard, the systemic intravenous delivery route shows first efficacy and safety in preclinical models and in preliminary clinical settings, representing the least invasive delivery route with the ability for clinical translation and patient compliance. However, it has to be explored whether the therapeutic effects of systemic and targeted delivery can be further refined in order to improve MSC-based therapies in the future.

It has been shown that regardless of the injection route only 1-5% of administered MSCs end within the target tissue and that most of cells are not even detectable 7-14 days post administration [34]. Thus increasing number of injections or cell concentrations seem necessary to increase the amount of MSCs within the injury site [34]. The recruitment of systemically applied MSCs into the target tissue is probably due to chemotactic stimuli released by injured cells. Therefore, only a limited time window might lead to therapeutic effects *in vivo*.

In this regard, the combination of MSC or MSC secretome with appropriate scaffold material would enable a more targeted application. Higher concentrations of paracrine factors released by MSCs can be preserved in a local microenvironment. Various biomaterials have been used as vehicles of delivery for cells and paracrine factors as well as a scaffold for extracellular matrix production and tissue formation. In the field of cardiovascular *in situ* tissue engineering (see chapter 1.1), the inclusion of bioactive substances has shown to increase host cell recruitment via an inflammatory process and enable tissue formation [35]. Aliginate particles can be formulated into porous scaffold marices as delivery vehicles for bioactive molecules or transplanted cells [36]. This strategy might also improve the limited cellular repopulation of electrospun heart valves described in chapter 4 and further support a faster host tissue formation.

5.5 REFERENCES

1 Friedenstein, A. J., Chailakhjan, R. K. & Lalykina, K. S. The development of fibroblast colonies in monolayer cultures of guinea-pig bone marrow and spleen cells. *Cell Tissue Kinet* **3**, 393-403 (1970).

2 Pittenger, M. F. *et al.* Multilineage potential of adult human mesenchymal stem cells. *Science* **284**, 143-147 (1999).

3 Wagner, W. *et al.* Comparative characteristics of mesenchymal stem cells from human bone marrow, adipose tissue, and umbilical cord blood. *Exp Hematol* **33**, 1402-1416, doi:10.1016/j.exphem.2005.07.003 (2005).

4 Miura, M. *et al.* SHED: stem cells from human exfoliated deciduous teeth. *Proc Natl Acad Sci U S A* **100**, 5807-5812, doi:10.1073/pnas.0937635100 (2003).

5 Riekstina, U., Muceniece, R., Cakstina, I., Muiznieks, I. & Ancans, J. Characterization of human skin-derived mesenchymal stem cell proliferation rate in different growth conditions. *Cytotechnology* **58**, 153-162, doi:10.1007/s10616-009-9183-2 (2008).

6 Zvaifler, N. J. *et al.* Mesenchymal precursor cells in the blood of normal individuals. *Arthritis Res* **2**, 477-488, doi:10.1186/ar130 (2000).

7 Pasquini, L., Nasto, R., Mie, M. E., Giuliani, B. & Periti, E. [Amniotic fluid analysis as a screening test in term and post-term pregnancy]. *Minerva Ginecol* **55**, 69-73 (2003).

8 In 't Anker, P. S. *et al.* Amniotic fluid as a novel source of mesenchymal stem cells for therapeutic transplantation. *Blood* **102**, 1548-1549, doi:10.1182/blood-2003-04-1291 (2003).

9 Cai, J. *et al.* Generation of human induced pluripotent stem cells from umbilical cord matrix and amniotic membrane mesenchymal cells. *J Biol Chem* **285**, 11227-11234, doi:10.1074/jbc.M109.086389 (2010).

10 Raynaud, C. M. *et al.* Comprehensive characterization of mesenchymal stem cells from human placenta and fetal membrane and their response to osteoactivin stimulation. *Stem Cells Int* **2012**, 658356, doi:10.1155/2012/658356 (2012).

11 Wang, H. S. *et al.* Mesenchymal stem cells in the Wharton's jelly of the human umbilical cord. *Stem Cells* **22**, 1330-1337, doi:10.1634/stemcells.2004-0013 (2004).

12 Lazarus, H. M. Bone marrow transplantation in low-grade non-Hodgkin's lymphoma. *Leuk Lymphoma* **17**, 199-210, doi:10.3109/10428199509056824 (1995).

13 Search. Titel: Mesenchymal Stem Cells. *ClinicalTrial.gov* (July 2017).

14 Wang, S., Qu, X. & Zhao, R. C. Clinical applications of mesenchymal stem cells. *J Hematol Oncol* **5**, 19, doi:10.1186/1756-8722-5-19 (2012).

15 Squillaro, T., Peluso, G. & Galderisi, U. Clinical Trials With Mesenchymal Stem Cells: An Update. *Cell Transplant* **25**, 829-848, doi:10.3727/096368915X689622 (2016).

16 Dominici, M. *et al.* Minimal criteria for defining multipotent mesenchymal stromal cells. The International Society for Cellular Therapy position statement. *Cytotherapy* **8**, 315-317, doi:10.1080/14653240600855905 (2006).

17 Calloni, R., Cordero, E. A., Henriques, J. A. & Bonatto, D. Reviewing and updating the major molecular markers for stem cells. *Stem Cells Dev* **22**, 1455-1476, doi:10.1089/scd.2012.0637 (2013).

18 Aslan, H. *et al.* Osteogenic differentiation of noncultured immunoisolated bone marrow-derived CD105+ cells. *Stem Cells* **24**, 1728-1737, doi:10.1634/stemcells.2005-0546 (2006).

19 Quirici, N. *et al.* Isolation of bone marrow mesenchymal stem cells by anti-nerve growth factor receptor antibodies. *Exp Hematol* **30**, 783-791 (2002).

20 Chen, G. *et al.* Monitoring the biology stability of human umbilical cord-derived mesenchymal stem cells during long-term culture in serum-free medium. *Cell Tissue Bank* **15**, 513-521, doi:10.1007/s10561-014-9420-6 (2014).

21 Rosland, G. V. *et al.* Long-term cultures of bone marrow-derived human mesenchymal stem cells frequently undergo spontaneous malignant transformation. *Cancer Res* **69**, 5331-5339, doi:10.1158/0008-5472.CAN-08-4630 (2009).

22 Kassem, M. Mesenchymal stem cells: biological characteristics and potential clinical applications. *Cloning Stem Cells* **6**, 369-374, doi:10.1089/clo.2004.6.369 (2004).

23 Mosna, F., Sensebe, L. & Krampera, M. Human bone marrow and adipose tissue mesenchymal stem cells: a user's guide. *Stem Cells Dev* **19**, 1449-1470, doi:10.1089/scd.2010.0140 (2010).

24 Riekstina, U. *et al.* Embryonic stem cell marker expression pattern in human mesenchymal stem cells derived from bone marrow, adipose tissue, heart and dermis. *Stem Cell Rev* **5**, 378-386, doi:10.1007/s12015-009-9094-9 (2009).

25 Guillot, P. V., Gotherstrom, C., Chan, J., Kurata, H. & Fisk, N. M. Human first-trimester fetal MSC express pluripotency markers and grow faster and have longer telomeres than adult MSC. *Stem Cells* **25**, 646-654, doi:10.1634/stemcells.2006-0208 (2007).

26 Ullah, I., Subbarao, R. B. & Rho, G. J. Human mesenchymal stem cells - current trends and future prospective. *Biosci Rep* **35**, doi:10.1042/BSR20150025 (2015).

27 Baraniak, P. R. & McDevitt, T. C. Stem cell paracrine actions and tissue regeneration. *Regen Med* **5**, 121-143, doi:10.2217/rme.09.74 (2010).

28 Breitbach, M. *et al.* Potential risks of bone marrow cell transplantation into infarcted hearts. *Blood* **110**, 1362-1369, doi:10.1182/blood-2006-12-063412 (2007).

29 Rubio, D. *et al.* Spontaneous human adult stem cell transformation. *Cancer Res* **65**, 3035-3039, doi:10.1158/0008-5472.CAN-04-4194 (2005).

30 Zhou, Y. F. *et al.* Spontaneous transformation of cultured mouse bone marrow-derived stromal cells. *Cancer Res* **66**, 10849-10854, doi:10.1158/0008-5472.CAN-06-2146 (2006).

31 Djouad, F. *et al.* Immunosuppressive effect of mesenchymal stem cells favors tumor growth in allogeneic animals. *Blood* **102**, 3837-3844, doi:10.1182/blood-2003-04-1193 (2003).

32 Rasmusson, I., Ringden, O., Sundberg, B. & Le Blanc, K. Mesenchymal stem cells inhibit the formation of cytotoxic T lymphocytes, but not activated cytotoxic T lymphocytes or natural killer cells. *Transplantation* **76**, 1208-1213, doi:10.1097/01.TP.0000082540.43730.80 (2003).

33 Ranganath, S. H., Levy, O., Inamdar, M. S. & Karp, J. M. Harnessing the mesenchymal stem cell secretome for the treatment of cardiovascular disease. *Cell Stem Cell* **10**, 244-258, doi:10.1016/j.stem.2012.02.005 (2012).

34 Kurtz, A. Mesenchymal stem cell delivery routes and fate. *Int J Stem Cells* **1**, 1-7 (2008).

35 Roh, J. D. *et al.* Tissue-engineered vascular grafts transform into mature blood vessels via an inflammation-mediated process of vascular remodeling. *Proc Natl Acad Sci U S A* **107**, 4669-4674, doi:10.1073/pnas.0911465107 (2010).

36 Sun, J. & Tan, H. Alginate-based biomaterials for regenerative medicine applications. *Materials* **6**, 1285-1309 (2013).

CURRICULUM VITAE

DEBORA KEHL

Address:	Badenerstrasse 394, 8004 Zurich
Date of Birth:	July, 30th 1989
Nationality:	Swiss / Spanish
Email:	debora.kehlgomez@gmail.com

Professional experience

PhD candidate, Program in Integrative Molecular Medicine **2014-2017**
Institute for Regenerative Medicine, University of Zurich, Switzerland

- Conducting several research projects independently, including conception of scientific questions, organization of resources, and data collection/analysis
- Developing and maintaining research collaborations with external national and international universities and hospitals, acting as a direct contact person and coordinator
- Writing and managing three ethical licenses according to the Human Research Act Switzerland, in order to acquire primary human material from collaborating hospitals
- Acquiring funding by writing and initiating research projects and structuring them into major milestones and deliverables
- Writing and proof-reading scientific papers, reports and reviews and regularly presenting scientific data/literature in public
- Direct supervision of medical and master students, imparting medical physiology knowledge, planning research projects and grading master theses

Master candidate, Program of Human Biology **2012-2014**
Swiss Center for Regenerative Medicine, University / University Hospital Zurich, Switzerland

- Assay and method development in order to answer new scientific questions
- Managing, creating and maintaining project plans and milestones independently
- Responsible for the coordination of human ethical licenses, keeping regular records of the implemented samples and preparing annual reports
- Writing and proof-reading scientific papers, reports and reviews and regularly presenting scientific data/literature in public

Educational qualifications

PhD candidate, Program Integrative Molecular Medicine, University of Zurich 2014-2017

Master of Science in Biology, Program Human Biology, University of Zurich 2012-2014
Cumulative grade: 5.9, Semester Award Winner (6=highest, 1=lowest)

Bachelor of Science in Biology, University of Zurich 2008-2011
Cumulative grade: 4.7 (6=highest, 1=lowest)

Professional training

GCP course 1,2 & 3, Clinical Trial Center, University Hospital Zurich	2017
Supervision of physiology lab classes and medical master students, University of Zurich	2014-2016
Project management for research, University of Zurich	2014
Laboratory animal science (LTK1), FELASA Category B, University of Zurich	2014
Training in acquiring funding for science, University of Zurich	2014
Scientific writing in English, University of Zurich	2012

Languages

German (native speaker)
Spanish (native speaker)
English (advanced, C2)
French (intermediate, B1)

Computer Skills

MS Office (working)
Data Analysis (Graph Pad Prism; working)
Photoshop Adobe (basic)
Homepage administration

Bibliography

Original peer-reviewed publications (first author):	2 published, 1 submitted
Original peer-reviewed publications (co-author):	5 published
Peer-reviewed review articles / book chapters (first author):	2 published, 1 submitted
Poster presentations (national/international):	3 presented

Fundraising / Scientific Awards

Semester Award Winner 2016, as supervisor of master student Sabrina Görtz, Faculty of Medicine, University Zurich	2016
Center for Applied Biotechnology and Molecular Medicine Start up grant, University of Zurich (as co-applicant)	2016
ImmunoTools Award 2016, ImmunoTools Germany	2016
Foundation for Research in Science and the Humanities, University of Zurich (as co-applicant)	2015
Semester Award Winner 2014, Faculty of Science, University of Zurich	2014
Alfred and Anneliese Suttner-Stöttner-Foundation (individual scholarship)	2014

PUBLICATIONS

PEER-REVIEWED RESEARCH ARTICLES

Kehl D, Mallone A, Generali M, Uldry AC, Heller M, Gantenbein B, Hoerstrup SP, Weber B **(2017)** A proteomic approach: hWJSC secretome retains the highest inflammation-mediated angiogenesis potential. *(in preparation)*

Kehl D*, Generali M*, Görtz S, Geering D, Slamecka J, Hoerstrup SP, Bleul U, Weber B **(2017)** Amntiotic fluid cells show higher pluripotency-related gene expression than allantoic fluid cells. Stem Cells and Development, Oct 1;26(19):1424-1437.

Kehl D, Görtz S, Wang C, Hoerstrup SP, Bleul U*, Weber B* **(2017)** Gestational age-dependent fetal fluid dynamics in the ovine developmental model. Reproduction, Fertility and Development. *(under revision)*

Generali M*, **Kehl D***, Capulli AK, Parker KK, Hoerstrup SP, Weber B **(2017)** Comparative analysis of poly-glycolic acid-based hybrid polymer starter matrices for in vitro tissue engineering. Colloids Surf B Biointerfaces, Jul 1;158:203-212. (Epup ahead of print)

Generali M, Casanova EA, **Kehl D**, Bode PK, Hoerstrup SP, Cinelli P, Weber B **(2017)** Endothelialized bioengineered vascular grafts based on peripheral blood mononuclear cell-derived induced pluripotent stem cells. *(in preparation)*

Capulli AK, Emmert MY, Pasqualini F, **Kehl D,** Caliskan E, Lind JU, Sheehy SP, Park SJ, Ahn S, Weber B, Gross JA, Hoerstrup SP, Parker KK **(2017)** JetValve: Rapid manufacturing of biohybrid scaffolds for biomimetic heart valve replacement. Biomaterials, Jul;133:229-241.

Slamecka J, Salminova L, McClellan S, van Kelle M, **Kehl D,** Laurini J, Cinelli P, Owen L, Hoerstrup SP, Weber B **(2016)** Non-integrating episomal plasmid-based reprogramming of human amniotic fluid stem cells into induced pluripotent stem cells in chemically defined conditions. Cell Cycle, 15(2):234-49.

Weber B, **Kehl D**, Bleul U, Behr L, Sammut S, Frese L, Ksiazek A, Achermann J, Stranzinger G, Robert J, Sanders B, Sidler M, Brokopp CE, Proulx ST, Frauenfelder T, Schoenauer R, Emmert MY, Falk V, Hoerstrup SP **(2016)** In vitro fabrication of autologous living tissue-engineered vascular grafts based on prenatally harvested ovine amniotic fluid-derived stem cells. J Tissue Eng Tegen Med, Jan;10(1):52-70.

Weber B, Robert J, Ksiazek A, Wyss Y, Frese L, Slamecka J, **Kehl D**, Modregger P, Peter S, Stampanoni M, Proulx S, Falk V, Hoerstrup SP **(2014)** Living-engineered valves for transcatheter venous valve repair. Tissue Eng Part C Methods, Jun;20(6):451-63.

Weber B, Dijkman PE, Scherman J, Sanders B, Emmert MY, Grünefelder J, Verbeek R, Bracher M, Franz T, Kortsmit J, Modregger P, Stampanoni M, Robert J, **Kehl D**, van Doeselaar M, Schweiger M, Brokopp CE, Wälchli T, Falk V, Zilla P, Driessen-Mol A, Baaijens FP, Hoerstrup SP **(2013)** Off-the-shelf human decellularized tissue-engineered heart valves in a non-human primate model. Biomaterials, Oct;34(30):7269-80.

PEER-REVIEWED BOOK CHAPTERS AND REVIEW ARTICLES

Kehl D, Weber B, Hoerstrup SP **(2016)** Bioengineered living cardiac and venous valve replacements: current status and future prospects. Cardiovasc Path, Jul-Aug;25(4):300-5.

Malheiro V, Enayati M, **Kehl D**, Bergmeister H, Weber B, Maniura-Weber K **(2016)** Macrophage cellular crosstalk in the body response to implantation. eCell and Materials. *(under revision)*

Kehl D*, Weber B*, Hoerstrup SP **(2013)** Section I. Amniotic Fluid Stem Cells: Amniotic fluid-derived cells: an autologous cell source for cardiovascular tissue engineering. Published in Applications of Perinatal Stem Cells, edited by Atala A. and Murphy S.V., Springer New York.

POSTER PRESENTATIONS

Poster presentation at Advances in Stem Cells and Regenerative Medicine **(2017)**, European Molecular Biology Laboratory (EMBL), Heidelberg, Germany

Poster presentation at the annual retreat of the Integrative Molecular Medicine Program **(2016)**, Magglingen, Switzerland

Poster presentation at the 6th Biennial Heart Valve biology & Tissue Engineering Meeting **(2014)**, London, UK (abstract published in a supplement of Global Cardiology: Science and Practice)

PUBLIC PRESENTATIONS

13th Winter Brain & Heart Symposium, University of Zurich, Sils Maria, Switzerland. Organization: Institute for Regenerative Medicine. **(2017)** Comparative analysis of the pro-angiogenic potential of different human mesenchymal stem cell sources.

Research colloquium, Division of Surgical Research, University Hospital Zurich, Switzerland. Organization: Prof. Dr. med. Gregor Zünd. **(2014)** Comparative analysis of the pro-angiogenic potential of different therapeutically relevant human mesenchymal stem cell sources

Stem Cell Symposium Zurich for Gynecologists, Klinik Hirstlanden, Zurich, Switzerland. Organization: Prof. Dr. Breymann, Vita34. **(2014)** Herstellung von lebenden “tissue engineerten” Herzklappen aus Stammzellen

ACKNOWLEDGEMENTS

It is my pleasure to acknowledge everyone who was important for the completion of my PhD, it would have never been possible without you.

First of all, I would like to thank Prof. Dr. Dr. Simon P. Hoerstrup for giving me the opportunity to pursue my PhD in his group. Thank you for the trust and confidence you always had in my work. I would like to further thank PD Dr. Dr. Benedikt Weber for his guidance through my PhD. Thank you for giving me the opportunity to work on diverse exciting projects and helping me to become an independent researcher being responsible for projects from the beginning to the end.

Furthermore, I would like to thank Prof. Dr. Arnold von Eckardstein for taking the chair of my committee and his insightful comments and encouragement. In addition, I would like to thank my two additional committee members, Prof. Dr. Christian Grimm and Prof. Dr. Benjamin Gantenbein, for their support and constructive advices.

Special thanks to Ulrich Bleul from the Vetsuisse faculty, University of Zurich, for his trust, continuous support and advice over the last years. I would also like to thank the Disease Biophysics Group, Harvard University, in particular Andrew K. Capulli and Prof. Kevin Kit Parker for our successful collaboration. Thank you Manfred Heller and Anne-Christine Uldry for sharing all your knowledge about mass spectrometry with me. Moreover, I would like to thank all collaborating medical doctors, practices and hospital for the primary human material obtained: Dr. Nicole Gross, Dr. Tamim Obeid, Prof. Dr. Roland Böni, Prof. Dr. Claudio Dora and Prof. Dr. Jürg Hafner. This work would not have been possible without the personal funding from the Alfred and Anneliese Suttner-Stöttner-Foundation as well as funding from the Foundation for Research in Science and the Humanities, University of Zurich and the CABMM Start up grant, University of Zurich.

In addition, I would like to thank my complete lab team (current and past) at the Institute of Regenerative medicine at Moussonstrasse. Especially I thank my beloved lab family – Melle, Ursi, Lab Mama Tine, Marko, Laura, Aga and Anna – for all their support and fun while working together. You always reminded me that live goes on, even when experiments failed the third time. It is a great pleasure being your friend! Further thanks to Sabrina for her exceptional teamwork and enthusiasm during her master thesis.

Finally, my deepest appreciation belongs to all my family and friends who always supported me realizing my dreams.

Nenita, muchas gracias por creer siempre en mi, sea lo que sea. Tu me has enseñado como lograr todo lo que quiera en la vida siempre y cuando tenga voluntad. Papi, danke für dis hilfriche mathematische Gen, dini unigschränkti Unterstützig und Liebi. Brüederli, erscht jetzt chasch mi Dr. nennä, au wänn scho vor 3 Jahr immer a das glaubt häsch… Danke dir und dä Laura! Marc, I love you, danke dass du immer a minere Sietä bisch, mir selbstvertraue gisch und (ab und zue) ab mine PhD Witzli lachsch. Au es grosses Danke a dich Angi, di bescht Mitbewohnerin und Fründin wos git.